Determining individual chromosome missegregation rates and the responses to aneuploidy in human cells

Joseph Thomas Worrall

A thesis submitted in partial fulfilment of the requirements for the degree of Doctor of Philosophy

August 2017

Statement of originality

I, Joseph Thomas Worrall, confirm that the research included within this thesis is my own work or that where it has been carried out in collaboration with, or supported by others, that this is duly acknowledged below and my contribution indicated. Previously published material is also acknowledged below.

I attest that I have exercised reasonable care to ensure that the work is original, and does not to the best of my knowledge break any UK law, infringe any third party's copyright or other Intellectual Property Right, or contain any confidential material.

I accept that the College has the right to use plagiarism detection software to check the electronic version of the thesis.

I confirm that this thesis has not been previously submitted for the award of a degree by this or any other university.

Signature:

Date: 21st August 2017

Publications during PhD enrolment

1. Phillips M*, Khadeir R* , **Worrall JT**, Sharpe K, Yuan M, Tookman L, Steele J, Lemoine N, Frezza C, Cutts R, Chelala C, Bomalaski J, Sheaff M, Ghazaly E, Szlosarek P. (2017). Macrophages mediate resistance to ADI-PEG20 in Mesothelioma. *Cancer Discovery*. In Review.

2. Quétier I, Marshall JJ, Spencer-Dene B, Lachmann S, Casamassima A, Franco C, Escuin S, **Worrall JT**, Baskaran P, Rajeeve V, Howell M, Copp AJ, Stamp G, Rosewell I, Cutillas P, Gerhardt H, Parker PJ, Cameron AJ. (2016). Knockout of the PKN family of Rho effector kinases reveals a non-redundant role for PKN2 in developmental mesoderm expansion. *Cell Reports*. 14(3):440-8.

3. Campbell GR, **Worrall JT**, Mahad DJ. (2014). The central role of mitochondria in axonal degeneration in multiple sclerosis. *Multiple Sclerosis Journal.* 20(14) 1806-13.

Conference abstracts: selected oral presentation

1. **Worrall JT** and McClelland SE (2016). Determining the missegregation rates of individual human chromosomes. *Molecular Biology of the Cell*. vol. 27. American Society for Cell Biology annual meeting, San Francisco, USA, December 2016.

2. **Worrall JT** and McClelland SE (2016). Determining the missegregation rates of individual human chromosomes. *Cytogenetics and genome research*. vol. 148, 131-131. 21st International Chromosome conference, Foz do Iguaçu, Brazil, July 2016. Runner up: Best Student Oral Presentation Award.

Collaborations

1. Single-cell sequencing analysis and RPE-1/DLD1 cells harbouring mutant CENP-A alleles were a generous collaboration with the Fachinetti laboratory, Institut Curie, Paris, France.

2. Figures in chapter 6, and data in chapter 7.1, were generated in collaboration with Dr. Sarah McClelland, Barts Cancer Institute, London, UK.

* Equally contributing authors

Abstract

Background.

Genomic instability and aneuploidy, which are ubiquitous hallmarks of cancer cells, encompass both structural and numerical chromosome aberrations. Strikingly, cancer cells often display recurrent patterns of aneuploidy which are thought to be contingent on selection pressures within the tumour microenvironment maintaining advantageous karyotypes. However, it is currently unknown if individual chromosomes are intrinsically vulnerable to missegregation, and therefore whether chromosome bias may *also* contribute to pathological aneuploidy patterns. Moreover, the earliest responses to chromosome missegregation in non-transformed cells, and how these are overcome in cancer, has remained elusive due to the difficult nature of isolating nascent aneuploid cells.

Results.

Individual chromosomes displayed recurrent patterns of biased missegregation in response to a variety of cellular stresses across cell lines. Likewise, a small subset of chromosomes accounted for a large fraction of segregation errors following one specific mechanism driving aneuploidy. This was supported by the discovery that chromosomes 1 and 2 are strikingly susceptible to the premature loss of sister chromatid cohesion during prolonged prometaphase arrest. Additionally, I have elucidated the arrangement of individual metaphase human chromosomes, highlighting missegregation vulnerabilities occurring at the metaphase plate periphery following nocodazole wash-out. Finally, I have developed a novel system for isolating nascent aneuploid cells, suggesting the earliest transcriptome responses to chromosome missegregation in non-transformed human cells involve ATM and BCL2-mediated apoptosis.

Acknowledgements

I am grateful to the Medical Research Council for providing the generous funding for this research and Barts Cancer Institute for the provision of excellent facilities.

I would first like to thank Dr. Sarah McClelland for providing unparalleled support, supervision and opportunities throughout this PhD. Sincere thanks is extended to the members of the McClelland lab for frequent sanity-checks, encouragement and experimental teachings. Additionally, I cannot express enough gratitude and appreciation to everyone in the “kindergarten” PhD office for providing the backbone to my most joyous times and memories from BCI – no matter how cramped the desk space.

This PhD would have been an insurmountable academic and personal endeavour, had it not have been for the unwavering support of my family and friends, to whom I dedicate this thesis.

Table of contents

List of figures

List of tables

List of abbreviations

2D	two-dimensional
3D	three-dimensional
A	adenine
aCGH	array-based comparative genomic hybridisation
APC/C	anaphase-promoting complex/cyclosome
AML	acute myeloid leukaemia
ANOVA	analysis of variance
ATM	ataxia-telangiectasia mutated
ATP	adenosine triphosphate
bp	base pair
BSA	bovine serum albumin
C	cytosine
CO_2	carbon dioxide
CDK	cyclin-dependent kinase
CENP-A	centromere-associated protein A
CENP-B	centromere-associated protein B
CENP-C	centromere-associated protein C
CENP-E	centromere-associated protein E
CEP	centromere enumeration probe
CIN	chromosomal instability
CLIP	chromosome linkage inner nuclear membrane
CNA	copy number alteration
CRC	colorectal cancer
DAM	deoxyadenosine methyl
DAPI	4’,6-diamidino-2-phenylindole, dihydrochloride

dATP	deoxyadenine triphosphate
DDK	Drf1-dependent kinase
DCC	dosage compensation complex
dCTP	deoxycytosine triphosphate
dGTP	deoxyguanine triphosphate
DIG	digoxygenin
DMSO	dimethyl sulfoxide
DNA	deoxyribonucleic acid
DNMT	deoxyribonucleic acid methyltransferase
dNTP	deoxynucleotide triphosphate
dTTP	deoxythymine triphosphate
DSB	double-strand break
dsDNA	double-stranded deoxyribose nucleic acid
dsEGFP	destabilised enhanced green fluorescent protein
EDF	extended depth of field
EDTA	ethylenediaminetetraacetic acid
EGFP	enhanced green fluorescent protein
FACS	fluorescence-activated cell sorting
FBS	foetal bovine serum
FISH	fluorescence *in situ* hybridisation
FISH-IS	fluorescence *in situ* hybridisation in suspension
G	Giemsa
G	guanine
G_0	gap 0 phase
G_1	gap 1 phase
G_2	gap 2 phase
GFP	green fluorescent protein
H_2O	water

H2A	histone protein 2A
H2B	histone protein 2B
H3	histone protein family H3
H3K4me2	histone H3 dimethyl lysine-4
H3K4me3	histone H3 trimethyl lysine-4
H4	histone protein family H4
HDAC	histone deacetylase
HR	homologous recombination
INM	inner nuclear membrane
ISWI	imitation switch
Kb	kilobase
Kbp	kilobase pair
KT	kinetochore
LB	Luria-Bertani
LOR	late origin of replication
M	mitosis
Mb	megabase
Mbp	megabase pair
MAP	mitogen-activated protein
MCC	mitotic check-point complex
mRNA	messenger ribose nucleic acid
nm	nano meters
NEB	nuclear envelope break-down
NER	nucleotide excision repair
NDR	nucleosome-depleted region
NHEJ	non-homologous end joining
NPC	nuclear pore complex
NPS	nucleosome positioning sequence

OD	optical density
ORI	origin of replication
PBS	phosphate-buffered saline
PCR	polymerase chain reaction
PFA	paraformaldehyde
PLK	polo-like kinase
PS	phosphatidyl serine
PSCS	premature sister chromatid separation
R	replication
RC	replication complex
rDNA	ribosomal deoxyribose nucleic acid
RFP	red fluorescent protein
RMA	repeated measure assistance
RMS	root mean squared
RNA	ribonucleic acid
RNAi	ribonucleic acid interference
ROS	reactive oxygen species
rpm	revolutions per minute
rSAP	recombinant shrimp alkaline phosphatase
S-phase	synthesis phase
siRNA	small-interfering ribose nucleic acid
SNF	sucrose non-fermentable
SNP	single nucleotide polymorphism
ssDNA	single-stranded deoxyribose nucleic acid
SMC	structural maintenance of chromosomes
SSC	saline sodium citrate
STBR	spot-to-background ratio
SUMO	small ubiquitin-related modifier

SWI	switch
SWR	switch-related protein
T	thymine
TBE	tris borate ethylenediaminetetraacetic acid
TBP	transcription initiator binding protein
UV	ultraviolet

1. Introduction

Preface

The complement of genetic material in eukaryotic cells is usually diploid – possessing pairs of homologous chromosomes. The diploid state appears to be advantageous because it is permissive for the balanced genetic exchange which occurs during recombination in the gametes, thereby enabling sexual reproduction. Surprisingly, there are notable exceptions in which the diploid state is perturbed without catastrophic cellular consequences. Numerous plant species are tetraploid (containing a multiple of the diploid chromosome number) and many species of fungi are haploid (half the diploid chromosome number) for a majority of their life cycle. Additionally, there is the phenomenon of aneuploidy – the gain or loss of whole chromosomes – which usually has deleterious consequences on cell fitness but is surprisingly well-tolerated by cancer cells.

The large variety of chromosome states observed, even between cells from a single organism, is still poorly defined and mechanistically unclear. Moreover, stably-maintained aneuploidies for particular chromosomes are likely an interplay of both selection and recurrent chromosome missegregation. Both possibilities are contingent on subverting the mechanisms which act to maintain a stable chromosome number between generations. Aneuploid cells may therefore, in-effect, bypass or dysregulate a putative 'aneuploidy sensing' pathway which is as-yet undefined.

In this introductory chapter I describe the structure and function of chromosomes, drawing particular attention to their molecular regulation, organisation and segregation which impacts upon aneuploidy mechanisms and responses in eukaryotic cells, with emphasis on aneuploidy in tumourigenesis.

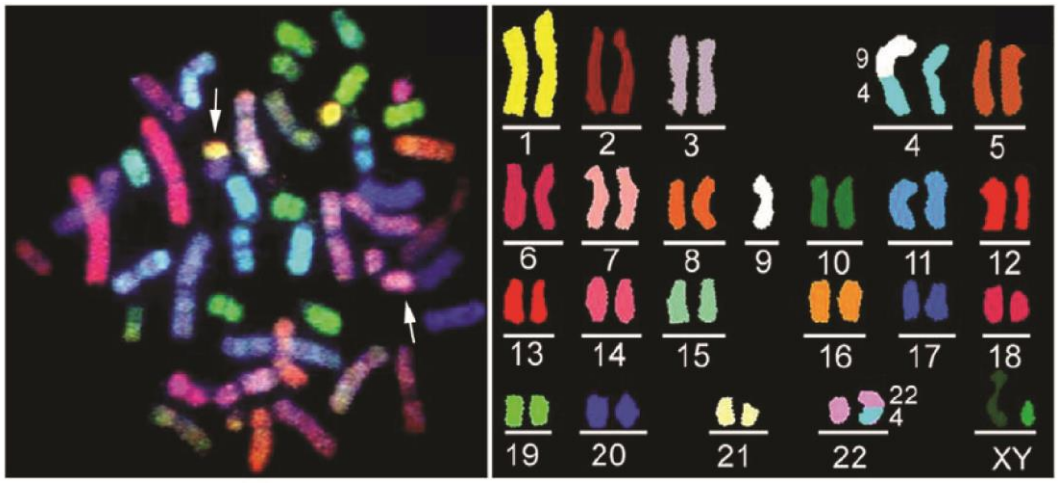

Figure 1.0. Spectral karyotyping of aneuploid cells. RGB display of hybridised metaphase spreads can be used to detect aberrant chromosome structure and number. Cancer cells often display recurrent patterns of aneuploidy and structural chromosomal instability. Arrows indicating chromosome translocations Figure adapted from[1].

1.1. Chromosomes

In eukaryotes, linear deoxyribonucleic acid (DNA) is tightly packaged into a higher-order structure known as chromatin, a DNA-protein composite containing histones and non-histone proteins. Hierarchical compaction of this nature allows a large amount of DNA to exist as discreet entities known as chromosomes which reside in the comparatively small volume of the nucleus of each cell[2]. Here I describe the molecular pathways concerning chromosome function, regulation and segregation during cell division.

1.1.1. Chromosome structure and function

The DNA comprising the human genome is divided unequally into 22 chromosome pairs, known as the autosomes, and two sex-determining chromosomes – XX in females and XY in males. The structure and organisation of chromosomes are governed by several requirements including gene expression control[3]. As such, human cells have evolved chromatin remodelling strategies that are capable of enormous plasticity under the control of complex, regulatory signalling networks[4].

Two structural features common to all chromosomes are the centromeric and telomeric regions, occurring at the central constriction and capping the ends of chromosomes, respectively. These regions contain highly-repetitive DNA sequences that serve several important functions. Although they are present in each chromosome, the length and position of these repetitive elements varies between chromosomes.

1.1.1.1. Chromatin architecture and remodelling

The basic repeating subunit of chromatin, known as the nucleosome, is highly conserved across species[5]. It is comprised of a 147bp segment of DNA wrapped around homodimers of each of the four histone proteins (H2A, H2B, H3 and H4) which assembles to form the histone octamer. The tight association between DNA and the octameric core afford protection from nuclease digestion and permit an initial compaction of linear genomic DNA of approximately 7-fold[6,7]. Nucleosomes serve to package the genome, but in doing so they also restrict the access of DNA-binding transcription factors, meaning there is a fine balance between DNA accessibility and packaging efficiency[8]. Gene expression in transcriptionally active areas of the genome is controlled by a number of regulators. Firstly, there is dynamic competition between transcription factors and nucleosomes for elements in gene promoters known as the *cis*-regulatory sequences[9]. Competition of this nature is regulated by enzymes known as 'chromatin modifiers' which covalently alter nucleosomes, and 'chromatin remodellers' which eject or reconfigure nucleosomes. Studies in yeast suggest that the chromatin architecture at promoters exists in two broad states – constitutive and highly regulated – with protein complexes for specific genes blurring the distinction in special cases[10,11].

Constitutive (open promoter) genes are spatially organised to allow the binding of transcription factors at the expense of nucleosomes, therefore promoting gene expression. The chromatin immediately upstream of the transcription start site of these genes typically contains a large nucleosome-depleted region (NDR) that is densely populated with poly(dA:dT) tracts[12–14]. These sequences are rigid in structure, thereby promoting nucleosome instability and inhibiting chromatin spooling[15]. Conversely, AA/TT dinucleotide repeats induce a chromatin curvature which promotes nucleosome assembly[16,17]. Regions of this nature which extend for more than 150bp are known as nucleosome positioning sequences (NPS). Notably,

transcriptional activator binding sites often reside in the NDR, increasing transcription factor binding efficiency and gene expression.

At regulated (closed promoter) genes, transcription factors compete with nucleosomes for occupancy of the *cis*-regulatory binding sites. These promoters are littered with NPS sequences of varying length, which dictate the nucleosome-transcription factor balance by altering the rigidity of promoter chromatin[18]. In most cases, there is at least one exposed binding site, between adjacent nucleosomes, on the linker DNA that permits a 'pioneer' access to the promoter which can then initiate chromatin remodelling in a controlled manner to expose further sites concealed by the nucleosome[19,20]. Transcription initiation can also vary between open and closed promoters. The transcription initiation binding protein (TBP) is an absolute requirement for TATA-less and TATA-containing promoters[21]. Whereas very few open genes contain TATA boxes, almost all closed promoters contain TATA boxes inside the proximal nucleosome edge, enhancing the requirement for chromatin remodelling and nucleosome displacement before TBP access and gene expression can occur[22].

The transition between chromatin states can also be achieved through the hydrolysis of adenosine triphosphate (ATP) by chromatin remodellers. These are specialised protein complexes that are classified by their mechanism of action. The imitation switch (ISWI) and sucrose non-fermentable (SNF) remodelling families assemble and organise chromatin by the deposition of nucleosomes[23]; the SWI/SNF family facilitate nucleosome ejection or movement, and the SWR1 family insert specialised histones into nucleosomes for reconstruction[24,25]. By cooperating the expression and localisation of remodelling complexes with environmental changes, chromatin architecture around promoters controls the expression of target genes with high temporal precision.

1.1.1.2. Centromeres

The repetitive sequence which specifies the centromere, known as α-satellite DNA, is organised into functional subdomains and is flanked by regions of heterochromatin. The centromere serves as more than a junction point between the two chromatid arms – it also coordinates the movement of chromosomes during mitosis and meiosis, regulates sister chromatid cohesion and helps synchronise chromatin condensation[26,27]. Most of the available data concerning centromere function describe its important role in mitosis, where it serves as the assembly site for microtubules through its interaction with a multi-protein complex, known as the kinetochore[28].

The centromeric α-satellite DNA is host to a specialised histone H3 variant, CENP-A, which is important, but not essential for, kinetochore assembly on the centromere (**figure 1.1a**)[29]. It has been shown that the octamer of histone proteins that form the nucleosome can assemble *in vitro* with purified CENP-A, suggesting that CENP-A is sufficient to replace endogenous H3 dimers at centromeric regions[30]. Unlike other histone proteins which are removed and reincorporated into chromatin during early S-phase, CENP-A nucleosomes are inherited in a semi-conservative manner with nascent-synthesised CENP-A loading occurring at the centromere during G_1[31]. This explains how CENP-A specificition at α-satellite DNA is faithfully maintained between generations[32,33]. It is now known that CENP-A does not completely replace histone H3 at centromeric sequences. Instead, H3-containing nucleosomes are interspersed with CENP-A-containing nucleosomes. These H3 histones are tagged with a dimethyl modification on lysine 4 (H3K4me2) which is essential for the specification and maintenance of CENP-A at centromeres. Interestingly, it has been shown that CENP-A contributes to the rigidity of the centromere through its interaction with H4, which is less flexible than the common H3-H4 interaction,

thereby providing a stable platform for downstream assembly of kinetochore components[34].

Centromeres are also distinguished from the rest of the genome by higher-order packaging. This relies on two other members of the CENP family – CENP-B and CENP-C. Targeting of CENP-B to the centromere is achieved through its interaction with the CENP-B protein binding motifs, the CENP-B boxes, which are deposited at alternating 171bp monomers (**figure 1.1b**)[35]. Functionally, this allows dimerization of conserved domains on adjacent CENP-B proteins so that the CENP-B boxes are brought in close proximity[36]. This looping of α-satellite DNA induces non-random phasing of CENP-A nucleosomes throughout the centromere[37]. Likewise, CENP-C has several targeting domains specifying it to centromeric DNA, where it is important for the dimerization of CENP-B and promoting other protein-protein interactions. During mitosis, CENP-C functions as a scaffolding protein, remodelling the centromeric architecture to create a chromatin environment which is permissive for the assembly of the inner kinetochore at metaphase[38].

Given that most centromeres are flanked by heterochromatin – transcriptionally silenced regions of the genome characterised by dense histone methylation – it is likely that the epigenetic environment surrounding the centromere plays an important role in either specifying the centromere, or aiding its function[39]. More recently, it has been suggested that heterochromatin might be important to limit kinetochore assembly to centromeric DNA[40]. Experimentally, this has been shown by heterochromatin restriction of CENP-A to the centromere, even in conditions when CENP-A is overexpressed[41]. Conversely, the removal of pericentromeric heterochromatin is permissive for the spread of CENP-A into flanking sequences, which may impact on kinetochore assembly and, therefore, chromosome segregation[42].

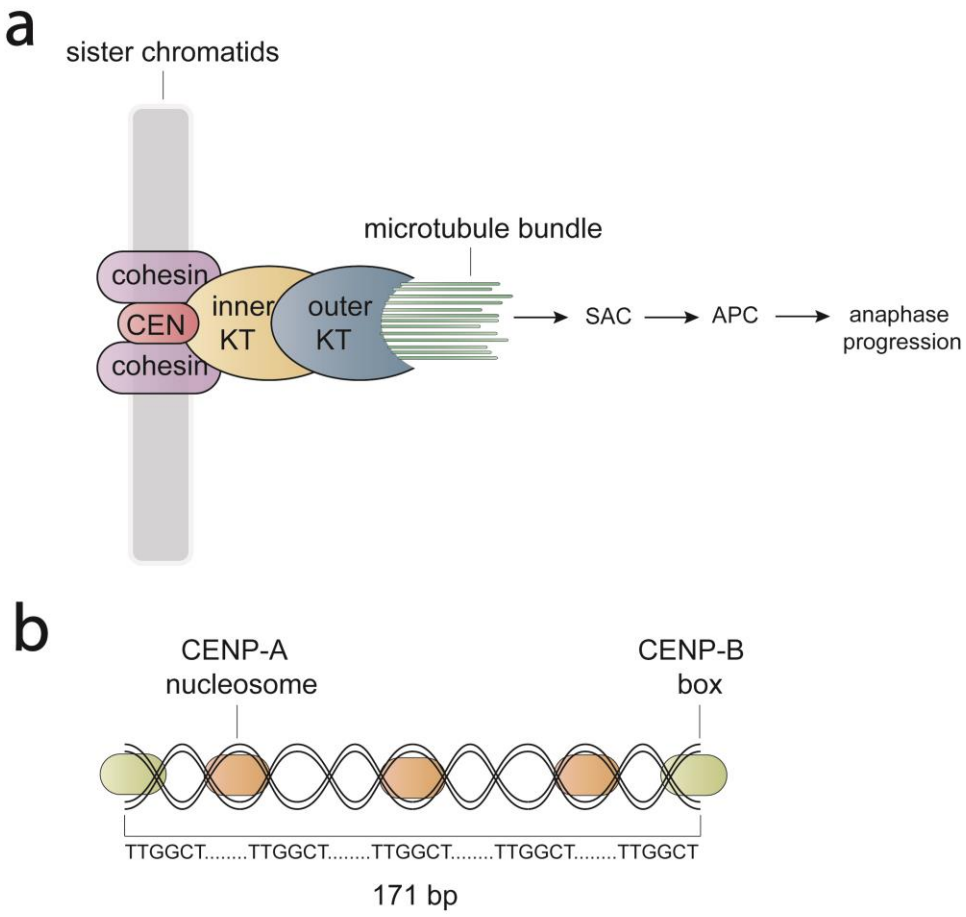

Figure 1.1. The structure and function of the centromere. (a) The inner and outer kinetochore (KT) components assemble on the repetitive α-satellite DNA of the centromere (CEN). (b) A specialised histone H3 variant, CENP-A, is incorporated into centromeric nucleosomes and facilitates kinetochore assembly in collaboration with CENP-B at CENP-B boxes.

1.1.1.3. Telomeres

As the name suggests – from the Greek nouns telos ('end') and meros ('part') – telomeres are found at the extremities of each chromosome arm. Much like centromeres, telomeres are specialised chromatin environments consisting of repetitive DNA sequences which are essential for chromosome function. Without telomeres, each round of genome duplication would lead to progressive chromosome attrition. Of equal importance is their ability to mask the ends of chromosomes which would otherwise be recognised as DNA breaks leading to cell-cycle arrest[43].

Human telomeres are characterised by multiple tandem repeats of the sequence TTAGGG proceeded by G-rich single-stranded overhangs at the 3' terminus. Telomeric DNA adopts an unusual conformation known as 'T-loop' where the telomeric ends fold back and invade the adjacent double-stranded DNA (dsDNA)[44]. These repeat regions are generated and maintained by a specialised reverse transcriptase, known as telomerase, which is unusual in that it carries its own RNA template.

The precise molecular mechanisms which recruit telomerase to the telomeres are still unclear; however it is known that Cdc13, a G-rich-specific DNA-binding protein which is necessary to protect telomeres against double-strand breaks (DSBs), is involved in telomerase recruitment[45–47]. These G-rich overhangs are also able to quadruplex with themselves, by virtue of the fact that each base serves as both an acceptor and donor for hydrogen bonds. This quaternary structure limits telomerase activity (preventing promiscuous telomere extension), suppresses recombination events and acts to protect the chromosome ends from exogenous DNA damage[47]. It has been shown that the length of the 3' G-overhang is essential for telomerase regulation and end processing, with the shortest telomeres eliciting the strongest telomerase recruitment at S-phase[48–50].

The transition between the repetitive regions of telomeres to transcriptionally-active euchromatin is not abrupt. Instead most, but not all, telomeres are underpinned by a dynamic and variable region known as the subtelomere, which may traverse up to 300kb[51,52]. The precise evolutionary origin of subtelomeric regions are unknown, but are likely to have arisen by many translocation and recombination events.

Functionally, subtelomeres may provide enhanced protection for telomeres; however it has recently been demonstrated that they are also able to rescue genes located at the ends of chromosomes from telomeric methylation, which would otherwise disrupt their expression[53,54]. Additionally, subtelomeres play an important role in meiosis, where they inhibit crossover events. This is important as it has been shown that meiotic recombination events near the ends of chromosomes could impair proper chromosome segregation[55].

1.1.2. The nuclear organisation of chromosomes

The nucleus is an organelle which is spatially separated from the cytoplasm by two membrane bilayers – the outer nuclear membrane and the inner nuclear membrane. The non-random arrangement of chromosome within the nucleus is important for many of their functions including transcriptional regulation, DNA stability and chromosome segregation during mitosis.

1.1.2.1. Radial chromosome positioning

Individual chromosomes can be stained with fluorescent probes by Fluorescence *in situ* Hybridisation (FISH). This technique revolutionised my understanding of the spatial organisation of DNA, as it allowed the sub-nuclear location of genetic loci to be mapped along an axis extending from the nuclear core to the inner nuclear membrane[56,57]. By mapping the radial positions of chromosomes, it is now known that many cell types have a preference for gene-dense chromosomes locating in the nuclear core and gene-poor chromosomes occupying the nuclear periphery; this is known to be conserved among primates and a similar phenomenon for chromosome size has been reported (**figure 1.2**)[57–59]. Confusingly, despite this general density phenomenon, there is little evidence that each chromosome has a defined '3D neighbourhood' of chromosome with which it resides[60].

The mobility of chromatin in the interphase nucleus is limited[61–63]. This has important implications for human disease, as the proximity of chromosomes becomes the limiting factor for the variety of chromosome translocations which can occur; only chromosomes which are sufficiently close may exchange genetic material by double-strand break repair[64]. This has been shown in both mouse and human lymphocytes[65]. It has also been reported that reciprocal translocations involving chromosomes with stochastic arrangements can disrupt nuclear organisation. This is most pronounced in the example of the recurrent t(11;22)(q23;q11) translocation

where chromosome 22, usually positioned in the nuclear core, is shifted towards the periphery when chromosome 11 is located more centrally than expected[56]. The radial positioning of chromosomes, given the consequences for translocations and other structural DNA aberrations, may have important implications for chromosome evolution[66].

Each chromosome, regardless of its position in the nucleus, occupies a well-defined territory[67]. At the boundary between adjacent territories, there are regions where chromatin is able to loop into the no-mans-land and form *cis* and *trans* associations between chromosomes[68]. Interestingly, it has been shown that the centromere is important for attenuating the association of looped sequences present on opposite arms of the same chromosome, preventing intra-chromosome translocations, although the mechanistic basis for this is still unclear[69]. Functionally, the looping of DNA may aid transcription of these regions. Recent data suggest that most of these looping regions are gene-dense and hyper-sensitive to DNase I treatment, indicative of highly-active promoter regulatory elements[70]. It has also been suggested that DNA looping may allow actively-expressed regions of the genome to explore a larger nuclear space, which is thought to be important for certain mRNA splicing events[71].

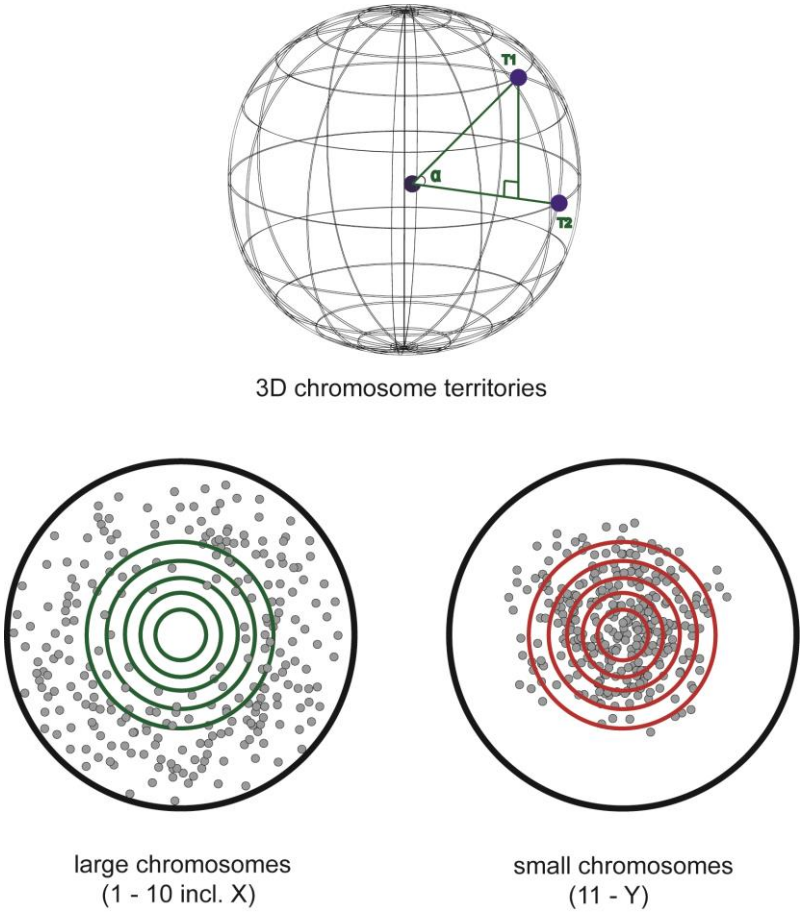

Figure 1.2. The radial positioning of chromosomes. Human chromosomes can be mapped radially within a nuclear sphere. Larger, gene-sparse chromosomes reside at the nuclear periphery while smaller, gene-dense chromosomes occupy the nuclear core (illustrative data points). Chromosomes occupy distinct territories which are clustered into neighbourhoods, defined radially by $[T_1T_2 \sin \alpha]$. Adapted from[59].

1.1.2.3. Chromatin domains

Within each chromosome territory, there is further clustering of active and inactive gene regions, known as chromatin domains[72]. The interaction of inactive domains occurs in two broad categories – centromere proximal and centromere distal – which is likely to reflect their reduced freedom of movement and are usually found within their own chromosome territory[73]. Conversely, active regions are able to associate over long distances, which may reflect their requirement to cluster around shared gene splicing machinery. Local chromatin domains form unique structures which correspond with replication timing during S-phase. Regions of the genome with active genes, the 'replication (R) bands', are known as early replicating and inactive genomic regions, the 'Giemsa (G)-bands', are late-replicating[74]. It has also been shown that late-replicating domains tend to cluster at the nuclear periphery and that replication timing can significantly affect chromosome translocations[75]. This is important as it suggests that aberrant S-phase execution may predispose to the structural rearrangement of chromosomes.

1.1.2.4. Nuclear membrane-associated chromatin

The inner nuclear membrane (INM), aside from being the physical boundary of the nucleoplasm, is important for cooperating gene expression, genome stability and initiating DNA repair[76]. The INM is traversed by filamentous lamin proteins and nuclear pore complexes which interact with perinuclear chromatin and play an important role in maintaining the structural and functional integrity of the genome[77].

It is now possible to detect loci which interact with the INM by fusing DAM methyltransferases to INM proteins and identifying *de novo* DNA methylation by sequencing[78]. Using this approach, it is now known that transcriptionally silent chromatin regions associate with perinuclear membrane proteins in both humans and flies[79]. Interestingly, treatment with histone deacetylases causes the release of

lamin-associated sequences from lamins, suggesting that gene silencing by methylation is sufficient to promote association with the nuclear membrane[79]. This further supports the view that heterochromatic regions of the genome preferentially occupy the nuclear periphery[80]. It is important to highlight that the nuclear periphery is not always associated with gene silencing. It has been shown in yeast that genes associated with nuclear pore complexes (NPCs) can promote transcription, and that treatment with histone deacetylases inhibitors can promote the reactivation of silent chromatin to active domains at the NPC[81,82]. The precise mechanisms governing expression at the nuclear periphery are blurred further by activation, or silencing, of some genes at the INM in a regulatory element-dependent nature. These data highlight the complex interplay between perinuclear compartments, genetic elements and the nuclear envelope.

In yeast cells, the nucleolus is comprised largely of repetitive ribosomal DNA (rDNA), abuts the inner nuclear membrane and is prone to homologous recombination events, which cause genomic instability[83]. Affinity purification and proteomic analyse have revealed two key proteins, Heh1 and Nur1, which form the CLIP (chromosome linkage INM proteins) complex which bridges the rDNA repeats to the INM. It has recently been shown that disruption of the CLIP complex releases rDNA repeats from the nuclear membrane leading to recombination events and the accumulation of genetic lesions – a phenotype which was rescued by reintroducing artificial tethering to the INM[84,85].

Additionally, it is known that other repetitive sequences can associate with perinuclear proteins – one of which is telomeres. Early work identified at least one protein, Mps3, which is able to promote clustering of the 32 yeast telomeres into 4-8 foci at the nuclear envelope[86]. This discovery led to the study of INM chromatin silencing at telomeres and it was shown that several telomere-binding proteins are important for perinuclear anchoring[87]. More recently, it has been shown that Mps3-

dependent telomere clustering is important to sequester transcription inhibitors which can otherwise erroneously silence non-subtelomeric genes[88].

Surprisingly, DNA insulted with double-strand breaks (DSBs) is actively relocated to the nuclear membrane, where it interacts with nuclear pore complexes[89]. This recruitment to the INM is dependent on Mec1, a kinase that delays cell-cycle progression in response to DSBs. Importantly, damaged loci do not cluster with telomeric attachment sites, and damaged telomeric sequences promote co-localisation of telomeres with the NPC, suggesting that damaged DNA may be targeted to the NPC regardless of its nuclear envelope attachment status. The role of NPCs and lamins in genome stability and maintenance of chromatin organisation is reinforced by a number of important studies. For example, mutations in lamin proteins are linked with chromatin architecture abnormalities and loss of nuclear structural integrity; and lamins have also been linked to transcriptional regulation by modulating the availability of transcription factors at the nuclear envelope[90,91].

It is possible that the inner nuclear membrane helps stabilise DNA by acting as a large support platform enabling cells to control the distribution of repetitive loci relative to each other. The INM may also limit long-range recombination events between susceptible loci, by keeping sister chromatids spatially separated during S-phase. The clustering of repetitive domains at the nuclear periphery may also permit genetic co-regulation, which can promote beneficial recombination diversity under stress. Together, the above data demonstrate that the nuclear periphery is an important organisational region, where transmembrane proteins act to minimise DNA damage and as tethers for chromosomal domains.

1.1.3. Mitotic chromosome assembly

Profound changes in chromatin structure occur during mitosis, when the duplicated genome is equally partitioned into two daughter cells. Disassembly of the nuclear envelope, at mitotic onset, occurs concurrently with the rearrangement of an amorphous chromatin mass, resolving as sister chromatid pairs which line up on the equatorial spindle. This sequence of carefully-coordinated events is known as chromosome condensation, or assembly, and is an absolute requirement for the faithful segregation of genetic material[92,93].

1.1.3.1. The structure and composition of SMC complexes

Mechanisms of chromosome condensation, DNA repair and sister chromatid cohesion rely on a families of proteins known as the structural maintenance of chromosomes (SMC) complexes. These essential genomic functions are carried out by the three SMC complexes: condensin, Smc5/6 and cohesin[94]. These complexes assemble around heterodimers of SMC proteins (named SMC1-5), which are obligatory for DNA binding activity and the hydrolysis of ATP.

Smc1 and Smc3 create a ring-like structure, which is important for entrapping sister chromatids until proteolytic cleavage of Ssc1 at anaphase onset[95,96]. The entrapment of DNA is also known to hold condensins in close association with their target site. However, whereas cohesion is bound at physiological ionic strength, the interaction of condensins has been shown to dissociate only at high salt concentrations, suggesting that condensins are also able to bind DNA directly[97]. It is currently unknown whether Smc5/6 is able to bind DNA directly, or if it forms a similar ring-like structure. Given the structural similarity with condensins and cohesin, this seems entirely plausible.

1.1.3.2. Condensins

The primary function of condensins is to establish proper mitotic chromosome structure and promote faithful chromosome segregation during meiosis and mitosis. There are two condensin complexes, referred to as condensin I and condensin II, that share two core subunits, which are independently coordinated by distinct regulatory subunits. The two core protein subunits belong to a larger family of ATPases called the structural maintenance of chromosomes complex. Condensins are able to hydrolyse ATP to promote both superhelical rigidity and DNA compaction[98,99]. Despite data suggesting that condensins are crucial for chromosome assembly, there is an abundance of conflicting literature on their precise mechanism of action.

The earliest stages of chromosome condensation are characterised by the hierarchical supercoiling of chromatin fibres. One of the SMC subunit of condensins, Smc2, first associates with chromatin fibres at the periphery of the nucleus and subsequently accumulates at prometaphase along the central axis of each chromosome. Importantly, NEBD is coincident with the relocalisation of Smc2 and condensin I recruitment to chromatin arms, suggesting that chromosome structural changes observed before and after NEBD may be mechanistically distinct. More recently, it has been suggested that topoisomerase II is important for the axial formation of chromosome arms and recruitment of condensin I subunits; however this cannot explain the activities of condensin II[100].

Chromosome bridges, DNA spanning between dividing chromosome masses at anaphase, are one of the most prominent segregation defects observed in condensin-deficient cells[101–103]. Segregation defects of this kind are thought to be linked to improper chromosome condensation in the preceding metaphase. Condensin depletion in human cells and Xenopus embryos has been shown to increase the formation of merotelic chromosome attachments, single kinetochores

attached to microtubules emanating from both spindle poles, raising the possibility that condensins are also important for bipolar orientation of chromosomes[104]. Chromosome assembly defects have also been observed in condensin-depleted *C. elegans* models. Unlike vertebrate chromosomes which have one kinetochore per sister chromatid, *C. elegans* have many kinetochores which assemble along the length of each sister chromatid pair, known as holocentric chromosomes[105,106].

1.1.3.3. Sister chromatid cohesion

The dissolution of sister chromatid cohesion is coordinated in a two-step process. The first, occurring during prophase, does not affect centromeric cohesion, which gives mitotic chromosomes their single constriction[107,108]. The activity of separase at the onset of anaphase is responsible for the cleavage of the SMC protein Scc1, triggering disjunction of sister chromatids[109,110]. Cohesin exists as different populations which are loaded onto chromatin at various stages of the cell cycle. In human cells, >90 % the cohesin bound on chromosomes becomes dissociated during early prophase, leading to soluble mitotic cohesin complexes in the cytoplasm which are spared separase cleavage[111]. Cohesin subunits tagged with a green fluorescence protein (GFP) suggests that the residence time of some chromosomal cohesin is shorter than 25 minutes, in both G_1 and G_2 cells[112]. However, a distinct population engages with chromatin for significantly longer and may represent the pool responsible for holding sister chromatids together[113].

The loading of cohesin onto chromatin requires ATP hydrolysis at all stages and is facilitated by the ATPase domain of Smc1 and Smc3 of the cohesin complex. This was first shown using mutated Smc1 and Smc3 proteins which could bind, but not hydrolyse, ATP which were able to form cohesin ring-like structures but failed to stably associate with DNA[114,115]. The DNA binding capacity of cohesin varies at different parts of the genome, with some requiring the presence of additional factors or proteins before a stable association can be formed. At every known site, the

Ssc2/4 complex is essential for binding in mammals, Xenopus and yeast[116–119]. Unsurprisingly, defects in either Ssc2 or Ssc4 precipitate as global failure of sister chromatid cohesion[120]. It is unlikely that Ssc2/4 functions solely in cohesin loading, given that *ssc2* mutation is also known to compromise Smc5/6 onto chromatin concurrently with defects in condensin[121,122].

Chromatin association of cohesin in Xenopus requires, in addition to Ssc2/4, the formation of the pre-replication complex (RC)[123]. Purified extracts from Xenopus larvae display associations between Ssc2/4 and Cdc7/Drf1-dependent kinase (DDK), which is an essential member of the pre-RC[124]. The sequential binding of various cofactors in this assembly have revealed the possibility that Ssc2/4-DDK may act prior to DNA replication, suggesting that Ssc2/4's functions include chromatin fibre trapping in addition to cohesin recruitment to chromatin.

The two phase process of cohesin removal from sister chromatids is under tight temporal control. Unlike the metaphase-to-anaphase transition, in which the separase-mediated cleavage is well characterised, the prophase pathway of cohesin dissolution is separase-independent and has yet to be fully elucidated. It is known that, during the prophase pathway, moderate dissociation is mediated by polo-like kinase (PLK) and Aurora B phosphorylation on the C-terminal domains of Scc3[125]. Given that cohesin removal can still occur in the absence of these proteins, they are unlikely to be requisite. Recent data suggests that the master regulator of prophase cohesin removal is Wapl, a protein which binds to the SMC scaffolding subunit Pds5. This was demonstrated in Wapl-depleted cells, resulting in the majority of cohesin remaining on chromatin arms[126,127]. The prophase pathway removes most, but not all, chromatin-bound cohesin. Centromeric cohesin is protected from this pathway because of a centromere-specific Sgo1[128,129].

The metaphase-to-anaphase transition is characterised by separase cleavage of Ssc1, the α-kleisin subunit of the cohesin complex[96]. A non-cleavable mutant Ssc1

in HeLa cells disrupts sister chromatid disjunction and blocks Rec8's removal from bivalent chromosomes[110]. The activity of separase is further regulated, in a cell-cycle-dependent manner, by the chaperone protein inhibitor, securin[130]. The phosphorylation of separase by Cdk1 on serine 1121 promotes the stable interaction with cyclin-B/Cdk1, rendering the protease domain catalytically null[131]. This function is of paramount importance, especially in pre-implantation mouse embryos and primordial germ cells, where securin levels are known to be lower than in other cell types[132,133].

Crucially, the activity of separase is prevented until all sister chromatid pairs are bioriented. Once all kinetochores are attached to microtubules the APC/C ubiquitinates securin and cyclin B, leading to their proteolysis [134]. This signalling cascades culminates with the cleavage of Ssc1 subunit of cohesin complexes at centromeric DNA, triggering sister chromatid disjunction[110].

An important emerging role for cohesin is in double-strand break repair in meiotic and mitotic cells[122,135]. Two distinct cohesin population engage in repairing DSBs in mitotic cells – cohesin recruited to the break point and cohesin already holding sister chromatids together when the break occurred[136,137]. Cohesin in meiotic cells is involved in generating reciprocal translocation events by DSB repair and generates the chiasmata, which secures bivalent chromosomes to each other until meiosis I[138]. It is known from yeast studies that the α-kleisin subunits Ssc1 and Rad21 present in mitosis are replaced by Rec8, which is specific to the meiotic cohesin complex[139]. Functionally, this may permit the repairing of DSBs by non-sister chromatid recombination and therefore promote genetic diversity. Human cells also swap these subunits for meiotic-specific variants, namely STAG3 replacing Scc3 and Smc1B (replacing Smc1), which are important for generating heterogeneity during oogenesis and spermatogenesis.

1.2. Mechanisms driving aneuploidy

1.2.1. DNA damage

The DNA of human cells is under continual assault by a barrage of exogenous DNA damage-inducing agents and cellular metabolites. These insults may alter the primary nucleotide sequence, which is a leading cause of many of human diseases. Unperturbed cells have the capacity to sense errors arising from DNA damage and have evolved regulatory networks which correct damage below a threshold, removing cells with damage which cannot be corrected by programmed cell death[140,141]. Aneuploid cells often display high rates of protein mis-folding due to protein stoichiometry imbalances[142,143]. It is also known that DNA damage is a major driver of chromosome instability and cause of aneuploidy[144–147]. This section describes the foundations of DNA damage phenotypes with examples of perturbations which give rise to aneuploid progeny.

1.2.1.1. DNA damage repair

Repair pathways which maintain the integrity of DNA are broadly divided into sub-categories, depending on their mechanism of action: base excision repair, nucleotide excision repair, double-strand break repair, direct repair and repair of cross-linked DNA.

The repair of DNA by base excision is initiated by the removal of the base by a DNA glycosylase to form an abasic site. This class of glycosylase enzymes are capable of recognising a wide range of aberrant nucleotides including deaminated, oxidised, reduced, alkylated and mismatched bases. In most cases, the removal of the base occurs by a process known as the abasic lyase reaction in which the 1'-aldehyde from the deoxyribose is reduced by a β-elimination reaction, leaving the 3'-sugar phosphate residue unsaturated[148]. This is proceeded by removal of the sugar 5' to the abasic site and the gap is filled by DNA polymerase and subsequently nick

ligated[149]. In human cells, this process is known simply as the short-patch base excision repair as the reaction only involves three enzymes: APE1, DNA ligase III and DNA Polβ. Glycosylases use simple diffusion and Brownian motion to detect distortions created by the formation of hydrogen bonds in the DNA backbone caused by base damage[150]. Careful analysis of their crystal structure has revealed that some glycosylases compress DNA helices on either side of the damaged base, which permits rotational movement, thereby exposing the glycosylic bond which can be hydrolysed by specialised domains[151]. These act as a proof-reading mechanism to ensure base repair specificity. The dysregulation of Polβ is a frequent occurrence in human cancers.

Of particular interest is the centrosome-associated abnormal localisation of gamma-tubulin during mitosis in nude mice with aberrant Polβ expression. These changes were shown to promote numerical aneuploidy and increase malignancy aggression, possibly as a result of mitotic checkpoint deficiency[152]. Therefore, it is likely that defects in base excision repair could manifest as stochastic errors which promote chromosomal instability (CIN) and tumour progression.

Lesions formed on DNA after exposure to chemicals, irradiation or proteins cross-linked to DNA are repaired by the process of nucleotide excision repair (NER). Insults of this nature are repaired by the enzymatic removal of the offending base by multi-protein complexes which envelope the damaged strand[153]. Excision repair is known to recognise a wide range of substrates; consequently, it is thought that rather than identifying chemical variation in the lesions, it is structural changes in the phosphodiester backbone which are the point of engagement[153].

Once identified, lesions are subject to incision and removal of an oligomer of 24-32nt in length, which can be filled in by template-strand complementarity. An assembly of 6 repair factors form a multi-protein complex responsible for all the activity associated with NER[154]. In humans, it is the nuclease activity of XPC, XPA

and RPA which confer the initial DNA binding specificity, although there is still some uncertainty over their preferences for damaged DNA. It was demonstrated that these three nucleases have different DNA binding affinities and are present in different abundances[154]. It is likely that a combination of all of these play an important role in the final excision nuclease complex assembly. DNA unwinding and kinetic proofreading during NER is devolved to a specialised protein complex, the TFIIH, consisting of 6 subunits with both 3'-5' and 5'-3' helicase activity[154]. The helicase subunit unwinds DNA 20bp downstream of the assembly site; if this happens to be a non-damaged site then disassembly of the complex is promoted by hydrolysis of ATP.

Conversely, sites of DNA damage provide a high-affinity binding site for other subunits which recruit the nuclease domains in to contact with the damaged nucleotide[155]. Excision, polymerase activity and nick ligation complete the nucleotide replacement. Of interest, the proof-reading activity of TFIIH to detect only damaged nucleotides is not absolute, and gratuitous repair of undamaged bases does occur in human cells and may be mutagenic[156].

In yeast models it has been shown that NER is a requirement for faithful chromosome disjunction. In the absence of the repair factors, Rad1, Rad2 and Rad4, there was a significantly elevated rate of spontaneous gain of chromosome XV in both diploid and haploid mutant strains[157]. Emerging data also suggest that the nuclease activity of XPA is required for the maintenance of proper centrosome number (2 centrosomes per cell) [188]. This *in vitro* work has shown that the loss of *Xpa* is associated with centrosome amplification and micronuclei formation. Interestingly, the concurrent loss of p53 showed a more severe phenotype than haploinsufficiency of either alone, suggesting that there is cross-talk between NER and p53 pathways to supress chromosomal instability in response to DNA damage.

Double-stranded DNA breaks are unusual in that they occur by exogenous damage, by ionising radiation and ROS, but also occur naturally as a mechanism for generating genetic variation (such as in V[D]J recombination) and meiotic cross-over events[158–160]. DSBs are repaired by either homologous recombination (HR) or non-homologous end-joining (NHEJ). The process of HR is a multi-step process which requires the damaged strand to invade its homologous template, mediated by Rad51, BRCA1 and BRCA2[161]. The resulting structure, known as a Holliday junction, is resolved in such a way that the 'lost base' information is retrieved from the homologous duplex. NHEJ involves the heterodimer of Ku proteins which recruit ligase4-XRCC4, ligating two ends of a double strand break irrespective of whether the arms are from the same chromosome[162].

Defective HR pathways are prevalent in a number of cancers with heterogeneous chromosome content. These are typified by BRCA1 and BRCA2-deficient breast cancers. The loss of either of these genes is coincident with loss of genome stability[163]. This is most likely due to defects in HR-mediated repair which gives rise to cells with translocations and large-region deletions. Additionally, BRCA1/2 act in a tumour-suppressive manner as they regulate the cell cycle by signalling to checkpoint complexes[164]. It is by these mechanisms that BRCA1/2 likely act to simultaneously supress tumour initiation and maintain genome stability.

A number of anti-cancer drugs cause cell death by inducing the formation of inter-strand DNA cross-links. During replication, cross-linked DNA impairs polymerase activity and leads to the formation of DSBs both *in vivo* and *in vitro* as a result of replication fork collapse[165]. At replication-induced DSBs there is nuclease digestion which degrades the cross-link in a 3' to 5' direction. The combined actions of Rad51 and Rad52 with RPA form a Holliday junction which can then be resolved by homologous recombination[166].

1.2.1.2. Cell cycle checkpoints

The eukaryotic cell cycle is characterised by four distinct phases: G_1, S, G_2 and M. Transition between these states is carefully controlled to ensure that deleterious events in one stage are not left uncorrected before the next stage commences[167]. Human cells possess many inter-connected pathways, known as checkpoints, which inspect the integrity of DNA before permitting the cell to proceed to the next phase of the cell cycle (**figure 1.3**)[168]. The term 'checkpoint' has been expanded to include the execution of more ambiguous responses such as apoptosis, DNA repair and arrest of cell-cycle progression as a general phenomenon, independent of DNA damage. For this reason, I reserve the use of 'DNA-damage checkpoint' exclusively for signalling cascades which arrest, or slow, the cell cycle as a direct result of DNA damage. In this context, checkpoints which monitor DNA damage are not uniquely activated by such an event. Rather, they are continually operative pathways whose members are upregulated during a damage response.

In most human cancers, aneuploid cells are often deficient in proteins which execute various stages of the cell cycle checkpoints[169–172]. Often, multiple key checkpoint proteins are mutated in a single cell, allowing the uncontrolled proliferation of aneuploid cells with accumulating DNA damage and increased karyotypic complexity. The underlying cause of this chromosomal instability (CIN) phenotype is complex, but some studies suggest that the primary cause is due to improper mitotic checkpoint signalling, allowing cells to proceed to anaphase with misaligned chromosomes[173].

The G_1/S checkpoint, also known as the restriction point in human cells, prevents entry into S-phase in response to DNA damage by preventing the initiation of replication. Ionising radiation leading to double-strand breaks activates ATM which phosphorylates Chk2 and p53. Chk2 initiates Cdc25a degradation or exclusion from the nucleus resulting in p-Chk2 (inactive) accumulation, thereby preventing Cdc45

phosphorylation and hence preventing replication initiation[174,175]. UV light, and UV-mimetic compounds, cause DNA damage which is recognised by ATR, leading to Chk1 and Cdc25 phosphorylation-mediated arrest in G_1. Regardless of which pathway initiates the arrest, p53 is crucial for the maintenance of the G_1/S arrest which occurs several hours after DNA damage detection[175]. During this period, p53 becomes phosphorylated on ser15 and ser20, by Chk2 and Chk1 respectively, preventing its export from the nucleus and activating target genes including p21 (inhibiting Cdk2-cyclin E S-phase progression)[176,177]. Inhibition of transition to S-phase is also prevented by p21 binding to Cdk4-cyclin D, preventing Rb phosphorylation which in turn inhibits E2F transcription factor-activation of S-phase genes[178].

Importantly, the G_1/S checkpoint is activated precipitously in response to excision repair processing cascades. In yeast, this has been shown in cells which are deficient in excision repair exhibiting no S-phase entry delay following UV radiation[178]. Interestingly, checkpoint activation occurs in these cells once they are in S-phase, perhaps as a result of UV-induced photoproducts causing replication blockade. The G_1/S checkpoint is therefore critical for limiting the proliferation of aneuploid cells.

The main signal transducers which promote this response are ATM and p53 – ATM activates p53 leading to cell-cycle arrest and subsequently p53-mediated apoptosis. This has been validated *in vivo* with p53 and ataxia-telangiectasia mutated kinase (ATM) -null mice which develop thymic lymphomas with high levels of aneuploidy[179]. Importantly these tumours exhibited elevated ROS, characteristic of aneuploid cells. In these cells, ROS-induced oxidative DNA damage is thought to contribute to the activation of ATM which prompted the speculation of an 'aneuploidy checkpoint'[180]. It is known that p53 is one of the most commonly mutated genes in cancer, with $p53^{-/-}$ tumours exhibiting high levels of aneuploidy and chromosomal instability[181]. It is

still controversial whether p53 loss is required for the proliferation of aneuploid cells. For example, in aneuploid embryonic kidney cells, many rounds of cell division occur before embryonic lethality despite wild-type p53 and some tumours exhibit aneuploidy before p53 loss[182]. It is possible that these tumours have impaired signalling either upstream or downstream of p53 which may impair the G_1/S checkpoint. This is seen is some tumours where overexpression of MDM2 (a p53 antagonist) or down-regulation of p53 activators (such as the hyper-methylation of the $p14^{ARF}$ promoter) proceeds tumourigenesis[183].

Damage which is left unrepaired and manages to evade the G_1/S checkpoint, or encountered during S-phase, leads to activation of the S-phase checkpoint[184]. The mechanisms underlying this checkpoint are still not fully resolved, however it is known that ubiquitinylation or sequestration (by p21) of PCNA may significantly slow the speed of replication fork progression[185]. The main body of data so far suggests that the predominant mechanism of the S-phase checkpoint is late origin of replication (LOR) firing suppression[186]. Unsurprisingly for such an essential checkpoint, it involves the cooperation of a large number of sensor and effector proteins.

When the insult is a double-strand break, BRCA1 and ATM initiate a kinase signal cascade which can proceed by either of two mechanisms – the classical ATM-Chk2 described above, and the phosphorylation of SMC1[187,188]. DNA insults by UV radiation activate the ATR-ATRIP heterodimer. Functionally, ATR is able to bind to RPA-coated single-stranded DNA, UV-induced lesions and directly to chromatin[189,190]. Recent data from work in Xenopus egg extracts has shown that Cdc7-Dbf4 kinase activity, required for Cdc25a licensing on to DNA, is downregulated following Chk1 phosphorylation by ATR[191].

Similarly to the ATM pathway, the ATR pathway is also able to promote replication fork recovery after DNA correction mechanisms by phospho-activation of BRCA1.

Work in yeast has demonstrated that replication fork arrest can be initiated by the presence of lesions in replicating DNA[192]. The recovery of such regions is dependent on the activity of the recombination proteins MUS81 and Rad51[193]. Mutant yeast strains in which these genes have been knocked out, or disrupted, accumulate lethal double-stranded DNA breaks with long single-stranded intermediates[194,195]. The occurrence of these breaks is not random in the genome, certain areas are more susceptible than others. For example, in human cells, ATR depletion is known to cause breaks in regions of the genome that replicate slower than others – known as fragile sites[196].

The G_2/M boundary is the final fail-safe guarding cells from entering mitosis with damaged DNA. If damage is detected, either ATR-Chk1 or ATM-Chk2 signalling cascades arrest cells in G_2, however the maintenance of arrest is predominantly by ATM-Chk2[197]. Cells are prevented from entering mitosis by the down-regulation of Cdc25 which modulates Cdc2-Cyclin B activity[164]. Early experiments interrogated Cdc25C-knockout mutant mice strains, revealing that Cdc25C is not essential for checkpoint activation. Rather, the phosphatase activity of Cdc25A was shown to be essential for G_2/M checkpoint activation following ionising radiation (IR)[198]. In addition, it is known that p38 and p38α are also important following IR and UV respectively[199,200].

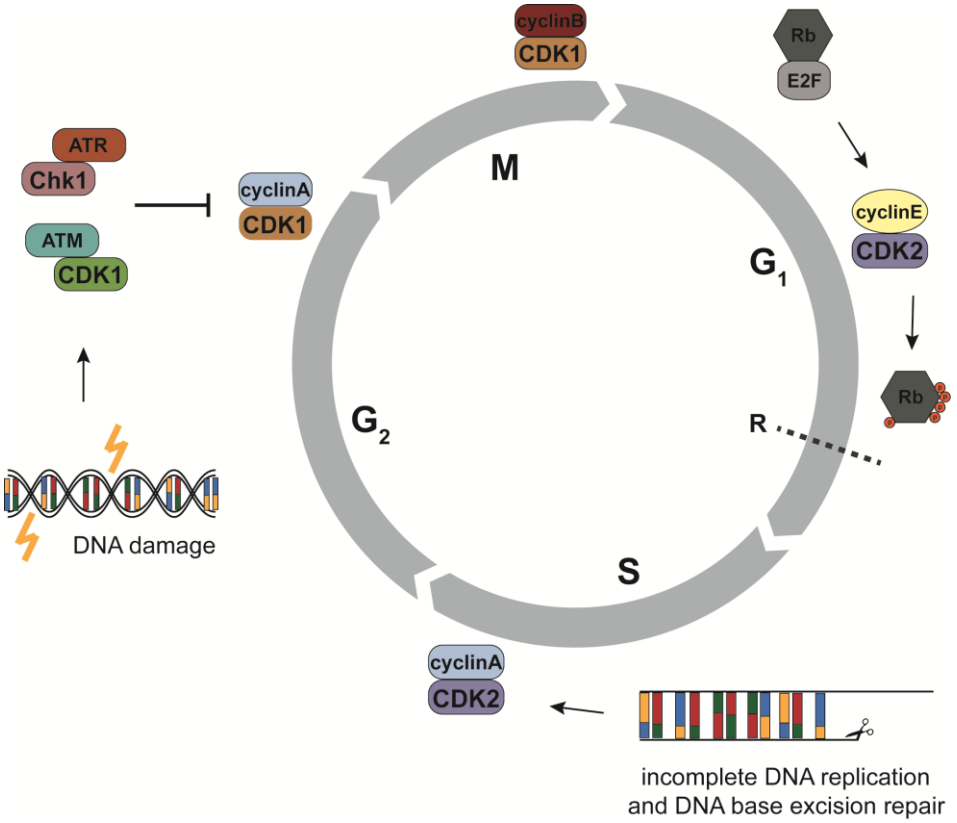

Figure 1.3. Cell cycle checkpoints and regulation. The cell cycle is regulated by a network of signalling cascades, which maintains genome fidelity. Progression through each of the four phases (G_1, S, G_2 and M) is controlled by cyclins and cyclin-dependent kinases (CDKs). Errors occurring during DNA replication at S-phase, or exogenous DNA damage accumulating throughout the cell cycle, restrict entry into mitosis until each checkpoint has been satisfied.

1.2.2. Replication stress

Replication of eukaryotic DNA is initiated from many origins, which are each 'licensed' by proteins which signal the start of S-phase[201–204]. The timing of replication at each origin is carefully orchestrated to ensure that nucleic acid resources, the accuracy and the speed are replication are balanced appropriately. There are many factors which can impede DNA synthesis, leading to the slowing, stalling and collapsing of replication forks – this is known as replication stress[205–207]. Replication stress can be thought of as a specialised form of DNA damage which has profound implication for genomic stability and cell survival. Unsurprisingly then, there are effector kinases that are shared between both replication stress and DNA damage pathways; the main sensors and effectors of replication stress being ATM and ATR[208–210]. Replication stress is rather unusual, compared to direct DNA damage, in the sense that the major underlying causes appear to be endogenous.

1.2.2.1. Replication-transcription collisions

The machinery for both transcription and replication operate on DNA simultaneously. Recent data has identified regions of the genome which are highly transcribed, particularly susceptible to double-strand breaks and replicated during early S-phase[211]. These are known as 'early replication fragile sites', and highlight the importance of collisions between protein complexes on DNA with separate agendas. It has been shown that, in some cases, DSBs can occur even before the convergence of the replication-transcription machinery at the nuclear periphery. This phenotype is surprising at it reveals that replication stress might be increased by the tethering of actively-transcribed genes to nuclear pore complexes[212]. The sequence of DNA itself may also determine its fragility to replication stress. For example: nascent RNA transcripts with particular AT/GC content have a propensity to form R-loop structures by re-hybridising with DNA emerging from behind the transcription complex, leading to polymerase stalling and

the replication fork collapsing[213]. Alternatively, if there is insufficient RNA-processing capacity at certain sites then this may inhibit dissociation of the replication complex from DNA, indirectly causing replication stress. To avoid these situations, human cells have the capacity to resolve R-loops by helicase and topoisomerase activity together with RNA-processing complexes that serve to prevent RNA from re-annealing with DNA[214,215].

1.2.2.2. Restarting at collapsed forks

If replication stress persists, or replication stress response pathways are abrogated, the fork may collapse. Recent data in mice and yeast suggest that ATR is crucial in restarting collapsed forks by recruiting and stabilising replication machinery in addition to preventing 'replisome' disengagement[216,217]. It has been shown that DNA breaks can occur following the collapse of a replication fork. Interestingly, treatment of human cells with fork-stalling agents leads to the presence of detectable breaks as early as four hours after fork collapse[218]. If the ATR pathway is abrogated in these cells, activation of DNA-PK and ATM are rapidly recruited to DSBs which may functionally compensate for ATR's absence[219].

It is thought that double strand breaks occur at collapsed forks as a result of endonuclease attack on persistent ssDNA or nucleotide gaps behind the fork[194]. Alternatively, the cell may be in a futile effort to correct stalled fork structures by initiating recombination or endonucleolytic cleavage repair pathways[218]. Curiously, fork structure resolution occurs significantly more frequently in the absence of signalling by ATR. One possibility is that HR-mediated processing of cleaved nucleotides in the absence of ATR permits fork restart without a checkpoint response, which may lead to permanent stalling of the replication fork[220]. If a fork reverses inappropriately, nascent-synthesised DNA is prone to degradation; although more recent data also suggest that reversal may, paradoxically, promote

fork restart and decrease the formation rate of DNA breaks by sheltering neighbouring DNA[220].

1.2.2.3. Replication stress in cancer

The timing of DNA polymerase activity at replication origins is crucial. It has been shown that re-replication and unscheduled initiation at these origins in human cells is controlled by Cdt1[221,222]. Overexpression of Cdt1 is associated with epithelial cancers with high-incidence of replication fork collisions and DNA breaks; an observation which can be recapitulated by injection of premalignant CDT1-overexpressing human cells into mice, generating genetically heterogeneous tumours[223–225]. Importantly, it has been shown that replication stress and impaired replication fork progression are present in human colorectal cancers (CRC) and are sufficient to promote chromosome missegregation, leading to aneuploidy[226]. Interestingly, this phenotype could be alleviated by supplementing chromosomally unstable colorectal cancer cells with nucleosides to suppress replication stress, suggesting that this mechanism plays a central role in maintaining the fidelity of the genome. This worked also demonstrated the existence of CIN-suppressor genes located on chromosome 18q which are subject to recurrent loss in CRC. Taken together these data provide evidence for a causal link between CIN and aneuploidy *in vivo* and show that there may be selective pressures for the generation and maintenance of discreet aneuploid karyotypes between tumour types.

It has been shown that the ATR pathway is upregulated in several cancer types, and that overexpression of ATR can lead to aneuploidy[227,228]. This is important as it known that loss of ATR in p53 null cells, or cells with oncogene-induced replication stress undergo senescence or apoptosis[229–231]. Together these data suggest that cancer cells depend on ATR for the maintenance of a CIN phenotype, and that

targeting ATR therapeutically may provide a mechanism for selective cell death in CIN^+ tumour cells[232].

1.2.3. The spindle assembly checkpoint

The spindle assembly checkpoint (SAC) detects unattached kinetochores, and delays anaphase onset until all chromosomes are attached on the spindle[233]. The Achilles heel of this molecular switch is that merotelic attachments, single kinetochores attached to microtubules from both spindle poles, are not detected by the SAC and these chromosomes can become trapped at the spindle equator during anaphase. Some data show that most of these 'lagging' chromosomes are eventually segregated to the correct cell; however, a proportion do not and result in aneuploid progeny[234,235]. There are many ways in which merotelic attachments can occur, and an elevated rate of merotelic attachments is a hallmark of CIN cancer cells[236]. The mitotic checkpoint complex (MCC) is responsible for this 'wait anaphase' signal and is comprised of a number of key proteins and signalling effector kinases including Mps1, MAD2, Bub1 and BUBR1. In mouse models of mosaic variegated aneuploidy, it has been shown that there is inactivation of BUBR1, demonstrating that disruption of MCC signalling is sufficient to disrupt faithful chromosome segregation[237]. However, the presence of MCC gene mutation in human cancers is rare and some data suggests that MCC gene methylation is a more common route to SAC disruption leading to CIN[238,239].

During the wait anaphase signal by the SAC/MCC, microtubule-kinetochore attachments are dynamically regulated by Aurora-B kinase which regulates microtubule turnover allowing merotelically attached kinetochores to be resolved before anaphase[240]. Aurora-B is also directly involved in the separation of duplicated centrosomes and, when overexpressed, centrosome amplification[240]. It has been shown that cancer cells cluster their extra centrosomes to form a pseudo-bipolar

spindle which permits bipolar cell division with an increased incidence of merotelic attachments and chromosome missegregation[241,242]. Together with Aurora-B kinase there are two main microtubule depolymerising proteins, MCAK and KIF2B, which reside at the kinetochore and are involved with the correction of erroneous attachments. Experimental knockdown of MCAK has been shown to increase the frequency of lagging chromosomes, and it has been reported that MCAK inactivating mutations are present in CIN colorectal cancer[243,244]. Taken together, these data suggest that merotelic attachments can lead to aneuploid daughter cells and provide a mechanism for the continual karyotype shuffling observed in many cancers.

1.2.4. Chromosome cohesion abnormalities

The cohesin complex is a ring-like structure which holds sister chromatids together until the onset of anaphase. At the metaphase-anaphase transition, this complex must be removed allowing the separation of genetic material[134,245]. STAG2, the main structural subunit of the cohesin complex, has been shown to play a fundamental role in maintaining the stability of the genome[272]. The relationship between STAG2 and chromosomal instability is complicated; *in vitro* knockdown of STAG2 in non-CIN cancer cell lines is correlated with increased aneuploidy and decreased cohesin, while genome sequencing of acute myeloid leukaemia (AML) samples revealed that very few STAG2 mutations are coincident with CIN[246]. The disparity between these results may be explained by recent work demonstrating that STAG2-dependent aneuploidy may be tissue specific, and likely to be linked to its secondary role as a transcriptional regulator[247].

1.3. Cellular consequences of aneuploidy

In general, the loss and gain of chromosomes has a detrimental effect on cellular fitness[248,249]. Studying the consequences of aneuploidy at the cellular level has remained challenging, in-part due to the lack of appropriate tools to study nascent aneuploid populations. Despite these challenges, important model systems have aided the understanding of the consequences of aneuploidy in yeast and mammalian cells; describing the impact of aneuploidy on: cell fitness, transcription, proteomic changes and genome stability[250–254].

1.3.1. Cell fitness and cell cycle changes

It has been suggested that CIN may allow chromosomal combinations to arise in cancer cells which impact on drug sensitivity both *in vitro* and *in vivo*[255,256]. There are also reports that some complex karyotypes increase the drug-efflux capacity of cancer cells, providing such sub-clones with a proliferative advantage under strong chemotherapy pressure and a poor clinical prognosis[257]. On the other hand, stratifying breast cancer patients based on CIN status may help to predict sensitivity to taxane therapy, a mitotic spindle stabilising agent that pushes CIN^+ cells towards cell death in mitosis or multinucleate apoptosis[258]. Paradoxically, these data demonstrate how CIN can both increase and decrease cellular fitness in a context-dependent manner.

The rates of cellular metabolism and timings of the cell cycle have been investigated in aneuploid cells. Using a chromosome transfer strategy, with selectable resistance markers, has allowed the study of single-chromosome aneuploidies in yeast[259,260]. It was found that all aneuploid cells proliferated significantly slower than isogenic euploid controls, with cell-cycle delays in G_1 and increased sensitivity to drugs targeting protein folding. Interestingly, although G_1 was delayed, only 2 out of 20

strains had a delayed metaphase-anaphase transition and 7 out of 20 had a delayed entry into mitosis. This may reflect the individual properties of each chromosome to illicit a particular phenotype, as G_1 delay time largely correlated with the amount of extra DNA[260]. It was also found that Cln2, responsible for promoting entry into the cell cycle, was significantly delayed in aneuploid strains, suggesting that aneuploidy interferes with the G_1-S transition upstream of *Cln2* transcription.

1.3.2. Genome stability

Defining the relationship between genome stability, aneuploidy and their combined effect on tumourigenesis has remained challenging. This is because these states are difficult to test experimentally and, as such, there is an abundance of conflicting data in cell culture models, animal models and how these may explain clinical data[236,261]. Some human cells may have stable aneuploidies which result from a transient lapse in genome stability, resulting in daughter cells with an abnormal karyotype which are faithfully inherited over time[262]. It is more likely however, especially in cancer, that aneuploidy results from an underlying CIN phenotype where whole chromosomes, chromosome fragments, and chromosome recombination events frequently occur[263]. One of the greatest technical challenges is to test whether spontaneously arising aneuploidies in-turn generate progeny with an increased likelihood of further missegregating chromosomes, or if an underlying CIN phenotype was the cause of the initial missegregation event.

It was first reported that cells with chromosomal instability were able to escape mitotic arrest following treatment with microtubule spindle poisons, leading to the suggestion that mitotic checkpoint attenuation was the underlying mechanistic basis of the CIN phenotype[264,265]. It was revealed a few years later however (by live-cell imaging) that spindle toxins increase the duration of mitosis in CIN cells; and they do not enter anaphase with misaligned chromosomes suggesting that a weakened

mitotic checkpoint is not the primary driving force of CIN[266,267]. It was also found that CIN^+ cells have elevated rates of lagging chromosomes at anaphase, indicating that unresolved mitotic spindle defects might by an important mechanism by which CIN and aneuploidy occur in human tumour cells.

To address whether aneuploid human cells are more vulnerable to further chromosome missegregation and genomic instability, lymphocytes from individuals with trisomies 13, 18 and 21 were isolated and chemically stimulated to proliferate *ex vivo*[268]. By analysing chromosome copy number using fluorescent centromere probes, it was found that trisomic individuals had a two-fold higher incidence of chromosome copy number alterations (CNA) than diploid individuals. Similar analysis of cells from patients with Turner syndrome (monosomy X) revealed that established monosomic cells are more than two-fold more likely to missegregate any of the autosomes investigated[269]. This suggests that spontaneous chromosome missegregation in human cells may be sufficient to generate CIN in cells with an otherwise stable karyotype.

These results have important implications for cancer initiation, as the loss of a tumour suppressor-rich chromosome, or gain of a chromosome harbouring oncogenes, may be sufficient to alter the mechanisms which regulate proliferation and induce CIN, simultaneously.

1.3.3. Transcriptional and proteomic reprogramming

From work in yeast it has been shown that expression of genes on aneuploid chromosomes is largely proportional to gene copy number[260]. Interestingly, aneuploid yeast strains also share a common gene expression signature, originally identified as a possible 'environmental stress response' which upregulates genes related to nucleic acid metabolism and ribosomal biogenesis[270]. This response

appears to be evolutionarily conserved across plants, yeast mice and humans, although the cause, nature and mechanism remain unclear[254]. In human cells, the presence of an extra chromosome has been shown to upregulate pathways involved with energy metabolism and autophagy, and causes down-regulation of DNA and RNA synthesis pathways[251]. Recent work has used a novel strategy to silence the extra copy of chromosome 21 in cells from Down syndrome patients[271]. It was demonstrated that genetic insertion of the X-inactivation gene on chromosome 21 could promote transcription repression through similar mechanisms as for the inactive X chromosomes in females. Silencing of the one extra copy of chromosome 21 by this method resulted in an 18-34 % increase in cell growth rate, suggesting that transcription is partly responsible for the compromised proliferation rate of aneuploid human cells. Importantly, chromosome silencing did not rescue proliferation to wild type levels, reflecting the multifactorial response to trisomy and that extra DNA alone, regardless of transcriptional state, may be sufficient to slow cellular growth. If there is an aneuploidy-sensing mechanism hard-wired into cells that regulates transcription, it raises the exciting possibility that it can be exploited therapeutically to target tumour cells whilst sparing healthy diploid cells.

The correlation between transcription and the proteome in aneuploid cells is unclear. Although gene expression is proportional to gene copy number, it has been shown that many proteins encoded by additional chromosomes do not scale in the same manner[260]. Importantly, many of the proteins that do not are part of larger multi-protein complexes, suggesting that protein stoichiometry imbalances may be influencing the proteolytic pathways in aneuploid cells[251]. This is an attractive hypothesis as it fits with the data demonstrating that aneuploid cells have a higher energetic demand, possibly due to the synthesis and degradation of superfluous proteins, and are sensitive to chemical inhibition of protein synthesis and folding[260,272].

More recently, proteomic dosage compensation has been observed in human cells in response to trisomy and tetrasomy, and post-translational mechanisms have been shown to further self-attenuate protein expression when the genes encoding them are present in excess[250,251]. This proteomic analysis further revealed the existence of a novel aneuploidy-related proteomic signature which is characteristic of redox homeostasis and altered metabolism, which could be alleviated by increasing protein turnover.

These results demonstrate that aneuploidy is sufficient to alter the metabolism and redox state of human cells which is subject to a negative feedback loop by both post-transcriptional and post-translational mechanisms. Both of these are important factors which increase the energetic burden in cells with abnormal karyotypes.

1.3.4. Aneuploidy tolerance

Human neurons and hepatocytes are known to harbour non-diploid chromosome complements[271,273]. Surprisingly, where they do arise, these aneuploidies do not appear to be deleterious to cellular function, and are not thought to predispose to tumourigenesis[274]. The mechanisms which allow some cell types to tolerate aneuploidy are currently unknown, and careful comparison with non-quiescent cells may reveal important transcriptional/proteomic reprogramming which occurs during cancer development and confers similar tolerance to a non-diploid genome.

There are thought to be numerous ways that cells can buffer the deleterious effects of aneuploidy. One hypothesis is that polyploidy, the entire genome present in multiple copies, may dilute the protein stoichiometric imbalances of a single extra chromosome[302]. It has been shown that there may be a strong selective pressure for this phenotype during tumour evolution, as many cancer types have a near tetraploid karyotype[275,276]. Further evidence of the need for superfluous-protein

regulation as a prerequisite to aneuploidy tolerance has been demonstrated by inactivation of UBP6[305]. UBP6 is a deubiquitinylating enzyme which regulates the activity of the proteasome. When UBP6 is inactivated, proteasomal turnover of proteins is accelerated and provides aneuploid yeast strains with a mechanism for reducing the proteotoxic effect of uncomplexed cytosolic proteins[277,278]. Upregulation of the proteasome by this mechanism was shown to be strongly correlated with increased aneuploid yeast proliferation rates. It has yet to be determined whether phenotypically-equivalent mutations are present in human cancers cells, and the subsequent impact this may have on proliferative capacity.

The integrity of DNA and progression of the cell cycle are tightly controlled by regulatory pathways which provide feedback to p53, a key cell cycle regulator. Aberrations which compromise any part of these processes ultimately lead to p53-dependent cell cycle arrest or delays, and it has been shown that this is also true for aneuploid cells[180,267,279,280]. Accordingly, it is unsurprising that p53 inactivation is a common occurrence in human cancers, acting as a driver of tumourigenesis and strongly correlated with a poor clinical outcome[279]. Interestingly, it has been shown that p53 mutations can act synergistically with progesterone, but not estrogen, stimulation to significantly increase chromosomal instability and aneuploidy in mammary epithelial cells[281]. Importantly, this reveals the existence of tumour microenvironment-specific differences in tumour suppressor inactivation and extent of aneuploidy *in vivo*.

1.4. The Aneuploidy-CIN relationship in cancer

Despite widespread aneuploidy in human cancers, there is little consensus on the exact role aneuploidy and chromosomal instability play in tumour development and progression. Much of the *in vivo* work to study chromosomal abnormalities has relied on mouse models with a spectrum of abnormalities in the key cell cycle checkpoints described above. The reliability and similarity to human carcinogenesis in these models is a topic of debate but have revealed that, somewhat paradoxically, aneuploidy and chromosomal instability can both promote and inhibit tumourigenesis[256,282–284]. The ubiquitous nature of aneuploidy across almost all cancer types is starting to be recognised as an important therapeutic target and is an active area of research.

1.4.1. Promoting tumourigenesis

It has been shown that mitotic checkpoint dysfunction, by overexpression of genes regulating the checkpoint, can lead to aneuploidy. Importantly, this is also true in human cancers, where overexpression of spindle assembly checkpoint genes occurs more frequently than their inactivation[285]. Experimentally, it has been shown that overexpression of mitotic check-point complex (MCC) protein MAD2 produces aneuploid tumours in various tissues including hepatomas, adenomas and, in some cases, intestinal tumours[286,287]. Interestingly, transient MAD2 overexpression is sufficient to promote tumour formation, suggesting that sustained mitotic checkpoint abnormalities are not a prerequisite for this phenotype[314]. Importantly, this may reflect the nature of aneuploid cells to perpetuate their own transformation through increased chromosomal instability. It has also been observed that the degree of overexpression of the outer-kinetochore protein HEC1 is correlated with the formation of aneuploid tumours in mice, and is a poor prognostic indicator in human

cancers[288]. These data suggest that there is a strong mechanistic relationship between cells with abnormal microtubule-kinetochore attachments, CIN and aneuploidy *in vivo*.

It has been demonstrated, through the analysis of array-based comparative genomic hybridisation (aCGH) and cytogenetics, that solid tumours show preferential loss of small chromosomes[289]. It is also reported that patients with chronic myeloid leukaemia have a significantly elevated rate of small chromosome gain; raising the possibility that the tumour microenvironment plays an important role in the propensity for different aneuploidies between malignancy types[290]. The most common aneuploidies in human gametes include chromosomes 21, 22, X and Y in sperm cells and chromosomes 16, 21 and 22 in oocytes[291–293]. Interestingly these also occur most frequently during early-stage astrocytomagenesis, potentially reflecting the nature of solid tumour cells to spontaneously lose small chromosomes, independent of oncogenic potential[289].

The recurrent gain of specific chromosomes in tumour cells supports the hypothesis that the loss of tumour suppressor genes, or the gain of oncogenes, through CIN mechanisms facilitates oncogenesis. For example, individuals with Down's syndrome (trisomy 21) are at a significantly higher risk of developing acute myeloid leukaemia and acute lymphoblastic leukaemia[294,295]. This is compounded by the observation that an extra copy of chromosome 21 is often present in haematological cancers, suggesting there may be a context-dependent selective pressure for cancer cells with discrete karyotypes[235]. Additionally it has also been shown that chromosomal instability, as a result of replication stress, can lead to the recurrent loss of three tumour suppressors on chromosome 18q, providing a putative mechanism which could drive CIN in colorectal cancers[226]. Taken together these data suggest that aneuploidy and CIN can facilitate and drive tumourigenesis.

1.4.2. Inhibiting tumourigenesis

Having established that the majority of aneuploidy and CIN phenotypes are tumorigenic, it is important to highlight that they can also inhibit tumour formation in a highly context-dependent manner[256,296,297]. It has been shown that inducing excessive CIN by treatment with spindle poisons leads to cell death following a gross aneuploidy phenotype, but the presence of CIN in cancer suggests there may be an optimal level of genome instability which is sufficient for tumour progression, without catastrophic genomic dysfunction[298].

Accordingly, it has recently been shown that the stratification of breast cancer patients on their 'CIN score' correlated with a poor prognosis; that is until a threshold of CIN was reached after which increasing genome instability correlated with increased survival outcome[255]. This suggests that aneuploidy and chromosomal instability are only tumourigenic within given limits, and raises the possibility that raising CIN beyond this threshold could be a novel therapeutic approach.

Returning to the example of trisomy 21, it is important to note that although there is a significant increased risk of leukemias, the incidence of solid tumours is markedly decreased[299]. These inhibitory effects have been investigated and reported linked to two key genes encoded on chromosome 21: *DYRK1A* and *DSCR1.* Although the underlying mechanism has not been fully elucidated, it is known that these genes are involved with the inhibition of the calci-neurin pathway of tumour angiogenesis[300].

It has also been reported that aneuploidy can inhibit tumourigenesis in tissues which are already prone to tumour formation, such as the liver[301]. By heterozygous deletion of one allele of CENP-E, a centromere protein important for chromosome congression, it was observed that the formation of spontaneous liver tumours was decreased by 50%[301]. Additionally it was also observed that when liver tumours did

occur in CENP-E$^{+/-}$ mice they were significantly reduced in volume, suggesting that mitotic dysfunction in cells with an inherent propensity to missegregate chromosomes can act as a tumour suppressive mechanism.

1.4.3. Aneuploidy as a therapeutic target

Therapeutic targeting of aneuploid human cells, whilst sparing diploid cells, is a very active research area with high impact potential. Many of the current compounds exploit the perturbed processes of metabolism and protein production in aneuploid cells ultimately leading to cell death and arrest through uncharacterised mechanisms. One such molecule is 17-AAG, an inhibitor of the protein-folding chaperone Hsp90 which associates with the endoplasmic reticulum[272]. Reducing the protein folding capacity of aneuploid cells that are already under proteotoxic stress is hypothesised to lead to AMP-mediated cell death. Further supporting this model, combination therapy of 17-AAG and AICAR, an energy stress-inducing compound, in trisomic mouse embryonic fibroblasts and human cell lines significantly reduced their proliferation compared to diploid control cells[272]. However it has been shown recently that these compounds are associated with unacceptably high side-effects in phase II clinical trials, but provide preliminary evidence that it is possible to target aneuploid cells specifically with small molecules[302,303].

More recently, the idea of targeting CIN cells specifically has been suggested. Cancer cells have been shown to cluster extra centrosomes to allow a pseudobipolar mitosis with increased incidence of merotelic attachments[241]. In the absence of a pseudobipolar spindle, cells proceed through mitosis with multipolar spindles leading to cell death[304]. An RNAi screen identified *HSET*, a kinesin motor protein involved in microtubule trafficking, as an important effector protein for extra centrosome clustering. Importantly, it has been shown that HSET is expendable in normal cells, possibly because there is some functional overlap with other kinesin

motor proteins, suggesting it may be possible to induce cell death in cells with extra centrosomes. Excitingly, small-molecule HSET inhibitors are already in clinical trials[305,306].

1.5. Methods for detecting aneuploidy

Experimental technologies for investigating aneuploidy can be broadly grouped into those which measure aneuploidy on a population-wide basis and those which give single-cell resolution. One critical consideration for any technique is the over or under estimation of aneuploidy rates due to the introduction of experimental artefacts during sample preparation and analysis. More recent approaches have tried to improve on legacy techniques by coupling high-throughput, population-based analysis with single-cell resolution. Here I discuss the advantages and disadvantages of the most widely used karyotype analysis techniques to detect aneuploidies in human cells.

1.5.1. Comparative genomic hybridisation

Comparative genomic hybridisation (CGH) technologies are microarray-based sequencing platforms which were developed to assess genomic aberrations in cancer[307,308]. The development of array-CGH (αCGH) permitted, for the first time, DNA copy number alterations to be correlated with population-wide chromosome abnormalities thus transforming clinical cytogenetics. In traditional αCGH, genomic DNA from a reference genome and the sample of interest are differentially hybridised with two fluorescent probes which competitively bind to nucleic acid targets immobilised on a solid support[309]. The amount of DNA hybridised to each array position, expressed as a $\log_2$ ratio of fluorescent signal relative to the reference genome, correlates with the ploidy of that particular genetic locus. There are two main factors which determine the resolution of αCGH array – the density of genome coverage and the size of the nucleic acid target. The most apparent benefit to using αCGH over traditional FISH is that one is able to detect multiple DNA copy number alterations simultaneously across the genome. These changes include

amplifications, deletions and duplications at any locus represented on the array. In this way, αCGH can be thought of as a concurrent and coordinated FISH experiment over thousands of loci, compared to traditional FISH which is limited by the availability of fluorophores which can visualised simultaneously[310].

Aneuploidy, in the broadest sense, encompasses both structural and numerical chromosome aberrations. Therefore, as αCGH is based exclusively on DNA hybridisation, it is unable to detect structural abnormalities such as inversions or reciprocal translocations as these are not reflected by chromosomal content. Additionally, only copy number changes which are present in the majority of the population, and therefore above the intrinsic noise of the analysis, will be detectable with αCGH[311]. These make αCGH unsuitable where subtle structural and numerical aneuploidies are to be detected.

1.5.3. Single-cell sequencing

The rapid development of next-generation sequencing has significantally reduced the cost and time to obtain a complete genome DNA sequence. This has realised the possibility of sequencing individual cells and detecting aneuploidies on a cell-by-cell basis. This has already been demonstrated for both mouse and human tissue samples from the brain, liver and skin[312]. A critical step in single-cell sequencing (SGS) is isolating and amplifying target DNA from individual cells. The isolation of single cells can be achieved through FACS, cell pickers or, more crudely, serial dilution. Preparation of the genomic library for sequencing begins with whole-genome amplification (WGA), where DNA is fragmented and end-ligated to be amplified by PCR. Libraries from individual sequencing lanes can subsequently be demultiplexed, subjected to quality control and mapped onto the genome of reference[313].

The copy number variation (CNV) can be determined using a Hidden Markov model which determines the read copy number for each genomic loci in turn, generating a resolution that is equal to, or greater than, αCGH[314]. Importantly, determining faithful chromosome copy number does not depend on high resolution sequencing data, as only 0.5-1% DNA sequence coverage per cell is necessary.

Single-cell sequencing is less subject to artefacts than traditional FISH as thousands of sequencing reads are analysed for each chromosome simultaneously, compared to a small number of loci by FISH[315,316]. Additionally, the preparation of the library and robotic fluidic systems can automate a large proportion of the wet lab work, further reducing costs. Unfortunately, although next-generation sequencing (NGS) is only a fraction of the former cost, it is still considered relatively expensive to sequence enough individual cells to obtain representative population aneuploidy rates, as a large number of single cells are required. Furthermore, it is not yet possible, at low coverage, to detect inversions and balanced translocations which precludes some usages, such as the study of chromothripsis[317]. It is also difficult to amplify and sequence such small quantities of DNA without significant risk of sequencing artefacts including GC bias during PCR amplification; although these can be mitigated using well-designed bioinformatic tools[318]. As NGS costs continue to drop precipitously, it is likely SCS will become a viable option for investigating clinical aneuploidy.

1.5.4. Flow cytometry

The use of flow cytometry to detect chromosome copy number has increased significantally in resolution in recent years and encompasses three broad applications: DNA profiling, population chromosome copy number and single cell chromosome copy number[319–322].

DNA profiling is a term used to describe the intensity of fluorescent staining of DNA intercalating dyes, where the intensity of DNA staining is proportional to the DNA content of each cell (**figure 1.4a**). Its most common application is to determine the cell cycle profile of a population, where cells in G_2/M have approximately double the fluorescence intensity of G_1 cells. Cells in S-phase have a spectrum of DNA intercalation between these two peaks. It is therefore possible to determine an approximate value of the ploidy for a population of cells by comparing the DNA profile of a sample population to a known diploid population – cells with aberrant ploidy are shifted towards the higher end of the fluorescence spectrum. The data from these experiments only provide a rough approximation of ploidy for two reasons; firstly, the intercalation of DNA dye may be incomplete or dependent on the cell type, which could cloak or distort subpopulation of cells. Secondly, aneuploid cell populations may not be homogenous which gives rise to noisy DNA profiles with less sharp peaks, particularly in cycling cells where there are a large number of karyotype states or polyploidy which makes analysis difficult.

The variation between chromosomes, with respect to size and base pair content ratio, lends favourably to interrogation with bivariate flow cytometry. Principally, chromosomes are stained with chromomycin A3, which specifically binds GC-rich DNA, and Hoechst 33258, with specificity for AT-rich DNA. These two dyes can be resolved by flow cytometry on naked human chromosome DNA, not only by DNA content, but by base pair ratio, which varies between each chromosome. Chromomycin and Hoechst have excitation maxima which are sufficiently separated that they can be excited by different lasers, however there is a considerable degree of overlap in emission spectra. It is for this reason that the only flow cytometry instruments capable of bivariate chromosome analysis have two spatially separated lasers required to obtain spatially separated emissions from each dye.

The primary drawback of flow cytometry is that a consequence of the specialised optical arrangement is a linear time delay between signals at the two detectors requires highly sensitive compensation electronics to correct the elliptical laser optics. Data output can be interpreted using a bivariate cluster algorithm, where aneuploidies in single chromosomes can be detected as an increase in dot-plot density in a given region (**figure 1.4b**)[323]. Chromosomes 9-12 are similar enough in their AT and GC ratios that they are not resolved using this method, which obscures aneuploidies of these chromosomes. Furthermore, bivariate chromosome analysis is not sensitive enough to determine small translocations and deletions[324]. However, larger structural chromosomal abnormalities may be visualised as a shift or separation in two dimensions on the plot.

It has recently been shown that, using specialised image cytometry technologies coupled with FISH, it is possible to visualise chromosome copy number alterations in a high-throughput, single cell approach[325]. This is able to couple the high-throughput requirements for population-based analysis with the resolution of single cell sequencing. I discuss the precise application of this technology in chapter 6 and demonstrate its practical applications for detecting aneuploidy in response to environmental stresses.

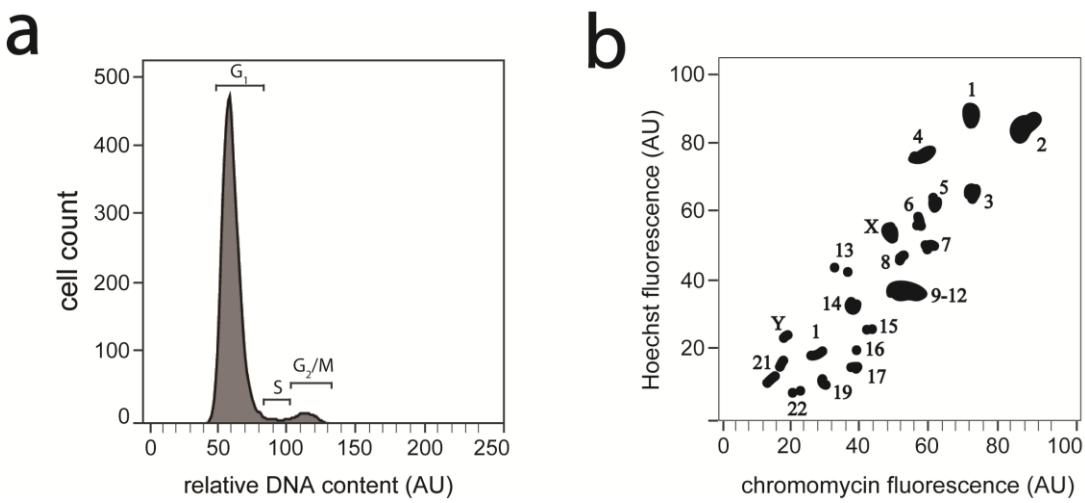

Figure 1.4. DNA analysis by flow cytometry. (a) DAPI-stained populations of fixed cells fluoresce proportional to their DNA content. Cell cycle profiles can determine the proportion of cells at each stage of the cell cycle and detect polyploidy by comparison to diploid population. (b) Staining chromosomes with chromomycin and Hoechst can detect aneuploidy using bivariate chromosome flow analysis (illustrative data points). Aneuploidy can be detected as an increase in the staining number or density at a defined regions compared to diploid control cells. Adapted from[326].

1.5.5. Fluorescence *in situ* hybridisation

Population-based studies of aneuploidy can be analysed in both dividing and non-dividing cells by decorating the DNA with fluorescent probes and/or DNA intercalating agents. In simple metaphase preparations, stained only with intercalating agents such as Giemsa, it is possible to detect a number of large chromosome abnormalities including translocations, deletions, inversions, insertions, amplifications as well as whole chromosome copy number variations[327–329]. Coupling DNA banding staining with fluorescent probes against individual genomic loci can help establish cytogenetic abnormalities with clinical phenotypes such as the BCR-ABL translocation t(9;22)(q34;q11)[330].The use of a single probes to measure aneuploidy rates can introduce false positive and negative results if there are duplication or deletions events at the probe-binding region which necessitates, in some cases, the use of dual probes against subtly different regions of the same chromosome, which can be expensive.

Additionally, the FISH procedure can introduce artefacts itself due to failure of probe hybridisation, probe clustering, or incomplete metaphase spreading[331,332]. FISH on interphase cells has the advantage of providing single cell copy number state and it is possible to couple this information with immunofluorescence to determine to down-stream spatial and temporal responses of aneuploidy with exquisite resolution.

Whole-chromosome FISH paints permit spectral karyotyping analysis which reveal whole chromosome copy number changes and gross genome translocation events[333–335]. The process is moderately expensive as it requires the use of chromosome-specific chromosome paint sets with five fluorescent dyes, which barcode each chromosome in metaphase preparations. Importantly, both structural and numerical aberrations can be detected using this method, which lends itself to clinical applications where there are known disease drivers caused by chromosome

abnormalities. One important consideration for clinical oncology applications is the process of aneuploidy speciation over time, as heterogeneous sub-populations evolve in response to subtle microenvironmental pressures.

The very nature of sampling size in populations of genetically diverse tumour samples therefore limits the probability that true aneuploidies are represented faithfully by these analysis methods.

2. Aims and objectives

Develop a novel system to isolate nascent aneuploid cells

The earliest responses to chromosome missegregation in non-transformed cells are largely unknown. In-part, this is due to technical limitations preventing the isolation of cells within the few hours following chromosome loss. The first aim of this PhD was to generate a novel, fluorescence-based aneuploidy reporter cell line to isolate nascent aneuploid cells. Analysis of monosomic populations isolated using this approach aimed to expose changes at the level of the transcriptome in response to aneuploidy, within 12 hours of chromosome loss.

Determine the missegregation rates of individual chromosomes

A ubiquitous feature of cancer cells is elevated chromosome missegregation and recurrent patterns of aneuploidy. The second aim of this PhD was to undertake the first high-throughput and systematic approach to elucidate the missegregation rates of individual human chromosomes in response to different cellular stresses. Further, this PhD aimed to characterise the mechanisms underlying the most striking differences between individual chromosome segregation error rates.

Elucidate the arrangement of metaphase chromosomes

The well-defined territories of interphase chromatin are intimately linked with ordinary function. At present, the only data for metaphase territories are derived from radial measurements in metaphase spreads, which are subject to significant artefacts. The final aim of this PhD was therefore to develop an image analysis tool to elucidate the arrangement of metaphase human chromosomes in the native metaphase plate.

3. Materials and Methods

3.1. Tissue Culture Assays

3.1.1. Reagents and cell culture

All cells were maintained in sterile conditions at 37 ºC with 5% atmospheric CO_2. Cell culture media was supplemented with 10% (v/v) foetal bovine serum (FBS; Gibco) and 1% (v/v) penicillin-streptomycin (Sigma). Cell lines were selected which had previously been characterised as chromosomally stable (**table 3.1**).

Cell lines were grown as adherent monolayers and passaged through trypsinisation. To trypsinise cells, media was removed by aspiration and cells were carefully washed twice in phosphate-buffered saline solution (PBS) at room temperature for 30 seconds. PBS was removed and 1x trypsin-EDTA (Sigma) was incubated with cells at 37ºC until cells had detached from the surface of the culture vessel. Cells were fully resuspended in at least five times the volume of trypsin in appropriate media supplemented with FBS - to inhibit the trypsin enzyme. Cells taken from this suspension were used to seed new culture vessels, containing fresh media, at the appropriate density for the application.

Cell line	Media	Cell type	CIN status
RPE-1 hTERT	DMEM – F12	retinal pigment epithelial	negative[336,337]
RPE-1 hTERT 12/3	DMEM – F12	retinal pigment epithelial	positive[336]
HCT116	DMEM	colorectal carcinoma	negative[336,337]
DLD1	DMEM	colorectal adenocarcinoma	negative[338]
BJ hTERT	DMEM	foreskin fibroblast	negative[339]

Table 3.1. A panel of transformed and non-transformed human cell lines. The panel of human cell lines used for the experiments in this thesis covered both transformed and non-transformed cell types from a range of tissues of origin. The chromosomal instability (CIN) status for each cell line had been previously characterised.

3.1.2. Plasmid transfections

Adherent cell monolayers in 6-well dishes were grown to approximately 60 % confluence for transfection. 6 µL Lipofectamine 2000 reagent (Life Technologies) was diluted in 150 µL Opti-MEM reagent (Life Technologies) and added in a 1:1 ratio with the required amount of plasmid DNA diluted in 700 µL Opti-MEM reagent. Following incubation for five minutes at room temperature, 250 µL of the DNA-lipid complex solution was added, drop-wise, to the surface of the media in each transfection well. After 24 hours, the media was replaced and cells grown for a further 24 hours. For stable cell line generation, transfected cells were passaged at low density into culture vessels supplemented with media containing G418 at a final concentration of 500 µg/mL (Sigma) to select for drug-resistant clones. The selection media in each well was replaced every three days for two weeks, after which time drug-resistant colonies had formed and were harvested for down-stream applications.

3.1.3. Small-molecule perturbation of the cell cycle

Nocodazole is a microtubule depolymerising drug which arrests cells in mitosis as they are unable to form a functional mitotic spindle. To arrest cells in mitosis, and to induce chromosome missegregation, cells were treated with 100 nM nocodazole (Sigma) dissolved in dimethyl sulfoxide (DMSO) for between 2 hours and 16 hours. To allow microtubule re-polymerisation, nocodazole was washed out of cells by completely replacing the media three times with PBS pre-warmed to 37 ºC for two minutes each, followed by fresh media pre-warmed to 37 ºC, twice. Cells were released from nocodazole for up to 24 hours to allow cells to proceed through mitosis. A variation of this protocol includes the physical removal of mitotic cells from the culture vessel by mitotic shake-off. Dislodgement of mitotic cells into suspension is achieved by gentle shaking of the culture vessel. To release mitotic cells from

nocodazole, mitotic cells in suspension following shake-off were harvested by centrifugation at 1,200 rpm for three minutes. The supernatant was aspirated and cells were resuspended in the appropriate media pre-warmed to 37 ºC, twice.

To synchronise cells at the G_2/M check-point, cells were treated with the CDK1 inhibitor RO-3306, dissolved in deionised water, for 14 hours at a final concentration of 9 µM. To allow cells to proceed through the mitotic checkpoint, RO-3306 was washed out of cells by completely replacing the media three times with PBS pre-warmed to 37 ºC for two minutes each, followed by fresh media pre-warmed to 37 ºC, twice. In experiments requiring cells synchronisation prior to nocodazole treatment, the final media wash contained 100 µM nocodazole.

3.1.4. Colony formation assay

Single cells sorted by FACS were counted in experimental triplicate using a haemocytometer (BioRad) and 100 cells from each condition were seeded into 6-well dishes from triplicate experiments and allowed to form colonies over a period of 10 days. After 10 days the number of colonies in each well were counted as follows. Colonies were stained with 5 mL 0.01 % (w/v) Crystal Violet in deionised water for one hour at room temperature on a rocker. Excess dye was removed and colonies were dissolved in 1 mL 2 % (w/v) Triton X-100 for a minimum of 16 hours with agitation. The optical density (OD) of 200 µL crystal violet-stained cell suspension was read at 570 nm on an optical density plate reader (Victor2D - 1420, Perkin-Elmer Inc.).

3.2. Fluorescence Microscopy

3.2.1. Live-cell imaging

Cells expressing a fluorescent histone H2B variant (H2B-RFP/GFP) were seeded into live-cell imaging dishes at low density at least two days prior to filming, mounted on an Olympus DeltaVision microscope (Applied Precision) and maintained at 37 ºC in CO_2-independent medium (L15, Sigma) for the duration of the experiment. Additionally, the DeltaVision stage environment was maintained at 5 % CO_2. Proliferating cells were imaged by acquiring seven 2.0µm optical sections in the Z-axis, with TRITC laser line band-pass filter (488/532 nm), at three-minute intervals for three hours, followed by 15-minute intervals for between 24 and 72 hours. Movies were analysed in the softWoRx Explorer 1.3 (Applied Precision). The timing of mitotic events was determined by analysis of cells going through mitosis during the three-minute time-lapse filming, to allow precise timings to be obtained. Nuclear envelope break-down, congression of the last chromosome and anaphase onset were easily identifiable at this temporal resolution. The fate of daughter cells was followed in the 15-minute time-lapse period.

3.2.2. Immunofluorescence

Cells were seeded onto microscopy coverslips were treated with 9 µM RO-3306 (Santa-Cruz) and/or 100 µM nocodazole (Sigma). After treatment, cells were washed once with 1x PBS, fixed and permeabilised with PTEMF solution (20 mM PIPES pH 6.8, 0.2 %, Triton X-100, 10 mM EGTA, 1 mM $MgCl_2$ and 4 % formaldehyde) for 10 minutes at room temperature. Fixed cells were blocked for 30 minutes in PBS + 3 % BSA, washed twice in 1x PBS (5 minutes, room temperature) and stored in 1x PBS at 4 ºC for at least two hours and up to two weeks before

immunostaining. For immunostaining, cells were incubated for one hour at room temperature in the appropriate primary antibody diluted in 1x PBS.

Following primary antibody staining, cells were washed three times with 1x PBS for five minutes each. Primary antibodies were detected by appropriate FITC/ TRITC/ Cy5-conjugated secondary antibodies (Life Technologies) for 30 minutes at room temperature, diluted in 1x PBS containing 1 µg/mL DAPI, followed by three five-minute washes with 1x PBS. Coverslips were mounted on glass microscopy slides in Vectashield (Vector laboratories). 3D fluorescent image stacks were acquired on an Olympus DeltaVision microscope in 0.2 µm steps, using the Olympus 20x, 40x, 60x or 100x UPlanSApo immersion oil objectives with a 1.4 numerical aperture.

3.3. Construction of a mammalian *dsEGFP* expression vector

3.3.1. Amplification of pEGFP-C1 vector

A pEGFP-C1-containing vector was obtained from a commercially available source (Addgene), as it had a suitable backbone for cloning into mammalian cell lines. The vector DNA was first amplified, for downs-stream applications, by transforming α-Select Gold Efficiency competent cells (Bioline Reagents). Competent cells stored at -80 ºC were thawed on ice for 15 minutes before addition of 10 ng plasmid DNA was added to 50 µL of cells. Cells were incubated with plasmid DNA, on ice, for a further 15 minutes prior to heat-shock. Competent cells were heat-shocked by incubating at 42 ºC in a water bath, without agitation, for two minutes before being immediately plunged into ice for five minutes. For one hour, cells were incubated at 37 ºC in a shaking incubator at a rate of 220 rpm in 350 µL of S.O.C medium to supressed catabolite production. Bacteria colonies were left to grow overnight at 37 ºC on Luria-Bertani (LB)-agar plates containing 50 µg/mL kanamycin. Single colonies were picked, used to inoculate 50 mL LB broth plates containing 50 µg/mL kanamycin, and grown overnight in a shaking incubator at 37 ºC, 220 rpm. DNA of the correct size was confirmed by running approximately 200 ng of plasmid DNA, recovered from overnight bacterial cultures by the QIAprep Spin Miniprep (Qiagen), on a 1 % (w/v) agarose gel stained with gel red (Biotium), with a 1 kb ladder (NEB), for one hour in Tris Borate EDTA (TBE) at 80 volts.

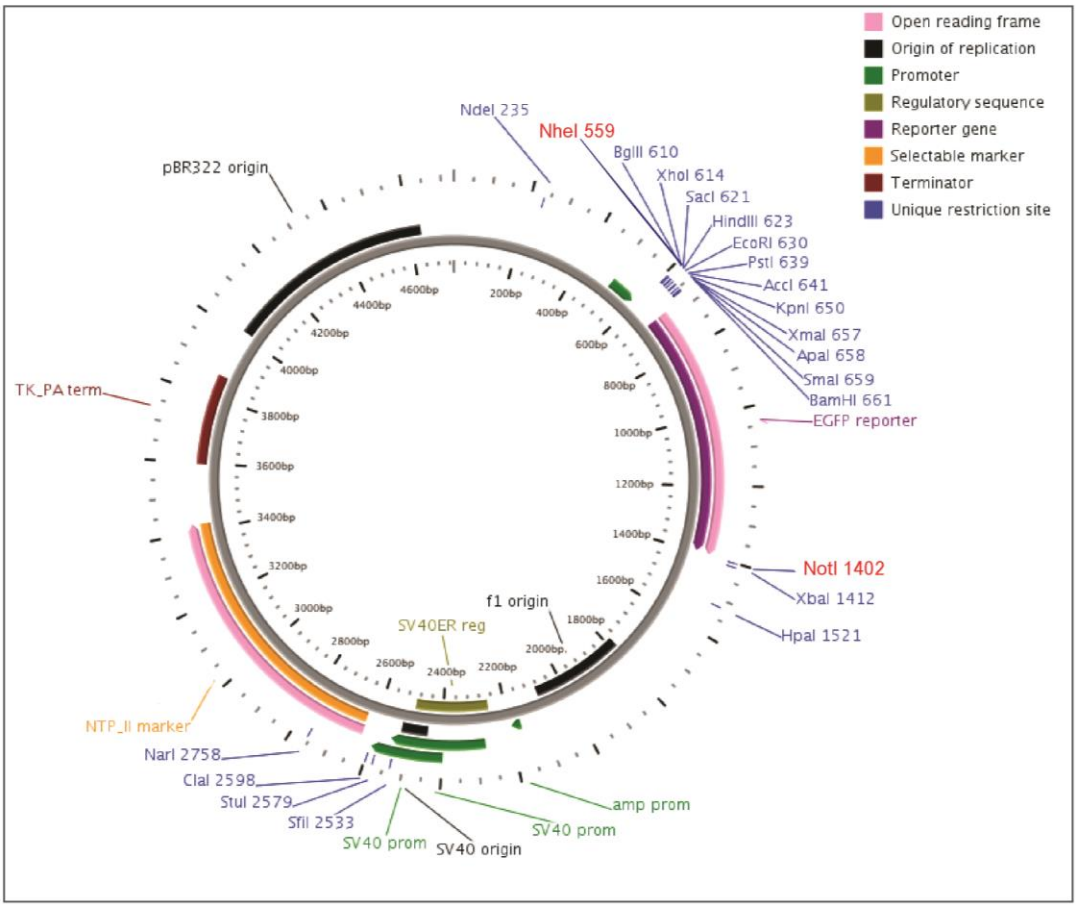

Figure 3.1. Diagrammatic representation of the pEGFP-C1 plasmid. The pEGFP-C1 plasmid contains a regular EGFP report gene at the C-terminus of a multiple cloning site (MCS). NheI and NotI were used to remove EGFP and dephosphorylated to prevent plasmid self-ligation. An origin of replication (pBR322) and kanamycin resistance cassette (NTPII) enabled *E.coli* amplification, selection and purification of plasmid DNA.

3.3.2. Cloning the dsEGFP gene into the pEGFP-C1 vector

The dsEGFP gene donor (Addgene #56474) and pEGFP-C1 backbone plasmid DNA were digested with the restriction enzymes NheI-HF and NotI-HF in CutSmart-4 buffer (NEB) for 1 hour to generate fragments with compatible 'sticky' ends. To prevent self-ligation, and therefore increase cloning efficiency, the pEGFP-C1 vector backbone was dephosphorylated with shrimp alkaline phosphatase in the supplied buffer (rSAP, NEB) for 30 minutes at 37 ºC, followed by enzyme inactivation at 65 ºC for five minutes. A sample of the digested vector DNA, and the total volume of dsEGFP-donor DNA, were separated on a 1 % (w/v) agarose gel stained with gel red (Biotium), with a 1 kb ladder (NEB), for one hour in TBE at 80 volts. The vector digestion was confirmed by the presence of a linear DNA band at the expected size (3879 bp). The dsEGFP fragment (843 bp) was excised from the gel using a sharp blade over a UV box and purified using a Zymoclean Gel DNA Recovery kit (Zymo Research) and the recovered DNA concentration assessed by spectrophotometry (Nanodrop ND-1000).

The vector backbone and dsEGFP plasmid DNA were incubated, at a molar ratio of 3:1, in the presence of T4 DNA ligase in the appropriate buffer (NEB) overnight at 16 ºC to allow the fragments to anneal and ligate. The resultant plasmid, pSMC50, was recovered following *E.coli* amplification, as described above, in bacterial media containing kanamycin antibiotic.

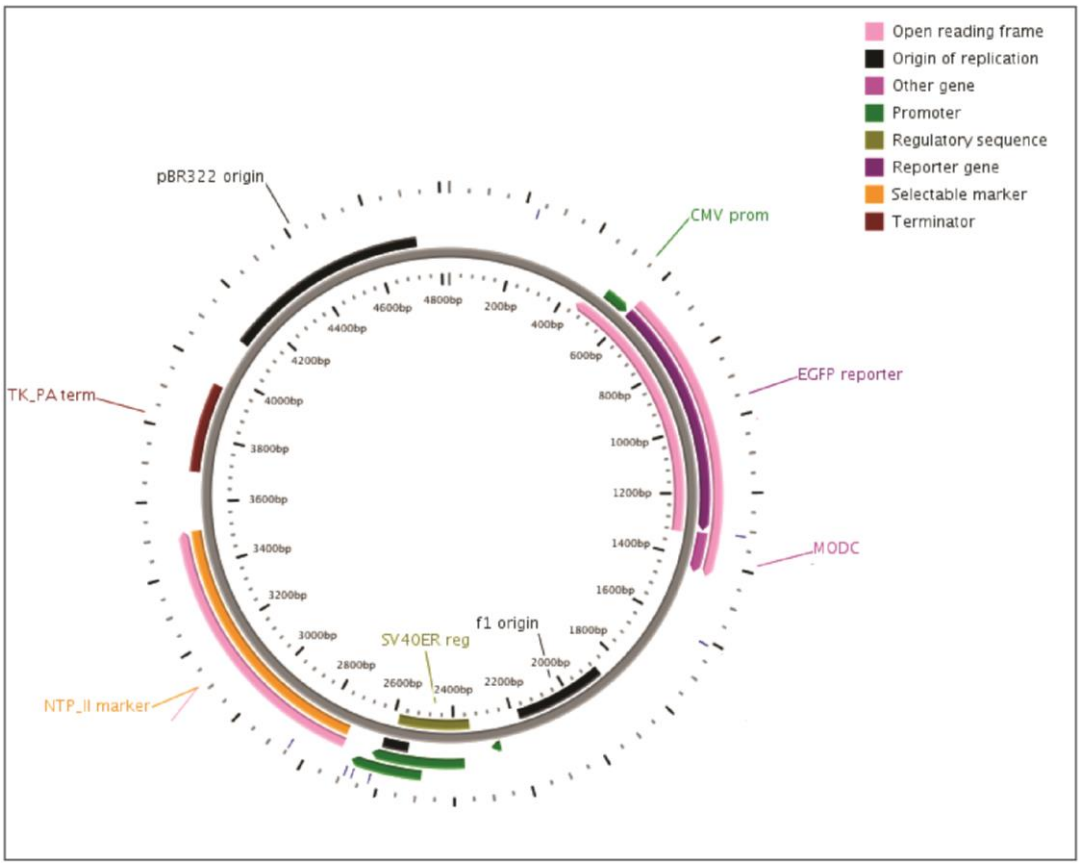

Figure 3.2. Diagrammatic representation of the dsEGFP-C1 plasmid. The dsEGFP-C1 plasmid contains an EGFP report gene with a mouse ornithine decarboxylase (MODC) domain at the C-terminus. An origin of replication (pBR322) and neomycin resistance cassette (NTPII) enabled transfected plasmid DNA expression and selection in human cells. High levels of expression were maintained by a cytomegalovirus (CMV) promoter immediately upstream of the dsEGFP gene.

3.4. Fluorescence *in situ* hybridisation

3.4.1. Traditional fluorescence *in situ* hybridisation

Cells were cultured on sterile glass microscopy slides until log-phase growth and fixed using freshly-prepared Carnoy's fixative solution (3:1 methanol-glacial acetic acid) for 10 minutes at room temperature. For cells sorted by fluorescence-activated cell sorting, samples were harvested by centrifugation at 1,200rpm for three minutes and fixed with Carnoy's fixative, in suspension for 10 minutes at room temperature, followed by settling onto glass slides. The fixative was allowed to evaporate and air-dried slides were immersed in 2x SSC for two minutes, without agitation, at room temperature. Samples were dehydrated through an ethanol series for two minutes each (70 %, 80 % and 100 %) and allowed to dry.

Each centromere enumeration probe (CEP, CytoCell) was equilibrated to room temperature for five minutes and uniformly mixed with a nuclease-free pipette tip. Solutions of complete hybridisation mixture consisted of 2µL of each probe and made up to a final volume of 10 µL with hybridisation solution B (CytoCell), briefly vortexed to mix, and pulsed in a microcentrifuge for 10 seconds. The probe mixture and sample slide were pre-warmed on a hotplate at 37 ºC for five minutes prior to hybridisation.

The probe mixture was spotted onto the sample slides and carefully covered with a nuclease-free coverslip. The probe and sample were denatured simultaneously for two minutes 75 ºC. After two minutes, the samples were placed in a light-proof, humid container at 37 ºC for at least eight hours. Post-hybridisation, the coverslip was carefully removed and the samples immersed in 0.2x SSC at 72 ºC for one minute without agitation. The sample slide was drained and submerged in PBS with DAPI (1 µg/mL) for two minutes. Sample slides were allowed to air dry at room temperature. Slides were prepared for fluorescence microscopy by addition 10 µL

of anti-fade reagent (Vectashield, Vector Laboratories) and sealed with a nuclease-free coverslip and non-aqueous fixative.

3.4.2. Fluorescence *in situ* hybridisation in-suspension

Cells in log-phase growth were treated with 100 µM nocodazole for eight hours and released following mitotic shake-off into fresh medium for 12 hours before analysis. Replication stress was induced by treatment with 0.2 µM aphidicolin for 24 hours. Cells from all experimental conditions were harvested, as previously described, and fixed by adding freshly-prepared 3:1 methanol-glacial acetic acid drop-wise to a pellet of PBS-washed cells. For hybridisation, cells were washed with 1x PBS with 3% BSA twice for five minutes, pelleted, and resuspended in 0.05% Tween20 and 2x Saline-sodium Citrate (SSC) in PBS. 1 $x10^6$ cells from this suspension were pelleted and the supernatant removed by pipetting. Cells were then resuspended in 40µL of complete hybridisation mixture containing 28 µL hybridisation buffer, 10µL nuclease-free H_2O and 2 µL CEP probe. Denaturing and probe hybridisation were performed in a thermocycler under the following conditions: 80 ºC (five minutes), 42 ºC (9 to 16 hours) and an optional storage step of 4 ºC. Following hybridisation, 200 µL of 2x SSC was added to each reaction mixture. Cells were pelleted and resuspended in 50 to 100 µL of 1x PBS before analysis (optional: DAPI, 1 µg/mL). All samples were analysed on the ImageStream^X cytometer by excitation with the 488 nm laser with a power of 100 mW at a 'high' flow speed.

3.4.3. Mitosis fluorescence *in situ* hybridisation

3.4.3.1. Anaphase fluorescence *in situ* hybridisation

Cells were treated with 100 µM nocodazole for eight hours. Following mitotic shake-off, cells were pelleted and seeded onto glass microscopy slides pre-coated with poly-L-lysine. After 60 minutes, cells were incubated for 10 minutes at room temperature with freshly prepared fixative solution (3:1 methanol-glacial acetic acid). Fixed cells were hybridised with centromere-specific probes with, and without, all-centromere probe according to manufacturer instructions (Cytocell), as previously described, and counter-stained with DAPI (1 µg/mL). For chromosome laggard rates, anaphase cells with lagging chromosomes were analysed from three independent experiments. Chromosome lagging rates were determined from the absolute number of CEP signals for specific chromosomes and the total number of chromosomes lagging in each anaphase judged by the all-centromere probe.

3.4.3.2. Late prometaphase fluorescence *in situ* hybridisation

Late prometaphase were identified by the presence of five or less uncongressed chromosomes 45 minutes post-nocodazole wash-out. Cells were analysed to determine the percentage of uncongressed chromosomes, split centromere rates and chromosome positioning in the metaphase plate. Uncongressed chromosome rates were determined from the total number of chromosomes uncongressed and the absolute number of CEP signals for specific chromosomes. The centromeres of individually stained sister-chromatid pairs were deemed to be ‘separated’ or ‘split’ if the centre of the two signals for each chromatid were greater than 2 µm apart, or were on opposing sides of the metaphase plate. The metaphase plate territory for individual chromosomes were interrogated by determining the distance of each sister chromatid pair from one end of the metaphase plate. Data were transformed

as a ratio of the distance from one end of the metaphase plate, to normalise for variation in metaphase plate length as a result of sample preparation. Chromosome territories at metaphase were analysed by generating frequency histograms of each chromosome for positions along the length of the plate.

3.5. Flow and Image Cytometry

3.5.1. Fluorescence-activated cell sorting

To sort RPE-1-4 cells by flow cytometry, a hierarchical gating strategy that measures parameters of each cell as it passes through the capillary-flow chamber was utilised. The first parameter identifies all cells, and is a readout of the total cell area, based on how much light is scattered from two lasers in the 'forward' (FSC) area and 'side' (SSC) area directions. Material below a threshold scatter of ~30,000-50,000 in both axes is determined to be debris and is excluded from the subsequent analysis and sorting. Of the 'all cells' population, doublet cells can be eliminated by plotting FSC-A (area) against FSC-H (height). Cells with a high ratio of their total area against height are likely to be two cells together and are excluded. Single cells are identified from clumps of cells, which still satisfy the area to height ratio, by gating those with a low total area side-scatter (SCA-A) and a low total width side-scatter (SCA-W).

3.5.2. Cell cycle analysis

The DNA content of single cells was used to determine population-wide changes in progression through the cell cycle. The cell cycle phases can be determined by plotting a frequency histogram of the relative amount of DNA in each cell. In proliferating cells, the majority of the population will be in G_1 and have a 2n DNA content that is visualised as the largest peak. Cells at various stages of S-phase, as the genome is being duplicated, will have an intermediate DNA content between 2n and 4n. Cells in G_2 and mitosis, following S-phase, can be distinguished as a DNA content with a fluorescence value roughly twice that of the G_1 peak. To prepare cells for cell cycle analysis, cells were fixed using 4% paraformaldehyde (PFA) at room temperature for seven minutes. Fixed cells were centrifuged out of the fixative solution at 1200 rpm for three minutes, and resuspended in a PBS + 0.2 % Triton X-

100 for three minutes to permeabilise the cell membrane. Permeabilised cells harvested by centrifugation at 1200 rpm for three minutes and resuspended in 500 – 1000 µL PBS containing DAPI at a final concentration of 1µ/mL and incubated for a minimum of five minutes at room temperature prior to analysis. Samples were analysed on a BD LSR Fortessa flow cytometer (BD Biosciences) by excitation of DAPI-stained cells with a 350nm laser and data recorded after a band-pass 450/50nm emission filter. For each sample, the DNA content of a minimum of 10,000 cells was acquired and the percentage of the population in each phase of the cell cycle determine in the FlowJo flow cytometry analysis software package (FlowJo LLC).

3.5.3. Apoptosis

In living cells, phosphatidyl serine (PS) is on the plasma membrane leaflet facing the cytoplasm. When cells are undergoing apoptosis, PS is transported to the outer plasma membrane where it binds, with high affinity, to the calcium-dependent lipid-binding protein, annexin V. The percentage of cells in early and late apoptosis, as well as dead cells, was determined by immunofluorescent staining of annexin V and the incorporation of DAPI by flow cytometry. Cells that are negative for both stains are living cells. Early apoptotic cells are identified by the presence of annexin V on the outer membrane, but are still impermeable to DAPI. Late apoptotic cells are positive for both DAPI and annexin V staining. Dead cells remove annexin V from the cell membrane by proteolysis, and are therefore only positive for DAPI.

Samples were harvested as previously described, washed once with PBS for three minutes, and stained for annexin V. Annexin V was stained using an anti-annexin V antibody conjugated to a far-red fluorophore (AlexaFluor 647, Thermo Fischer). Annexin binding buffer (1X, 140 mM NaCl, 10 mM HEPES, 2.5 mM $CaCL_2$, pH 7.4) was added in a ratio of 25:1 with the conjugated antibody and incubated with the

sample for 15 minutes at room temperature. DAPI, diluted to a final concentration of 1 mg/mL in 200 µL of annexin binding buffer, was added to the samples and incubated for five minutes at room temperature prior to analysis. Reference voltages for each laser on the flow cytometer were set using stained and unstained control cells. Cells were excited simultaneously with light of wavelength 450 nm and 647 nm. Annexin V and DAPI staining was recorded through the 450/50 and 670/14 band-pass filters, respectively. A minimum of 10,000 cells were recorded for each experiment.

3.5.4. Image cytometry analysis

Data obtained by the ImageStream^X were analysed in IDEAS 6.2 (Merck Millipore). Samples for each chromosome and experimental condition were obtained separately and contained within a single data file. For each sample between 500 and 40,000 individual cells were analysed.

Raw data files were opened in the IDEAS software package and the built-in compensation matrix applied. This correction is necessary to remove fluorescent noise introduced from the spatial alignment between channels, the flow speed, camera background normalisation and the level of brightfield gain. During acquisition, the EDF element was used to increase the focus range from 4 µm to 16 µm, allowing close to 100% of cells to be focused. Single cells are distinguished from cell aggregates by low area and high aspect ratio.

The gating of single cells was manually verified by visual observation of brightfield images in the selected region. Plotting the Gradient Root Mean Squared (RMS) value of the brightfield channel allowed only cells that were in-focus to be analysed. In-focus cells have a high Gradient RMS value. For some samples, where the hybridisation efficiency was weaker, a further gate was applied to select for only cells

in the sample above a threshold of probe signal intensity. This was achieved by plotting the total intensity of fluorescence in each cell, versus the Raw Max Pixel intensity within the cell. Cells with hybridised probe have an average total fluorescence, and a high Raw Max Pixel intensity. Single, in-focus, hybridised cells were then analysed for the chromosomal content of a particular chromosome by applying a 'spot mask' and 'spot counting' feature to the centromere probe signals for each image. The masking parameters were determined on user-defined variables: the radius of the spot and the spot-to-background ratio (STBR). The STBR is the spot pixel value divided by the background fluorescence of the bright detail image. The spot mask therefore denotes a region that is of appropriate area to be considered a centromeric signal, and the boundary at which the signal diminishes. Where the radius value is x, this suggests that the denoted area of a single spot should have a minimum value of $2x+1$ pixels. Regions that satisfy the spot mask criteria in single cells are enumerated by the spot-counting wizard. For the wizard to accurately determine chromosome ploidy, true populations were denoted for both $2n-1$ and $2n+1$ cells for a minimum of 25 images. The wizard then compiles the common features for over 250 elements and assigns each image a spot count.

The images obtained of CEP spots are 2D projections of 3D images, to encompass the entire volume of the nucleus. If a cell is aligned so that the two centromere signals are in the same x, y position, but different z positions, they sometimes appear as a single focus, because they overlap following image projection. To correct for this, CEP signal intensity was plotted as a histogram from the original spot count data which correlates with the amount of probe hybridised, rather than the spot count. Disomic cells had a medium (M) intensity of hybridisation signal intensity, representing two spots. Cells with one spot that had lost a chromosome will fall below the value represented by two standard deviations above the mean fluorescent intensity; cells that had gained a chromosome will fall above two standard deviations

of the mean of the hybridisation signal intensity. Events that are classified as one spot by the software usually fell into the medium range for intensity in the majority of cases. This suggests that, for the reasons stated above, they are disomic cells with aberrant ploidy-spot relationship. Cells designated as one spot that fell outside the 2 standard deviation window were deemed to be true monosomies. Cells designated as $2n+1$ by the spot-counting wizard were manually verified by visual inspection of each image and correlating it with the 2 standard deviation cut-off above the mean diploid fluorescence intensity.

3.6. DNA analysis

3.6.1. Genomic DNA extraction

Genomic DNA was extracted from cell lines using the DNeasy Mini kit (Qiagen). For control experiments, where starting material was not limiting, DNA was extracted from 1 x10^6 cells. For all experimental conditions sorted by FACS, genomic DNA was extracted from at least 50,000 cells. To extract genomic DNA, harvested cells were centrifuged and resuspended in 200 µL PBS and 20 µL proteinase K, to remove proteins from the sample. Following resuspension, 200 µL buffer AL was added and the sample thoroughly vortexed and incubated at 56 ºC for 10 minutes. 200 µL of ethanol absolute was added to the sample and mixed by vortexing. The mixture was pipetted into a DNeasy Mini spin column and centrifuged at 6000 xg for one minute. DNA in the column was washed twice by addition of 500 µL buffer AW1 and AW2 followed by centrifugation, at 6,000 xg for one minute and 20,000 xg for three minutes, respectively. DNA was eluted by centrifugation at 12,000 xg in a variable volume of nuclease-free PBS (60 to 200 µL), depending on the sample. For elution in a total volume of 60 µL, the DNeasy Mini column was washed with 2x 30 µL PBS to increase the total yield.

The absolute DNA concentration was determined by a spectrophotometer (Nanodrop ND-1000), where the ratio of absorbance at 260 nm and 280 nm was at least 1.8, and therefore considered to be DNA of sufficient quality for down-stream applications.

3.6.2. Southern blot

Cells from clone RPE-1-4F were harvested and resuspended in 200 µL PBS + 20 µL proteinase K, to digest proteins. Genomic DNA was extracted as previously described. To fragment the genome, 1 µg of genomic DNA was restriction-digested

with XhoI and KpnI-HF in the supplied buffers (NEB), followed by heat-inactivation at 80 ºC for 10 minutes. Genome fragmentation was confirmed by imaging each sample on a 0.8 % (w/v) agarose gel, stained with gel red, after running for 100 minutes at 65 volts in TBE.

To transfer DNA to the membrane the following procedure was implemented: A nitrocellulose membrane and three sheets of blotting were wetted by brief immersion in 0.4 M NaOH. Two of the blotting papers served as wicks for the transfer, and the third was overlaid on the gel support stand to prevent direct contact with the acrylic. The gel was rinse briefly with de-ionised water and placed on top of the acrylic support surface. The nitrocellulose membrane was laid carefully across the top of the gel, ensuring no air bubbles were trapped which would prevent proper transfer of DNA to the membrane. To this, the two sheets of additional blotting paper were stacked, followed by dry paper towels, increasing the total thickness to approximately 7 cm. A further piece of acrylic was stacked on to the assembly to allow the stable balance of a 500 gram weight, to weight the entire assembly and promote capillary diffusion of the NaOH through the nitrocellulose membrane. The transfer assembly was allowed to stand and the DNA transferred to the membrane for a minimum of 16 hours at room temperature

The membrane was carefully removed and washed in neutralisation buffer (Sigma). Before hybridisation with labelled probes, the membrane was blocked in salmon sperm DNA. To prepare the complete blocking agent, pre-hybridisation solution (Sigma) was incubated in a water bath at 42 ºC. Salmon sperm (Sigma) was denatured for 5 minutes at 95 ºC, immediately chilled on ice, and added to the pre-warmed hybridisation solution to a final concentration of 50 µg/mL. The membrane was carefully rolled into a hybridisation tube, complete hybridisation blocking solution added, and placed in a revolving hybridisation oven for five hours at 42 ºC.

For hybridisation, fluorescently-labelled pSMC50 probe was added to 10 mL hybridisation solution (Sigma), pre-warmed to 49 ºC, up to a final concentration of 10 ng/mL. The pre-hybridisation solution was discarded from the membrane and the hybridisation solution added, followed by incubation for 16 hours at 49 ºC. A 6X wash solution; consisting of 180 mL 20X SSPE (Sigma), 12 mL 10 % SDS and 408 mL deionised water; was pre-heated to 49 ºC and used to wash the blot on a shaking incubator for 15 minutes at 49 ºC. An aliquot of the 6X wash solution was diluted three times in deionised water, pre-heated to 49 ºC and used to wash the blot for 30 seconds. Hybridised blots were visualised on an Odyssey CLx imaging system (Licor) with a one minute and three minute exposure time.

3.6.3. Polymerase chain reaction and probe labelling

3.6.3.1. Generating fluorescently-labelled *dsEGFP* probes

The dsEGFP gene host plasmid, pSMC50, was digested with DNAse I – a restriction enzyme with no known sequence specificity – for 10 minutes at 37 ºC to generate a library of pSMC50 DNA molecules between ~100 bp and ~1,000 bp in length. DNA digestion was confirmed by running approximately 100 ng of the digestion mixture on a 1 % agarose gel for 30 minutes before down-stream applications. Precipitation of 1 µg of the fragment library was achieved by adding 1/10 volume of sodium acetate (pH 5.2, 3 M) and two volumes of ethanol absolute to the mixture, freezing at -70 ºC for 30 minutes then centrifuging at 12,000 rpm for 15 minutes. The supernatant was removed carefully by pipetting and the pellet washed with 70 % ethanol and allowed to air dry at room temperature. The pellet was resuspended in 20 µL of labelling buffer (Ulysis), denatured at 95 ºC for 5 minutes, snap cooled on ice and briefly centrifuged to redeposit DNA to the bottom of the tube. To this mixture was added 1 µL of ULS Alexa Fluor® 488 labelling stock solution (Ulysis) and incubated at 80 ºC for 15 minutes. The reaction was stopped by plunging the sample

into ice. Labelled DNA was recovered from the reaction mixture by a gel filtration-based spin column (BioRad) according to the manufacturer's instructions. The labelling efficiency, quality and concentration of labelled DNA was determined by a spectrophotometer (Nandrop ND-100).

3.6.3.2. Generating digoxygenin-labelled *dsEGFP* probes

Digoxygenin-labelled probes were generated by amplifying the target sequence by polymerase chain reaction (PCR). To a microcentrifuge tube was added the following reagents: PCR buffer with $MgCL_2$, PCR DIG-probe dNTP synthesis mix (Roche; 200 µM dATP, dCTP, dGTP, 130 µM dTTP, 70 µM DIG-dUTP), 0.5 µM forward PCR primer, 0.5 µM reverse PCR primer, 0.75 µL enzyme mix (Roche) and 50 pg template plasmid DNA (or 50 ng genomic DNA, depending on the application; Table 3.2). The total reaction volume was brought to a total of 50 µL with PCR-grade water (Roche). For the PCR reaction, 0.2 µL microfuge tubes and DNA amplified by thermocycling (Table 3.2). The PCR amplification was confirmed by running 5 µL of the sample mix on a 1 % (w/v) agarose gel for one hour. Successful probe labelling was confirmed by comparing the gel shift of the DIG-labelled PCR products with the unlabelled control PCR reaction.

3.6.4. Single-nucleotide polymorphism array

The ploidy of each sample was determined by a Genome-Wide Human SNP Array 6.0 (Affymetrix) and data analysed in the Chromosome Analysis Suite (CAS, Affymetrix). Data were transformed from global references obtained from signals in the CAS normalised reference library. Normalised signals were $\log_2$ transformed, and the copy number variation of a single SNP between samples was estimated from the weighted $\log_2$ ratio.

Target	Forward Primer	Reverse Primer
GFP	ATCGACTTCAAGGAGGACGGCAAC	ATGAACTTCAGGGTCAGCTTGCCG
IPCR(A)	AAGATCCGCCACAACATCGAGGAC	ATGGCGGACTTGAAGAAGTCGTGC
IPCR(B)	TGAGCAAAGACCCCAACGAGAAGC	TGTAGTTGCCGTCGTCCTTGAAGAAG
β-globin	CCAATCTGCTCACACAGGATAGAG	CCTTGAGGCTGTCCAAGTGATTCAGG

Stage	Temperature / Time	
Denaturing	90 ºC / 30 seconds	
Denaturing	90 ºC / 30 seconds	
Annealing	62 ºC / 90 seconds	X 25–35 cycles
Extension	72 ºC / 120 seconds	
Storage	≤4 ºC / ∞	

Table 3.2. Polymerase chain reaction primers and thermocycling. Forward and reverse primers were used to amplify gene target sequences using the stated forward and reverse primers (5’ to 3’ sequences shown). DNA amplification was achieved by thermocycling.

3.6.5. Metaphase spreads

Cells were treated with colcemid for six hours, harvested and resuspended in pre-warmed hypotonic solution (1:1; 0.4 % KCl 0.4 % Sodium citrate) at 37 ºC for seven minutes. Pelleted cells were resuspended by adding freshly-prepared fixative (3:1 methanol-glacial acetic acid) in a drop-wise fashion to prevent clumping and incubated for 30 minutes at room temperature. Metaphase spreads were obtained by dropping the fixed cell suspension onto clean glass microscopy slides from a height of between 1.5 and 1.8 meters and allowed to air-dry before storage at 4 ºC for up to three months prior to analysis.

3.6.6. Single-cell sequencing

Samples from control and experimentally-induced aneuploid cells sorted by FACS were sent to a collaborator for single-cell sequencing analysis using AneuFinder as previously reported[314]. Briefly, sequence reads are determined as non-overlapping bins with an average length of 1 Mb, a GC correction is applied, and binned sequences are analysed using a Hidden Markov model to differentiate aneuploidies from zero (nullisomy) to 10 (decasomy) chromosome copies. To negate the inherent sample variation introduced by sequencing single cells, a stringent quality control step was included that uses multivariate clustering analysis to excluded samples of insufficient quality. Chromosome copy number is plotted as a genome-wide state with clustering of cells based on the similarity of copy number profiles.

3.7. Transcriptome Analysis

3.7.1. RNA extraction

EGFP-positive and negative cells were collected by FACS as previously described. Cells were pelleted by centrifugation at 1200 rpm for three minutes and 350 µL RLT lysis buffer (Qiagen) added drop-wise to a loosened cell pellet. Cells in lysis buffer were homogenised by passage through a P200 pipette tip and one volume of 70 % ethanol added and mixed by vortexing. The sample was transferred to an RNeasy Mini Spin column (Qiagen) and centrifuged for 15 seconds and 12,000 rpm to bind total RNA to the column. RNA was washed by addition of 700 µL buffer RW1 and 15 second centrifugation at 12,000 rpm. To remove all traces of ethanol from the RNA sample, 500 µL Buffer RPE was added to the column and centrifuged at 12,000 rpm for two minutes. Total RNA from each sample was eluted by applying 50 µL RNase-free water directly to the column and centrifuging for one minute at 12,000 rpm. The total RNA concentration and RNA quality were analysed on a spectrophotometer (Nanodrop ND-1000).

3.7.2. Determination of dsEGFP insertion frequency

Total RNA from each sample was analysed using the GeneChip Human Transcriptome Array 2.0 (Affymetrix). Raw data from the array were transformed to normalise for quantile variation between samples, and correct for background noise, using the conservative RMA transformation function within the Affymetrix Power Tool software package (Affymetrix). RMA-transformed data were smoothed by plotting mRNA expression across the genome as a 1000-point moving average of Log_2 expression values.

3.7.3. Transcriptome responses to monosomy 6

Raw transcriptomics data files were normalised by SST-RMA transformation within the Transcriptome Analysis Console software package (Affymetrix). Differences in expression for each probe between samples were determined by one-way, unpaired ANOVA where significance was $p<0.05$. The fold change for each gene was plotted on a linear scale from -4 to +4. Data were plotted as pathway maps using the built-in WikiPathways compatibility function[340].

3.8. Mathematical proofs

3.8.1. Chromatid geometry

The centre of a best-fit ellipse of metaphase DNA, stained with DAPI, was determined using ImageJ. The major and minor axis length were defined using built-in analysis tools within ImageJ. Individual centromere signals were determined by thresholding fluorescent images to remove background and absolute x, y coordinates for individual signals were exported (**figure 7.1a**).

The relative metaphase positions (**figure 7.1b**) were determined as follows:-

o = x ,y

oA = Δx

AB = Δy

$\therefore$ oB = $\sqrt{(\Delta x^2+\Delta y^2)}$

$\theta_2 = 180- \theta$ or $\theta_2 = ABS ((180-(\tan^{-1}(\Delta y/\Delta x))-\theta)$

Relative metaphase position = oC

$\cos \theta_2$ = oC/oB

$\therefore$ oC = oB $\cos \theta_2$

$\therefore$ oC = $(\sqrt{(\Delta x^2+\Delta y^2)})\cos(180-\theta)$

or

$(\sqrt{(\Delta x^2+\Delta y^2)})\cos(180-(\tan-1(\Delta y/\Delta x))-\theta)$

The angular deviation between sister chromatids (figure 7.1c) was determined as follows:-

o = x, y

AE = Δx

AB = Δy

$\therefore$ BE = $\sqrt{(\Delta x^2+\Delta y^2)}$

CD = ΔoCoD (see relative metaphase positioning proof)

cosθ = CD / BE

$\therefore \theta = \cos^{-1}$(ΔoCoD / BE)

$\theta_2 = 90 - \theta$

$\therefore \theta_2 = 90 - (\cos^{-1}$(ΔoCoD / BE))

Raw data for ellipse centre coordinates (x, y), metaphase rotation angle (θ), major axis length, and sister chromatid coordinates (x, y) were extracted from each image by a custom ImageJ macro command (**chapter 10.1.2**). The mathematical calculations above were performed on extracted data using a Microsoft Excel function workflow (**chapter 10.1.6**).

3.9. Statistics

Where required, data were normalised to the appropriate control before analysis. Statistical analyses of *in vitro* assays were performed in GraphPad Prism 5.4 (GraphPad). Data with two experimental conditions were analysed using a two-tailed Student's T-test assuming unequal variance. For two or more treatment groups, significance between mean values was determined by one-way ANOVA with Tukey's post-hoc test to correct for family-wise errors.

Chi-squared significance and p-values were calculated by comparing the observed and expected values for the independent variables (aneuploidy-vulnerability and metaphase plate region) from a 2x2 contingency table.

Unless stated otherwise all graphs plot the mean, with error bars showing +/- one standard deviation of the mean, of triplicate biological repeats. Asterisks have been used to denote the significance value between experimental conditions, adhering to the following nomenclature: $p<0.05$ (*); $p<0.01$ (**); $p<0.001$ (***); $p<0.0001$ (****).

4. Developing a novel system to isolate nascent aneuploid cells

4.1. Optimising a drug-induced chromosome missegregation strategy

Aneuploidy has detrimental consequences for cell fitness; therefore, the preservation of a diploid karyotype between generations is a fundamental priority of proliferating human cells[260,341,342]. Elucidation of the earliest responses to aneuploidy in human cells is severely limited by the lack of appropriate tools to isolate aneuploid cells in the few hours following chromosome missegregation, before cells undergo apoptosis[145,180,259]. To circumvent these issues, and investigate the early responses to chromosome missegregation, I devised an experimental strategy to isolate nascent populations of aneuploid cells using a fluorescence-based aneuploidy-reporter cell line (**figure 4.1**).

The insertion of an enhanced green fluorescent protein (EGFP) transgene into a single chromosome locus would enable the isolation of populations of cells which have lost this chromosome by fluorescence-activated cell sorting (FACS). I have chosen to create my initial aneuploidy-reporter cell line using retinal pigment epithelium cells (RPE-1-hTERT; RPE-1 herein); a chromosomally-stable, non-transformed cell line which has been immortalised by constitutive expression of telomerase[343]. This cell line is well-suited for the outlined experimental strategy as it is has a low rate of spontaneous chromosome missegregation, and thus control and aneuploid (EGFP-negative) populations are biologically distinct and can be used for comparative analysis of the early responses to aneuploidy[226,337].

The analysis of the responses to aneuploidy requires enough cells to be able to utilise population-based approaches, such as gene expression arrays and transcriptomics, which require tens of thousands of cells[344]. Since the rate of spontaneous chromosome missegregation in RPE-1 cells is very low, chromosome missegregation will be artificially elevated using small molecule inhibitors of mitosis.

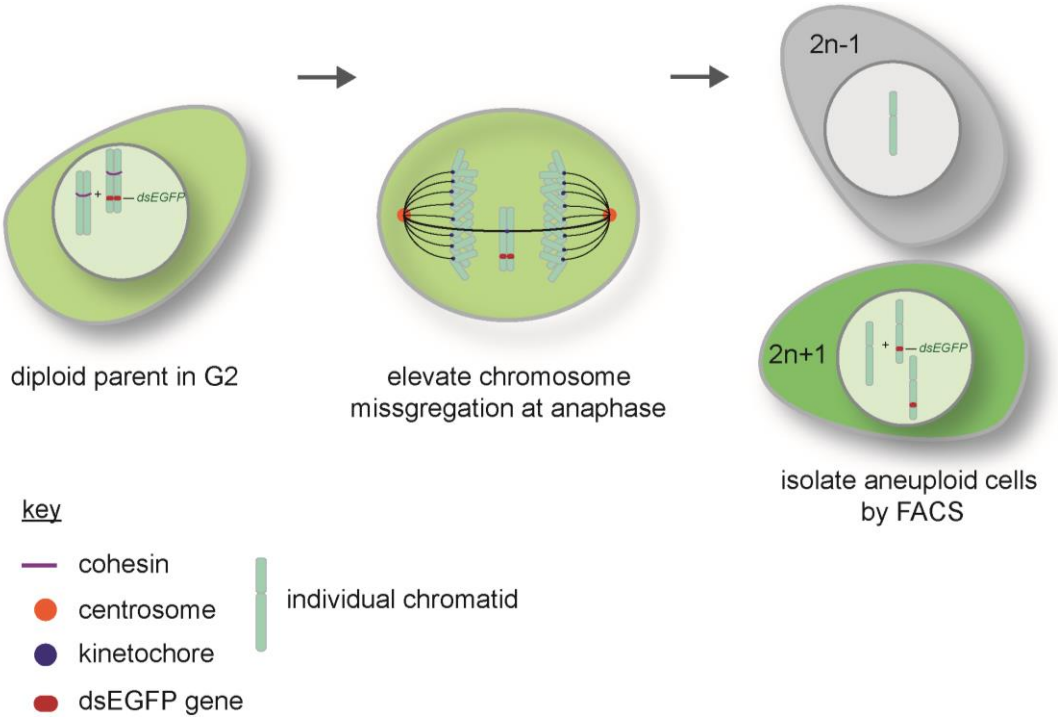

Figure 4.1. Experimental strategy for isolating aneuploid cells using FACS. A chromosome reporter strategy, based on fluorescence-activated cell sorting (FACS), was devised. A de-stabilised green fluorescence protein (*dsEGFP*) gene would be inserted into a single chromosome. Elevating aneuploidy using small molecule inhibitors of mitosis (nocodazole) would, in some cells, lead to reporter chromosome missegregation. This would generate a pool of aneuploidies, a sub-population of which would have missegregated the reporter chromosome and could be identified by EGFP fluorescence (lack thereof). Cells would be sorted by FACS post-chromosome missegregation and used for down-stream experiments.

4.1.1. The rate of micronuclei formation

Nocodazole is a microtubule depolymerising agent which causes cells to arrest in mitosis due to a failure to assemble a mitotic spindle[345]. Upon wash-out of the drug, spindle assembly can resume but is prone to the formation of improper kinetochore-microtubule attachments, leading to high rates of chromosome missegregation at anaphase (**figure 4.2a**)[235,346,347].

The primary cause of aneuploidy following nocodazole wash-out is thought to be mediated by merotelic chromosome orientation – individual kinetochore attachment to microtubules emanating from both spindle poles[234]. To determine the efficiency of nocodazole in inducing chromosome missegregation, I used a simple assay based on quantifying the percentage of cells with a micronucleus[348]. Micronuclei are a well-established surrogate measure of aneuploidy, caused by lagging chromosomes at anaphase which become trapped outside the main nuclear body (**figure 4.2b**)[349].

It has been shown that prolonged treatment with nocodazole can cause DNA damage due to a long-term arrest in mitosis[350–352]. It will be important for down-stream experiments that DNA damage caused by the chromosome missegregation strategy is minimised so aneuploidy-related, not DNA damage-related, phenotypes are elucidated.

Anticipating that DNA damage would be elevated following a 16-hour nocodazole treatment, an additional experiment was included where cells had been pre-synchronised at the G_2/M checkpoint by 14-hour small-molecule inhibition of CDK1 (using RO-3306) followed by a short 2-hour nocodazole treatment (referred to as 14r+2n herein)[353,354]. Following arrest, cells were washed in fresh media to remove nocodazole and allowed to proceed through the cell cycle for 24 hours before analysis.

Basal levels of micronuclei in control cells were low (**figure 4.2c**). Treatment of RPE-1 cells with nocodazole for 2 hours did not significantly increase aneuploidy compared to the untreated control. Following 16 hours nocodazole wash-out, chromosome missegregation was significantly elevated, in-line with the literature (***p<0.001)[337]. Pre-synchronising cells at G_2/M followed by 2-hours nocodazole wash-out (14r+2n) significantly elevated chromosome missegregation above 2-hour treatment alone and to approximately similar rates as for 16-hour nocodazole treatment (***p<0.001).

These data confirm that I are able to induce chromosome missegregation using small molecule inhibitors of the cell cycle. Importantly, it is possible to significantly elevate aneuploidy following a short (2-hour) nocodazole wash-out by pre-synchronising cells at the G_2/M boundary, which I anticipate to be important to minimise DNA damage.

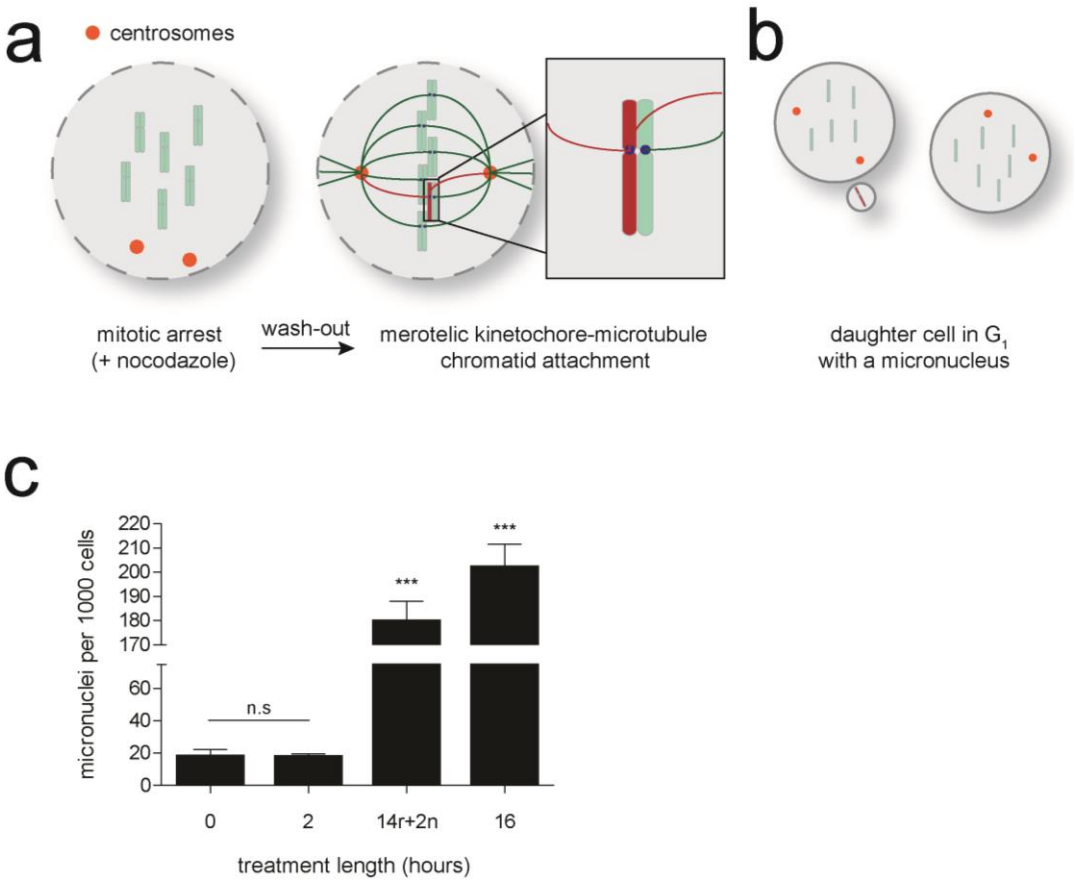

Figure 4.2. Micronuclei formation rates following nocodazole wash-out. (a) Treatment with the microtubule spindle poison nocodazole leads to mitotic arrest due to a failure to assemble a mitotic spindle. Following nocodazole wash-out, chromosomes form merotelic attachments on the spindle. (b) Micronuclei are extra-nuclear compartments containing whole chromosome or chromosome fragments which arise following a faulty mitosis. (c) Micronuclei rates are elevated following a faulty mitosis induced by 14r+2n and 16 hours nocodazole. One-way ANOVA with Tukey's post-hoc multiple comparison; ***p<0.001.

4.1.2. DNA damage in nocodazole-arrested cells

As described above, DNA damage occurring during induction of chromosome missegregation is deleterious to my experimental strategy, resulting as a consequence of a prolonged mitotic arrest and should be therefore be minimised. To quantify DNA damage levels in each condition, the extent of DNA damage was determined by immunofluorescent staining of γ-H2AX, a phosphorylated histone H3 variant that is incorporated at sites of DNA damage[355–357]. Cells were deemed to be positive for DNA damage if they contained three or more discreet γ-H2AX foci, as previously described[226].

Nocodazole treatment for two hours did not significantly elevate DNA damage in prometaphase RPE-1 cells above the untreated control (**figure 4.3a and 4.3b**). Extended treatment with nocodazole for 16 hours significantly increased unresolved DNA damage at prometaphase, in line with the literature (***$p<0.001$)[350–352,358]. Importantly, pre-synchronising cells at G_2/M before a 2-hour nocodazole treatment did not elevate DNA damage; conversely, a small decrease was observed, although this did not reach significance. This slight decrease in DNA damage may reflect a longer time in G_2 to correct errors that occurred during DNA replication[359]. Importantly, pre-synchronising cells before 2-hour nocodazole wash-out reduced DNA damage to levels comparable to that observed in the untreated control cells (**figure 4.3a and 4.3b**). This demonstrates that the induction of chromosome missegregation can be uncoupled from drug treatment-induced DNA damage in RPE-1 cells.

In practise, despite the concomitant elevation of DNA damage, the 16-hour nocodazole treatment is a more cost effective and efficient means of elevating chromosome missegregation. Therefore, during some of the optimisation steps below, I continue to use this treatment. However, during isolation of aneuploid cells for further downstream analysis in future experiments I will pre-synchronise cells

before nocodazole treatment using RO-3306 to minimise DNA damage, ensuring I can analyse nascent responses specific to aneuploidy and not DNA damage.

4.1.3. Centromere signal in the micronucleus

DNA which is missegregated is broadly categorised into two groups: whole chromosomes and acentric chromosome fragments[360–362]. Micronuclei can therefore contain either whole chromosomes (positive for centromere staining) or partial chromosomes (lacking centromeric staining). Ideally, my experimental outline is to investigate the response to whole-chromosome aneuploidy. To determine the induction of whole-chromosome aneuploidy, untreated and nocodazole-treated RPE-1 cells were stained with an anti-CREST antibody, marking the kinetochore and therefore centromere of each chromosome, and percentage of CREST-positive micronucleI was quantified 24 hours after nocodazole wash-out. This allowed the percentage of whole chromosomes in the micronuclei to be quantified.

In untreated cells, 42 % of micronuclei contained at least one CREST signal (**figure 4.3c and 4.3d**). Following 2-hour nocodazole wash-out the percentage of whole-chromosomes entrapped in a micronucleus was not significantly different ($p=0.36$). After an extended mitotic arrest with 16-hour nocodazole, all micronuclei contained at least one CREST signal (***$p<0.001$). Interestingly, 14r+2n was intermediate, with 57.5 % of micronuclei containing whole chromosomes, potentially reflecting the increased likelihood of whole chromosomes being missegregated following DNA damage in 16 hours nocodazole rather than an artefact of synchronising cells[363].

Therefore, elevating missegregation using 14r+2n generates a mixed population of whole-chromosome and partial-chromosome aberrations and should be considered when analysing in down-stream applications.

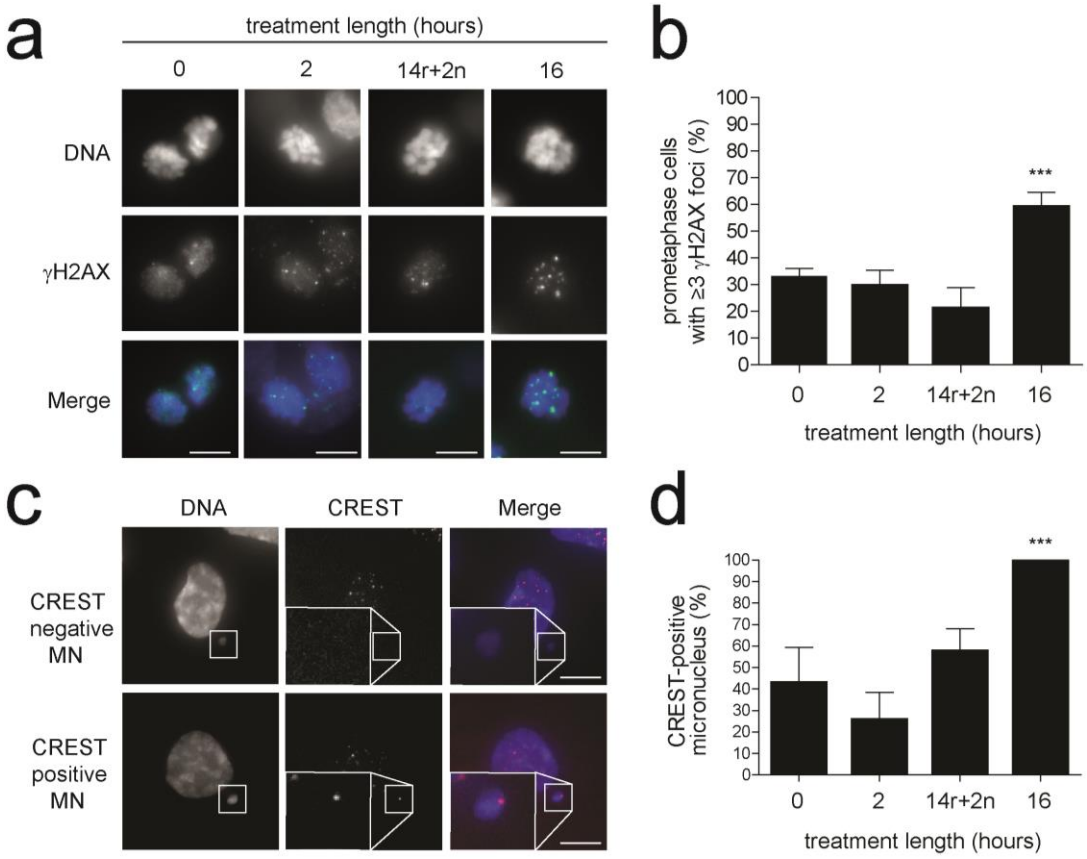

Figure 4.3. Prometaphase DNA damage and micronuclei characterisation following nocodazole wash-out. (a & b) DNA damage is increased in prometaphase cells arrested in mitosis by extended nocodazole (16 hours, ***p<0.001) but not a 2-hour nocodazole arrest in synchronised cells (14r+2n). (c & d) Whole-chromosome missegregation was identified using a centromeric stain, CREST, at 24 hours following nocodazole wash-out. The percentage of CREST-positive micronuclei (MN) was elevated following 16 hours nocodazole but not for any other treatment. Inset: CREST negative and positive micronuclei. Boxes: Micronucleus. One-way ANOVA with Tukey's post-hoc multiple comparison; ***p<0.001. Scale bars: 15 μm.

4.1.4. p21 and p53 nuclear stabilisation following chromosome missegregation

It has been shown that, following chromosome missegregation, p21 and p53 are stabilised in the nucleus and limit the proliferation of aneuploid cells by inducing cell-cycle arrest[180,337,364,365]. I hypothesised that populations of RPE-1 cells with an assortment of aneuploidies would stain positive for nuclear p21 and p53, and could therefore be isolated by fluorescent activated cell sorting – thereby providing an alternative strategy to that proposed in the primary experimental outline, should it prove difficult to execute (**figure 4.4a *cf*. figure 4.1**).

The nuclear stabilisation of p21 and p53 in control and nocodazole-treated RPE-1 cells was analysed 24 hours following drug wash-out. Cells were classified by the presence of a micronucleus (MN), indicating that chromosome missegregation had occurred in the preceding anaphase[366]. The sister of a cell that harboured a micronucleus was identified by proximity and classified as MN-positive, as it would have a high chance of aneuploidy, where an MN represents a change in chromosome number.

To analyse every cell in the image set, a macro was written for ImageJ which would automatically quantify the p21 and p53 nuclear staining intensity, therefore reducing the requirement for time-intensive manual analysis (**figure 4.4b** & **chapter 10.1.1**).

Chromosome missegregation induced by 16-hour nocodazole wash-out significantly increased nuclear p21 and p53 stabilisation in micronuclei-positive cells, as expected (**figure 4.4c-e**, ***$p<0.001$). Interestingly, micronuclei-positive (MN+) cells following 14r+2n did not show significantly elevated p21 or p53 stabilisation compared to the internal control cells without micronuclei (MN-). However, it is still unclear from this experiment whether p21 and p53 are stabilised in the nucleus as a response to aneuploidy or the DNA damage induced under these conditions. In

MN+ cells following 14r+2n, where DNA damage is abrogated, no p21 or p53 stabilisation was observed which suggests that this approach cannot be used to differentiate between diploid and aneuploid cells, without significant DNA damage artefacts at this time point. Therefore, below I continue optimising the reporter chromosome-based approach for aneuploidy detection.

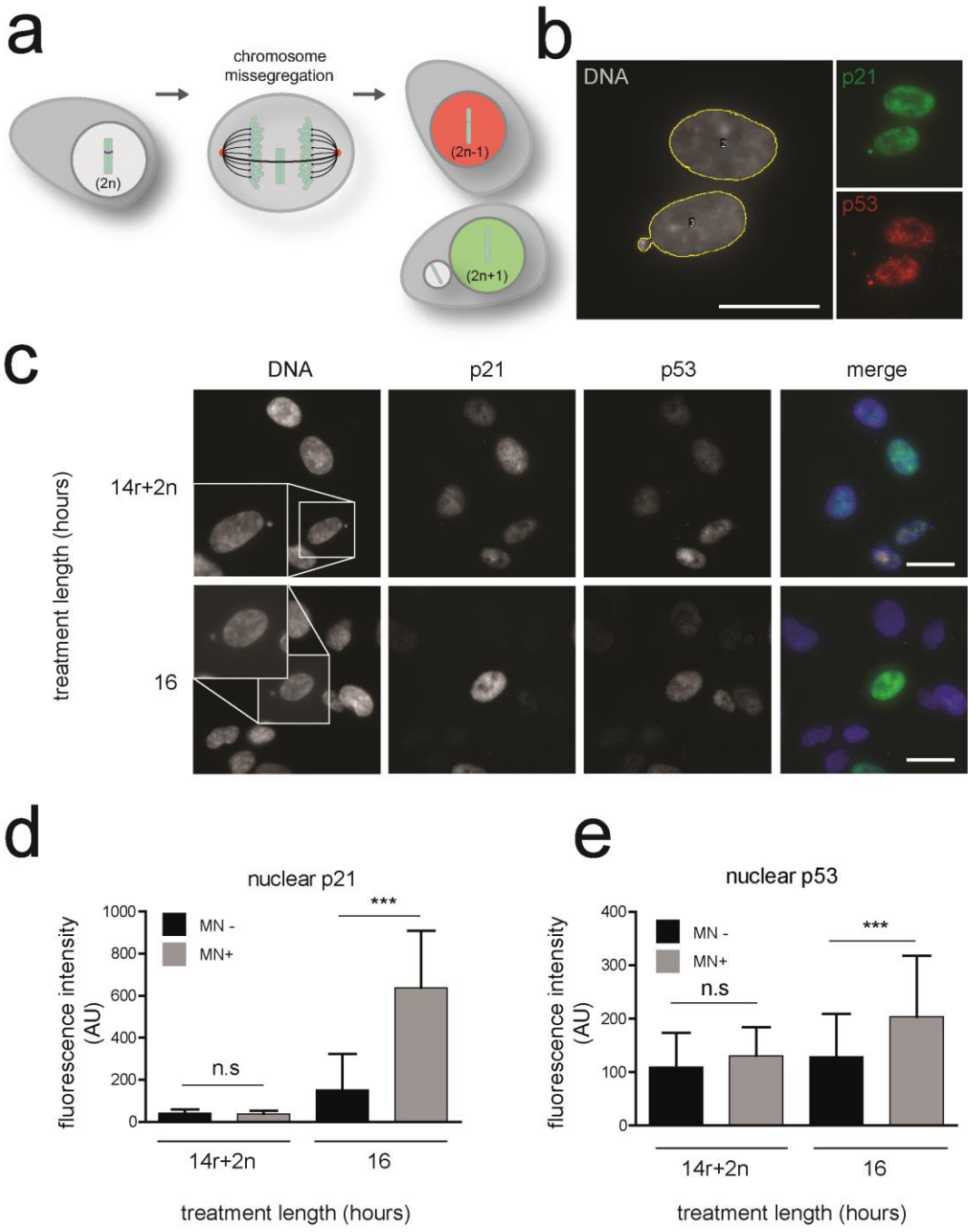

Figure 4.4. p21 and p53 nuclear stabilisation following nocodazole wash-out. (a) Nascent aneuploid cells have been shown to stabilise p21 and p53 in the nucleus[337]. (b) An automated image analysis tool to quantify nuclear p21 and p53. (c, d and e) Micronuclei-positive cells were also positive for p21 and p53 following 16-hour nocodazole arrest (***p<0.001). AU: arbitrary units. One-way ANOVA with Tukey's post-hoc multiple comparison; ***p<0.001. Scale bars: 50 µm.

4.2. Generating RPE-1-hTERT cells expressing *dsEGFP*

4.2.1. Construction of a mammalian expression vector harbouring *dsEGFP*

To isolate aneuploid cells requires rapid EGFP turn-over following reporter chromosome loss. However, EGFP is a very stable protein, with a half-life of over 24 hours, therefore I have taken advantage of a destabilised-EGFP (dsEGFP) protein which has a C-terminal Mouse Ornithine Decarboxylase (*ODC1*) domain which targets EGFP for rapid proteasome-mediated degradation (**figure 4.5a**)[367–369].

A plasmid cassette harbouring *dsEGFP*, a kanamycin antibiotic resistance gene and a selectable Geneticin (G418) resistance gene was designed (**chapter 3.3.1 and 3.3.2**). The identity of the resulting plasmid (pSMC50) was checked by restriction digestion using NheI and NotI that produced bands of the expected sizes (3879 bp and 843 bp, **figure 4.5b**), confirming the successful generation of the expression construct.

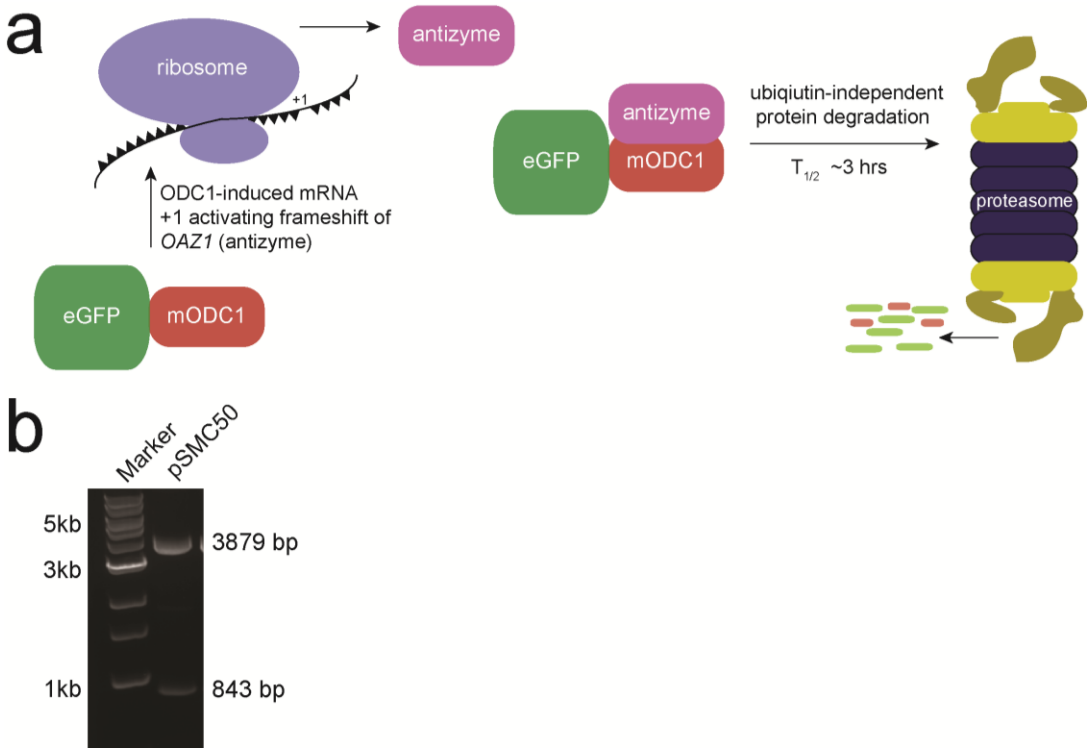

Figure 4.5. Generating a destabilised *EGFP* expression cassette. (a) The mouse ornithine decarboxylase domains (mOCD1)-tagged green fluorescent protein (EGFP) should be rapidly degraded by proteasomal targeting. (b) Successful expression cassette plasmid generation was confirmed by agarose gel electrophoresis, producing bands at 3879 bp and 843 bp when digested with NotI and NheI. Ladder: 1 Kb.

4.2.2. Inserting the *dsEGFP* gene into RPE-1 cells

To maximise the chances of integration into a single chromosome, RPE-1 cells were transfected with a dilution series (1µg, 500ng, 200ng and 100ng) of plasmid DNA. To isolate cells which had stably taken up the plasmid, cells were re-plated at low density and treated with Geneticin for 10 days. Geneticin is an antibiotic which is broken down by a selectable marker on the pSMC50 plasmid cassette – neomycin[370]. Following selection, the only plate with single-cell colonies arose from RPE-1 cells transfected with 1µg plasmid DNA, suggesting that these population had taken up the plasmid. A total of five clones were isolated, RPE-1-[1-5], expanded over 14 days, and characterised for expression of *dsEGFP*.

By conventional fluorescence microscopy the EGFP signal was faint, but visible in RPE-1 clones. RPE-1 clones 1, 2, 4 and 5 expressed *dsEGFP* to similar degrees by fluorescence microscopy (control; **figure 4.6a**). No detectable EGFP signal was observed in clone 3.

To confirm the proteasome dependency of EGFP degradation, and more easily visualise *EGFP* expression conclusively, each clone was treated with MG132, a small-molecule inhibitor of the proteasome, for 24 hours[371]. As expected, apart from clone 3 which remained negative, EGFP fluorescence intensity increased in each clone following proteasome inhibition, confirming the proteasome dependency of the mODC1 domain (**figure 4.6a and 4.6b**).

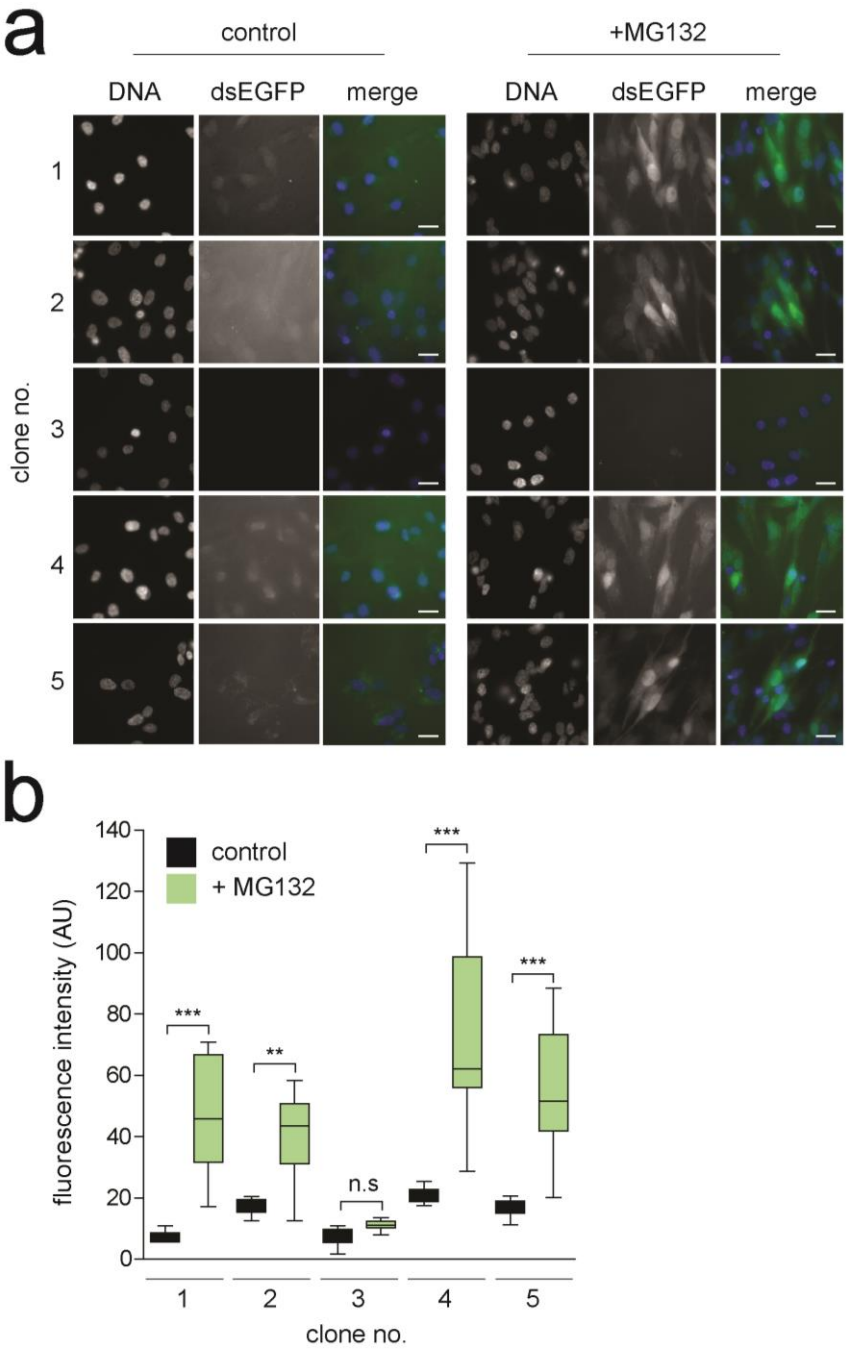

Figure 4.6. Proteasome inhibition in RPE-1 clones. Five RPE-1 clones were isolated and expanded. (a & b) Following treatment with MG132 for 24 hours, to inhibit the proteasome, four out of five clones were positive for EGFP. Contrast for images are the same row-wise (not column-wise) for each clone. Two-tailed t-test assuming unequal variance; **p<0.01, ***p<0.001). AU: arbitrary units. Scale bars: 50 µm.

4.2.3. Determining the half-life of dsEGFP in RPE-1 cells

The half-life of dsEGFP in RPE-1 cells is an important parameter to determine, as rapid EGFP turnover is required to isolate aneuploid cells in the few hours following chromosome loss. RPE-1 clone 4 (RPE-1-4) was initially chosen for further analysis as the cellular morphology was the most consistent with the parental RPE-1 cells by phase-contrast and fluorescence visual inspection. To obtain a first estimation of EGFP half-life, RPE-1-4 was treated with a time-course of the proteasome inhibitor MG132 over 24 hours. As expected, EGFP fluorescence increased progressively with MG132 treatment time, doubling in intensity every ~ 4 to 6 hours (**figure 4.7a and 4.7c**).

To confirm the half-life of dsEGFP, using a population-based assay in thousands of cells, RPE-1-4 cells were treated with a time-course cycloheximide. Cycloheximide is a small-molecule inhibitor of protein synthesis, which blocks translation elongation by interfering with a critical ribosomal mRNA-binding pocket[372]. Following cycloheximide treatment EGFP fluorescence decay was measured by flow cytometry. The half-life of dsEGFP was determined to be ~4.5 hours in RPE-1-4 cells, compared to over 24 hours for regular EGFP (**figure 4.7b and 4.7d**)[367–369].

The rapid turnover of dsEGFP (and therefore fluorescence in cells which lose the reporter chromosome) should be permissive for the isolation of EGFP-negative cells by fluorescence-activated cell sorting, for use in down-stream experiments.

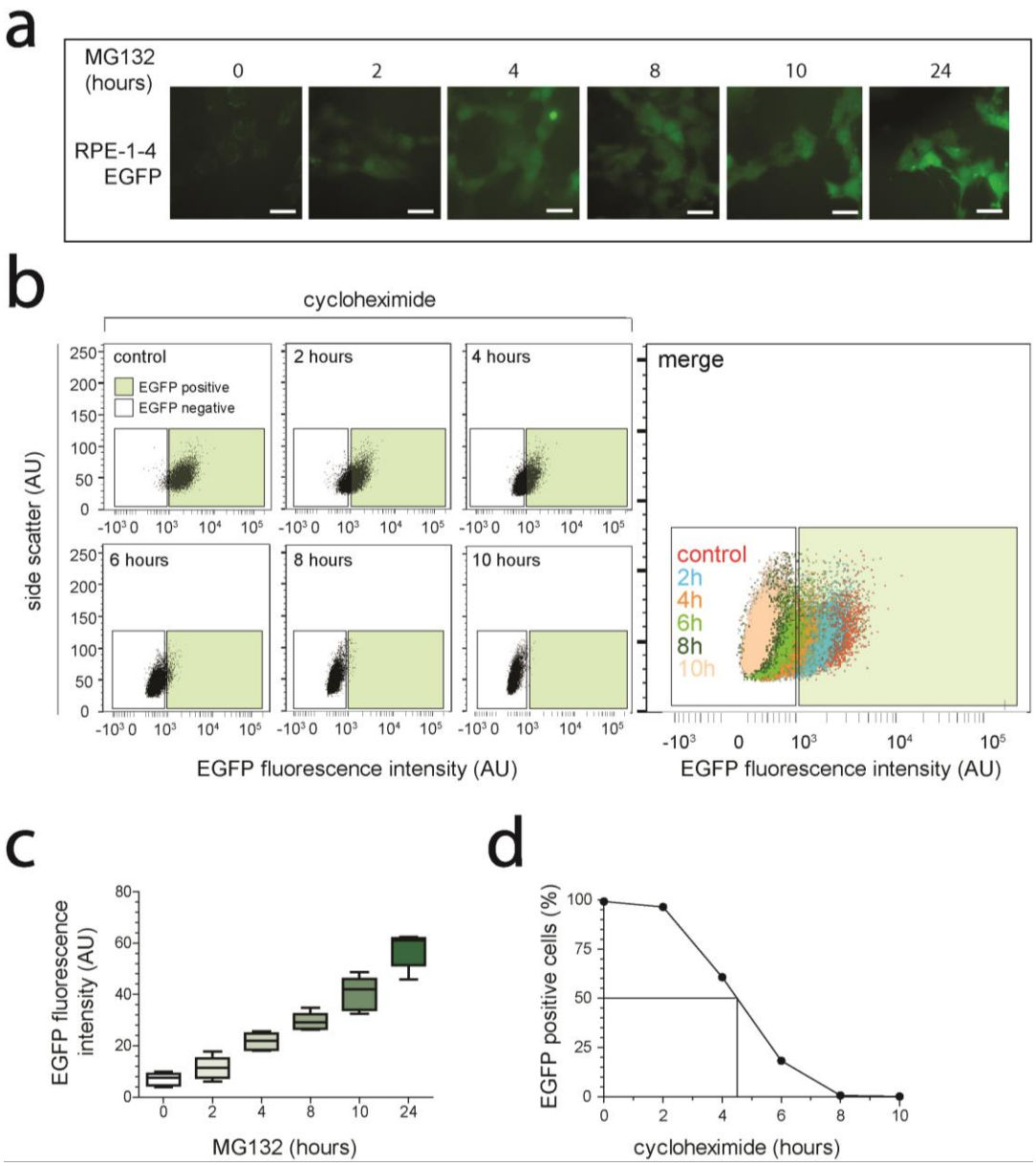

Figure 4.7. Characterising the half-life of dsEGFP in RPE-1-4. RPE-1-4 was phenotypically the most similar to the parental RPE-1 cell line. (a and c) A time-course of MG132 proteasome inhibition in RPE-1-4 increased EGFP fluorescence intensity (arbitrary units; AU). (b & d) Treatment with the protein synthesis inhibitor cycloheximide revealed the dsEGFP half-life to be ~ 4.5 hours in RPE-1-4 by flow cytometry (n=10,000 cells, from a single experiment). AU: arbitrary units. Scale bars: 50 µm.

4.2.4. Sorting RPE-1-4 cells by flow cytometry

To enable a clear separation between the EGFP-negative and positive cells in subsequent experiments, RPE-1-4 cells expressing the highest 20 % EGFP fluorescence (named RPE-1-4F herein) were collected by fluorescence-activated cell sorting (FACS) and used for down-stream experiments (**figure 4.8**).

To sort single RPE-1-4 cells by flow cytometry a hierarchical gating strategy, which measures parameters of each cell as it passes through the capillary-flow chamber, was used. Parental RPE-1 cells were used to set the reference voltage for the laser that excites EGFP (B530/30-A) so that, on a logarithmic scale of arbitrary fluorescence intensity, cells fluoresced with a maximum intensity of 10^3 EGFP arbitrary units (AU). This is important as cells from clones RPE-1-4 which fluoresced greater than this could be easily identified and represented at least a doubling in EGFP signal. Single, EGFP-positive cells were sorted using by FACS using a BD FACSAria II (BD Biosciences) and re-cultured for down-stream applications.

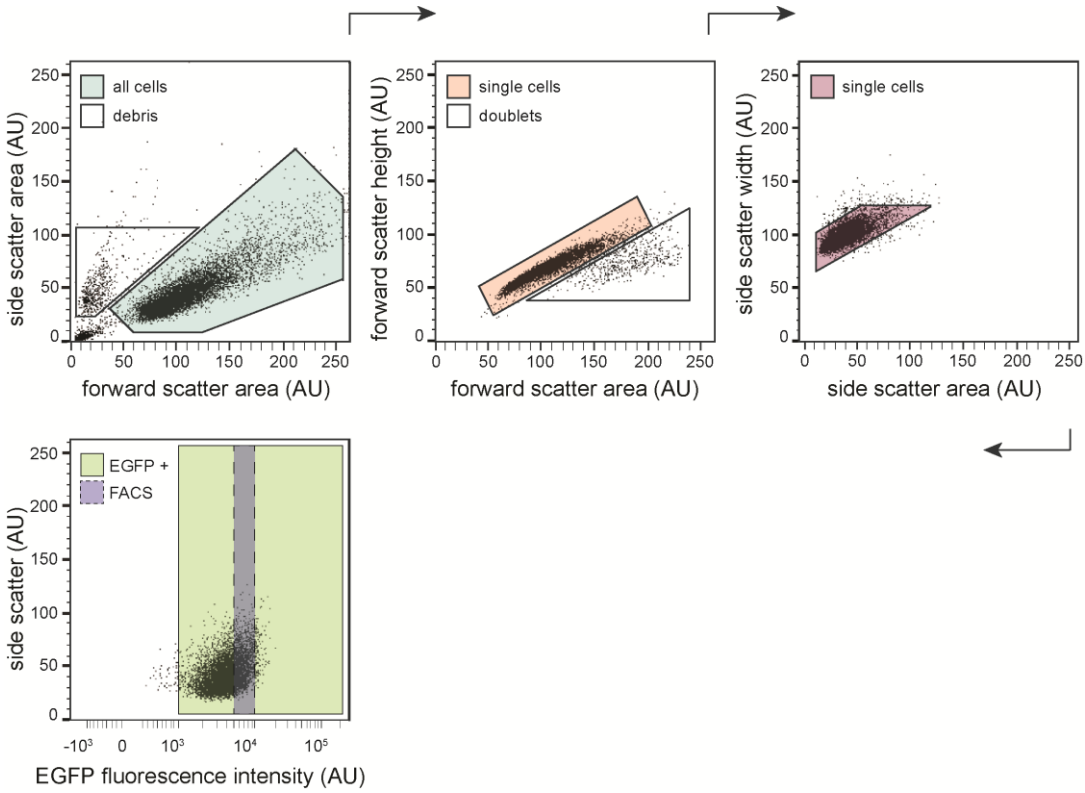

Figure 4.8. Sorting a pure population *dsEGFP*-expressing RPE-1-4 cells. A narrow window of RPE-1-4 cells were sorted by fluorescence-activated cell sorting (FACS) to ensure there were no EGFP-negative cells contaminating the cell line (subsequently: RPE-1-4F). Single, EGFP-positive RPE-1-4 cells were isolated by ensuring cellular debris, doublets and EGFP-negative cells were excluded by a hierarchical gating strategy. AU: arbitrary units.

4.3. *dsEGFP* is expressed from a single chromosome in RPE-1-4F cells

To isolate nascent populations of cells which are aneuploid for a single chromosome necessitates the *dsEGFP* gene be exclusively expressed from a single chromosome. To determine if RPE-1-4F was expressing *dsEGFP* from a single chromosome, several approaches to interrogate the chromosome insertion frequency, as well as insertion locus/loci, of the *dsEGFP* gene were attempted (Southern blot, inverse-PCR, digoxygenin-labelled custom DNA probes). The only method with which I were able to successfully determine chromosome insertion frequency was fluorescence *in situ* hybridisation.

4.3.1. Enumerating *dsEGFP* integration frequency by FISH

Fluorescently-labelled DNA probes complementary to the original plasmid, harbouring the *dsEGFP* gene sequence, were generated which would hybridise to the *dsEGFP* gene when performing fluorescence *in situ* hybridisation (FISH) on interphase cells and metaphase spreads. By co-hybridising with known centromere enumeration probes (CEP), the number of chromosomes containing the *dsEGFP* gene in RPE-1-4F cells could be determined. The successful *dsEGFP* probe-labelling reaction was confirmed by spectrophotometry (**figure 4.9a**).

FISH was performed on interphase cells and metaphase spreads from RPE-1-4F cells, co-staining for unique centromeres and the *dsEGFP* gene. A clear fluorescent signal was observed, suggesting that the FISH procedure was working as expected. Importantly, the *dsEGFP* gene had integrated into a single chromosome, as evident by the presence a single *dsEGFP* focus in interphase cells and two foci on replicated sister chromatid arms in metaphase spreads (**figure 4.9b and 4.9c**).

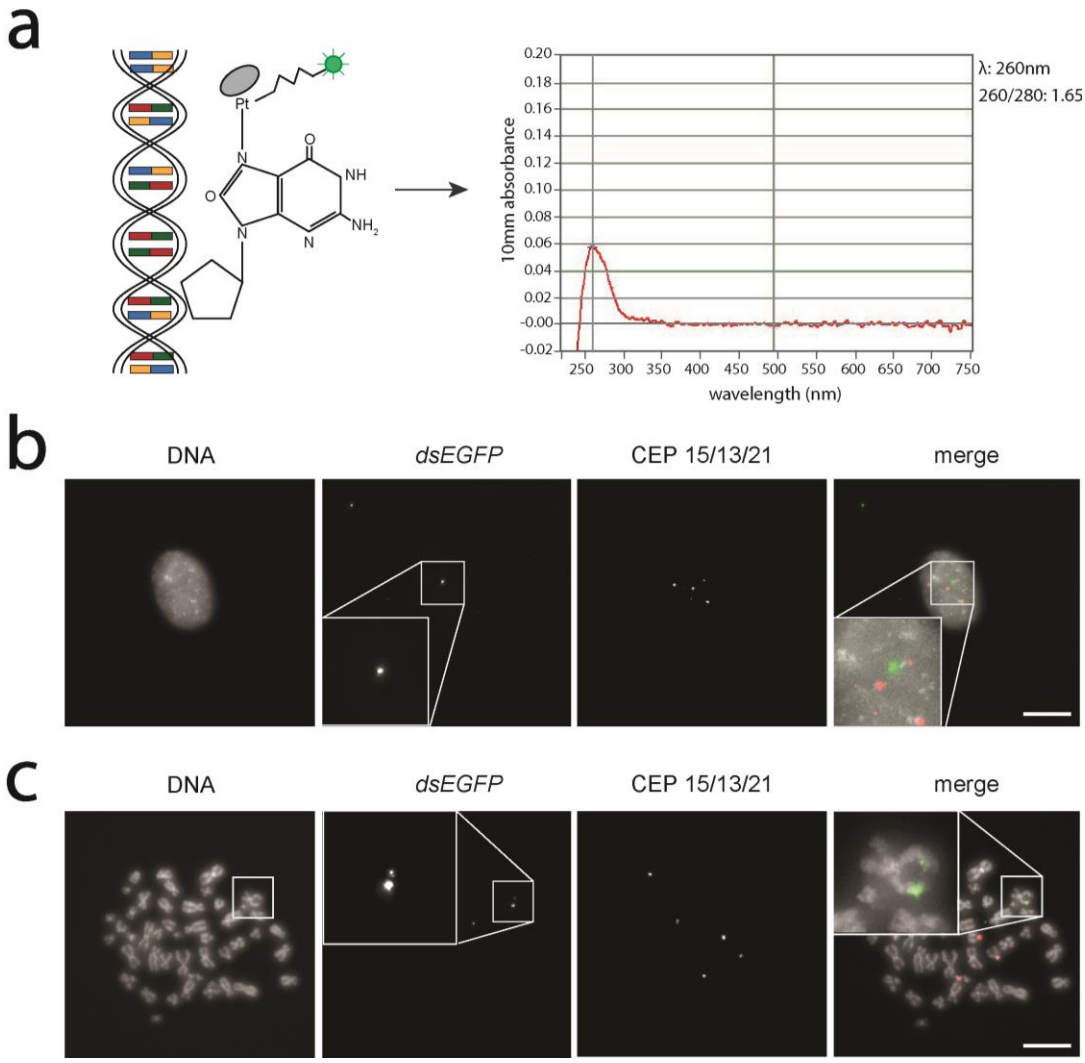

Figure 4.9. The *dsEGFP* gene integrated into a single chromosome in RPE-1-4F cells. (a) DNA probes conjugated with Alexa-488 dye were generated and the probe quality checked by spectrophotometry. (b) Fluorescence *in situ* hybridisation (FISH) with *dsEGFP* probes and known centromere enumeration probes (CEP; chromosomes 15, 13 and 21) revealed a single integration in interphase cells. (c) FISH on metaphase spreads confirmed the *dsEGFP* gene had integrated on the distal q-arm of an unidentified chromosome. (c, inset) One signal could be observed on each sister chromatid as expected following DNA replication. Scale bars: 30µm.

4.4. Summary

Here I have optimised a drug-induced chromosome missegregation strategy and generated a fluorescence-based aneuploidy reporter cell line. The main benefit of using the mitotic inhibitor drugs described (sequential RO-3306 synchronisation followed by a short nocodazole wash-out) is that I are able to significantly elevate chromosome missegregation, without generating DNA damage, in a cell line with otherwise low spontaneous aneuploidy rates. Moreover, the rapid loss of EGFP fluorescence in my single-chromosome aneuploidy-reporter cell line should enable the isolation of monosomic cells by FACS for down-stream experiments.

It is important to highlight that it is still unclear whether there is the potential for EGFP loss by other transcriptional or post-translational mechanisms independent of aneuploidy; or if EGFP signal is lost during apoptosis. Therefore during my analysis in chapter 5 I draw particular attention to these caveats where applicable.

5. Isolation and characterisation of monosomic human cells

5.1. Isolation of aneuploid cells by fluorescence-activated cell sorting

To isolate populations of aneuploid cells by fluorescence-activated cell sorting (FACS), RPE-1-4F cells were arrested in mitosis with nocodazole for either 2 hours alone, 2 hours in synchronised cells or 16 hours. Cells which had arrested in mitosis were clearly visible by traditional bright-field microscopy with a characteristic rounded morphology. Mitotic RPE-1-4F cells were harvested by shake-off and allowed to proceed through mitosis into G_1 for 12 hours. This ensures that the vast majority of cells harvested for FACS have been arrested in mitosis by nocodazole, therefore aneuploid cells would not be diluted in a larger number of cells that had not reached mitosis before nocodazole wash-out.

Control and nocodazole-treated RPE-1-4F cells were collected and counter-stained with DAPI, a fluorescent DNA-intercalating dye which does not stain living cells[373]. Counter-staining exclusion is crucial as dead cells no longer express dsEGFP, and would otherwise be erroneously counted and/or sorted as aneuploid.

In control RPE-1-4F, dsEGFP-negative cells occurred in the population at a rate of 0.32 %. This is higher than the expected value of 0.0002 % (the chance of the reporter chromosome missegregating in 1/100 cells) suggesting that a large proportion of untreated GFP-negative cells have lost GFP fluorescence via an aneuploidy-independent mechanism (**figure 5.1a and 5.1b**). Two hours treatment with nocodazole alone did not significantly elevate the rate of report-chromosome missegregation above the untreated control, as expected from observed micronuclei formation rates under these conditions (**figure 4.3c; chapter 4.1.2**). As expected, two hours treatment with nocodazole wash-out in pre-synchronised cells significantly increased the percentage of EGFP-negative cells in the population (***$p<0.01$). Likewise, the percentage of EGFP-negative cells in the population following 16-hour

nocodazole wash-out was significantly greater than the untreated control (***p<0.001).

These data suggest that a prolonged (16-hour), or a short (2-hour in synchronised cells), nocodazole arrest is able to elevate the rate of reporter-chromosome loss in the EGFP-negative population. Due to a wide range of EGFP fluorescence, it was not possible to identify EGFP- double positive cells (with two copies of the reporter chromosome; 2n+1), which would be expected to exhibit approximately twice the EGFP fluorescence of diploid cells. Of note, EGFP-positive cells represent a population in which an assortment of aneuploidies (for unlabelled chromosomes) is likely, and should not be mistaken for completely diploid.

EGFP-negative and EGFP-positive cells were sorted by FACS following both 16-hour and 14r+2n wash-out in this way for the subsequent characterisation experiments described below.

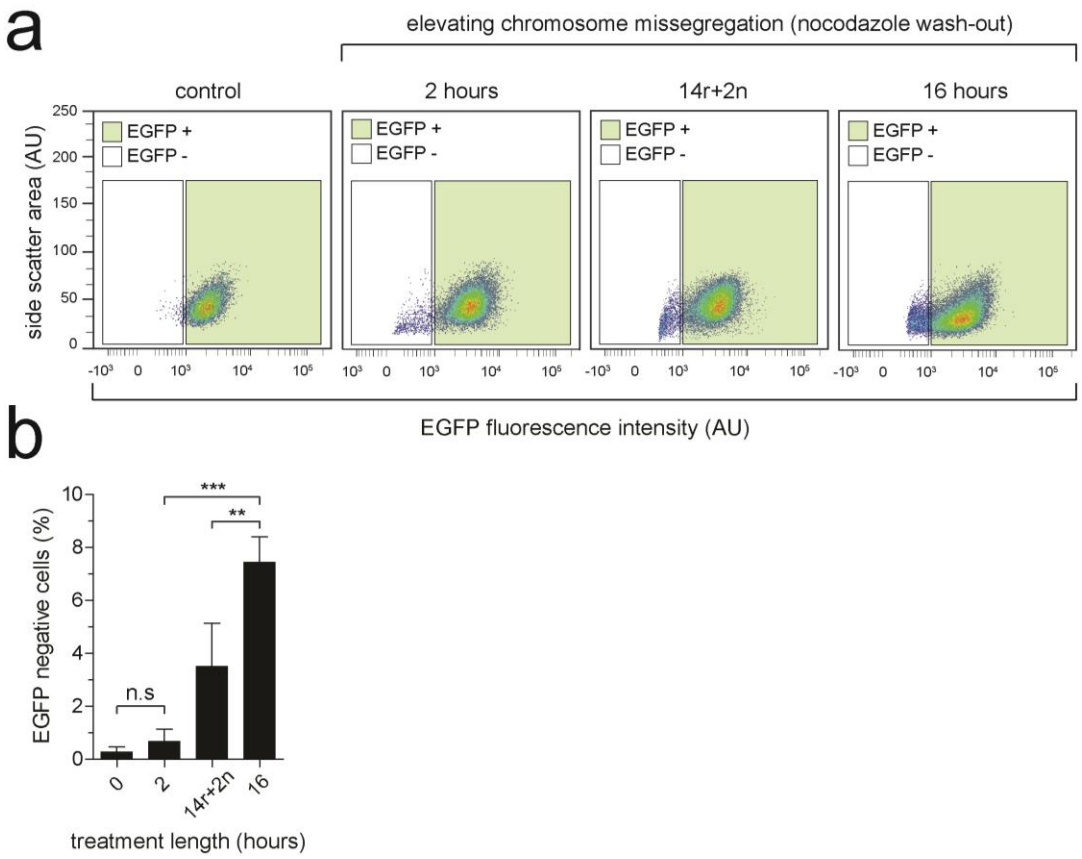

Figure 5.1. The loss of dsEGFP fluorescence following nocodazole wash-out. (a) Aneuploidy, as judged by the loss of dsEGFP expression by flow cytometry, was rare in untreated RPE-1-4F cells (control). The loss of dsEGFP was increased following nocodazole wash-out. (b) Treatment with nocodazole for two hours did not significantly elevate the rate of dsEGFP-negative cells in the population. Elevating aneuploidy by both 14r+2n and 16 hours nocodazole wash-out significantly increased the rate of dsEGFP loss in RPE-1-4F cells. AU: arbitrary units. One-way ANOVA with Tukey's post-hoc multiple comparison; **p<0.01, ***p<0.001).

5.2. Determining the identity of the reporter chromosome

Having isolated EGFP-negative cells, I wanted to identify the reporter chromosome. Given that I had preliminary data suggesting the dsEGFP gene was located on a single chromosome (**see chapter 4.3.1**), it is was likely that EGFP-negative cells were aneuploid for a single chromosome, and so I proceeded with down-stream analyses for confirmation. Unfortunately, temporary problems were encountered with *dsEGFP* FISH probe hybridisation efficiency. Therefore below, I characterise EGFP-negative cells, using alternative strategies, to determine the reporter chromosome identity.

5.2.1. SNP array

Changes in chromosome copy number can be determined by assessing the allelic frequency of single-nucleotide polymorphisms (SNP) – changes to a single base at many susceptible genomic loci[374]. EGFP-positive and negative RPE-1-4F cells sorted by FACS following 14r+2n and 16h nocodazole wash-out were sent for SNP array analysis (Affymetrix). Additionally, control samples from parental RPE-1, untreated RPE-1-4F, HCT116 and HCT116+3 cells were also analysed to calibrate the SNP array sensitivity.

5.2.1.1. HCT116 SNP array

HCT116 cells are a near-diploid, chromosomally-stable human colon carcinoma cell line of male origin that are known to have lost their Y chromosome in ~90% of cells[338]. Accordingly, the SNP array revealed the presence of a single X chromosome (Log_2=-0.5) and complete loss of the Y chromosome (log_2=<1). HCT116 cells are also known to harbour three stable-propagated chromosome translocations on one of each chromosomes 10, 16 and 18 allele (**figure 5.2a**)[276,338]. Comparison between the published karyogram and the SNP array revealed the

translocation on chromosome 10q is a result of short chromosome 10q duplication (log_2=0.5, **figure 5.2b**). The translocated chromosome 16 allele is a large translocation and duplication involving chromosome 8q, visible by the G-banding pattern and amplification of chromosome 8q (log_2=0.5,). Finally, the chromosome 18p translocation results from a duplication of a region at the distal end of chromosome 17q (log_2=0.5). HCT116+3 cells possess a known gene amplification site on chromosome 3q[375]. I were unable to detect the chromosome 3q amplification (log_2<0.5, **figure 5.2c**). These data demonstrate that SNP array is sensitive to whole chromosome copy number alterations and population-wide translocations. However, gene amplifications cannot be detected due to the inherently low resolution of population-based genomic assays.

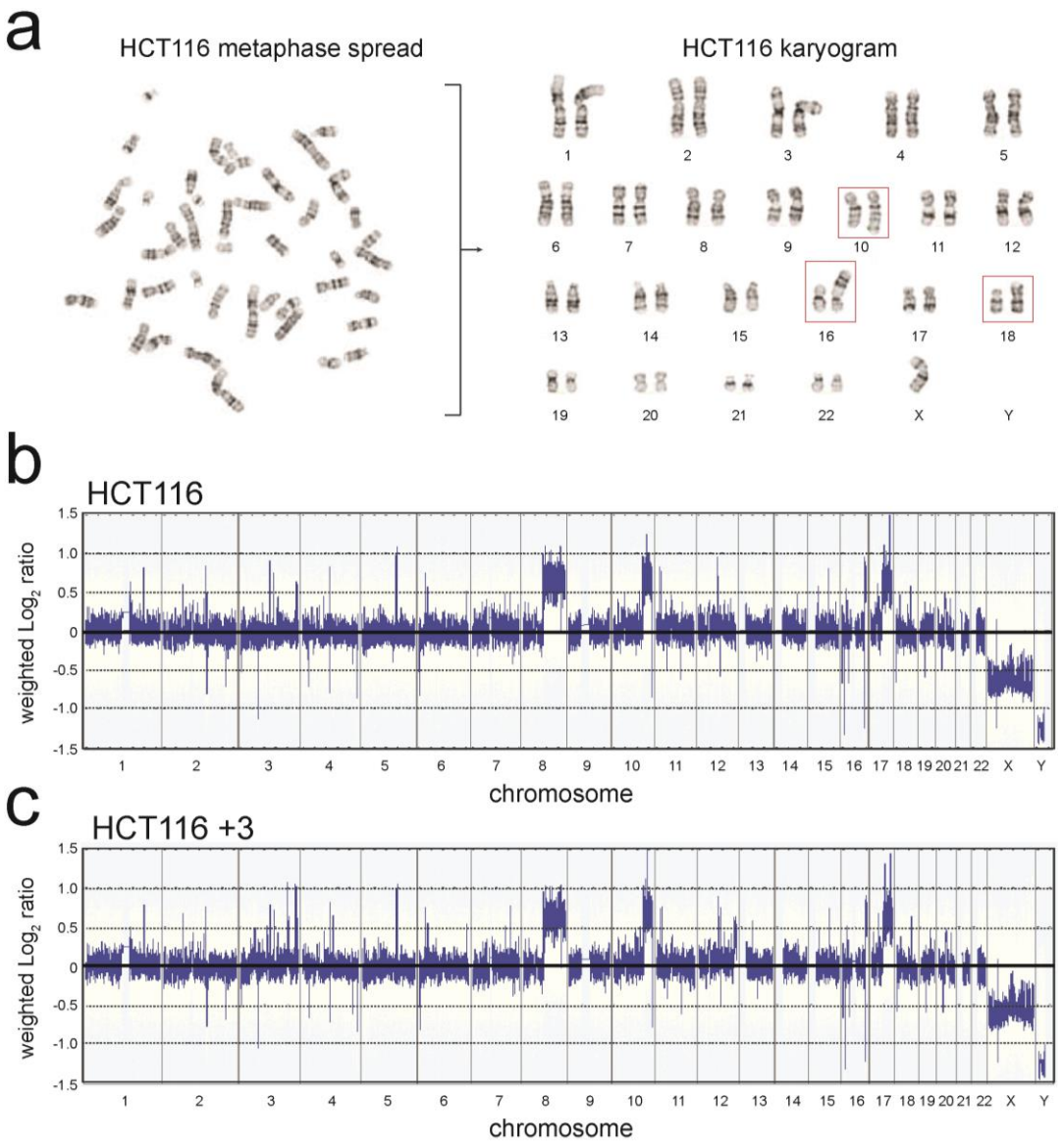

Figure 5.2. HCT116 and HCT116+3 single nucleotide polymorphism array. (a) HCT116 cells are known to harbour three stably propagated translocated alleles[276]. (b) Single nucleotide polymorphism (SNP) array revealed the translocations to be t(10q:10q), t(18q:16p) and t(17q:18p). (c) A sub-clone of HCT116 with a chromosome 3 amplification was undetectable above the level of background noise.

5.2.1.1. RPE-1 SNP array

Parental RPE-1 cells, of female origin, are ostensibly diploid however some isolates are known to display stably-propagated aberrations particularly of chromosomes 10 and 12[336,376]. I were unaware of the additional chromosome 12 aberration in some RPE-1 isolates prior to generating my aneuploid reporter clone (RPE-1-4F) in RPE-1 cells.

SNP array analysis confirmed both gain of chromosome 12 (log_2=0.25) and amplification of chromosome 10q in parental RPE-1 cells (log_2=>0.5; **figure 5.3a**). Fortuitously, in RPE-1-4F cells, the trisomy of chromosome 12 was not observed, suggesting that this clone originated from the small percentage of cells not carrying trisomy 12 in my isolate of RPE-1 cells (**figure 5.3b**). This is important as trisomy 12 in my aneuploidy reporter strategy would have been a direct conflict of the experimental aim – to induce aneuploidy. No other significant gross chromosomal changes were observed.

EGFP-negative RPE-1-4F cells were sorted by FACS following both 14r+2n and 16 hours nocodazole wash-out. The variability in DNA content induced by both treatments was similar (**figure 5.3c and figure 5.3d**). Unfortunately, I were unable to detect a significant change in chromosome copy number in EGFP-negative RPE-1-4F cells by SNP array following either drug treatment. This could reflect the sensitivity of the SNP array to detect changes in whole chromosome copy number where the aneuploidy is not present in every cell, suggesting that my EGFP-negative population is not sufficiently enriched for a specific monosomy above the noise for detection by SNP array. The enrichment of monosomy in the EGFP-negative population, and the level required for SNP array detection, are therefore unclear from this data.

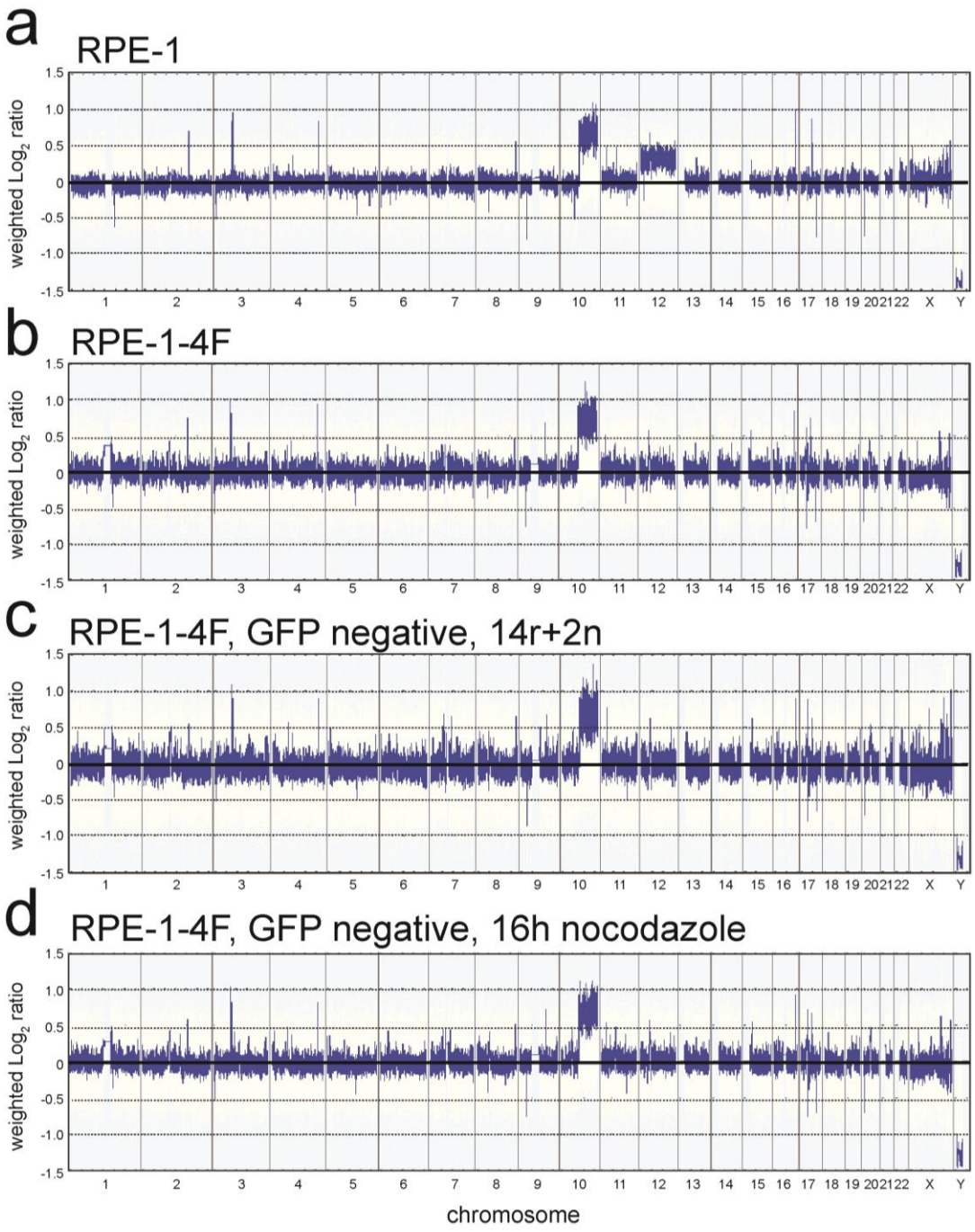

Figure 5.3. RPE-1 single nucleotide polymorphism array. RPE-1 cells were sent for SNP array analysis. (a) RPE-1 parental. (b) RPE-1-4F control. (c) RPE-1-4F, 14r+2n, EGFP-negative. (d) RPE-1-4F, 16 hours nocodazole, EGFP-negative.

5.2.2. Transcriptome analysis

Another approach to determine the elusive reporter chromosome was devised based on gene transcript levels. This approach would serve two purposes – to identify the reporter chromosome and additionally obtain population transcriptome data for EGFP-negative cells. The loss of one copy of a chromosome would be expected to reduce the global mRNA, for the genes encoded by that chromosome, by approximately 50%. This approach makes the assumption that transcription compensation mechanisms would not obscure the data within 12 hours following missegregation; for example by dosage compensation by the alleles from the remaining homologous chromosome, as previously reported in stable aneuploid populations[377,378].

Total RNA was extracted from parental RPE-1, untreated RPE-1-4F, and EGFP-negative and positive RPE-1-4F cells sorted by FACS, to be sent for transcriptome analysis. Initially, RNA extracted from up to 20,000 EGFP-negative cells was insufficient in yield and quality to send for RNA sequencing. To overcome these limitations, the experiment was scaled to enable sorting of ~ 300,000 EGFP-negative, aneuploid cells per experiment. Yields from these larger experiments were sufficient in RNA quality and RNA concentration to send for transcriptome analysis (Affymetrix GeneChip Human Transcriptome Array 2.0).

Data from the transcriptome array were RMA-transformed to correct for background noise and normalise for quantile variation between samples. RMA-transformed data were smoothed by plotting a 1000-point moving average of Log_2 mRNA expression across the genome. Between untreated RPE-1-4F and parental RPE-1 cells there was little variation in gene expression patterns for most chromosomes (**figure 5.4a**). Genes from chromosome 12, however, were significantly down-regulated compared to parental RPE-1 cells as a result of the known trisomy in this cell line, confirming the SNP array observation.

Significant changes in mRNA expression in EGFP-negative, aneuploid cells were observed (**figure 5.4b**). The variation of mRNA expression increased in comparison to untreated RPE-1-4F cells. Additionally, notable differences above this base-line were observed for chromosomes 1q, 5, 6 and 15. Chromosome 1q exhibited a marked drop in expression (up to -15.9 %), chromosome 5 increased (up to +40.39 %), chromosome 6 expression had fallen (up to -28.37 %) and chromosome 15 expression had significantly increased (up to 66.12 %).

These data suggest that the EGFP-negative populations are enriched for monosomy 6 cells, and thus chromosome 6 is a candidate to be harbouring the EGFP transgene. Although monosomy enrichment was sufficient to be observed by transcriptome analysis, monosomy 6 was not enriched enough to be seen by SNP array suggesting that some of the analysis down-stream applies to populations which are not 100 % monosomic. This could further be a consequence of sorting EGFP-negative cells which are not aneuploid, due to a transient loss of EGFP signal or other mechanisms which spontaneously alter EGFP intensity following nocodazole wash-out.

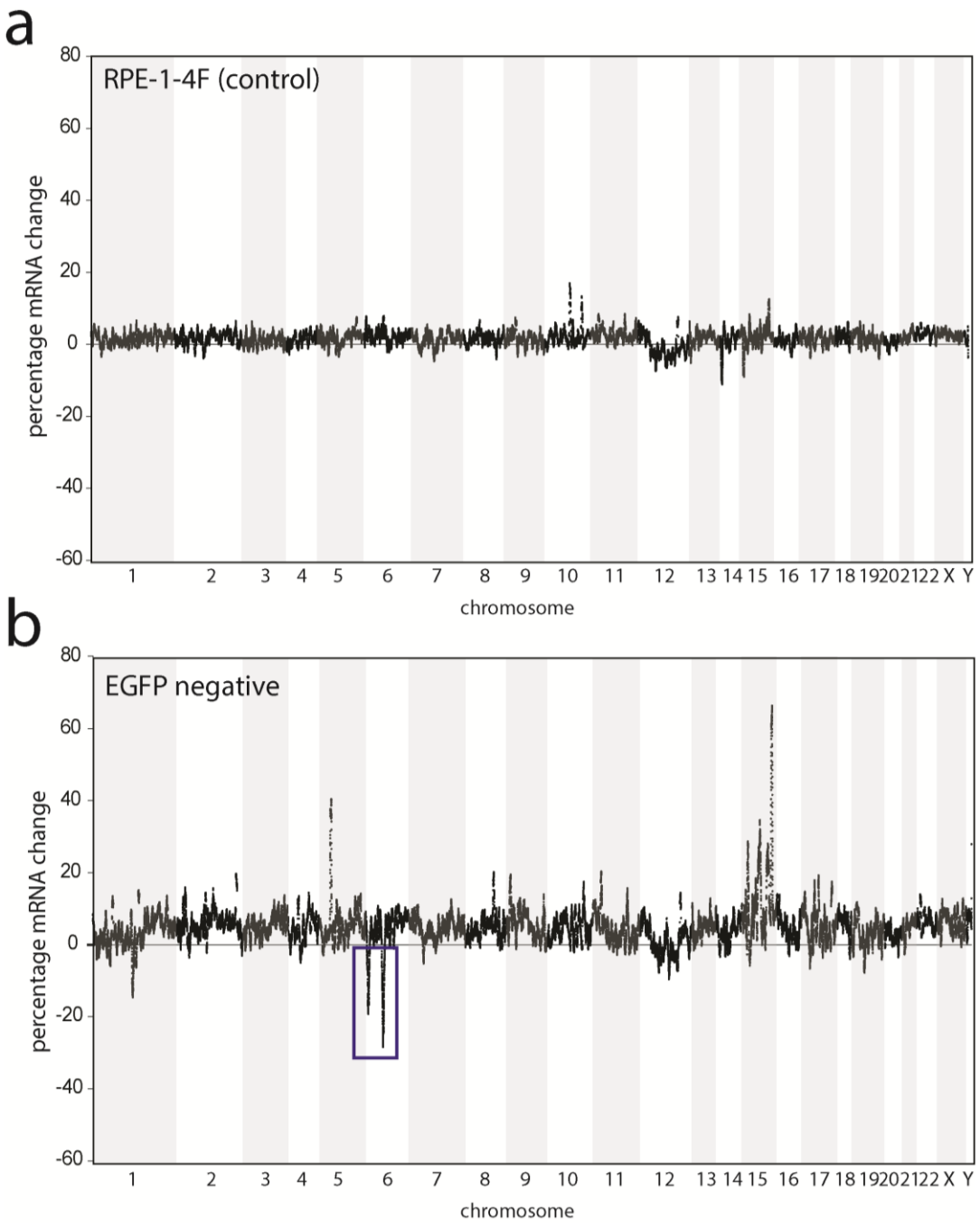

Figure 5.4. RPE-1-4F transcriptome analysis. RPE-1 cells sorted by FACS were sent for transcriptome analysis. (a) RPE-1-4F mRNA normalised to parental RPE-1 global mRNA. No differences were observed for any chromosomes except chromosome 12. (b) RPE-1-4F, 14r+2n, GFP-negative. mRNA were normalised to parental RPE-1. Blue box: chromosome 6 gene down-regulation.

5.2.3. FISH analysis of chromosome 6 in EGFP-negative and positive cells

To confirm the identity of the reporter chromosome, centromeric FISH was performed on EGFP-negative and positive cell sorted by FACS, post-nocodazole treatment. The signal to noise ratio for centromere probes specific to chromosome 6 and a control, chromosome 11, were sufficient to score aneuploidy rates in 1000 cells for each condition.

Importantly, EGFP-positive cells remained largely diploid for both chromosome 6 and chromosome 11 (**figure 5.5 and 5.5b**). Conversely, dsEGFP-negative cells were enriched for cells containing either nullisomy or monosomy 6 (74.9 %), whereas chromosome 11 monosomy remained comparable to the EGFP-positive, diploid cells.

These data suggest that chromosome 6 is the identity of the *dsEGFP* reporter chromosome which is lost in EGFP-negative RPE-1-4F cells post-nocodazole wash-out. However, I could not validate this with SNP array, suggesting EGFP-negative monosomy enrichment needs to be improved. Down-stream analysis of aneuploid cells isolated in this way may be a useful tool for assessing the early responses to aneuploidy in human cells. However, further optimisations of the methods used to induce missegregation (to induce greater whole-chromosome aneuploidy) and ways to enhance monosomy enrichment are required for extensive characterisation using this novel approach. The McClelland lab is currently developing more precise ways to isolate highly-enriched monosomy population for single chromosomes which will augment the data presented below in future experiments.

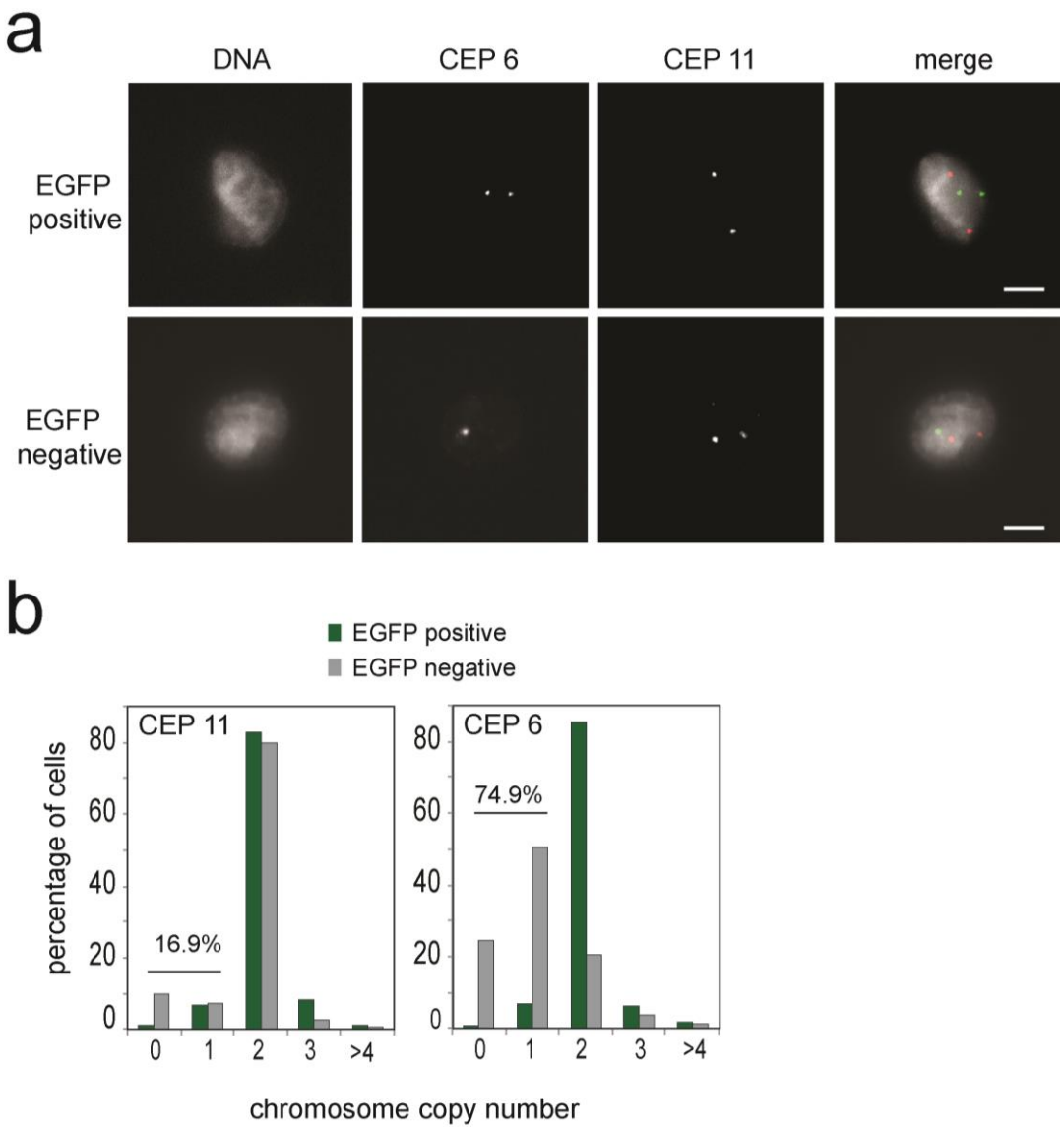

Figure 5.5. Fluorescence *in situ* hybridisation of cells RPE-1-4F cells sorted by flow cytometry. RPE-1 cells sorted by FACS were settled onto glass slides and hybridised with CEP probes. (a) RPE-1-4F dsEGFP positive and negative cells sorted by FACS were stained with chromosome 6 and 11 CEP probes. (b) Chromosomes 6 and 11, in EGFP-negative cells, were lost at a rate of 74.9 % and 16.9 %, respectively. n=1000 cells. Scale bars: 20 µm.

5.3. Characterisation of aneuploid cells

In this section, I begin to characterise the phenotypic responses of non-transformed human cells to chromosome missegregation, albeit from a less than 100 % pure population of cells. Therefore, the data described below are likely to underrepresent the *de facto* responses to monosomy in human cells and form the preliminary basis for further experimentation to validate the data presented in this chapter.

5.3.1. Cell cycle arrest and apoptosis

It is known that non-transformed cells arrest in the subsequent G_1 following chromosome missegregation[337,379–382]. To confirm this phenotype in my aneuploidy-reporter cell line, EGFP-positive and negative RPE-1-4F cells were fixed and stained with DAPI, and the DNA content of single cells analysed by flow cytometry (**figure 5.6a**). EGFP-positive cells showed a cell-cycle profile consistent with that expected for proliferating diploid cells 12 hours following release from mitotic arrest, with the emergence of S-phase and G_2/M peaks (4.99 %). In contrast, EGFP-negative cells had arrested in G_1, as expected, and were not observed at either S or G_2/M (0.00 %).

To determine the survival rate of aneuploid human cells, EGFP-positive and negative cells were seeded at low density and allowed to form colonies over 10 days. The colony outgrowth of the EGFP-negative cells was significantly reduced, as determined by crystal violet staining and absolute colony counts (**figure 5.6b**; **p<0.01). One important consideration is that EGFP-positive cells are not strictly diploid, as a small fraction of cells will also have missegregated unlabelled chromosomes. Therefore these data are more reflective of enriched *vs*. non-enriched aneuploid population survival.

To determine the mechanism(s) of reduced colony outgrowth, EGFP-positive and negative cells were interrogated for markers of apoptosis. Apoptotic cells were identified by the incorporation of DAPI, and the presence of annexinV on the cell membrane, of unfixed samples at 12 and 24 hours post-nocodazole wash-out by flow cytometry[373]. These preliminary data reveal that 36.9 % of EGFP-negative cells were in late apoptosis by 12 hours post-nocodazole wash-out, compared to 0.2 % for the untreated control (**figure 5.6c and 5.6e**). By 24 hours, the fraction of EGFP-negative cells in late apoptosis had decreased to 3.1 % whilst the percentage of dead EGFP-negative cells had risen from 13.8 % to 61.6 %, compared to just 0.8 % for the untreated control (**figure 5.6d and 5.6e**). These data demonstrate that the majority of EGFP-negative cells die via apoptosis within 24 hours of nocodazole wash-out.

Unfortunately, from this experiment alone, the distinction between two main possibilities is still unclear. Are EGFP-negative cells dying via apoptosis *because* they are aneuploid? Or, alternatively, are EGFP-negative cell arising independently of chromosome loss for reasons which are inducing apoptosis (possibly induced by unknown nocodazole-related effects)?

I had already observed ~ 20 % of cells in the EGFP-negative population with a diploid chromosome 6 content, therefore it is not possible to determine the contribution of diploid *vs*. aneuploid cells to the overall apoptotic fraction. The McClelland lab has previously observed aneuploid cells surviving beyond 12 hours following missegregation by live-cell imaging, therefore it is likely that a proportion of the EGFP-negative cells are in late apoptosis (or dead) despite the absence of chromosome missegregation in the preceding anaphase.

However, EGFP-negative cells (although diluted ~ 20 %) may still reveal interesting transcriptome changes occurring in the early response to chromosome missegregation in nascent aneuploid cells. These results are described below.

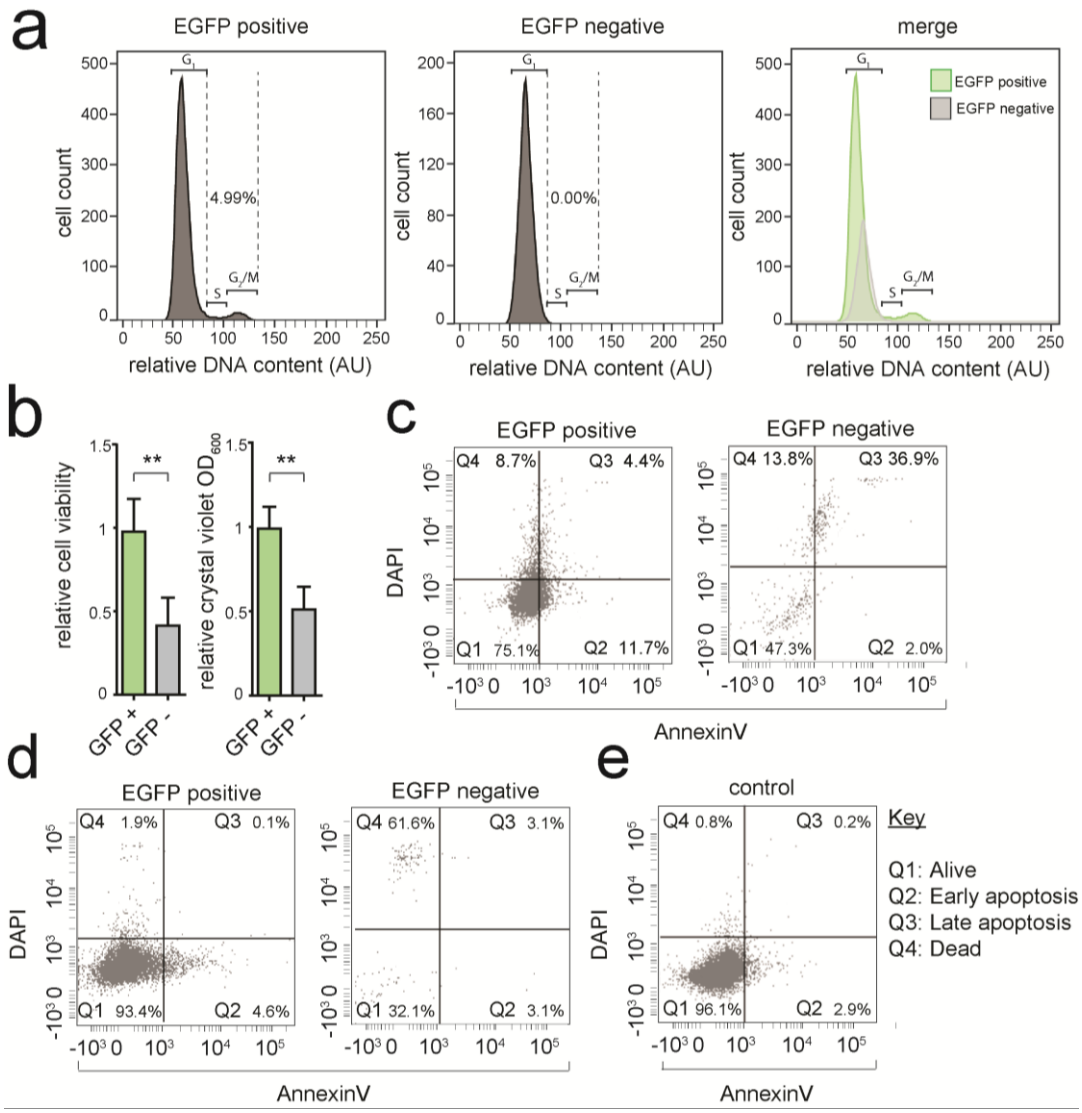

Figure 5.6. The early responses to aneuploidy in RPE-1 cells post-nocodazole wash-out. (a) EGFP-negative populations arrest in G_1 12 hours post-nocodazole wash-out. (b) EGFP-negative cells have significantly reduced colony outgrowth 10 days post-nocodazole wash-out, normalised to post-FACS control RPE-1-4F cells (two-tailed t-test assuming unequal variance; **p<0.01). (c) EGFP-negative populations display apoptosis by 12 hours. (d) Cell death occurs in 61.6 % of EFP-negative cells by 24 hours. (e) Apoptosis in untreated RPE-1-4F cells post-FACS is low. (a, c, d, e; preliminary data; n=10,000 from a single experiment). AU: arbitrary units.

5.3.2. Transcriptome analysis of the early responses to aneuploidy

5.3.2.1. Cell cycle regulators

The transcription level of mRNAs encoding for proteins involved in cell-cycle progression were interrogated by comparison of global mRNA from EGFP-negative cells normalised to EGFP-positive cells (**figure 5.7**). The relative transcriptome changes were normalised on a scale ranging from -4 (red) to +4 (green), where a lower number reflects lower mRNA transcription.

All cyclin-dependent kinases (CDK) associated with progression through the cell cycle were down-regulated, as were their binding targets, for all phases of the cell cycle. Of particular note, transcripts encoding CDK4 and E2F1, required for progression from G_1 through to S-phase, were among those most significantly down-regulated (***$p<0.001$). Additionally, three potent up-stream enhancers of p53 activation namely MDM2, ATM and p300 were significantly elevated ($p<0.01$, $p<0.01$ and ***$p<0.001$, respectively).

These data suggest that the EGFP-negative population is arresting in G_1 through the inhibition of cell cycle progression proteins and down-regulation of the E2F family of transcription factors, required to execute the initiation of S-phase. Moreover, it implies that the earliest responses to aneuploidy involve the upregulation of genes which promote p53 engagement and stabilisation in the nucleus, as previously reported[294]. Interestingly, the expression of p53 was not significantly different in EGFP-negative cells, suggesting that the p53 stabilisation in response to aneuploidy occurs prior to p53 expression changes. This is supported by the observation that MDM2 is upregulated, a known consequence of the negative feedback loop in the MDM2-p53 interaction[469].

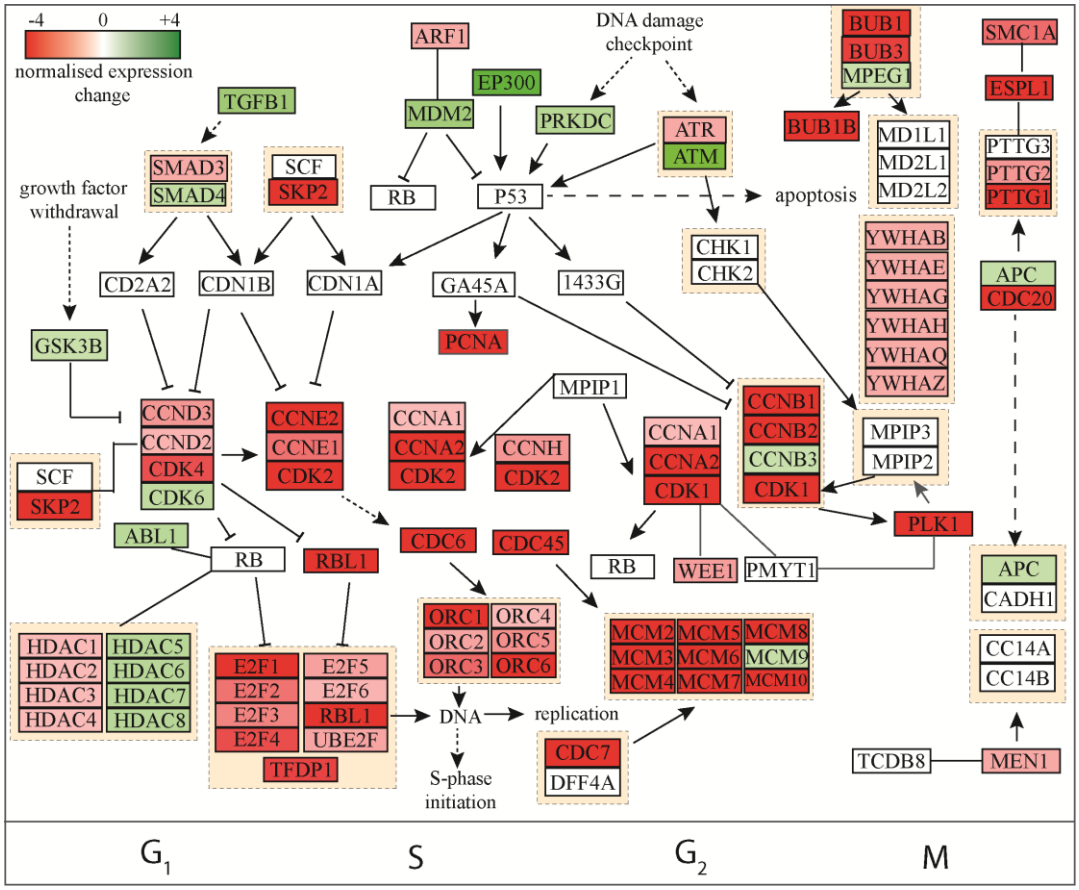

Figure 5.7. Transcriptome analysis of cell cycle proteins in EGFP-negative RPE-1-4F cells. mRNA encoding for proteins involved in the cell cycle were down-regulated in the EGFP-negative population. Increases were observed for *EP300* (p300; ***p<0.001), MDM2 (**p<0.01) and ATM (**p<0.01) suggesting the onset of DNA damage and cell-cycle arrest. Data normalised to EGFP-positive.

5.3.2.2. G1/S checkpoint down-regulation

Of particular interest is the level of transcripts encoding for regulators of the transition from G1 to S phase of the cell cycle. Strikingly, all transcripts coding for pro-cell cycle progression proteins, including E2F transcription factor family proteins and retinoblastoma proteins were significantly down-regulated (**figure 5.8**). Additionally, several proteins required for DNA replication and S-phase execution were significantly down-regulated, most notably POLƐ, MCM2 and RPA2 (***p<0.001). Additionally, there was an increase in transcripts for the cell cycle CDK regulators, CDKN2B (***p<0.001). All members of the origin recognition complex (ORC) family of proteins remained unchanged compared to the untreated control (data not shown).

The effects of these changes are likely to promote a complete cessation of cell cycle progression and engaging the DNA damage response pathway. The upregulation of RPA2 suggests either that a short nocodazole wash-out in synchronised cells is inducing single-stranded DNA formation, or that the link between aneuploidy and the DNA damage response is mediated by RPA2. I propose that the latter is more likely, given that I did not observe significant unresolved DNA damage at prometaphase following a short nocodazole wash-out in synchronised cells (**figure 4.3a and 4.3b; chapter 4**). It is also unclear if some genes may be down-regulated due to haploinsufficiency of the reporter chromosome and it would be important to correct for this in further analysis of these data.

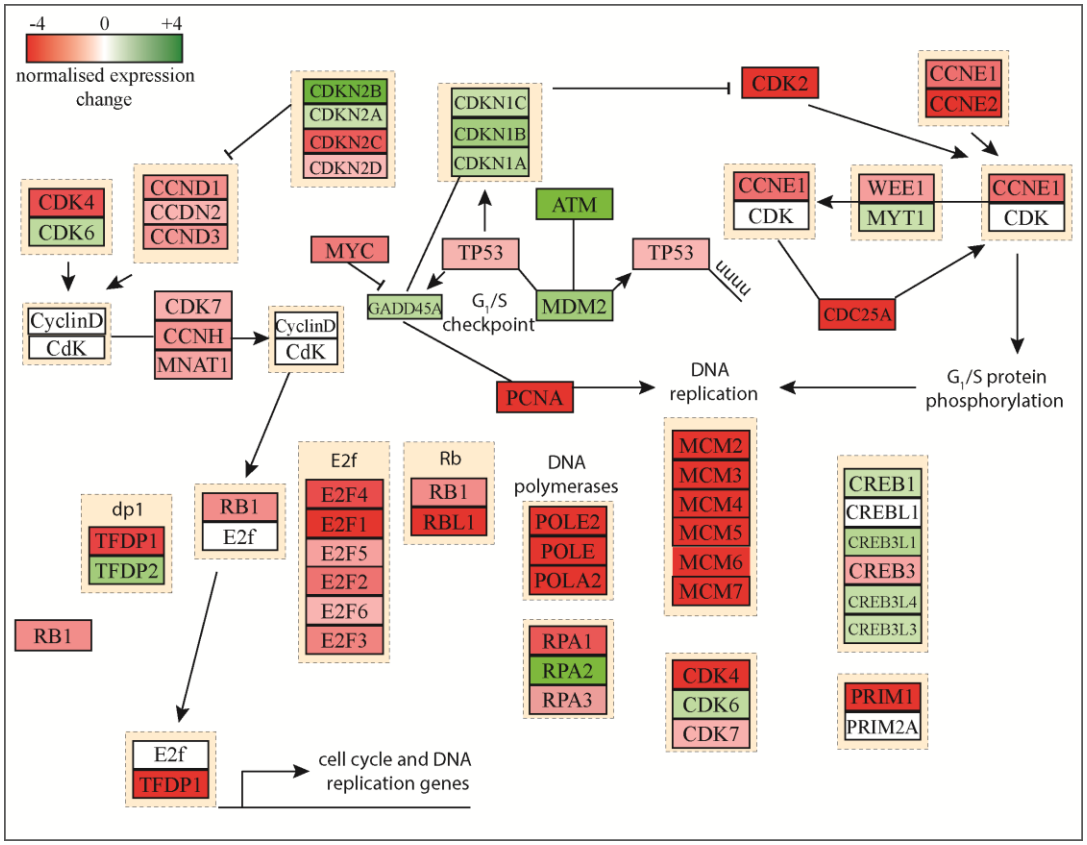

Figure 5.8. Transcriptome analysis of DNA damage-related proteins in EGFP-negative RPE-1-4F cells. Gene expression profiles of proteins involved in the DNA damage repair demonstrated an increase in the upstream DNA damage pathway activation occurs in nascent aneuploid cells including MDM2 and RPA2. Data normalised to EGFP-positive.

5.3.2.3. DNA damage response and apoptosis

I had previously reported the activation of apoptosis in EGFP-negative cells (**figure 5.6c**). The up-regulation of BCL6, and down-regulation of BCL2, mRNA therefore confirmed the induction of apoptosis already seen by AnnexinV staining in this population (**figure 5.9**; ***p<0.001). Although BCL2 was down-regulated, this did not correlate with an increase of the pro-apoptotic protein BAX or BAK1. Moreover, an increase in transcripts for the pro-apoptotic protein BCL2L11 was also observed (**p<0.01).

These data suggest that the late apoptotic fraction of EGFP-negative cells at 12 hours following nocodazole wash-out are dying through the intrinsic apoptosis response[383]. One important consideration is that the EGFP-negative population may be sensitised to stress arising during FACS following nocodazole wash-out. Therefore, although the induction of apoptosis was not observed in untreated RPE-1-4F post-FACS (**figure 5.6e**), this possibility cannot be ruled out by these experiments alone.

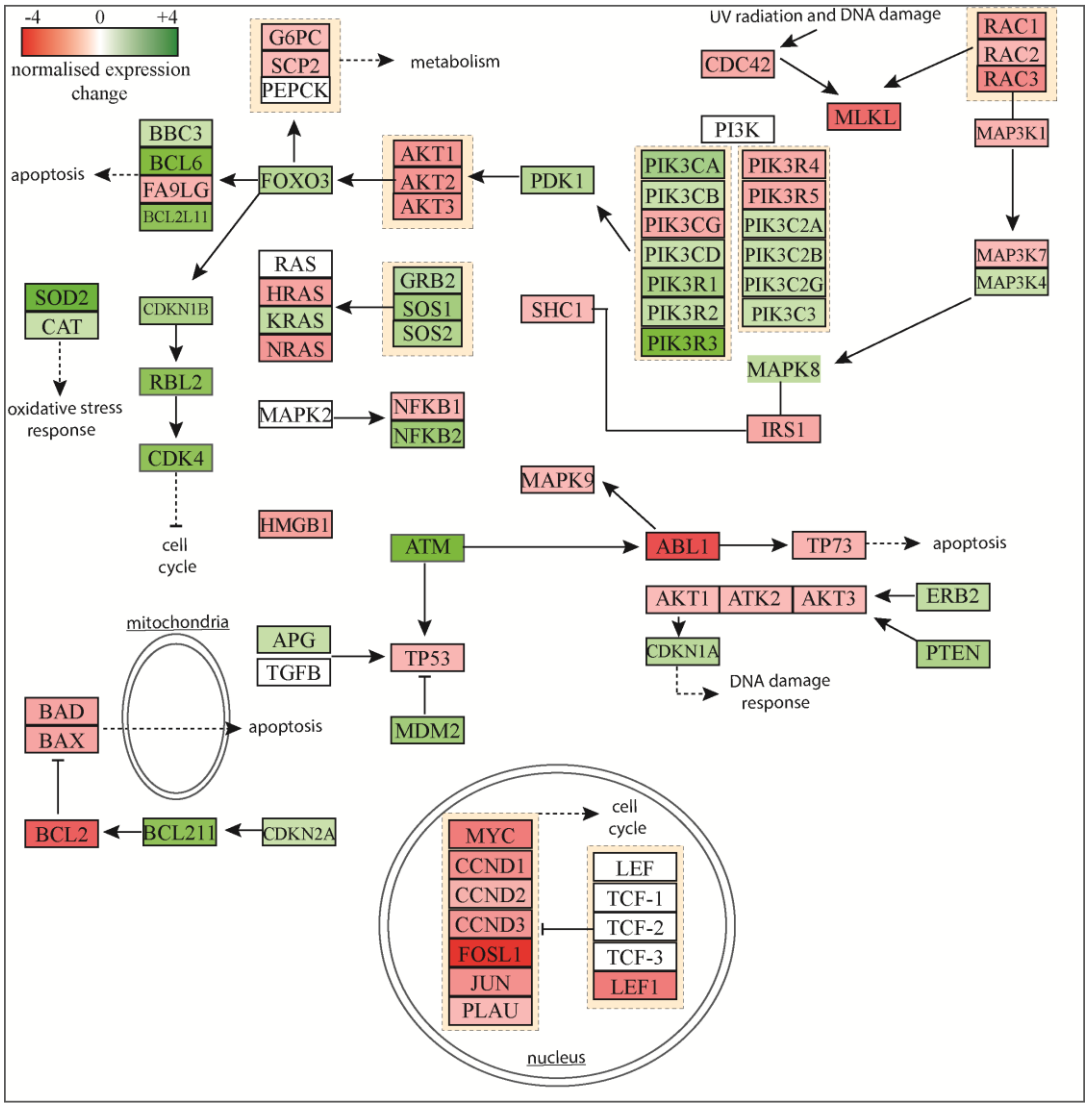

Figure 5.9. Transcriptome analysis of apoptotic signalling networks in EGFP-negative RPE-1-4F cells. Gene expression profiles of proteins involved in the pro- and anti-apoptotic responses suggests a significant increase in pro-apoptotic factors occurs in nascent aneuploid cells. Data normalised to EGFP-positive.

5.4. Summary

In chapter 5, I have applied the chromosome missegregation strategy and aneuploidy reporter cell line from chapter 4 to enrich for EGFP-negative cells and sort this population by FACS. Using a combination of transcriptome analysis and traditional FISH, I have identified a ~75 % monosomy 6 enrichment in my EGFP-negative population. Moreover, I have started to assess the validity of this system for isolating aneuploid cells as early as 12 hours following chromosome loss. Populations of cells isolated in this way behave similarly to the literature, arresting in G_1 and undergoing apoptosis, although whether EGFP loss is a cause or consequence of these phenotypes is still being investigated.

Furthermore, my preliminary transcriptome pathway analysis indicates that many of the expected consequences of chromosome loss are in agreement with my results, particularly the down-regulation of cell cycle progression proteins and increased transcription of pro-apoptotic proteins. However, it is apparent that further optimisations of this system are required to improve the enrichment of monosomic cells for down-stream applications to determine nascent aneuploidy responses more faithfully.

6. The missegregation rates of individual chromosomes

Preface

Due to technical limitations, the rate of spontaneous chromosome missegregation in human tissues is currently unknown. Recent *in vitro* studies and mouse models estimate the rate of spontaneous chromosome gain or loss to be around once in every 100 cell divisions, and this is likely to vary between cell lines with different tissues of origin[312,343]. However, the rates of chromosome gain and loss for the majority of individual chromosomes have yet to be determined in a robust and systematic manner.

Human chromosomes are very different to each other and this intrinsic variation may pre-dispose particular chromosomes to missegregation (**figure 6.1a**). This question is of fundamental interest to the fields of cell biology and medicine as it is currently unclear how patterns of aneuploidy in human disease arise, and if certain chromosomes are vulnerable to missegregation[384,385]. The available next-generation technologies, such as single-cell sequencing, are still expensive for routine analysis. Moreover, manual FISH scoring is artefact-prone and labour intensive, thus there is high demand for novel approaches to assess the rates of individual human chromosome missegregation[386,387].

Here, I implement a high-throughput image cytometry–based technology to detect whole-chromosome copy-number alterations (CNA) in response to a variety of cellular stresses, revealing striking difference in individual chromosome missegregation rates and patterns of aneuploidy across cell lines with different tissues of origin.

6.1. An image cytometry-based approach to detect aneuploidy

A variety of methods for imaging cells in flow have been refined following the advent of traditional flow cytometry. Such approaches have included flying spot scanning, slit scanning, mirror tracking and strobed illumination cytometry[388–390]. One of the greatest challenges for analysing single cells by flow cytometry is achieving imagery with high enough spatial resolution, fluorescence sensitivity and accuracy to combine with brightfield images of each cell in the flow. Over the last 10 years, advances in computing and optical filtration have combined all of these important parameters, permitting the practical application of imaging flow cytometry.

One such example is the ImageStream^X cytometer, a commercially available instrument which combines high resolution multispectral imaging with electronic cell tracking, producing images of comparable quality and resolution as a conventional 60X fluorescent microscope[391]. With a maximum throughput of 300 cells per second, the ImageStream^X produces 60,000 images of 10,000 cells in 30 seconds. Combined with the data analysis software package – IDEAS – this system can quantify over 250 individual features per cell, opening up a realm of high-throughput fluorescent imaging and analysis possibilities[391].

It has previously been shown that the ImageStream^X can accurately detect monosomies and trisomies in clinical acute myeloid leukaemia samples, with a detection sensitivity and false discovery rate of ~ 1 %[325]. I wanted to test the ImageStream^X system in my own hands, to determine if I could also detect aneuploidy in a high-throughput manner. If possible, it was my intent to use this technology to determine the missegregation rates of individual human chromosomes, in response to a variety of cellular stresses, as outlined in the preface to this chapter.

6.1.1. Optimising aneuploidy detection by the ImageStream^X

Individual chromosomes were labelled with fluorescent α-satellite centromere enumeration probes (CEP) by FISH in suspension (FISH-IS). Fluorescent and bright-field images of single cells were then obtained using the ImageStream^X cytometer (**figure 6.1b**). Images were analysed, and the ploidy for each chromosome determined, using the IDEAS software package[325].

Single cells passing through the flow chamber are distinguished from cell aggregates by low area and high aspect ratio. The extended depth of field (EDF) element was used to increase the focus range from 4 µm to 16 µm, allowing close to 100% of cells to be focused. Single, in-focus cells were then analysed for the ploidy of individual chromosomes by applying a 'spot mask' and 'spot counting' feature to the centromere probe signals for each image (**figure 6.1b**).

The images obtained of CEP spots are 2D projections of 3D images, to encompass the entire volume of the nucleus. If a cell is aligned so that the two centromere signals are in the same plane, they appear as a single focus, because they overlap following image deconvolution and projection (**figure 6.1c**).

To correct for this discrepancy, CEP fluorescence signal intensity was plotted as a histogram which correlates with the amount of probe hybridised, as well as the spot count (**figure 6.1d**). Disomic chromosomes (e.g. RPE-1 chromosome 18) had a medium intensity of hybridisation signal, representing two spots. Cells with one spot (e.g. HCT116 chromosome X) will have approximately 50% of the hybridisation intensity and fall in the low range; cells which had gained a chromosome will have 150% of the hybridisation signal intensity, falling in the high range (e.g. HCT116 stained for both chromosome 18 and X). For the majority of cells with a single CEP spot, where disomy is anticipated (e.g. RPE-1 chromosome 18), the total fluorescence for that cell was observed in the medium range of intensity (>99 %).

This suggests that they are disomic cells with aberrant ploidy-spot relationship in which the two signals are eclipsed following image projection, appearing as a single focus.

Given this, it is anticipated that there will be a small error margin of ploidy misclassification in my particular ImageStream^X configuration, of approximately 1 %, as previously reported[325]. Therefore, complementary approaches such as traditional FISH and single-cell sequencing will be used to validate these data.

6.1.2. An assessment of aneuploidy detection by the ImageStream^X

To make a preliminary assessment of whether chromosome missegregation rates were accurately detected with the ImageStream^X, chromosome missegregation was elevated in an otherwise chromosomally-stable cell line – HCT116[337,338]. This cell line was exploited for the initial assessment of the ImageStream^X as it was fortuitously amenable to the FISH-IS optimisation, in addition to its biological relevance (**see section 6.2.4**).

HCT116 cells were treated with an 8-hour nocodazole wash-out strategy, to elevate chromosome missegregation. Following a 12-hour wash-out, monosomy and trisomy rates were analysed by image cytometry and conventional fluorescence microscopy for a panel of chromosomes, covering a range of chromosome sizes and anticipated ploidy states (chromosomes 12, 16, 18 and X; monosomy X is anticipated because HCT116 are of male origin). The ploidy of individual chromosome was determined in 1,000 cells by conventional FISH and 20,000 cells by image cytometry. Importantly, monosomy and trisomy rates obtained by image cytometry were in good agreement with those scored by conventional FISH (**figure 6.1e**; R^2=0.9816).

There are currently no centromeric probes available for six chromosomes which have high centromere sequence similarity to each other; chromosomes 5, 13, 14, 19, 21 and 22. Unfortunately, I were unable to optimise the commercially available telomere probes for these chromosomes for image cytometry analysis. In some of the experiments below, the aforementioned chromosomes were analysed using traditional telomeric FISH; these data are highlighted throughout this chapter.

These data demonstrate that I have a robust experimental workflow to systematically determine the aneuploidy rates for most human chromosomes in many thousands

of cells per experiment. I are therefore able to assess chromosome copy number alterations, with high accuracy, to determine if certain chromosomes are more vulnerable to missegregation. This is an important question as determining the missegregation rates of individual chromosomes may help elucidate the basis for the recurrent aneuploidy patterns observed in human diseases – do aneuploidy patterns arise mainly through selection pressure or is there *also* continual missegregation of particular chromosomes?

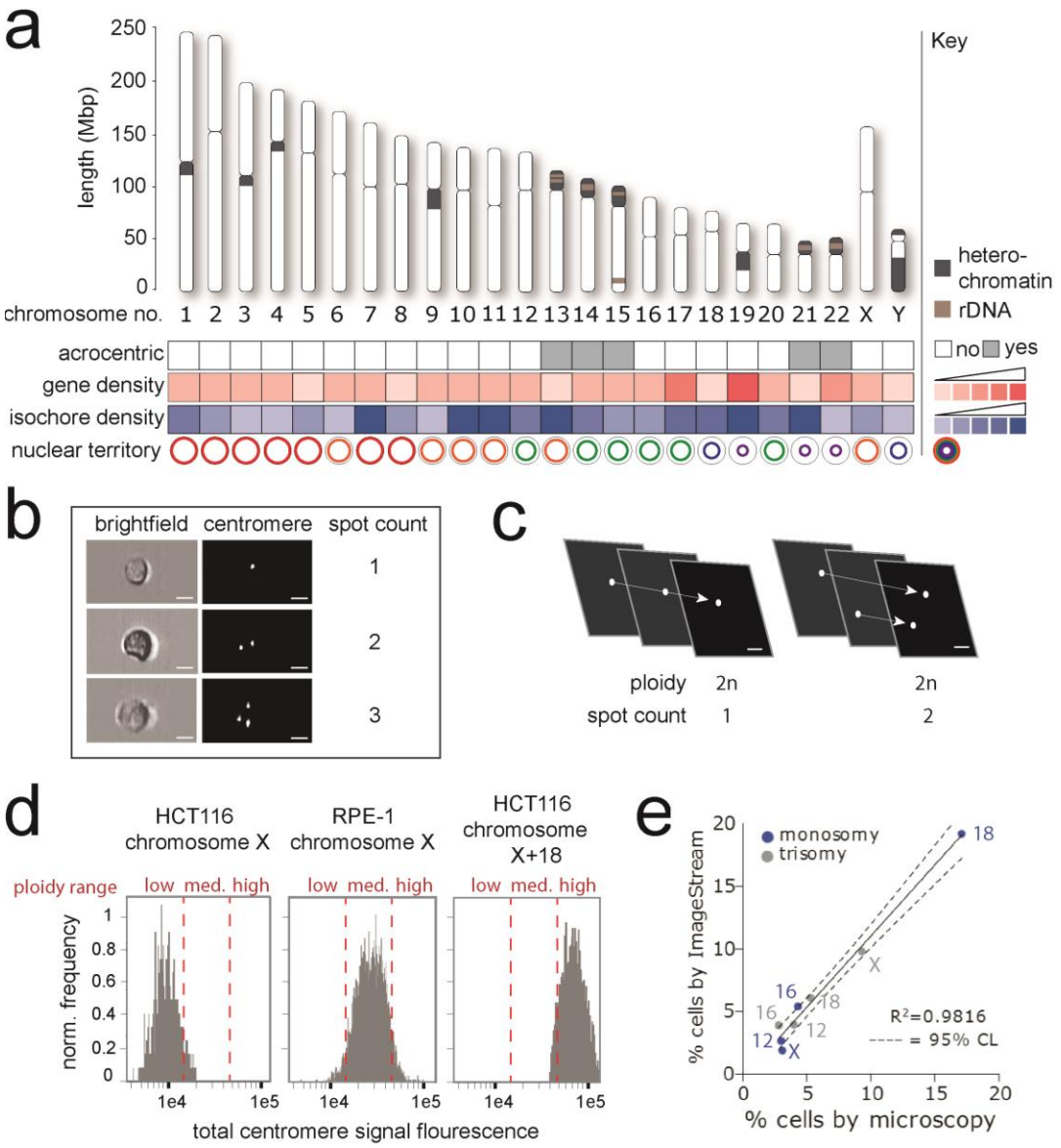

Figure 6.1. Aneuploidy can be accurately detected by image cytometry. (a) Human chromosome attribute map. Chromosomes display heterogeneity in physical characteristics, composition and interphase nuclear arrangement. (b) Centromere enumeration probes can be detected by image cytometry. (c & d) Overlapping centromere signals can be resolved by population-based histogram fluorescence quantification. (e) Aneuploidy rates scored by image cytometry are in good agreement with those by traditional scoring methods for a range of chromosomes within the 95 % confidence limits (CL; R^2 = 0.9816). Scale bars: 20 µm.

6.2. Aneuploidy rates following nocodazole wash-out

Chromosome missegregation can arise because of chromosome spindle malorientation occurring during mitosis[265,392]. To mimic spindle orientation defects, cell were arrested in mitosis for 8 hours with nocodazole. Nocodazole depolymerises microtubules which can reassemble upon wash-out, leading to chromosomes that are not correctly bioriented on the spindle, due to an increased frequency of merotelic attachments, as previously described in chapter 4 (**figure 4.2a**) After an 8-hour mitotic arrest, nocodazole was washed out for 12 hours to allow cells to complete mitosis, after which the of ploidy of single cells was analysed, before significant cell death (and therefore selection) has occurred[339].

Here, I characterise the aneuploidy rates for individual human chromosomes following nocodazole wash-out in cell lines of different tissue origin, ploidy and tumorigenic status. Addressing the issue of chromosome missegregation following nocodazole wash-out is a fundamental priority for two reasons; firstly, the rate of merotelic attachments are known to be increased in human cancers and therefore patterns of aneuploidy might arise from the chromosomes most prone to orientation defects[234,248,393]. Secondly, nocodazole wash-out is a popular strategy for increasing chromosome missegregation in cell biology studies[346,394–396]. Therefore, it is important to interrogate whether segregation error rates and aneuploidy observed *in vitro* support the prevailing assumption that chromosomes missegregate with equal frequencies following nocodazole wash-out[236].

I chose to assess the rates of aneuploidy in RPE-1, BJ, HCT116 and RPE 12/3 (with a stable chromosome 12 trisomy) cells as these cell lines have been established in culture for many years, are derived from different tissues of origin and are karyotypically well-defined[236].

6.2.1. RPE-1 aneuploidy rates following nocodazole wash-out

RPE-1 cells are a chromosomally stable, non-transformed cell line of epithelial origin which were used for my aneuploidy reporter strategy in chapters 4 and 5. It was anticipated that the rate of spontaneous chromosome missegregation would be low in this cell line, therefore elevated aneuploidy rates could be detected for individual chromosomes above this baseline.

In untreated RPE-1 cells, basal levels of aneuploidy were low, as expected for a chromosomally stable cell line – and from the micronuclei formation rates already observed in untreated RPE-1 cells (**figure 6.2**; grey dots and **figure 4.2c**; chapter 4). On average, chromosomes were lost at a frequency of 1.83 %. However, chromosome 8 was lost more frequently than the mean over triplicate experiments (3.49 %; $p<0.05$). The average chromosome gain rate was 1.03 % with no individual chromosomes varying significantly from the mean.

I next determined aneuploidy rates following microtubule disruption with 8-hour nocodazole wash-out, to elevate merotely. Twelve hours post-nocodazole wash-out, an increase in chromosome missegregation was observed, as expected (**figure 6.2**; blue and red dots). The average rate of chromosome gain was 3.92 %. However, I did not observe uniform chromosome gains. Strikingly, chromosomes 1, 3, 4, 7 and 10 were gained at significantly higher rates than all other chromosomes tested (3.59, 3.97, 10.20, 5.48 and 5.09 %, respectively; $*p<0.05$).

Chromosome loss also showed similar patterns, with chromosomes 1, 3, 4, 7, 10 and 18 being lost at high rates (6.39, 10.95, 5.20, 5.56, 5.83 and 5.43 %, respectively; $*p<0.05$). Chromosome 2 loss rates appeared elevated above the mean, but marginally failed to reach significance ($p=0.063$). For chromosomes 3, 4, and 18 the loss rate was not equal to the gain rate. This was unexpected, given that the McClelland lab has not observed cell death following chromosome

missegregation at this time point. One explanation is that chromosomes trapped in micronuclei, which do not reincorporate into the main nucleus, are being lost during the FISH-IS sample preparation, as only the nuclear chromosome content is analysed.

These data demonstrate that the contribution of each chromosome to the overall missegregation rate is unequal, with certain chromosomes being prone to aneuploidy following nocodazole wash-out. They further reveal that nocodazole, thought to increase global chromosome missegregation stochastically and equally for all chromosomes, is actually inducing the missegregation of a small subset of chromosomes. Moreover, these data highlight that recurrent patterns of aneuploidy in human disease may result from previously-uncharacterised properties of individual chromosomes.

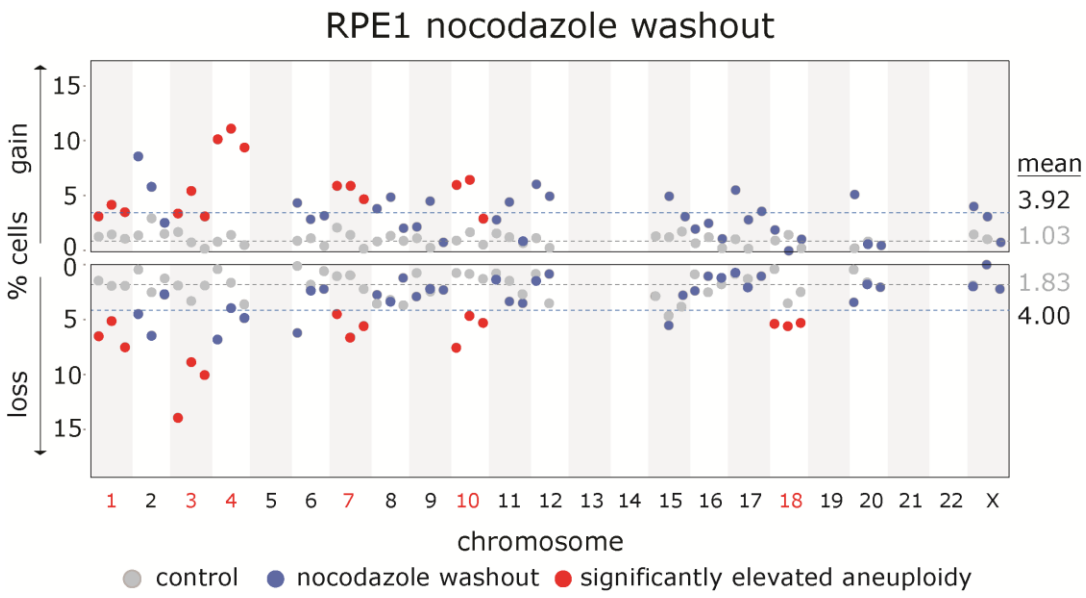

Figure 6.2. RPE-1 aneuploidy rates following nocodazole wash-out. Aneuploidy rates were determined for a large panel of human chromosomes with commercially available centromere probes. Basal levels of aneuploidy were low in unperturbed cells (grey dots; 1.03 % gain, 1.83 % loss). Global chromosome missegregation was elevated following mitotic disruption with 16-hour nocodazole wash-out (blue dots; 3.92 % gain, 4.00 % loss). Aneuploidy involving chromosomes 1, 3, 4, 7, 10 and 18 were observed more frequently than the global average, suggesting they are prone to missegregation following mitotic insult (red dots). All dots represent independent experiments. Red dots represent significant aneuploidy deviation from the mean using a two-tailed t-test (*p<0.05).

6.2.2. RPE-1 aneuploidy rates: single-cell sequencing validation

To further validate the missegregation rates using an independent methodology, control and nocodazole-treated RPE-1 cells were analysed by single-cell sequencing.

Single-cell sequencing is a recent technological development which allows the genomic content of single cells to be analysed. The advantages of single-cell sequencing over conventional sequencing approaches is that it allow genomic aberrations to be detected with exquisite resolution, providing highly-accurate determination of chromosome copy number alterations on a per-cell basis. Single cells were sorted by flow cytometry, to obtain a pure G_1 cell fraction, and sequenced by a collaborator using proprietary AneuFinder software as previously described[314,386]. Samples were frozen and analysed 12 hours following nocodazole release, therefore the majority of cells sequenced were in G_1 and were of sufficient DNA quality for analysis (data not shown).

In untreated RPE-1 cells, basal levels of aneuploidy were low, in-line with the data obtained by image cytometry (**figure 6.3**; top panel). In all cells, I observed a gain of chromosome 10q, confirming the data from SNP array analysis of untreated RPE-1 cells already observed in my hands (**see chapter 5.2.1.1**). One of the single cells sequenced harboured four copies of chromosome 10q, in addition to partial gains of chromosomes 6, 10p, 12 and X. Monosomy X was observed in a single cell; and partial trisomy of chromosome X in two single cells. These data validate basal levels of aneuploidy to be low in untreated RPE-1 cells, as observed by image cytometry.

Following nocodazole wash-out aneuploidy was elevated, as expected (**figure 6.3**; bottom panel). The known chromosome 10q aberration in this cell line was observed in all cells, as for the untreated control. Importantly, chromosomes 1, 2, 3, 4, 7, 10 and 18 were lost in between 10-30 % of cells, confirming the data obtained by image

cytometry. Additionally, chromosomes 5, 12 and 21 were observed to be lost in one single cell, out of the 12 analysed. In “cell 1”, the missegregation of six chromosomes was observed simultaneously, and accounted for a fraction of the chromosome loss rates not observed by image cytometry. This is likely a cell that underwent a multipolar division and would therefore be excluded, based on area and aspect ratio, by the ImageStream^X.

Importantly, these data are in good agreement with the missegregation rates observed by image cytometry. Therefore, I conclude that the ImageStream^X is a robust system for determining the missegregation rates of individual human chromosomes in a high-throughput manner, which I have validated by two further independent methodologies (traditional FISH on glass slides and single-cell sequencing).

Furthermore, these data confirm chromosome missegregation rates to be unequal following nocodazole wash-out, demonstrating that a subset of chromosomes are more vulnerable to merotely. If I exclude cell 1 from my analysis, which presumably went through a multipolar division, I do not see either the high gain or loss rates for chromosome 4 as observed by image cytometry. One explanation is that the CEP probe for chromosome 4 is subject to cross-hybridisation artefacts between centromeres, a possibility which is raised in the corresponding manufacturer data sheet for this probe, and may be exacerbated through unknown means following nocodazole wash-out. Finally, chromosome 2, which was borderline significant by image cytometry ($p=0.063$), was lost in 25 % of cells by SCS. One explanation is the experimental variance for chromosome 2 in a single experiment accounted for the failure to reach significance, as two of three experiments were above the mean and more closely aligned with the data obtained by SCS (**figure 6.2 *vs*. 6.3**).

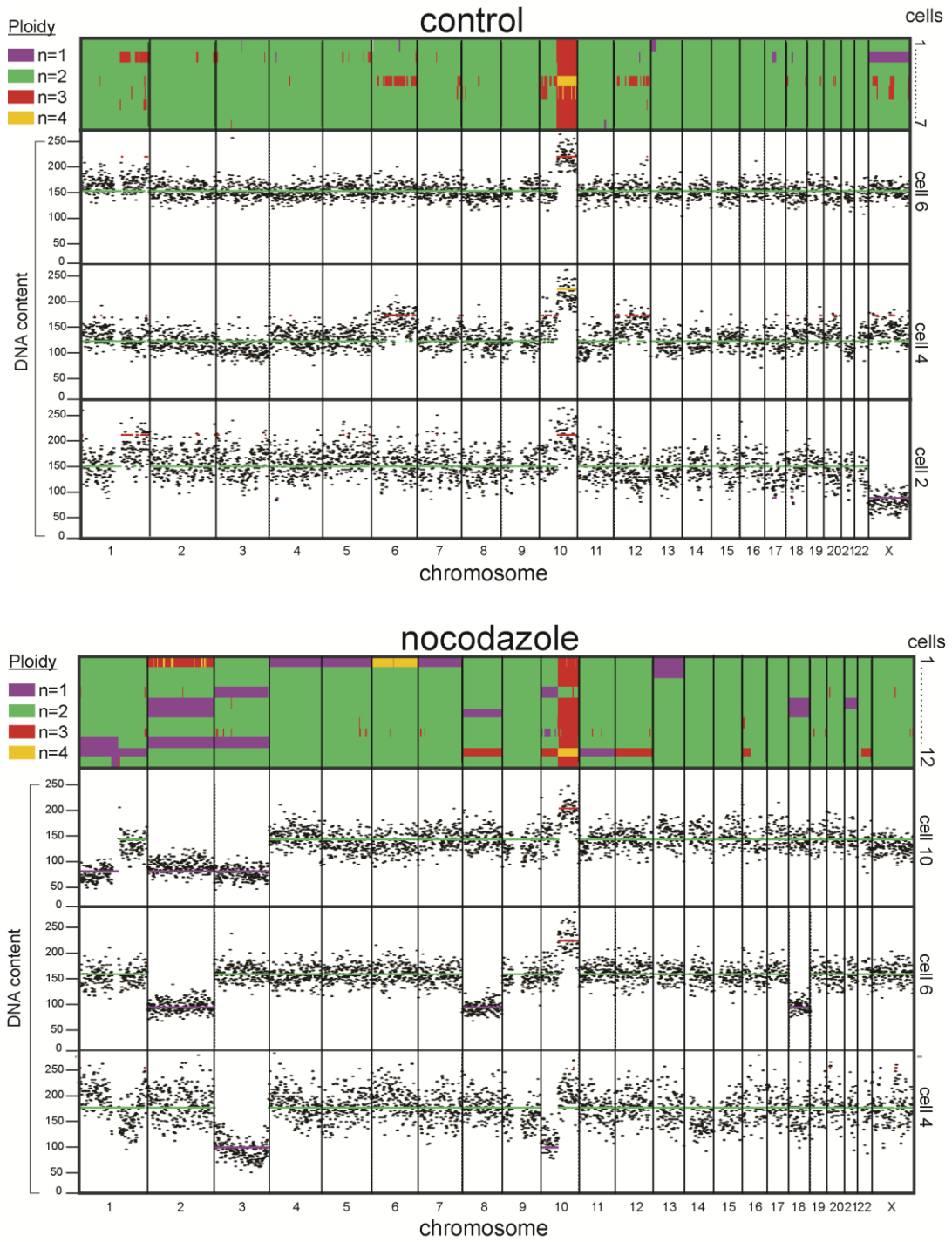

Figure 6.3. RPE-1 single cell sequencing following nocodazole wash-out. Aneuploidy rates for all chromosomes were determined by single cell sequencing in RPE-1 cells. Aneuploidy rates for control (top panel) and nocodazole wash-out (bottom panel) broadly reflected those observed by image cytometry. Representative DNA profiles for individual cells are shown.

6.2.3. BJ aneuploidy rates following nocodazole wash-out

To determine if the patterns of aneuploidy observed in RPE-1 cells could be attributed to the intrinsic properties of a small subset chromosomes, or was a cell line-specific phenomenon, the nocodazole wash-out was repeated in BJ cells, a non-transformed, immortalised cell line of fibroblast origin.

Basal levels of aneuploidy in untreated BJ cells were low and uniform for both monosomy and trisomy (1.66 and 1.92 %, respectively; **figure 6.4**; grey dots). The only exception was chromosome 4 which was gained at nearly twice the mean rate for all other chromosomes (2.62 %), possibly as a result of probe cross-reactivity described in section 6.2.2. These findings are in agreement with preliminary data demonstrating low basal rates of anaphase errors in this cell line and the expectation that missegregation rates would be low in chromosomally-stable cells[339].

Following nocodazole wash-out, I observed an increase in the rate of chromosome gain and loss, as expected (3.75 and 4.32 %, respectively; **figure 6.4**; blue and red dots). Chromosomes 1, 3, 10, 18 and 20 were lost more frequently than the mean, in good agreement with the patterns observed in RPE-1 cells; demonstrating that a small subset of chromosomes are particularly vulnerable to missegregation (6.84, 6.16, 6.48, 5.43 and 5.87 %, respectively; *$p<0.05$). Overall, rates of chromosome gain were more similar to the corresponding chromosome loss rates, in comparison to RPE-1 cells. Chromosome 4 was the only chromosome tested which was gained more frequently than the mean (17.79 %; *$p<0.05$).

These data corroborate that the intrinsic properties of chromosomes 1, 2, 3, 4, 10 and 18 make them vulnerable to missegregation following nocodazole wash-out. Moreover, patterns of aneuploidy in human disease may be influenced by the intrinsic properties of a select few chromosomes which are vulnerable to recurrent missegregation. This is a particularly important discovery as it highlights a

previously-uncharacterised requirement for individual chromosome-level resolution of aneuploidy mechanisms; the absence of which obfuscates the interplay between selection pressures and karyotype complexity in aneuploid human diseases.

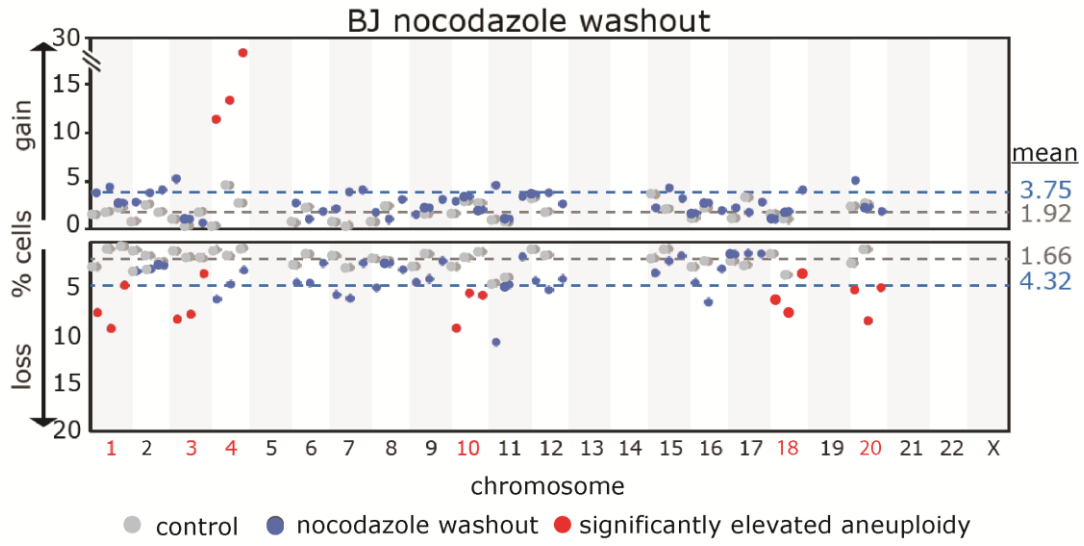

Figure 6.4. BJ aneuploidy rates following nocodazole wash-out. Aneuploidy rates were investigated in a second cell line, BJ, of fibroblast origin. Basal levels of aneuploidy were low in unperturbed cells (grey dots; 1.92 % gain, 1.66 % loss). Global chromosome missegregation was elevated to similar levels following microtubule disruption with 8-hour nocodazole wash-out (blue dots; 3.75 % gain, 4.32 % loss). Significantly elevated aneuploidies were similar to RPE-1 cells, involving chromosomes 1, 3, 4, 10, 18 and 20 (red dots). All dots represent independent experiments. Red dots represent significant aneuploidy deviation from the mean using a two-tailed t-test (*p<0.05).

6.2.4. HCT116 aneuploidy rates following nocodazole wash-out

To elucidate if non-random missegregation could be observed in human cancers, I took advantage of a chromosomally-stable, transformed cell line HCT116, originally derived from male colon carcinoma tissue. Determining the rates of missegregation in a transformed cell line may provide additional insight into the intrinsic propensities of chromosomes to missegregate in cancer cells, with potentially important implications for tumourigenesis and cancer evolution. Additionally, this would allow us to investigate whether recurrent patterns of non-random aneuploidy occur for the same subset of chromosomes observed in RPE-1 and BJ cells.

In untreated HCT116 cells, basal levels of chromosome gain were higher than expected for a chromosomally-stable cell line, and compared to RPE-1 cells (1.96 %; **figure 6.5**, grey dots; *p<0.05). Particularly, chromosomes 6, 12 and 16 were being gained at rates approximately twice that of the mean for all other chromosomes tested (3.87, 3.37 and 4.57 %, respectively; *p<0.05). However, this could also represent a low level of previously-uncharacterised stable aneuploidy in the population as I cannot distinguish between these possibilities with this experiment.

The average rate of basal chromosome loss was 1.83 % in untreated HCT116 cells. Of note, HCT116 cells are derived from the male colon and therefore monosomic for chromosome X. In my hands, I find that basal levels of chromosome X loss was zero (which is likely an artefact of the detection limit of the ImageStream^{X}), indicating that HCT116 cells with stable nullisomy X karyotype are extremely rare. Additionally, chromosome 12 was lost significantly less frequently than the mean (0.37 % loss; *p<0.05). For all other chromosomes tested, basal rates of chromosome loss were low and uniform, as expected.

Following nocodazole wash-out chromosome missegregation was elevated, as expected. The average rate of chromosome gain was 5.31 %, significantly higher than that observed for either RPE-1 or BJ cells following identical treatment (*p<0.05). Chromosomes 3, 4, 9, 15 and X were gained at significantly higher rates than the mean, representing a modest overlap in aneuploidy patterns compared to RPE-1 and BJ cells (7.37, 11.22, 10.04, 8.54 and 10.32 %, respectively; *p<0.05). Given that the mean trisomy rate was higher than both RPE-1 and BJ cells following nocodazole wash-out, there may be a greater degree of CIN or aneuploidy in this cell line than previously reported.

The average chromosome loss rate following nocodazole wash-out was similar to the chromosome gain rate (5.81 *vs*. 5.31 %, respectively). Likewise, it was observed that the mean monosomy rate was significantly greater than both RPE-1 and BJ cells (5.81 *vs*. 4.00 and 4.32, respectively; *p<0.05). The loss of chromosomes 8 and 17 were observed only at rates comparable to the untreated control cells (3.00 and 2.14 %, respectively). Conversely, chromosome 18 and 20 were lost at significantly higher rates than the other chromosomes analysed (17.94 and 11.22 %, respectively; *p<0.05).

These data demonstrate that a small number chromosomes – 3, 4, 18 and 20 – are susceptible to missegregation in both transformed and non-transformed cell lines following errors that occur during mitosis. However, it is possible that there are several further features of HCT116 cells – such as tissue origin and transformation status – which influence chromosome missegregation rates for those chromosome which are distinctly vulnerable in HCT116 cells. The McClelland lab is trying to elucidate if the large translocation of one chromosome 18 allele, which I also report in chapter 5, could account for the high rate of chromosome 18 loss in these conditions.

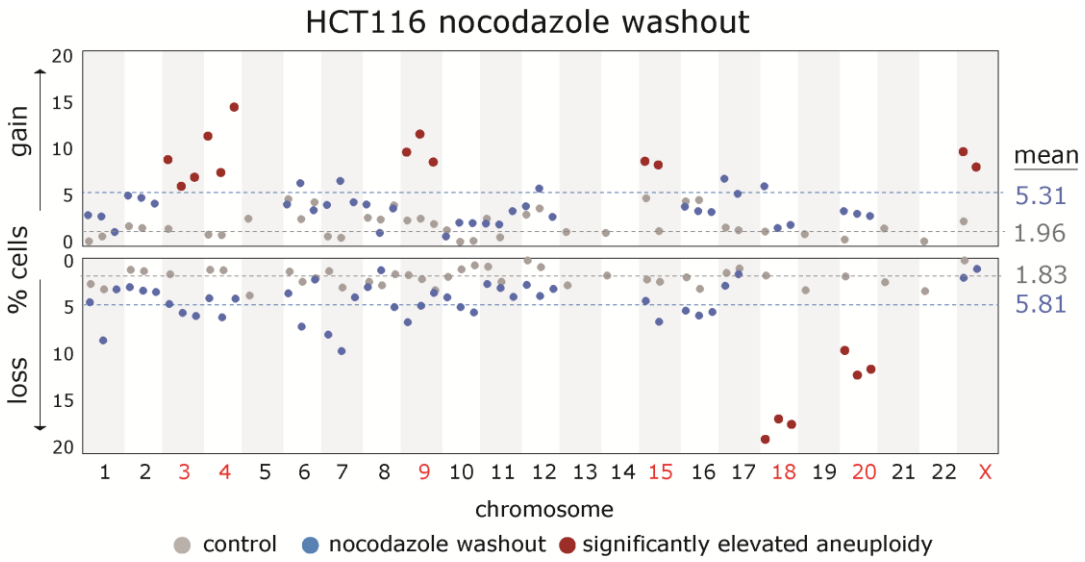

Figure 6.5. HCT116 aneuploidy rates following nocodazole wash-out. Aneuploidy rates were investigated in a transformed cell line, HCT116, of human colon carcinoma origin. Basal levels of aneuploidy were higher than RPE-1 and BJ cells in unperturbed cells (grey dots; 1.96 % gain, 1.83 % loss; *p<0.05). Global chromosome missegregation was elevated to higher levels than RPE-1 and BJ cells following microtubule disruption with 16-hour nocodazole wash-out (blue dots; 5.31 % gain, 5.81 % loss; *p<0.05). The most frequently elevated aneuploidies were strikingly different to RPE-1 and BJ cells, involving chromosomes 3, 4, 9, 15, 18, 20 and X (red dots). All dots represent independent experiments. Red dots represent significant aneuploidy deviation from the mean using a two-tailed t-test (*p<0.05).

6.2.5. RPE-1 12/3 aneuploidy rates following nocodazole wash-out

It has already been observed that the presence of extra chromosomes leads to genomic instability[236,336]. Specifically, RPE-1 cells harbouring a stable chromosome 12 trisomy (RPE-1 12/3) are susceptible to an increased frequency of DNA damage and anaphase chromosome bridges[336]. In my hands, I have already confirmed the stable maintenance of a chromosome 12 trisomy by SNP array in this cell line (**see chapter 5.2.1.1**). Therefore, image cytometry was used to determine whether the presence of an extra chromosome generates recurrent patterns of missegregation for specific chromosomes in RPE-1 12/3 cells. This is an important question as it is currently unclear if aneuploidy itself influences patterns of pathological chromosome missegregation. Additionally, the missegregation rates for chromosomes 5, 13, 14, 19, 21 and 22 were analysed by conventional telomeric FISH on glass slides (preliminary data shown).

In untreated RPE-1 12/3 cells, basal levels of chromosome gain and loss were significantly higher (approximately twice) that observed for untreated, disomic RPE-1 cells (**figure 6.6**; grey dots; 2.17 and 2.53 %, respectively; *$p<0.05$). The chromosome 12 trisomy was present in 82.4 % of cells, as expected from my SNP array observations (**figure 6.6**, bottom panel). No individual chromosomes loss rates in untreated cells varied significantly from the mean. Conversely, chromosomes 4, 16, 20 and X were gained at significantly higher rates than the mean (4.02, 3.03, 3.18 and 5.01 %, respectively; *$p<0.05$), highlighting that certain chromosomes may be vulnerable to missegregation in unperturbed aneuploid cells by the presence of a single extra copy of chromosome 12.

In RPE-1 12/3 cells, following nocodazole wash-out, an increase in chromosome missegregation was observed (**figure 6.5**; blue and red dots). The mean

chromosome loss rate, but not gain rate, was significantly higher than that observed for diploid RPE-1 cells under the same conditions (4.00 *vs*. 5.27 %; *p<0.05). Chromosomes 1, 3 and 10 were lost at significantly higher rates than the other chromosomes tested, a pattern which was similar, but incomplete, to that observed for diploid RPE-1 and BJ cells (7.64, 7.41 and 8.01%, respectively; *p<0.05).

These data demonstrate that basal chromosome missegregation is elevated in aneuploid cell lines by the presence of a single extra copy of chromosome 12, as previously reported[336]. Strikingly, this phenomenon is exaggerated following nocodazole wash-out where overall chromosome loss rates are ~ 25 % greater than diploid RPE-1 cells. Interestingly, patterns of chromosome missegregation following nocodazole wash-out were similar, but not identical, to those observed for diploid RPE-1 cells. This suggests that the presence of an extra chromosome influences patterns of aneuploidy, at least in this cell type. Further validation of other trisomies and cell lines are required for extensive characterisation.

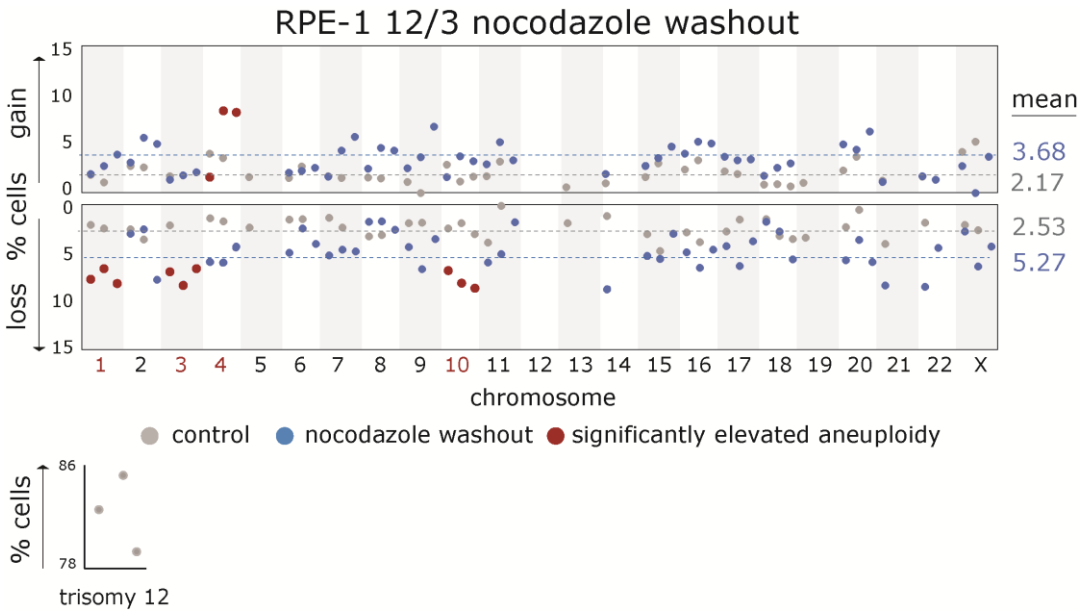

Figure 6.6. RPE-1 12/3 aneuploidy rates following nocodazole wash-out. Aneuploidy rates were investigated in a sub-clone of RPE-1 cells containing a stable chromosome 12 trisomy. Basal levels of aneuploidy were higher than RPE-1 cells in unperturbed cells (grey dots; 2.17 % gain, 2.53 % loss; two-tailed t-test *p<0.05). Global chromosome gain was elevated to a similar rate as diploid RPE-1 cells, but chromosome loss was greater, following microtubule disruption with 8-hour nocodazole (blue dots; 5.31 % gain, 5.81 % loss; two-tailed t-test *p<0.05). The most frequently-elevated aneuploidies were broadly similar to RPE-1 and BJ cells, involving chromosomes 1, 3, 4 and 10 (red dots). Chromosomes 5, 13, 14, 19, 21 and 22 were scored in at least 200 cells from independent experiments using traditional manual scoring with telomeric probes. All dots represent independent experiments. Red dots represent significant aneuploidy deviation from the mean using a two-tailed t-test (*p<0.05).

6.3. Aneuploidy rates following DNA replication stress

DNA replication stress can induce chromosome missegregation through the formation of dicentric chromosomes and chromosome bridges[226]. It is also known that replication stress is increased in aging cells and human colorectal carcinomas[397,398]. However, the mechanisms underlying pathological aneuploidy patterns observed in conditions of high replication stress are currently unknown and therefore of high therapeutic interest.

Moreover, it is known that one major mechanism generating replication stress is collisions between the replication and transcription machinery[399–401]. I therefore hypothesised that gene-dense chromosomes, where replication-transcription collisions may be elevated[402], may be more prone to structural aberrations which could generate aneuploidy-prone chromosomes. To interrogate these important questions, patterns of aneuploidy were determined by image cytometry following replication stress induced for 24 hours, with low-dose DNA polymerase II inhibition, using aphidicolin[403]. This treatment length was chosen to allow the majority of cells to proceed through at least one erroneous S-phase[339].

6.3.1. RPE-1 aneuploidy rates following DNA replication stress

As expected, replication stress-induced chromosome missegregation was elevated in RPE-1 cells at 24 hours post-aphidicolin treatment (**figure 6.7**; blue and red dots). The mean gain and loss rates were not significantly different to the rates following nocodazole wash-out, demonstrating that global aneuploidy is similar under different cellular stresses (3.79 and 4.73 %, respectively). However, chromosomes 2, 4 and 20 were gained at significantly higher rates than the mean (10.56, 5.37 and 7.25 %, respectively; *$p<0.05$).

Additionally, chromosomes 3, 4, 6, 16 and 18 were lost significantly more frequently than the mean following the induction of DNA replication stress (5.83, 5.69, 5.98, 6.82 and 9.27 % respectively; *$p<0.05$). I have therefore discovered that high aneuploidy rates can be observed for chromosomes that were not elevated following nocodazole wash-out, namely for chromosomes 6 and 16. One important consideration is that these data only reflect changes in centromere number. Therefore, structural aberrations which result in centromere duplication or loss following DNA replication stress cannot be differentiated in this experiment and may lead to a false discovery rate.

These data demonstrate that similar patterns of chromosome loss can be observed in the same cell type (RPE-1) under different cellular stresses (nocodazole wash-out *vs*. replication stress). Importantly, they also highlight that some patterns of chromosome missegregation, for example chromosomes 6 and 16, are induced by different mechanisms. Moreover, the lack of high chromosome 1 missegregation following replication stress, observed after nocodazole wash-out, raises the possibility that there are multiple routes to aneuploidy which may be chromosome and error-type specific.

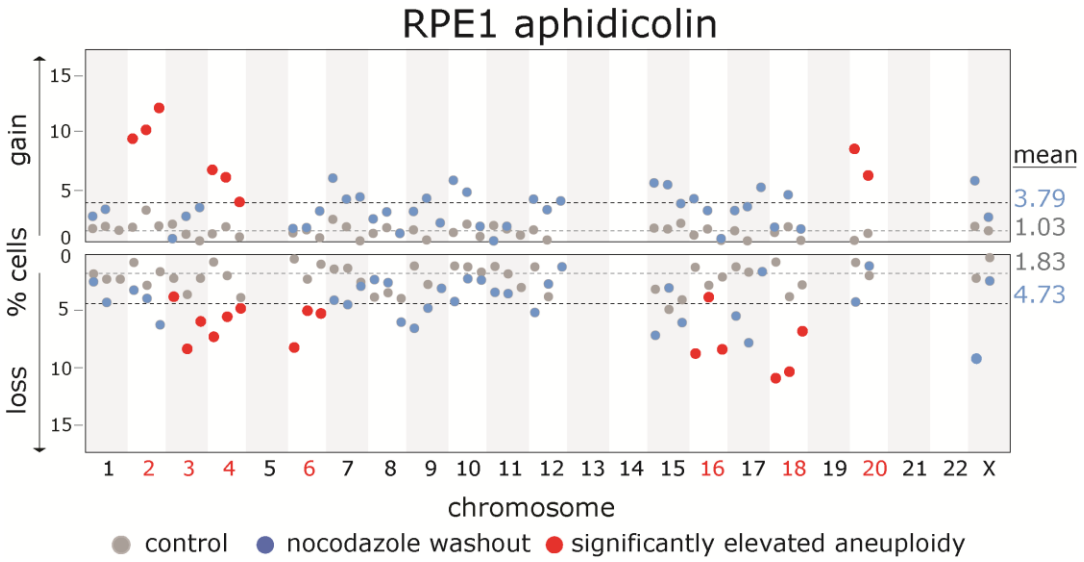

Figure 6.7. RPE-1 aneuploidy rates following DNA replication stress. Aneuploidy rates were investigated in RPE-1 cells following 24 hours of replication stress induced by aphidicolin. Global chromosome missegregation was elevated to a similar rate as RPE-1 cells following mitotic stress (blue dots; 3.79 % gain, 4.73 % loss). The most frequently elevated aneuploidies were those involving chromosomes 2, 3, 4, 6, 16, 18 and 20 (red dots). All dots represent independent experiments. Red dots represent significant aneuploidy deviation from the mean using a two-tailed t-test (*p<0.05).

6.3.2. BJ aneuploidy rates following DNA replication stress

To determine if the patterns of aneuploidy observed following DNA replication stress in RPE-1 cells was intrinsic missegregation behaviour of these few chromosomes, or a cell line-specific phenomenon, I treated BJ cells with low-dose aphidicolin for 24 hours.

As expected, chromosome missegregation was elevated in BJ cells induced with replication stress (**figure 6.8**; blue and red dots). The mean rate of chromosome loss was 3.70 %. However, some individual chromosomes were significantly less frequently monosomic in the population, with chromosomes 1 and 8 being lost at a rate approximately half that of the mean (1.66 and 1.82 %, respectively; *p<0.05). Conversely, chromosomes 3 and 18 were monosomic at rates significantly higher than the mean, an interesting observation given that these chromosomes were also lost at high rates following replication stress in RPE-1 cells (5.84 and 10.86 %, respectively; *p<0.05). Of further interest, chromosomes 6 and 16 which displayed high monosomy in RPE-1 cells were not missegregating above the mean in BJ cells, highlighting that there may be cell-line specific difference for particular chromosomes following DNA replication stress.

The mean rate of chromosome gain was elevated, and similar to the loss rate, following DNA replication stress (3.44 *vs*. 3.77 %, respectively). Chromosomes 2, 4 and 20 were all gained at significantly higher rates than the mean, representing a complete overlap in trisomy pattern with RPE-1 cells (6.18, 12.57 and 6.84 %, respectively; *p<0.05). All other chromosomes tested were gained at similar rates.

Taken together, these data demonstrate that patterns of aneuploidy following DNA replication stress are recurrent between cell types with different tissues of origin. Moreover, there are individual chromosomes which are prone to missegregation only following nocodazole wash-out (1 and 10), DNA replication stress (6 and 16) or

both (2, 3, 4, 18 and 20). The underlying mechanistic basis for these recurrent patterns and differences are still unclear, as chromosome-specific rates of aneuploidy are likely to reflect a range of individual chromosome characteristics and vary subtly between cell types.

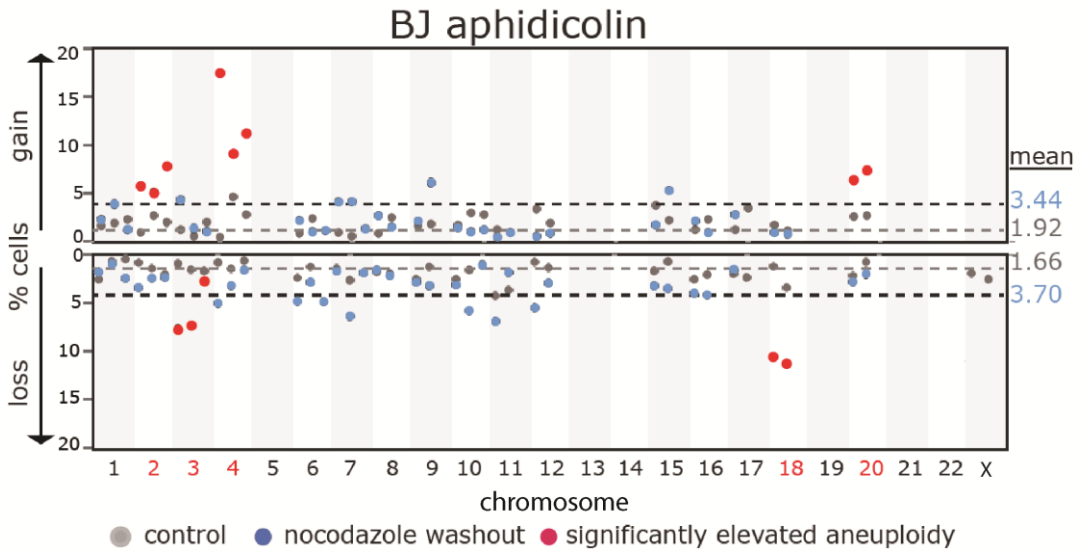

Figure 6.8. BJ aneuploidy rates following DNA replication stress. Aneuploidy rates were investigated in BJ cells following 24 hours of replication stress induced by aphidicolin. Global chromosome missegregation was gain was elevated to a similar rate as RPE-1 cells, but chromosome loss was marginally reduced (blue dots; 3.44 % gain, 3.70 % loss). The most frequently elevated aneuploidies were broadly similar to RPE-1 cells, involving chromosomes 2, 3, 4, 18 and 20 (red dots). All dots represent independent experiments. Red dots represent significant aneuploidy deviation from the mean using a two-tailed t-test (*p<0.05).

6.3.3. HCT116 aneuploidy rates following DNA replication stress

It is known that DNA replication stress is increased in colorectal carcinomas (CRC)[398]. I wanted to test the effect of replication stress in a cancer cell line, particularly colorectal cancer as it is known that CIN+ CRCs are associated with replication stress[226]. Importantly, HCT116 are CIN- and therefore a good tissue-type and cancer-specific control to determine patterns of aneuploidy following replication stress-induced chromosome missegregation. Additionally, the karyotype of HCT116 cells had already been extensively characterised by SNP array, and patterns of aneuploidy following nocodazole wash-out elucidated for this cell line (see **chapter 5.2.1.1** and **chapter 6.2.4**, respectively). The missegregation rates for chromosomes 5, 13, 14, 19, 21 and 22 were also analysed by conventional telomeric FISH on glass slides (preliminary data shown).

HCT116 cells were treated with low-dose aphidicolin for 24 hours, as for RPE-1 and BJ cells. As expected, chromosome missegregation was elevated following DNA replication stress (**figure 6.9**; blue and red dots). The mean rate of chromosome gain and loss were significantly higher than that observed for either RPE-1 or BJ cells under the same conditions (4.07 and 8.26 %, respectively; *$p<0.05$), implying that there are unique characteristics of HCT116 cells which predispose to replication stress-induced chromosome missegregation.

Overall, there was a wide range of chromosome gain rates following replication stress from individual experiments (0.46 to 10.66 %). Of note, chromosomes 4, 7 and 15 were being gained at a rate significantly above all other chromosomes (6.47, 6.29 and 8.06 %, respectively; *$p<0.05$).

Similarly, there was a wide range of chromosome loss rates across all chromosomes tested from independent experiments (0.46 to 29.4 %). Chromosomes 6, 18, 21 and X were lost at significantly higher rates than the mean (13.11, 14.91, 13.77 and 27.90

%, respectively; *p<0.05). The loss of chromosome X in HCT116 cells (27.90 %) was the highest rate of chromosome missegregation I observed for any cell line under any cellular stress, which is interesting as HCT116 cells are of male origin and therefore monosomy X in untreated cell; the loss of chromosome X therefore represents an extraordinary nullisomy population following DNA replication stress. Given that basal levels of monosomy X in HCT116 cells are undetectable in this assay, it is likely that this population will undergo apoptosis.

These data demonstrate that HCT116 cells missegregate chromosomes more frequently than non-transformed RPE-1 and BJ cells following DNA replication stress. They also reveal differences in chromosome missegregation patterns compared to RPE-1 and BJ cells, implying that there may be characteristics of transformed cells which promote instability of a different subset of chromosomes. One key observation is that there was a modest overlap between HCT116 cells following nocodazole wash-out and replication stress, suggesting that certain chromosomes are intrinsically vulnerable and others depend on the underlying mechanism in this cell line.

It is important to reiterate that only changes in centromere number for each chromosome are quantified. Furthermore, I have not formally validated these results by single-cell sequencing. These data therefore form the basis for further experiments elucidating how replication stress generates aneuploidy in cancer.

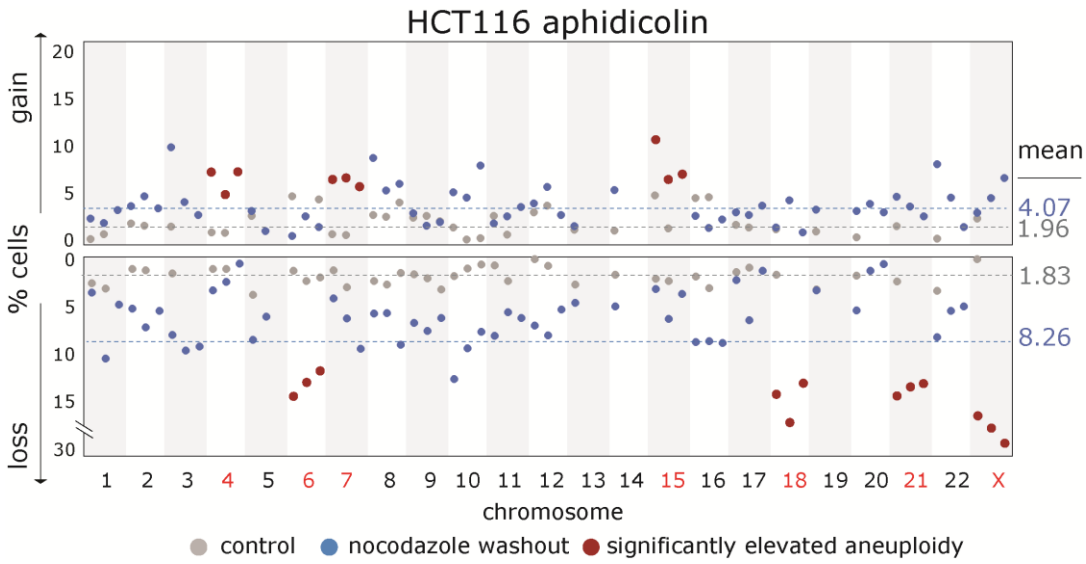

Figure 6.9. HCT116 aneuploidy rates following replication stress. Aneuploidy rates were investigated in HCT116 cells following 24 hours of replication stress induced by aphidicolin. Global chromosome missegregation was gain was elevated to a similar rate as RPE-1 and BJ cells, but chromosome loss was significantly increased (blue dots; 4.07 % gain, 8.26 % loss; *p<0.05). Significant chromosome gain was observed for chromosomes 4, 7 and 15; significant chromosome loss was observed for chromosomes 6, 18, 21 and X (red dots). Acrocentric chromosomes were scored manually in at least 200 cells from independent experiments using traditional manual scoring. All dots represent independent experiments. Red dots represent significant aneuploidy deviation from the mean using a two-tailed t-test (*p<0.05).

6.3.4. RPE-1 12/3 aneuploidy rates following DNA replication stress

Following the observation of recurrent patterns of missegregation in diploid and aneuploid RPE-1 cells after nocodazole wash-out, I wondered if similar patterns could be observed, and whether missegregation rates would be exaggerated in a similar way, following DNA replication stress in the trisomic RPE-1 cell line already discussed in this chapter – RPE-1 12/3 (**section 6.2.5**). One hypothesis is that the presence of an extra chromosome may increase chromosomal aberrations, following replication stress, by increasing the frequency of novel translocation involving the trisomic chromosome 12. Additionally, the missegregation rates for chromosomes 5, 13, 14, 19, 21 and 22 by were analysed by conventional telomeric FISH on glass slides (preliminary data shown).

RPE-1- 12/3 cells were treated with low-dose aphidicolin for 24 hours. Chromosome missegregation was elevated following DNA replication stress, as expected (**figure 6.10**; blue and red dots). The mean rates of chromosome gain and losses were comparable to HCT116 cells, but significantly higher than that observed for both diploid RPE-1 and BJ cells (4.37 and 6.31 %, respectively; *$p<0.05$). This is interesting as it suggests that the presence of a single extra chromosome is sufficient to increase aneuploidy globally following replication stress versus diploid RPE-1 cells.

Chromosomes 2, 4, 7 and 14 were gained at significantly higher rates than the mean, indicating that aneuploid cells also become frequently trisomic for a small subset of chromosomes following replication stress (4.64, 6.87, 9.15 and 11.58 %, respectively; *$p<0.05$). Interestingly, chromosomes 2 and 4 were also gained at high rates in diploid RPE-1 cells under the same conditions (chromosome 7 failed significance $p=0.64$ and chromosome 14 was not analysed in diploid RPE-1 cells),

confirming that patterns of chromosome gain are similar, but not identical, between diploid and aneuploid cells induced by DNA replication stress.

Furthermore, chromosomes 3, 13, 16, 18 and X were lost at high rates, which is in good agreement with the majority of significant monosomies in diploid RPE-1 cells (8.00, 13.02, 10.78, 10.51 and 13.95 %, respectively; *$p<0.05$). Chromosome 4 marginally failed significance ($p=0.064$) due to a large variation between experiments. Of note, chromosomes 8 and 15 were very stable and lost at rates comparable to that of untreated control cells (3.41 and 3.46%, respectively).

These data support the hypothesis that patterns of aneuploidy arising following DNA replication stress in diploid and aneuploid populations, derived from the same cell type, are recurrent and may be caused by inherent of properties of individual chromosomes. Additionally, the rates of aneuploidy following cellular stress were elevated by the presence of an additional chromosome 12, corroborating a similar observation following nocodazole wash-out (**section 6.2.5**), and the literature[336].

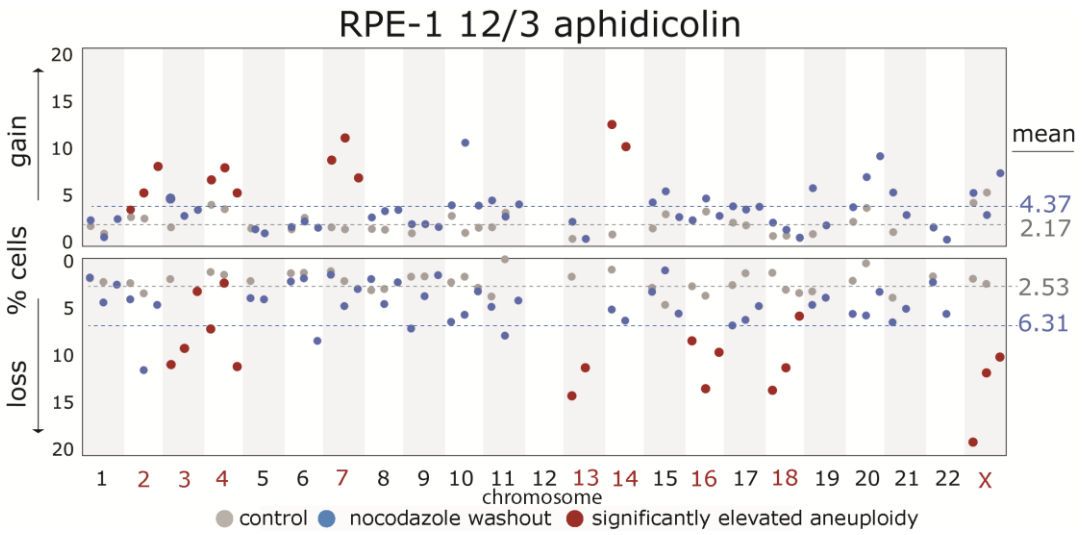

Figure 6.10. RPE-1 12/3 aneuploidy rates following DNA replication stress. Aneuploidy rates were investigated in a sub-clone of RPE-1 cells containing a chromosome 12 trisomy. Global chromosome gain and loss rates were marginally elevated compared to diploid RPE-1 cells (blue dots; 4.37 % gain, 6.31 % loss). The most frequently elevated aneuploidies were broadly similar to RPE-1 and BJ cells, involving chromosomes 2, 3, 4, 7, 13, 14, 16, 18 and X (red dots). Acrocentric chromosomes were scored manually in at least 200 cells from independent experiments using traditional manual scoring. All dots represent independent experiments. Red dots represent significant aneuploidy deviation from the mean using a two-tailed t-test (*p<0.05).

6.4. Aneuploidy rates following centromere protein A depletion

The centromere protein A (CENP-A), a specialised histone H3 variant, is known to play a role in specifying the centromere of human chromosomes, is important for down-stream assembly of kinetochore components and therefore important for the faithful segregation of chromosomes (**figure 6.11a**)[404]. It is currently unclear whether certain chromosomes are more vulnerable to the loss of centromere specification and fidelity. One important concept here is the idea of centromere strength – the notion that stability of chromosome attachment to the mitotic spindle is proportional to the recruitment of kinetochore components[291]. A critical limiting factor for kinetochore recruitment to centromeres is CENP-A, as CENP-A levels determine CENP-B recruitment which in-turn acts as a scaffold for the inner centromere complex[405–407]. Moreover, CENP-A levels are proportional to chromosome size. Therefore, I wanted to ask whether patterns of chromosome missegregation could be observed following CENP-A depletion[408].

6.4.1. An inducible CENP-A depletion system

To assess the role of CENP-A, and therefore centromere size and strength, in faithful chromosome segregation, I obtained cell lines with an inducible degradation motif-tagged CENP-A from a collaborator which were previously characterised[409]. These cell lines were derived from diploid RPE-1 cells, already described in this chapter (**section 6.2.1**); and DLD1 cells, a human colorectal carcinoma cell line. In each cell line, both alleles of CENP-A had been replaced with CENP-A mutants tagged with an auxin-inducible degradation (AID) domain and a GFP fluorophore (**figure 6.11b**).

It was previously shown that CENP-A degradation following addition of auxin was rapid, with a half-life of 16 minutes[409]. However, CENP-A already established at centromeres was protected from degradation until the next cell cycle when CENP-A is unloaded from the centromere. Therefore to completely remove all CENP-A, a total auxin treatment time of 48 hours was necessary to allow cells to proceed through one complete round of cell division in the absence of CENP-A.

To test whether I could observe complete CENP-A degradation in my hands, RPE-1-CENPA-AID-GFP and DLD1-CENPA-AID-GFP cells were treated with auxin for 48 hours. CENP-A-GFP was easily visualised in untreated cells by fluorescence microscopy and could be observed as punctate GFP spots (**figure 6.11c**; control). As expected, CENP-A was completely depleted by 48 hours in the presence of auxin in both RPE-1 and DLD1 cell lines (**figure 6.11c**; +48h IAA). These data demonstrate that these cell lines are capable of a complete and expeditious degradation of the CENP-A protein and can therefore be used to determine the rates of chromosome missegregation following centromere and kinetochore assembly disruption.

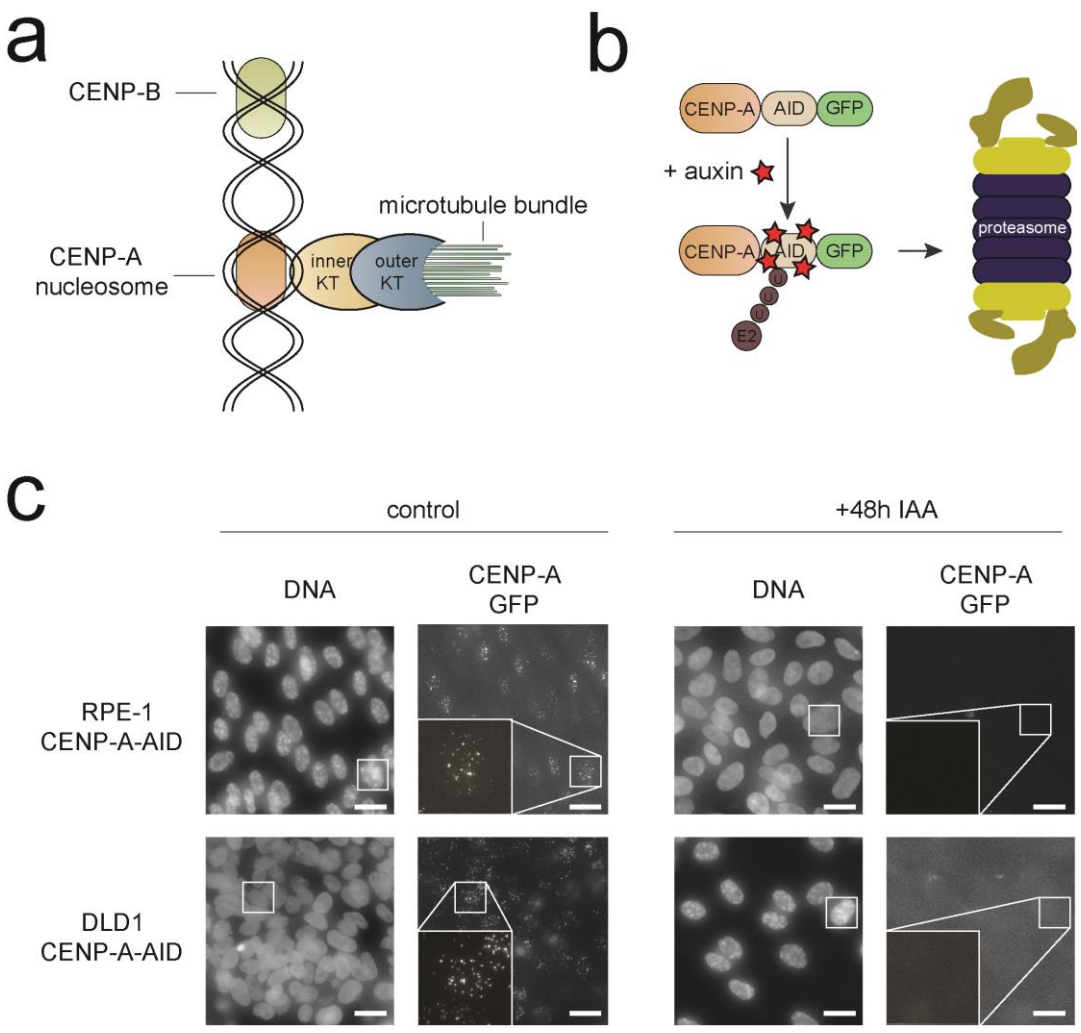

Figure 6.11. An inducible CENP-A degradation system. (a) CENP-A is incorporated at centromeric DNA sequences and helps assembly of down-stream kinetochore components which are required for chromosome biorientation. (b) CENP-A tagged with an auxin-inducible degradation (AID) domain and a GFP fluorophore is degraded by the proteasome following addition of auxin. (c) CENP-A is completely degraded following 48 hours auxin treatment in RPE-1 and DLD1 cells. Inset: CENP-A foci with and without auxin treatment. Scale bars: 50 µm.

6.4.2. RPE-1 aneuploidy rates following CENP-A depletion

RPE-1-CENP-A-AID cells were used to determine whether differences in centromeric CENP-A generates aneuploidy patterns following CENP-A depletion. First, the mean rate of chromosome gain and loss were determined in unperturbed cells and found to be marginally lower in control RPE-1-CENP-A-AID cells compared to control parental RPE-1 cells, although this did not reach significance (**figure 6.12**; grey dots; 0.82% *vs.* 1.03 % and 1.26 % *vs.* 1.83 %, respectively).

RPE-1-CENP-A-AID cells were treated with auxin for 48 hours to remove CENP-A. As expected, chromosome missegregation was elevated following CENP-A removal (**figure 6.12**; blue and red dots). There was a range of chromosome loss rates across all chromosomes tested. However, chromosomes 4, 9, 15, 16 and X were missegregating significantly more frequently than the mean (8.85, 6.61, 7.97, 7.90 and 8.21 %, respectively; *$p<0.05$). Additionally, global chromosome gain (1.29 %) was not as high as would be expected given the monosomy rates across the population (4.68 %). Across all chromosomes, trisomy rates higher than the mean of the untreated control cells was not observed, suggesting that trisomic cells may undergo apoptosis before 48 hours and are therefore undetectable. One way to test this would be to assess cell death at this time point.

These data suggest that the loss of CENP-A at the centromere, which is an indirect measure of centromere strength, generates chromosome-specific missegregation patterns. Furthermore, variations in centromere length, and thus CENP-A, between chromosomes may determine the rates of chromosome missegregation when the fidelity of kinetochore assembly is compromised.

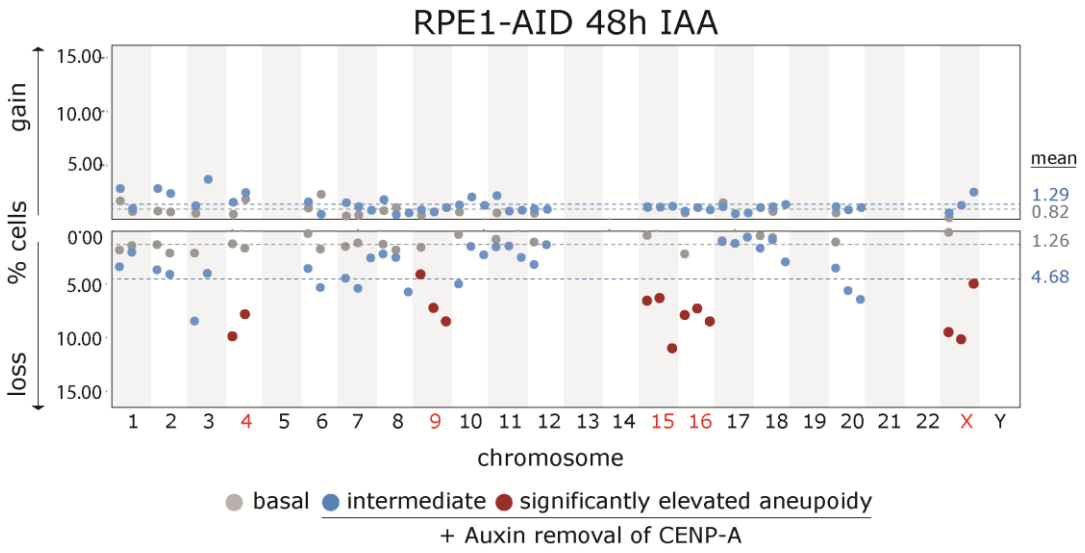

Figure 6.12. RPE-1 aneuploidy rates following CENP-A depletion. Aneuploidy rates were investigated in RPE-1 cells following 48 hours of CENP-A depletion induced by auxin (IAA). Basal levels of aneuploidy were low in untreated cells (grey dots; 0.82 % gain, 1.26 % loss). Global chromosome missegregation was elevated following removal of CENP-A for at least one cell cycle (blue dots; 1.29 % gain, 4.68 % loss). No chromosomes with significantly elevated trisomy rates were detected. The most frequently elevated chromosome losses were for chromosomes 4, 9, 15, 16 and X (red dots). All dots represent independent experiments. Red dots represent significant aneuploidy deviation from the mean using a two-tailed t-test (*p<0.05).

6.4.3. DLD1 aneuploidy rates following CENP-A depletion

A transformed, chromosomally-stable colorectal carcinoma cell line, DLD1, was used to determine whether the patterns of chromosome loss observed following CENP-A depletion in RPE-1 cells were cell line-specific. Similarly to RPE-1 cells, DLD1 cells had both endogenous alleles of CENP-A replaced with AID-tagged mutants.

First, the mean rate of chromosome gain and loss were determined and found to be marginally higher in untreated DLD1-CENPA-AID cells compared to untreated RPE-1-CENPA-AID cells, but this did not reach significance (**figure 6.13**; grey dots; 1.10 % *vs.* 0.82% and 1.97 % *vs.* 1.26 %, respectively).

DLD1-1-CENP-A-AID cells were treated with auxin for 48 hours to remove CENP-A. As expected, chromosome missegregation was elevated following CENP-A removal (**figure 6.13**; blue and red dots). Mean chromosome loss rates were similar to those observed in RPE-1 cells following CENP-A removal (4.61 % *vs.* 4.68 %), however average chromosome gain rates were significantly greater (1.82 % *vs.* 1.29 %; *$p<0.05$). Strikingly, chromosomes 1, 6, 7 and 18 were missegregating above the mean across independent experiments which corresponded to a complete non-overlapping of aneuploidy-prone chromosomes between the cell lines (**figure 6.13**; red dots; 5.77, 6.97, 8.32 and 5.45 %, respectively; *$p<0.05$). Additionally, global chromosome gain was also not as high as would be expected given the monosomy rates across the population in DLD1 cells, similarly to RPE-1 cells (1.82 %).

These data suggest that chromosome missegregation rates following a destabilisation of the centromere and/or kinetochore are cell line dependent. Alternatively, they may highlight intrinsic differences in centromere fidelity between transformed and non-transformed cell types.

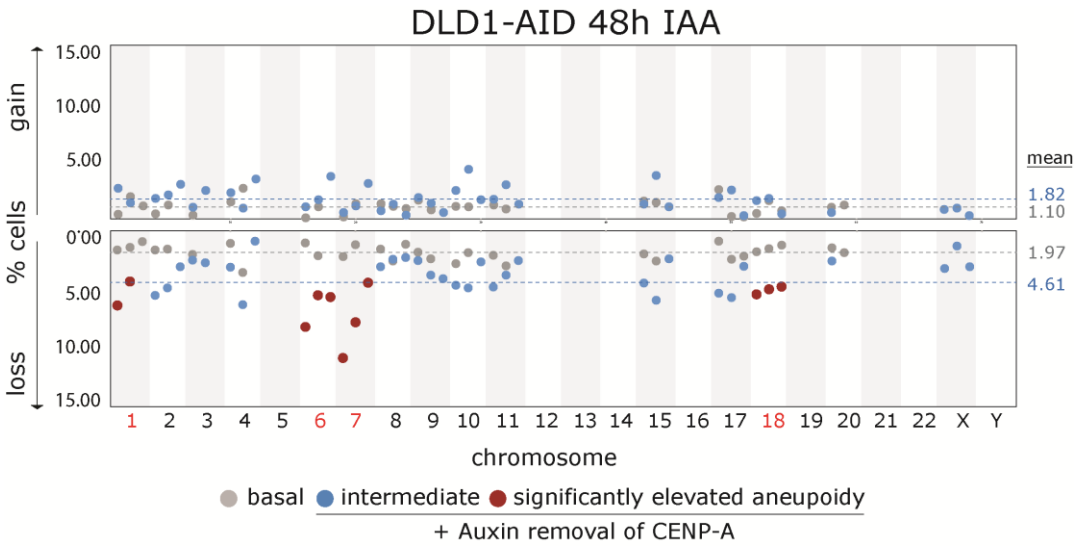

Figure 6.13. DLD1 aneuploidy rates following CENP-A depletion. Aneuploidy rates were investigated in DLD1 cells following 48 hours of CENP-A depletion induced by auxin (IAA). Basal levels of aneuploidy were low in untreated cells (grey dots; 1.10 % gain, 1.97 % loss). Global chromosome missegregation was elevated following removal of CENP-A for at least one cell cycle (blue dots; 1.82 % gain, 4.61 % loss). No significantly-elevated chromosome gain rates were detected. The most frequently elevated chromosome losses were strikingly different to RPE-1 cells following CENP-A depletion, involving chromosomes 1, 6, 7 and 18 (red dots). All dots represent independent experiments. Red dots represent significant aneuploidy deviation from the mean using a two-tailed t-test (*p<0.05).

6.5. Summary

I have implemented a high-throughput approach to determine individual-chromosome aneuploidy rates in unperturbed cells and reported how these rates change in response to a variety of cellular stresses. The discovery that individual chromosomes missegregate with different frequencies following nocodazole wash-out is a novel observation with high biological significance due to the importance of merotely in human disease and the ubiquitous nature of nocodazole in the study of aneuploidy. Importantly, this phenomenon was not cell-line specific, as a small subset of chromosomes behaved similarly in cell lines derived from different tissues of origin.

Moreover, individual chromosomes were missegregated with significantly elevated frequencies following replication stress, revealing that particular chromosomes are intrinsically vulnerable and others are contingent on the underlying mechanism inducing aneuploidy.

Furthermore, I have demonstrated that CENP-A-dependent centromere specification sensitises a small number of chromosomes to CENP-A depletion. Strikingly, aneuploidy patterns observed in the absence of CENP-A were not recurrent between RPE-1 and DLD1 cells, exposing a previously-unrecognised potential for cell line-dependent variation in CENP-A levels at individual centromeres.

7. Visualising individual chromosome dynamics during mitosis

7.1. Individual chromosome segregation behaviour at anaphase

Preface

It is widely reported in the literature that conditions which elevate aneuploidy often generate segregation errors at anaphase[410–412]. Indeed, it is possible to stratify segregation errors into a variety of sub-categories in an attempt to refine the underlying mechanism and impact on chromosomal instability phenotypes. Segregation errors are broadly split into two categories: lagging chromosomes (caught at the centre of dividing mitotic figures) and chromosomes bridges (thin DNA strands which span between the dividing mitotic figures)[226,413]. A prominent gap in my current understanding, based on the available literature, is the lack of data concerning chromosome-level resolution of segregation errors and therefore the contribution of individual chromosomes to the overall error rate.

My data from chapter 6 highlighted that a subset of chromosomes account for a disproportionate amount of the population-wide aneuploidy following cellular stress in multiple cell lines, induced through different mechanisms. Therefore, it is clear that there is a burgeoning requirement to elucidate if there are differences between individual chromosome segregation errors at anaphase, and their contribution to the overall error rate. I hypothesised that aneuploidy-prone chromosomes may account for a significant proportion of segregation errors observed at anaphase following nocodazole wash-out.

Here, I quantify lagging chromosome rates at anaphase with single chromosome-level resolution. Strikingly, I reveal that individual chromosomes undergo different routes to aneuploidy, even under the same cellular stress. Moreover, I expose the phenomenon of ‘premature sister chromatid separation’ (PSCS) for particular aneuploidy-prone chromosomes following nocodazole wash-out[414,415].

7.1.1. RPE-1 individual chromosome segregation error rates

RPE-1 cells were arrested in mitosis with nocodazole for eight hours followed by a release for one hour to allow cells to proceed through to anaphase. The 8-hour nocodazole arrest length was the same as for chapter 6, so a fair comparison between aneuploidy rates and segregation errors could be made. A panel of highly-aneuploid (1, 2, 3, 4, 7 and 10) and relatively stable (6 and 17) chromosomes were marked with two-colour FISH with centromeric α-satellite probes to determine the lagging rates for each chromosome at anaphase (**figure 7.1a**).

Strikingly, at least one chromosome 1 allele was observed lagging between the mitotic figures in ~ 50% of anaphases (**figure 7.1b**). Staining simultaneously for chromosome 1 and an all-centromere mark, and scoring missegregation as a function of all lagging chromosomes per cell, revealed that chromosome 1 accounted for 43 % of all lagging chromosomes at anaphase. Chromosomes 2 and 10 accounted for a further 22 % and 12 % of all laggards, respectively. These data demonstrate that over three-quarters of all lagging chromosome at anaphase are accounted for by just three aneuploidy-prone chromosomes following nocodazole wash-out in RPE-1 cells.

Conversely, I did not observe a significant increase in the lagging rates for chromosomes 3, 4 and 7, despite the observation that these chromosomes are frequently aneuploid under these conditions (**chapter 6.2.1**). However, it is possible that these chromosomes undergo cryptic non-disjunction, where chromosome missegregation occurs without a lagging intermediate.

To test the hypothesis that chromosomes 3, 4 and 7 may undergo cryptic non-disjunction, the percentage of monosomy/trisomy was scored following nocodazole wash-out in cells without lagging chromosomes (**figure 7.1b**). Importantly, chromosomes 3, 4 and 7 displayed non-disjunction at rates which were comparable

to the aneuploidy rates obtained by flow cytometry (4.67 %, 6.00 % 5.00 %, respectively), demonstrating that chromosomes undergo different routes to aneuploidy, even under the same cellular stress.

I next wondered if individual chromosomes take longer to align at metaphase, and if this may provide indications as to the underlying chromosome biology causing the striking differences in segregation error rate. Given that the McClelland laboratory has observed chromosome alignment to take approximately 45 minutes following nocodazole wash-out, the percentage of unaligned chromosomes was determined at this time point[339]. Interestingly, the frequency that individual chromosomes were unaligned at 45 minutes post-nocodazole wash-out displayed high heterogeneity. Chromosome 1 unalignment was highest, occurring in 37 % of prometaphase cells (**figure 7.1c and 7.1d**). All other chromosomes tested were unaligned in between 12 % and 22 % of prometaphase cells.

These data may reflect the disparity in the distances chromosomes have to congress to align at metaphase – chromosomes residing in the interphase nuclear core will require less time to congress to the spindle equator than those occupying the interphase nuclear periphery.

To assess whether unalignment for individual chromosomes was eventually resolved given extra time, cells were prevented from entering mitosis by inhibiting proteasome-dependent securin breakdown with MG132 for a further 2 hours, immediately following nocodazole wash-out. Despite the inhibition of securin cleavage, some sister chromatids were observed on opposing sides of the metaphase plate, suggesting cohesion failure and premature sister chromatid separation (**figure 7.1e**, PSCS). Strikingly, chromosome 1 displayed PSCS in 46.06% of prometaphase cells (**figure 7.1f**). PSCS was also observed for chromosome 2 (30.2 %) and to a lesser extent for the other chromosome analysed (5.59 to 15.34 %). These data suggest that there may be chromosome 1 and 2 -

specific sister chromatid cohesion fatigue following mitotic arrest. Moreover, PSCS was not observed for chromosome 1 in metaphase spreads following 8 hours nocodazole treatment alone, suggesting that microtubule pulling forces are required for this phenotype (**figure 7.1g and 7.1h**).

These data demonstrate that the chromosome missegregation rates, determined in chapter 6, likely reflect the intrinsic properties of individual chromosomes. Furthermore, the vulnerability of subsets of chromosomes following nocodazole wash-out may influence pathological aneuploidy patterns observed in human disease, through multiple routes to aneuploidy. Importantly, I have shown that routes to aneuploidy are not homogenous for individual chromosomes, even under the same cellular stress, highlighting a previously-uncharacterised need for chromosome-level characterisation of molecular mechanisms which generate CIN.

A further unexpected consequence of nocodazole arrest was the elevated rate of PSCS for chromosomes 1 and 2, demonstrating that there may be chromosome-level differences in cohesin establishment or maintenance, exposing a potentially novel route by which patterns of aneuploidy might arise in human disease.

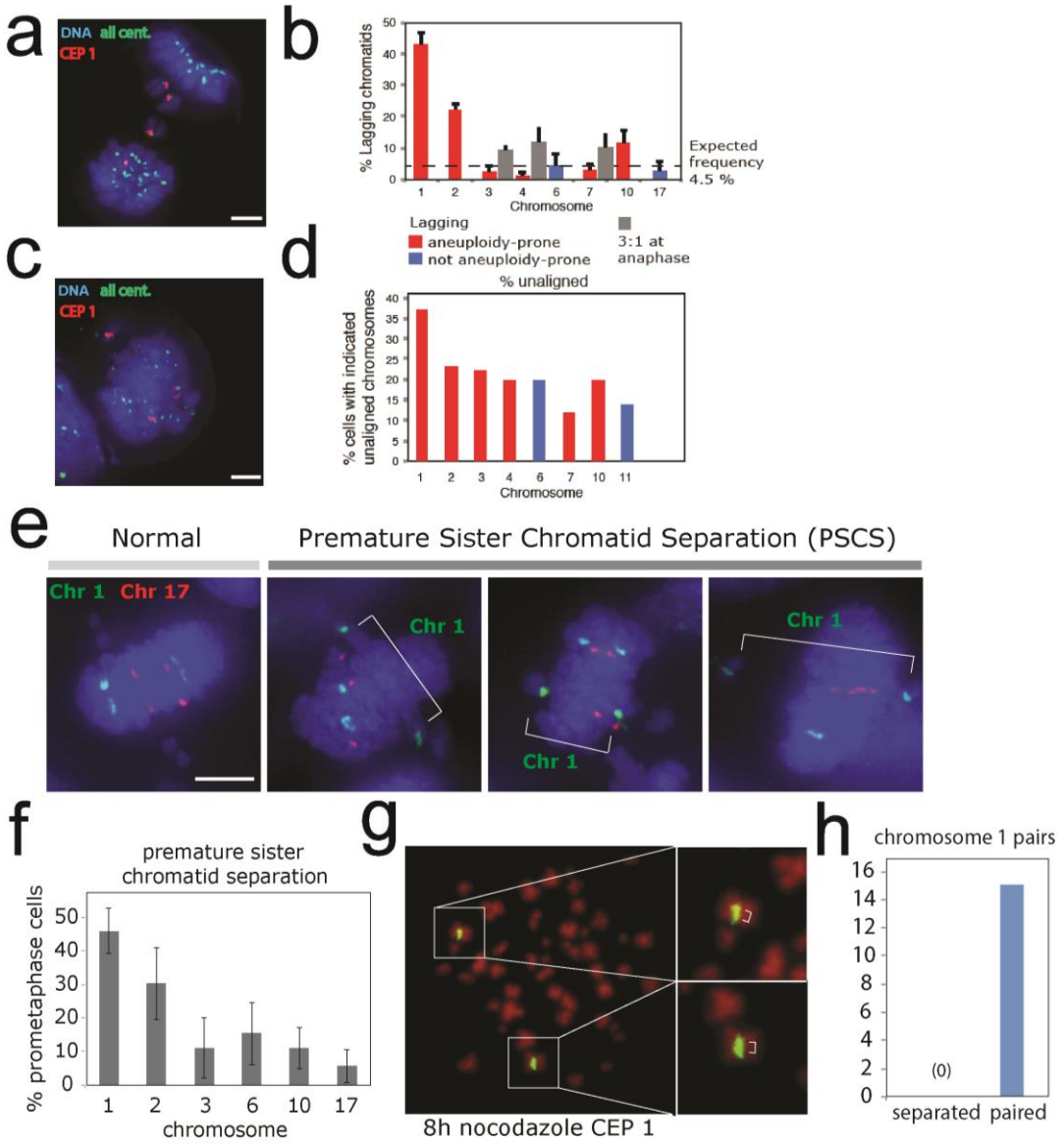

Figure 7.1. Characterising RPE-1 segregation errors following nocodazole wash-out. (a & b) Lagging and non-disjunction rates for a panel of chromosomes. (c & d) Chromosome 1 is frequently misaligned at late prometaphase; n=1. (e & f) Chromosome 1 and 2 are vulnerable to premature sister chromatid separation (PSCS). (g & h) PSCS is not observed at metaphase in the absence of microtubule pulling forces. Inset: non-separated chromosome 1 chromatids. Data by Dr. Sarah McClelland. Scale bars: 5 µm.

7.2. Metaphase chromosome territories

Preface

It is known that chromosomes occupy well-defined territories in the interphase nucleus[67,416]. What is less clear, is whether the spatial arrangement of chromosomes during interphase gives rise to similar patterns in the metaphase plate as cells proceed to sister chromatid alignment at the spindle equator. Early work demonstrated the potential for non-random arrangement of chromosomes in metaphase spreads[417,418]. However, this approach is subject to significant artefacts due to experimental reproducibility and subtle fluid mechanic disturbances as chromosomes settle onto the solid glass support – thus obscuring the true arrangement. Moreover, assessing the arrangement of chromosomes in the unperturbed metaphase plate has the additional advantage of enabling the elucidation of sister chromatid geometry.

I hypothesised that if patterns of chromosome alignment at metaphase were observed, they may be able to explain chromosome missegregation behaviour – it is possible that there are regions of the metaphase plate which are more prone to chromosome missegregation.

The geometry of individual metaphase sister chromatid pairs (including relative metaphase position, inter-centromere distance, inter-homologue distance and inter-centromere angle) are currently unknown. Determining these parameters at metaphase may reveal differences in underlying chromosome biology which could explain the non-random chromosome missegregation patterns observed in chapter 6.

7.2.1. The geometry of metaphase chromosomes

Given that interphase chromosome territories are subtle, I anticipated the same would be true at metaphase[64,419]. Determining the geometry of sister chromatid pairs in the metaphase plate would therefore necessitate the precise analysis of hundreds of metaphase chromosomes stained for specific centromeres by FISH with α-satellite probes. Manual geometric measurements of such large image sets using the image analysis program, ImageJ, can be labour-intensive and prone to analysis artefacts introduced by human error. To circumvent the issues associated with manual measurements, I developed a macro plugin for ImageJ which elucidates chromatid geometry, regardless of the orientation of the metaphase plate in the image (**chapter 10.1.2**). Using this novel approach, I undertook the first systematic and high-throughput assessment of metaphase chromosome arrangement to test whether specific chromosomes occupy preferred domains.

The metaphase plate region was defined by best-fit ellipse analysis of DAPI-stained DNA. The metaphase measurements defined both the major and minor axis length as well as the rotation of the plate around the ellipse centre from 0 to 180 degrees (**figure 7.2a**). The ellipse centre served an important function as a reference to which the normalised positions of sister chromatids could be radially mapped. Coordinates for the centre of individual centromere signals were expressed as the distance from the ellipse centre in both x and y dimensions (Δx and Δy, respectively).

To calculate the relative metaphase position, chromatids were mapped as the radial distance from the ellipse centre when aligned on the major axis, to standardise the positions in the plate (**figure 7.2b**). To achieve this, standard trigonometric functions were applied to the Δx and Δy coordinates (for proofs, see Materials and Methods, **chapter 3.8**). These formulae accounted for the positioning of sister chromatids relative to the major and minor axes, as well as the orientation of the metaphase

plate ellipse. To further account for metaphase orientation and length variation, relative chromatid positions were expressed as the normalised radial distance from the centre of the ellipse (**figure 7.2b**).

The angle (θ_1) between sister chromatids pairs was calculated as the deviation from parallel to the major axis, where [$\theta_1 = 0$] represents parallel chromatid alignment (**figure 7.2c**). Furthermore, inter-centromere distance and inter-homologue distance were calculated from the hypotenuse length between centromere pairs and relative distance on the major axis, respectively.

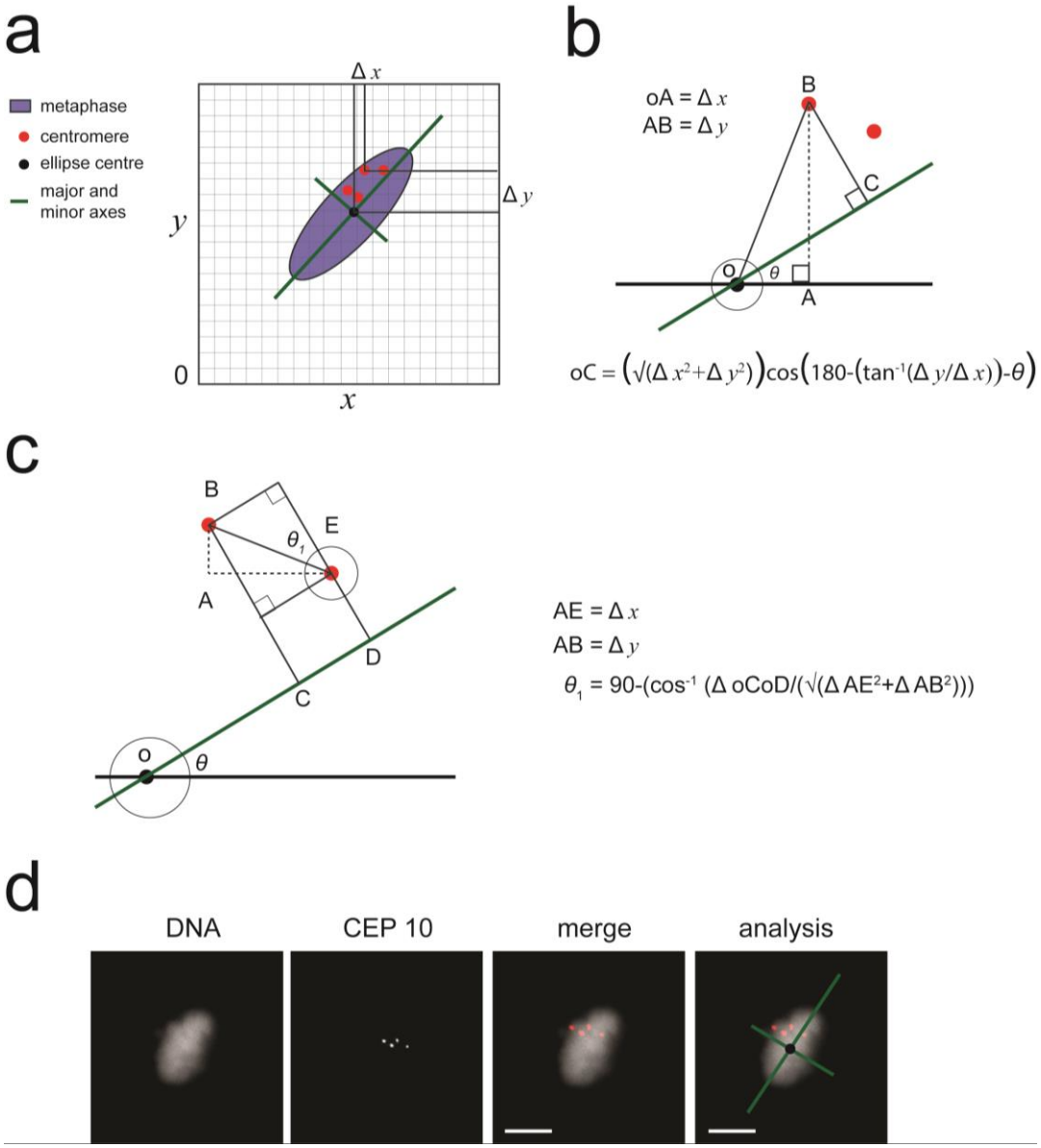

Figure 7.2. The geometry of metaphase chromosomes. (a) The coordinates of metaphase chromatids relative to the centre of the metaphase plate ellipse. (b) The relative metaphase plate position of individual chromatids can be determined by trigonometry in any metaphase orientation. (c) The perpendicular angle deviation between sister chromatid pairs. (d) Representative images illustrating chromatid positioning and metaphase geometry analysis. Scale bars: 5 µm.

7.2.2. RPE-1 metaphase chromosome geometry

7.2.2.1. Radial metaphase chromosome positioning

The normalised radial positioning of metaphase chromosomes in unperturbed RPE-1 cells, relative to the centre of the metaphase plate, were calculated as described (**figure 7.3a and section 7.2.1**). Radial metaphase chromosome positions were graphed on a cumulative frequency plot, to reveal average positional trends. Strikingly, radial distance from the metaphase centre showed a positive correlation with chromosome size – larger chromosomes at the metaphase periphery and smaller chromosome at the metaphase centre (**figure 7.3b and 7.3c**; R^2= 0.3783). Average chromosome position was defined at 50 % cumulative frequency: 15>18>17>3>11>16>8>X>6>20>10>7>4>2>9>1 (central to peripheral**; figure 7.3d**).

Of particular interest: chromosomes 1, 2, 4, 7, 10 and 18, which were frequently missegregated following nocodazole wash-out (**see chapter 6.2.1**), occupied average positions in two contiguous regions of the metaphase plate (**figure 7.3d**; aneuploidy-prone regions, *p<0.05). This suggests that chromosome arrangement at metaphase may predispose to aneuploidy, particularly at the metaphase periphery following nocodazole wash-out. Replication stress-induced aneuploidy-prone chromosomes were not found to be located in the aneuploidy prone regions, indicating this phenomenon may be related to microtubule dynamics (p=0.3173).

To determine if homologous chromosome pairs had preferred territories at metaphase, individual chromatid positions were graphed as a normalised density plot (**figure 7.3e**). Interestingly, although chromosomes showed broad size-related positioning, homologous chromosomes were infrequently confined to strict metaphase territories (example: chromosome 4; **figure 7.3e;** blue boxes**)**.

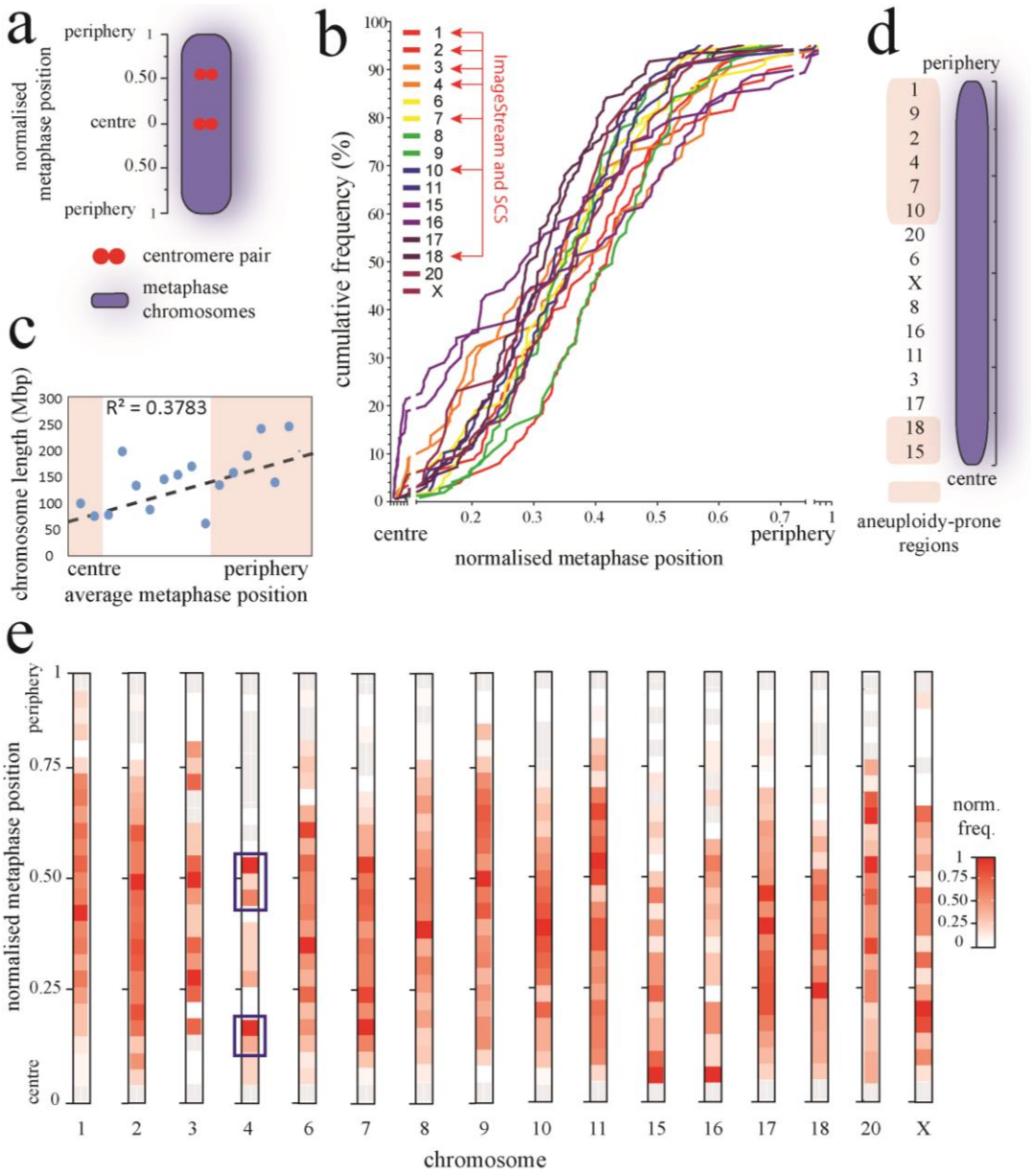

Figure 7.3. The radial positioning of metaphase chromosomes in RPE-1 cells. (a) Radial metaphase position can be expressed in metaphase length. (b) Cumulative frequency of metaphase positions reveals a size-dependent positioning phenomenon. (c) Chromosome size is correllated with radial metaphase position (R^2=0.3783). (d) Average chromosome position with aneuploidy-prone regions. Nocodazole-induced aneuploidy-prone significance by chi-squared *p<0.05 (0. 0117). (e) Individual chromsomes occupy a range of positions at metaphase. Blue boxes: example of chromosome 4 territories. Red arrows: significantly elevated aneuploidy in nocodazole wash-out. n=2820 from three independent experiments.

7.2.2.2. Inter-homologue distance

Given that chromosomes broadly exhibited size-dependent positioning at metaphase, I hypothesised that there may be a tendency for homologous chromosomes pairs to be spatially separated from one another by a regular distance, and this could contribute to the positioning phenomenon (**figure 7.4a**). To test this hypothesis, the distance between homologous chromosome pairs along the major metaphase axis was enumerated as a function of total metaphase distance, to account for variability in overall metaphase plate length. Strikingly, most homologous chromosomes were usually found within 25 % of the metaphase plate length from one another, irrespective of overall position (**figure 7.4b**). This was not true for chromosomes 1, 2 and 17 where chromosomes were frequently found beyond this distance. Excluding these three chromosomes, it was rare to find homologous chromosomes separated by greater than 50 % of the metaphase plate length.

The chromosome spacing phenomenon is most easily conceptualised using chromosome 4 as an example. The distribution of chromosome 4 at metaphase was broadly restricted to two readily-identifiable metaphase regions, [0.13-0.17] and [0.46-0.54], of the normalised radial distance from the metaphase centre (**figure 7.3e**; blue boxes). However, the spacing of chromosome 4 homologs was infrequently greater than 0.08 (8 %) of the metaphase plate length (**figure 7.4b**, chromosome 4). This suggests that chromosome 4 homologs congress to the same region of the spindle equator, thereby establishing territories in one of two regions in the majority of instances.

These data demonstrate that there may be mechanisms which govern the relative spacing of homologous chromosomes pairs – possibly as a result of interphase chromosome territory preservation through to metaphase.

7.2.2.3. Inter-centromere distance

The distance between centromeric signals of sister chromatid pairs can be used as a surrogate measure of cohesion. To investigate if particular chromosomes were more vulnerable to cohesion weakening (but not complete PSCS, described in chapter 7.1.1) at metaphase, and therefore increased missegregation at anaphase, inter-centromere distance was measured as described above (**chapter 7.2.1**). The mean inter-centromeric distance in untreated RPE-1 cells was 1.84 µm – less than the 2 µm limit defined for faithful sister chromatid cohesion (**figure 7.4c**) [256].

Conversely, the inter-centromeric distance for chromosomes 3, 9 and 18 were significantly greater than the mean, suggesting that some chromosomes may be more prone to weakened cohesion at metaphase (*$p<0.05$). This is interesting as chromosomes 3 and 18 were observed missegregating at significantly higher frequencies in this cell line following nocodazole wash-out, suggesting that cohesion weakening at metaphase may be compounded by a global increase in merotely after nocodazole wash-out.

Moreover, the average position of chromosomes 9 and 18 were found in the peripheral, aneuploidy-prone regions at metaphase. It is therefore a possibility that, in addition to the intrinsic properties of individual chromosomes, sister chromatid cohesin strength is influenced by the relative position occupied at metaphase. For chromosome X, no chromatids were separated by a large enough distance to be analysed, because of sister centromere signal overlapping.

One important consideration for the experiments described above is that, in my hands, the FISH signals of centromeric α-satellite probes are not as accurate for determining cohesion as immunofluorescent inter-kinetochore distances analysis. One explanation is that there may be incomplete probe binding or subtle differences between signals on sister chromatid pairs, even within the same metaphase plate.

Therefore, my data may be prone to artefacts introduced by differences in probe hybridisation. My image analysis tool finds the Gaussian-fitted centre point of fluorescent signals and measures the distance between non-overlapping signals. In this way, the inter-centromere distances defined here are more useful for inferring general weakening of centromeric cohesion rather than the *de facto* distance between sister centromeres.

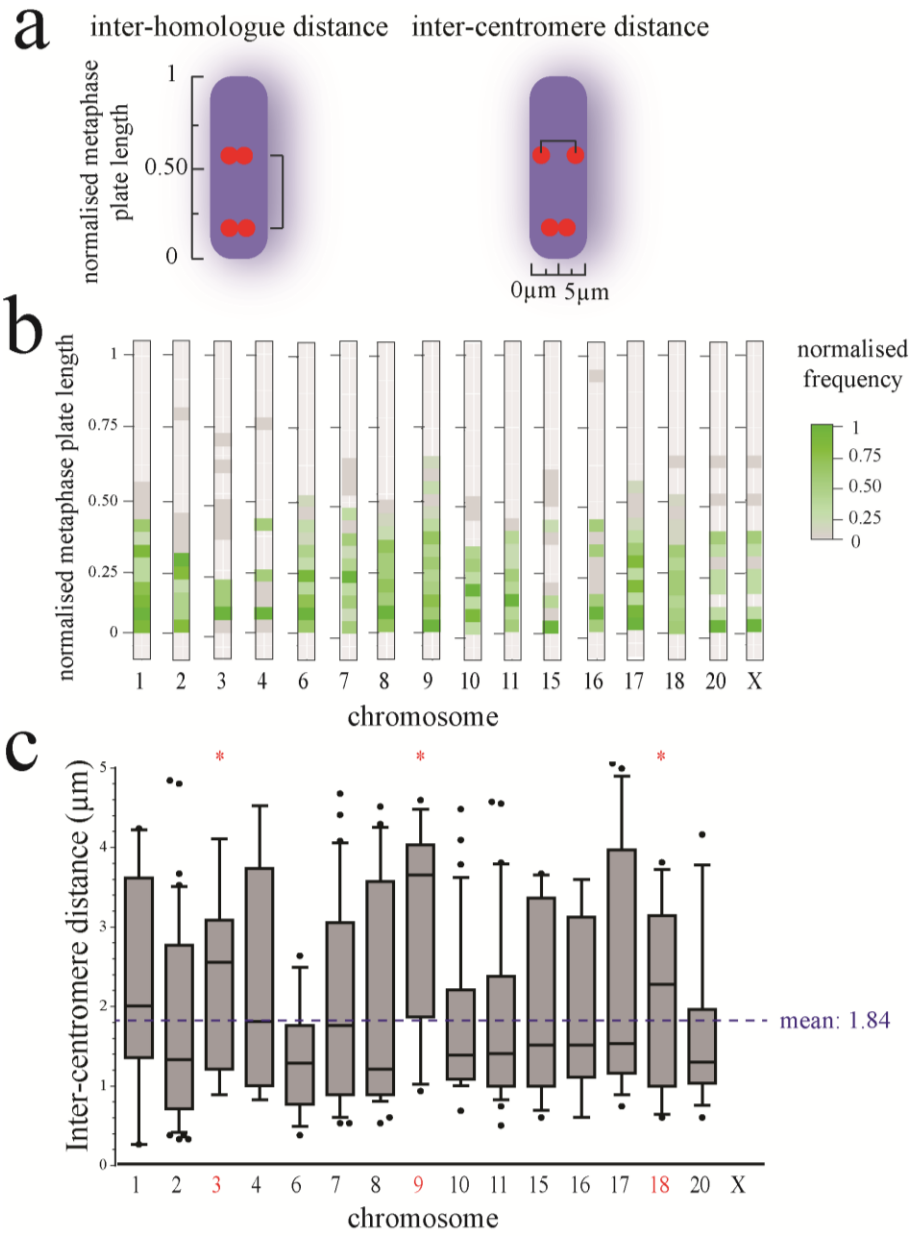

Figure 7.4. The separation of sister chromatids and homologous chromosomes in RPE-1 cells. (a) The distance between homologous chromomes can be expressed relative to metaphase plate length. Intercentromere distance was calculated between sister chromatid pairs; n=722. (b) Homologous chromosomes are rarely separated by greater than 50 % of the total metaphase length. (c) Sister chromatids 3, 9 and 18 are frequently separated by greater than 2 µm. Whiskers inclusive of 90 % to 10 % minimum and maximum values; n=325 from three independent experiments. Asterisks represent significant difference from the mean using a two-tailed t-test (*p<0.05).

7.2.2.4. Inter-centromere angle

It is currently unknown if there are differences in the angle between sister chromatid pairs at metaphase. This is interesting to determine, as gross irregularities in sister chromatid orientation may proclude faithful kinetochore-microtubule attachments and therefore segregation behaviour. It has already been demonstrated that the outer-kinetochore components are rotationally felxible, thereby increasing attachment to K-fibers at the metaphase periphery[420]. I wanted to ask a similar question of the individual chromatids themselves. To test this, deviation from perpendicular to the angle of the major axis of the metaphase plate between sister centromeres was calculated by trigonometry. I find that the vast majority of human metaphase sister chromatid pairs align within 0º – 6º of perpendicular to the major axis in untreated RPE-1 cells (**figure 7.5**). Occasionally, angles larger than 6º were observed for all chromosomes except 3, 4, 11 and 15. For chromosome X, no chromatids were separated by a large enough distance to calculate the angular deviation.

These data suggest that sister chromatid arrangement is tightly controlled to maintain near-perpendicularity with the major axis of the metaphase plate, as is expected for properly bioriented chromosomes at metaphase[421–423]. To examine this further, tracking with high temporal resolution of individual centromeres, marked by fluorescent centromere proteins, could be used to detect whether chromosomes which ultimately lag at anaphase first exhibit positioning or geometric defects.

A further consideration is that my data are determined from images projected from 3D, thus increasing the chance that my data are misrepresentative of the true chromatid geometry, as has been shown for inner and outer kinetochore components[420]. However, as my data reflect a larger-scale observation they are likely less influenced by image projection artefacts, although this has yet to be validated.

Figure 7.5. The rotation of sister chromatids at metaphase in RPE-1 cells.

Rose plot frequency histograms of the angular rotation between sister chromatids. Inner and outer circles are 0.5 and 1 frequency markers, respectively. Sister chromatids rarely rotate greater than 6 º from perpendicular to the major axis for most chromosomes. n=350 from three independent experiments.

7.2.3. BJ metaphase chromosome geometry

7.2.3.1. Radial metaphase chromosome positioning

To determine if size-dependent chromosome positioning applied broadly across multiple cell lines, BJ metaphase chromosome positions were determined as previously described (**chapter 7.2.1**). Similarly to the observation in RPE-1 cells, the average chromosome position at metaphase correlated with chromosome size (**figure 7.6b and 7.6c**; R^2=0.7537). The average chromosome position was defined at 50 % cumulative frequency, with chromosomes ordered as follows (central to peripheral): 18>20>16>15>11>10>8>17>X>6>4>7>3>9>2>1(**figure 7.6a**).

The most notable differences in chromosome positioning between cell lines was for chromosomes 3 and 20, found predominantly at the metaphase centre and periphery, respectively, in RPE-1 cells. This is important because chromosomes 18 and 20 were highly aneuploid following nocodazole in BJ cells (**chapter 6.2.2**), suggesting that central metaphase positioning may also contribute to the propensity of chromosomes to missegregate in addition to metaphase periphery vulnerabilities (**figure 7.6b**; aneuploidy-prone regions). In both nocodazole wash-out and replication stress, aneuploidy-prone chromosomes were found significantly more frequently in the aneuploidy-prone metaphase regions, confirming that regions of the metaphase plate are vulnerable to missegregation across cell lines (*p<0.05).

Analysis of individual chromosomes revealed a distribution throughout the metaphase plate which correlated with chromosome size but not individual chromosome territories (**figure 7.6c**). Chromosome positions were similar to, but not indistinguishable from, those observed in RPE-1 cells. For example, chromosome 16 positioning was discreet in RPE-1 cells but continuous in BJ cells. Additionally, chromosome 4 was more evenly distributed than in RPE-1 cells.

These data therefore highlight that chromosome arrangement at metaphase is broadly size-dependent but individual chromosomes are not restricted to particular domains. Furthermore, chromosome positioning at metaphase may predispose to aneuploidy of particular chromosomes, potentially by compounding the effects of other intrinsic chromosome characteristics, such as cohesion weakening and kinetochore-microtubule stability.

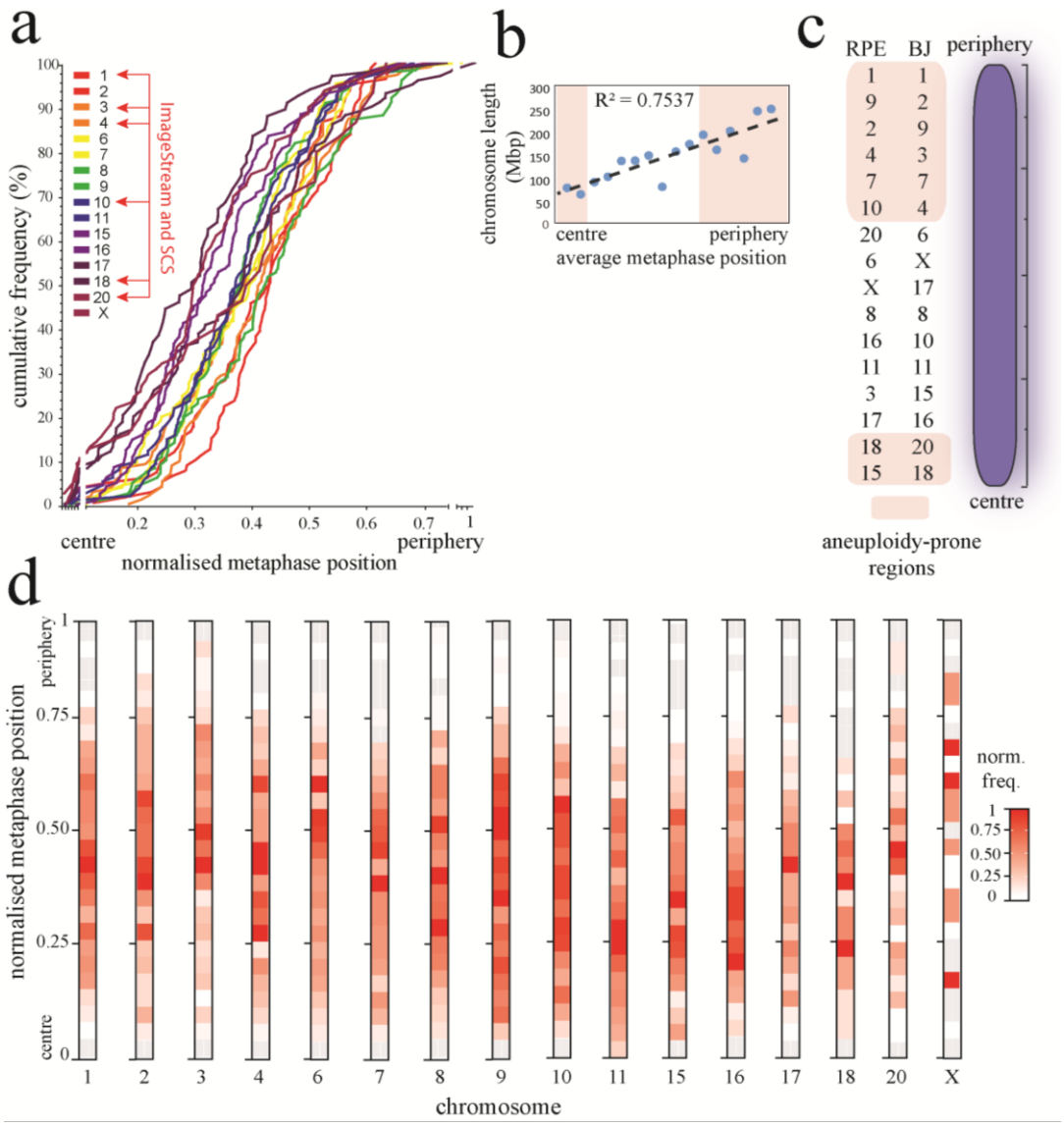

Figure 7.6. The radial positioning of metaphase chromosomes in BJ cells. (a) The cumulative frequency of metaphase plate positions reveals a size-dependent positioning phenomenon which was similar to that observed in RPE-1 cells. (b) Chromosome size is correllated with radial metaphase position (R^2=0.7537). (c) Comparison of average chromosome positions with aneuploidy-prone regions highlighted. Aneuploidy-prone significance by chi-squared *p<0.05 (0.0389; nocodazole wash-out and replication stress) (d) Chromatids occupy a range of positions and territories at metaphase to a lesser degree than RPE-1 cells. Red arrows: significantly elevated aneuploidy in nocodazole wash-out. n=3206 from three independent experiments.

7.2.3.2. Inter-homologue distance

Overall, homologous chromosome pairs were infrequently separated by greater than 50 % of the total metaphase length, similarly to RPE-1 cells (**figure 7.7a**). However, there were notable differences for some chromosomes. For example, chromosomes 3 and 11 were less-regularly spaced in BJ cells compared to RPE-1 cells, although there was no clear association between positioning of homologous chromosomes and differences in the missegregation rates of individual chromosomes.

These data suggest that whilst homologous chromosomes broadly appear to be found less than 50 % of the metaphase away from one another, there may be cell line-dependent variation in the regulation of homologous chromosome spacing. One explanation is that subtle difference in chromosome territories between cell lines is exacerbated in homologous chromosome positions at metaphase. As BJ cells are male and possess only one X chromosome it was not possible to obtain homologous distance data for this chromosome.

7.2.3.3. Inter-centromere distance

Similarly to RPE-1 cells, there was a range of inter-centromere distances in untreated BJ cells. The average inter-centromeric distance was 1.71 μm (**figure 7.7b**). Interestingly, the inter-centromeric distance for chromosome 1, 2, 7 and 9 was significantly above the mean, which correlated with their average position at the periphery of the metaphase plate, in the aneuploidy-prone regions. Indeed, these represent four out the five chromosomes furthest from the metaphase centre.

These data support the hypothesis that metaphase positioning may influence inter-centromeric distance. One way to test this hypothesis would be to analyse the inter-kinetochore distances along the length of the major axis of the metaphase plate.

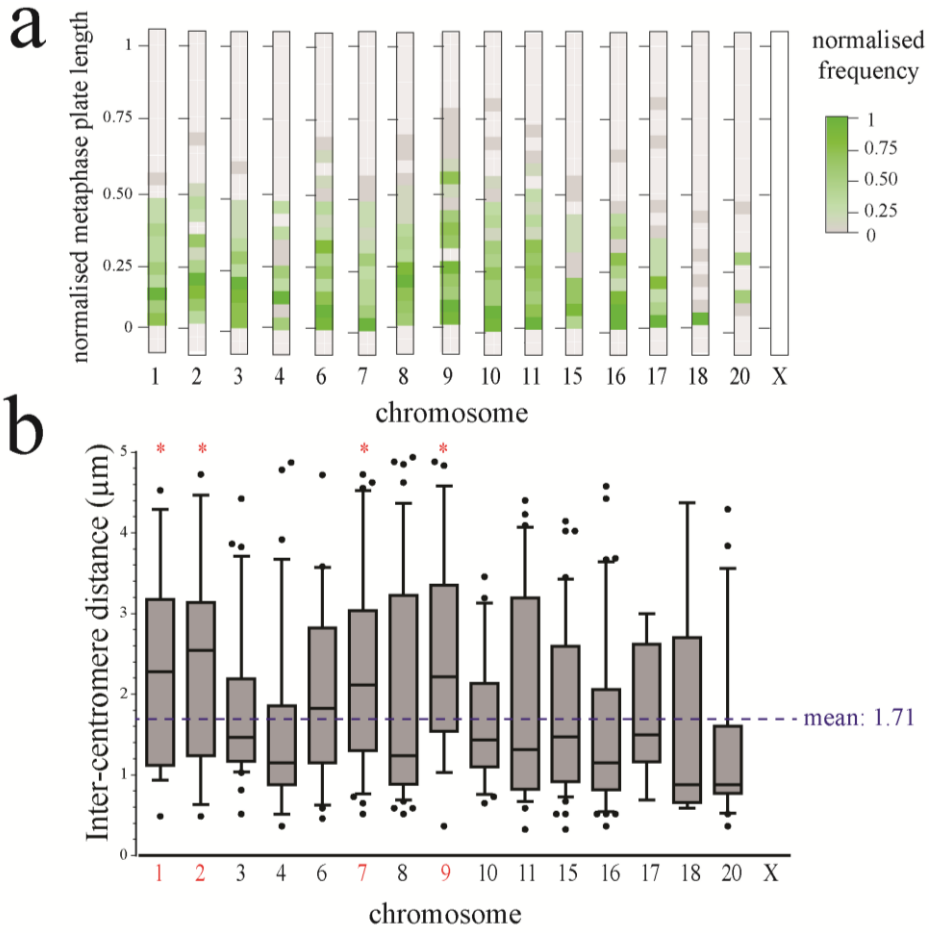

Figure 7.7. The separation of sister chromatids and homologous chromosomes in BJ cells. (a) Homologous chromosomes are rarely separated by greater than 50 % of the total metaphase length. Similar patterns are observed between BJ and RPE-1 cells; n=821. (b) Sister chromatids 1, 2, 7 and 9 are frequently separated by greater than 2 µm. Whiskers inclusive of 90 % to 10 % minimum and maximum values. n=463 from three independent experiments. Asterisks represent significant difference from the mean using a two-tailed t-test (*p<0.05).

7.2.3.4. Inter-centromere angle

The angle between sister chromatid pairs were similar to those observed in RPE-1 cells, with the majority of chromatid pairs exhibiting an angular deviation of less than 6º (**figure 7.8**). There was no obvious correlation between inter-centromere distance and the angular deviation, suggesting that sister chromatid alignment is tightly coordinated regardless of centromeric cohesion. However, angles greater than 6 º were not observed for chromosomes 16, 18 and 20 which, on average, occupy the most central metaphase positions in BJ cells. Of particular note, angles greater than 20 º were observed for chromosomes 1, 2 and 9 which occupy positions at the equatorial periphery.

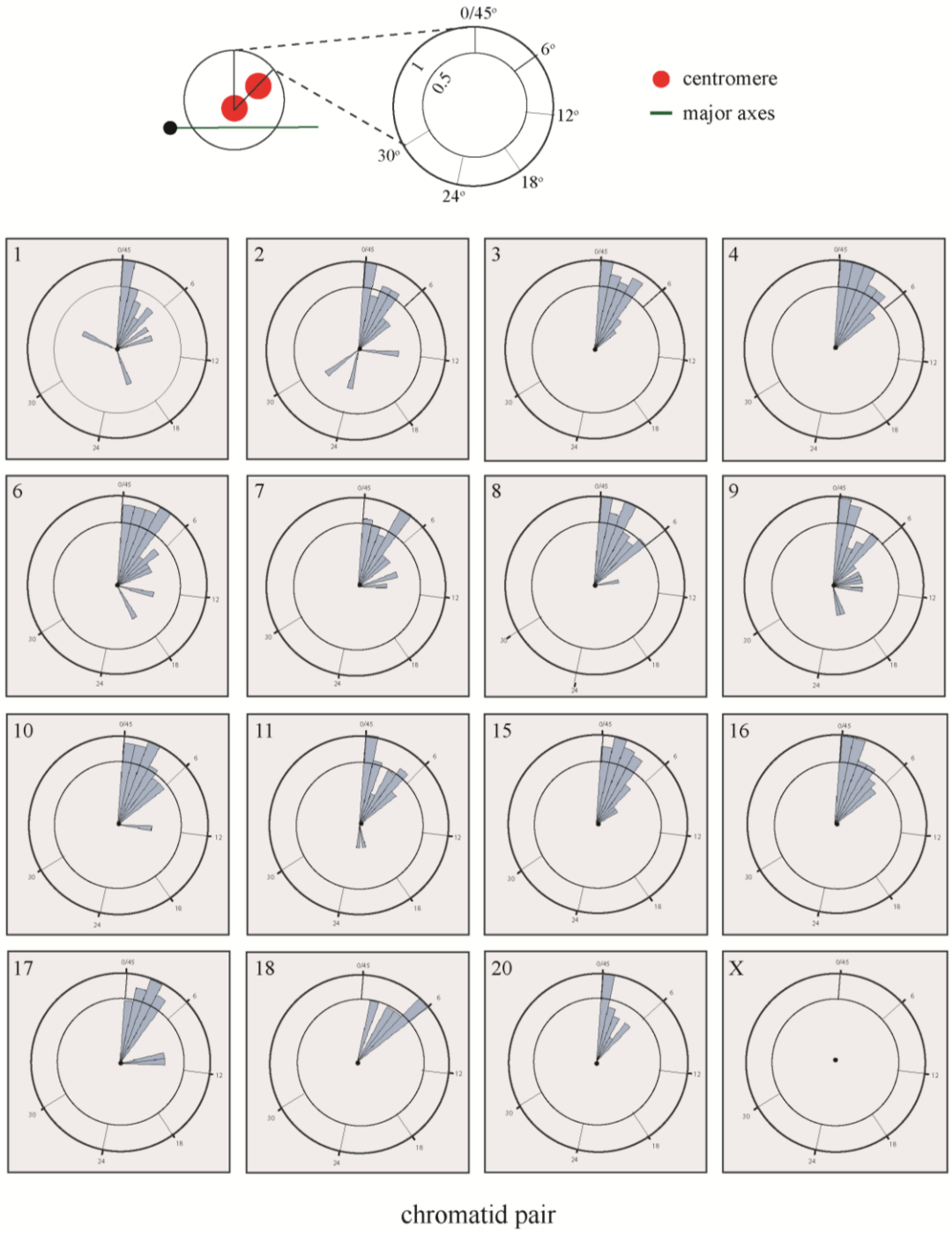

Figure 7.8. The rotation of sister chromatids at metaphase in BJ cells.

Rose plot frequency histograms of the angular rotation between sister chromatids. Inner and outer circles are 0.5 and 1 frequency markers, respectively. Sister chromatids rarely rotate greater than 6 º from perpendicular to the major axis for most chromosomes. n=479 from three independent experiments.

7.2.4. RPE-1 metaphase chromosome geometry post-nocodazole

Condensed chromosomes congress to the spindle equator during prometaphase by microtubule-dependent translocation[424–426]. It is currently unknown how metaphase positioning might be affected by an 8 hour period in the absence of microtubules, as is the case for nocodazole wash-out. One hypothesis is that chromosome position may be altered by Brownian motion of chromosomes during this period of microtubule absence. Additionally, I wanted to determine whether aneuploidy-prone chromosomes remained clustered at discrete metaphase regions, as previously observed in unperturbed RPE-1 and BJ cells. To answer these questions, the position of metaphase chromosome were analysed 45 minutes after release from an 8-hour nocodazole arrest, to allow time for chromosomes to congress to the spindle equator.

7.2.4.1. Radial metaphase chromosome positioning

The radial positioning of metaphase chromosomes in RPE-1 cells post-nocodazole arrest, relative to the centre of the metaphase plate, were calculated as described above. The relative chromosome positions were plotted as cumulative frequency along the metaphase axis, to reveal general positional preferences. Interestingly, size-dependent chromosome position at metaphase was observed, with chromosome order being similar to that reported in untreated RPE-1 and BJ cells (**figure 7.9a and 7.9b**). Chromosomes of intermediate size were arranged in accordance with their size throughout the plate. Average chromosomes arrangements were defined centrally to peripherally in the following order: 18>16>15>17>11>8>6>X>10>20>4>9>7>2>3>1 (**figure 7.9c**). In agreement with the data without nocodazole arrest, aneuploidy-prone chromosome are located significantly more frequently in the aneuploidy-prone metaphase regions (*$p<0.05$).

Furthermore, the position of individual chromatids was plotted as a density plot and revealed similar patterns to those observed for untreated RPE-1 and BJ cells (**figure 7.9d**). Of special interest, chromosome 1 – highly missegregated following nocodazole wash-out – was observed in a diffuse pattern relative that observed in untreated RPE-1 cells (**figure 7.9d**; blue boxes *cf.* **figure 7.3e**; chromosome 1). It is possible that the premature loss of sister chromatid cohesion (PSCS; **chapter 7.1.1**) may result in two phenotypes: one in which the sister chromatids are separated and remain uncongressed; the other where PSCS still occurs but individual sisters congress to a number of metaphase geographies in a stochastic manner. This could account for the diffuse pattern of chromosome 1 positions observed at metaphase following nocodazole wash-out.

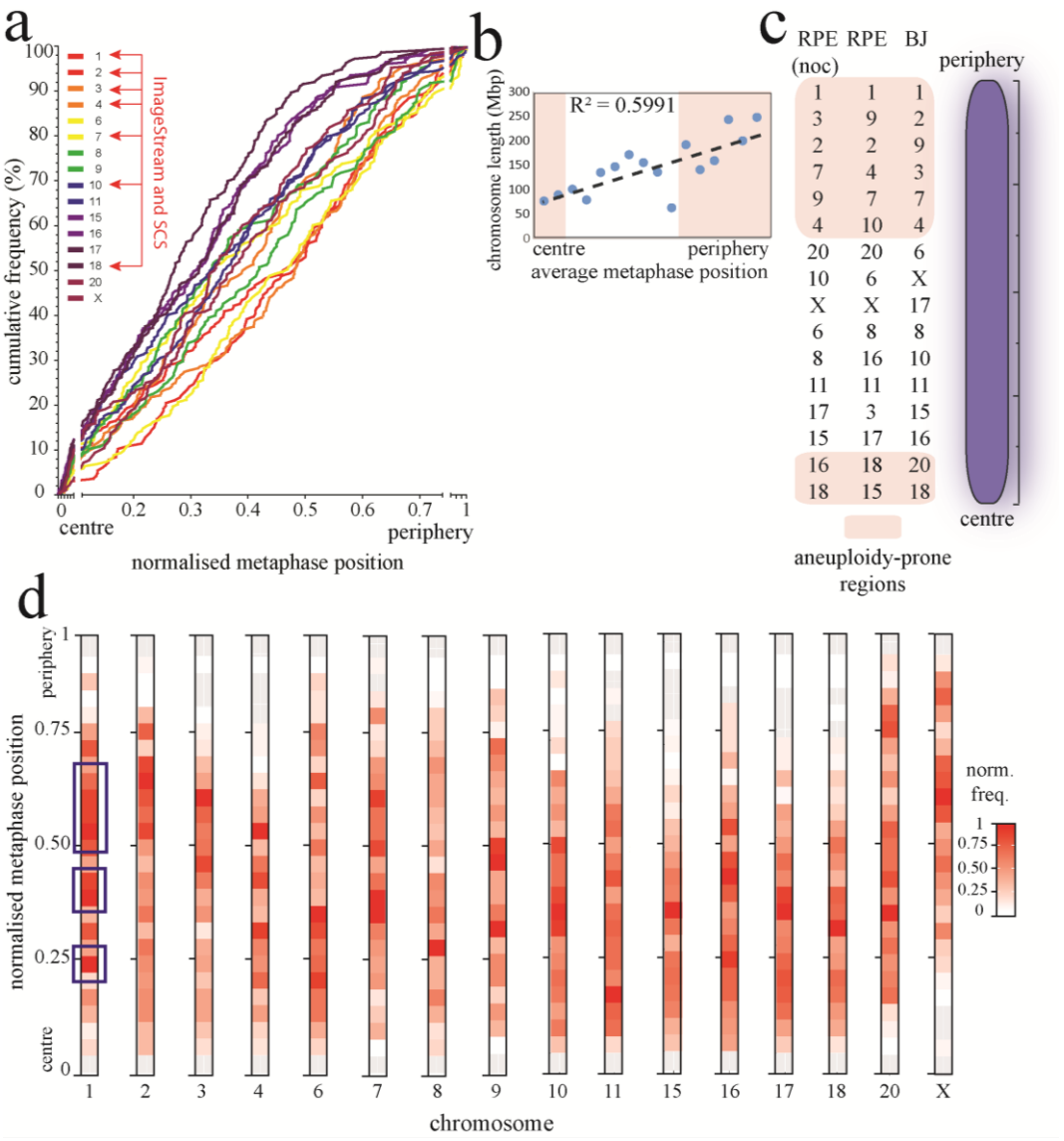

Figure 7.9. The relative position of metaphase chromosomes post-nocodazole wash-out in RPE-1 cells. (a) Radial metaphase plate positions reveals size-dependent chromosome positioning, similar to that observed in untreated RPE-1 cells. (b) Chromosome size is correllated with radial metaphase position (R^2=0.5991). (c) Average chromosome positions with aneuploidy-prone regions. Aneuploidy-prone significance by chi-squared *p<0.05 (0.0117). (d) Chromatids occupy a range of positions at metaphase. Red arrows: significantly elevated aneuploidy in nocodazole wash-out. Blue boxes: example of diffuse chromosome 1 territories n=3436 from three independent experiments.

7.2.4.2. Inter-homologue distance

The distance between homologous chromosome pairs along the major metaphase axis was enumerated as a function of total metaphase length, to account for variability in overall metaphase plate length. Interestingly, chromosomes 1, 3, 6, 7, 9 and 16 were rarely found more than 8% of total metaphase length apart (**figure 7.10a**). Additionally, for all chromosomes analysed, it was rare to find homologous chromosomes greater than 50% of the metaphase length apart. These data suggest that homologous chromosomes with well-defined metaphase territories tend to congress next to each other. They also suggest that homologous chromosome positioning is largely unaffected by microtubule disruption and therefore Brownian motion.

7.2.4.3. Inter-centromere distance

To investigate if particular chromosomes were more vulnerable to cohesion loss at metaphase following microtubule disruption, and therefore increased missegregation at anaphase, inter-centromere distance was measured as described above. The mean inter-centromeric distance was low and uniform compared to untreated RPE-1 cells (0.77 µm), which was not anticipated given my observation that chromosomes display PSCS following nocodazole wash-out (**figure 7.10b**).

One important consideration is that only chromosomes which are aligned in the plate are analysed, therefore unaligned chromosomes displaying PSCS are excluded. Additionally, the low and uniform inter-KT distance could represent unattached kinetochores which are not under microtubule tension yet.

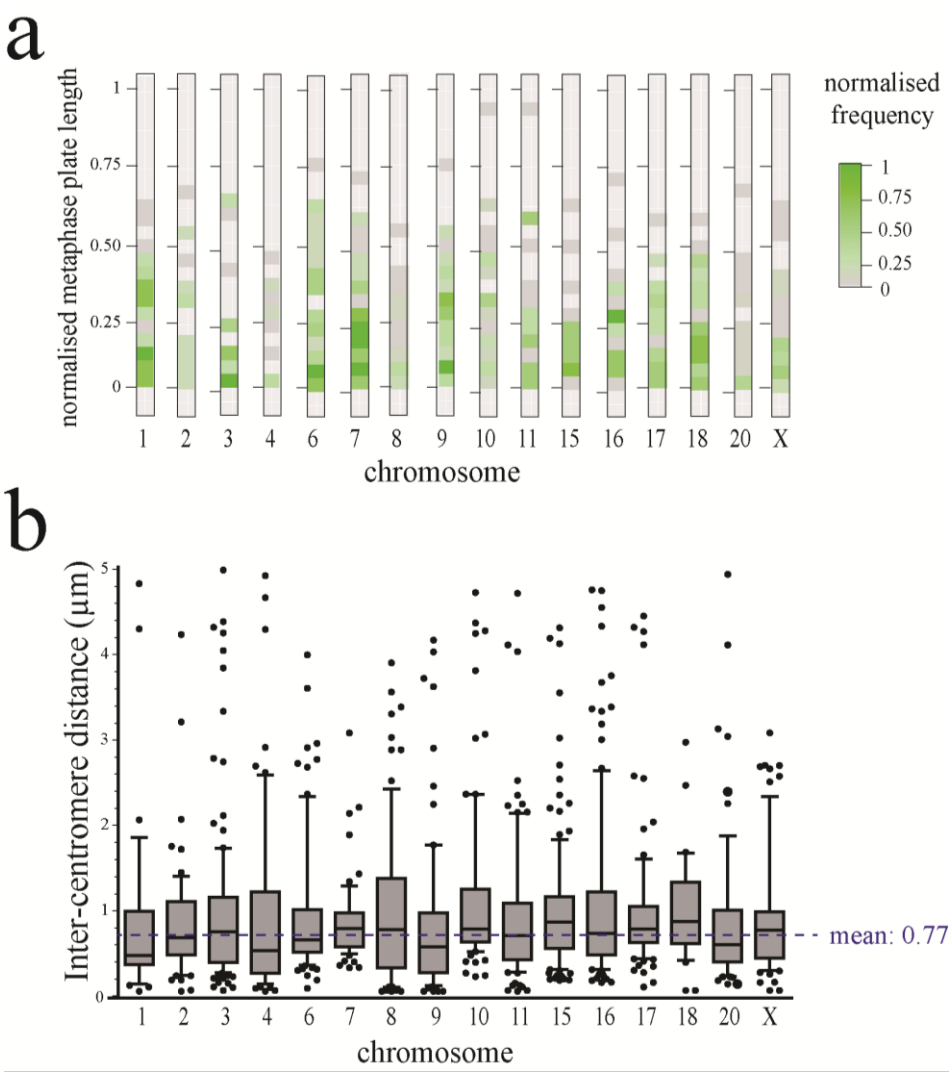

Figure 7.10. The separation of sister chromatids and homologous chromosomes in RPE-1 cells post-nococodazole wash-out. (a) Homologous chromosomes are rarely separated by greater than 50 % of the total metaphase length. Similar patterns are observed between treated and untreated RPE-1 cells; n=663. (b) Average sister chromatid separation did not exceed 1 µm for any chromosome. Whiskers inclusive of 90 % to 10 % minimum and maximum values. No significant deviation from the mean was observed with a two-tailed t-test. n=1335 from three independent experiments.

7.2.4.4. Inter-centromere angle

The deviation from perpendicular to the angle of the major axis of the metaphase plate was calculated by trigonometry as previously described. I find that most human metaphase sister chromatid pairs align within 0º – 6º of perpendicular to the major axis in RPE-1 cells following nocodazole wash-out, in-line with those aboserved for both untreated RPE-1 and BJ cells (**figure 7.11**). Occasionally, angles larger than 6º were observed for all chromosomes except 6, 17 and 20. Suprisngly, chromosomes 3, 4, 8 and 16 had an increased number of chromosomes which deviated by more than 6º, and chromosome 1 infrequently had sister chromatids that deviated by as much as 36º. These data suggest that sister chromatid arrangement is tightly controlled to maintain near-perpendicularity with the major axis of the metaphase plate.

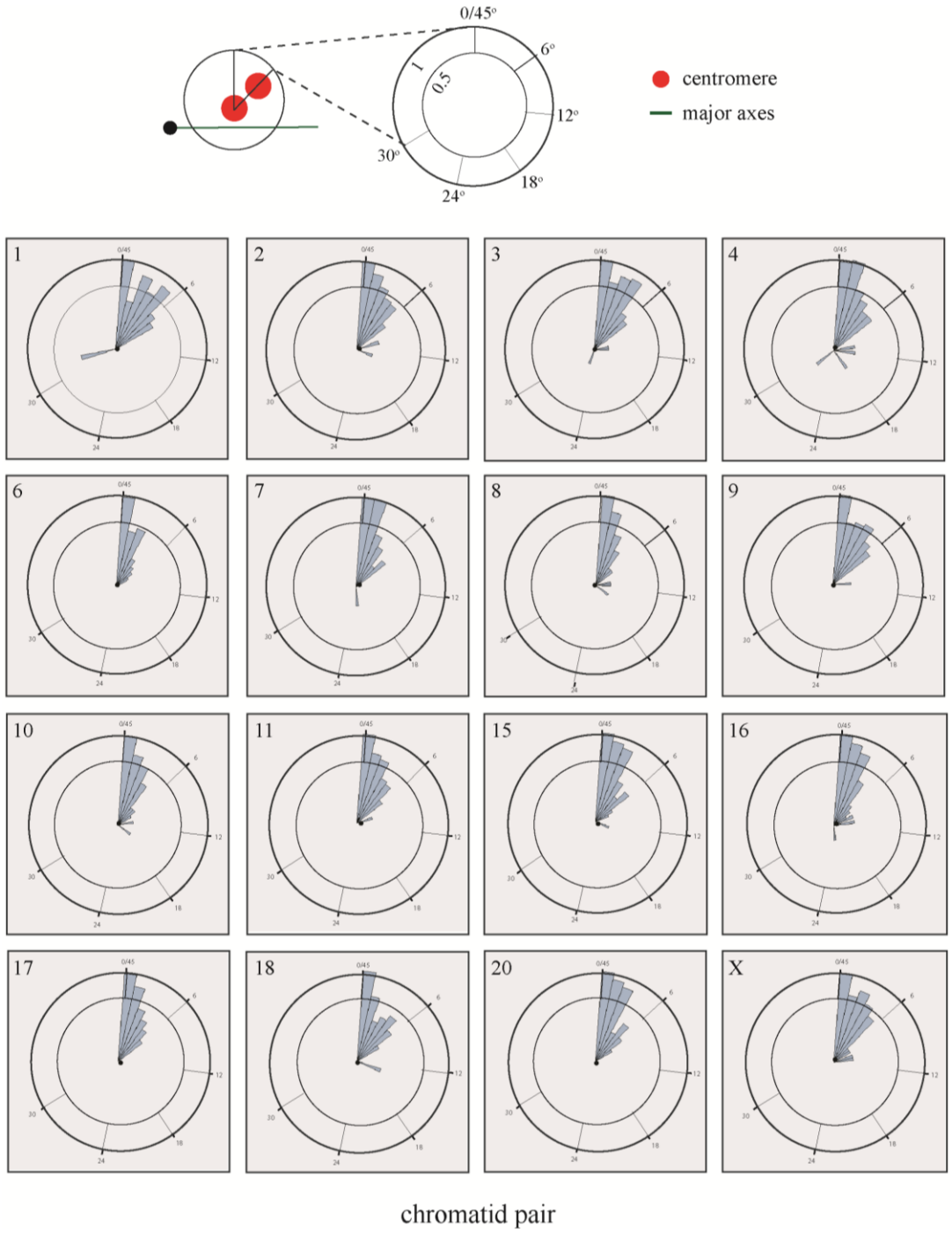

Figure 7.11. The rotation of sister chromatids at metaphase in RPE-1 cells post-nocodazole wash-out. Rose plot frequency histograms of the angular rotation between sister chromatids. Inner and outer circles are 0.5 and 1 frequency markers, respectively. Sister chromatids rarely rotate greater than 6 º from perpendicular to the major axis for most chromosomes. n=1415 from three independent experiments.

7.3. Summary

Chromosome missegregation rates are not equal across the human genome. The most frequently aneuploid chromosomes following mitotic insult are display recurrent patterns across cell lines of different origin (**figure 7.12a**). Additionally, patterns of aneuploidy can be observed under different cellular stresses, highlighting the intrinic instability of a small number of chromosomes. I have shown that aneuploidy-prone chromosomes are missegregated via different mechanisms following nocodazole wash-out (PCSC and non-disjunction). Strikingly, chromosomes 1, 2 and 10 accounted for three-quaters of lagging chromosomes at anaphase. Chromosome 3, 4 and 7 missegregated without a lagging intermediate (cryptic non-disjunction), demonstrating that individual chromosomes missegregate through different mechanisms, even under the same cellular stress. Furthermore, chromosome arrangement at metaphase is size-dependent (**figure 7.12c**). I reveal a trend whereby chromosomes which are aneuploidy-prone following nocodazole wash-out are clustered at the metaphase centre and periphery (**figure 7.12b**). Taken together, these data highlight the importance of chromatid geometry and stability of the centromeric chromatin environment for faithful chromosome segregation in human cells.

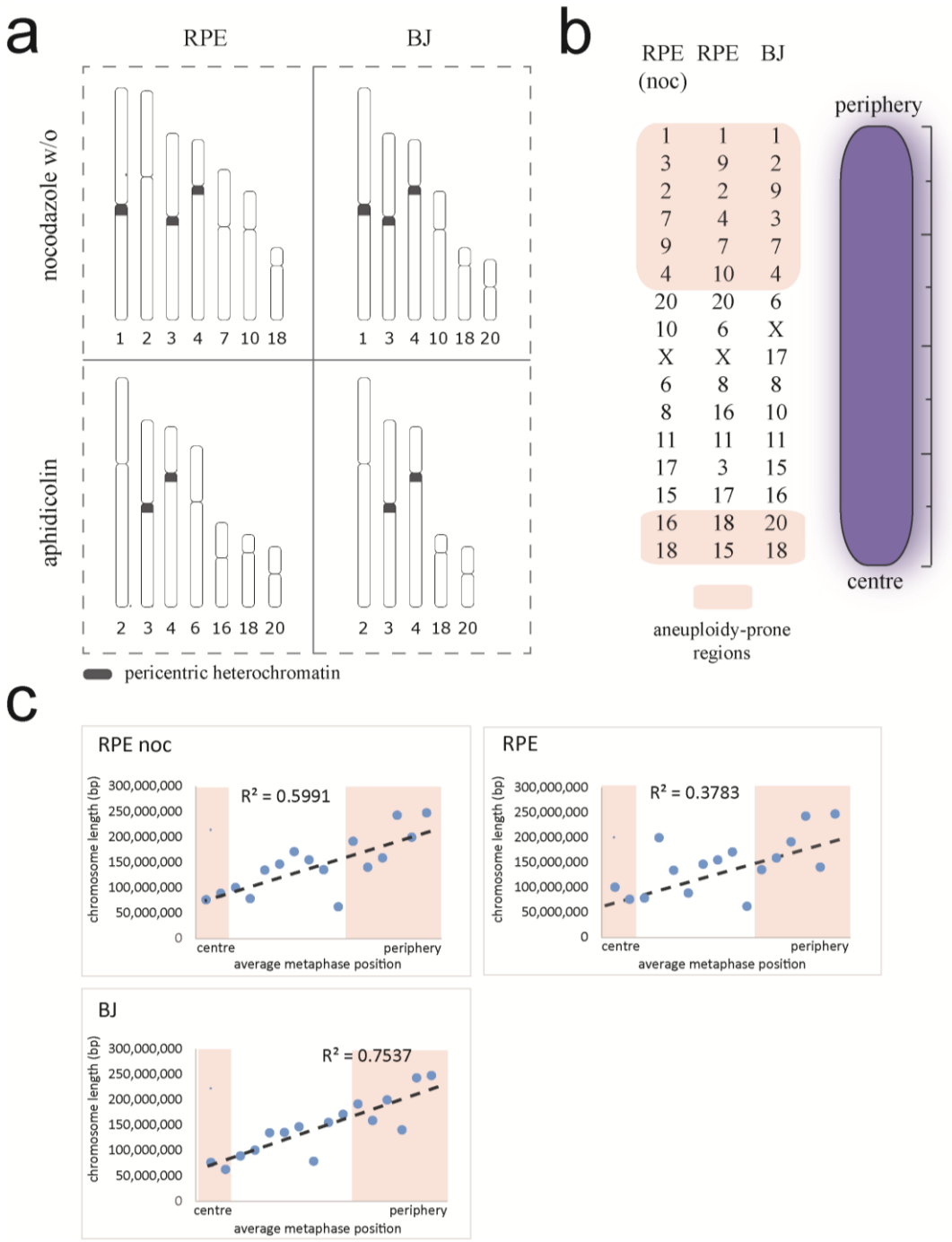

Figure 7.12. Chromosome missegregation and positioning summary. (a) There are recurrent patterns of aneuploidy across cell lines and cellular stresses. (b) Anupoidy-prone chromosomes are frequently found in discreet metaphase territories. (c) Overview of size-dependent metaphase chromosome positioning across cell lines and stresses.

8. Discussion

8.1. Overview

The early responses to aneuploidy in human cells, and the missegregation rates of individual human chromosomes, are poorly characterised. In part, these important questions have remained unanswered due to technical limitations obscuring the resolution of early aneuploidy responses, and the lack of appropriate technologies to accurately assess *de novo* aneuploidy rates for single chromosomes.

In this thesis, I have demonstrated it is possible to isolate aneuploid cells as early as 12 hours following the missegregation of a single chromosome using a novel strategy. Isolation of monosomic cells with this system has revealed some of the transcriptional responses that occur immediately following chromosome missegregation in human cells. Most notably, the expression of the pro-apoptotic BCL2-family proteins and up-stream p53-interacting proteins, MDM2 and p300, are significantly upregulated.

Additionally, I have implemented an image cytometry-based method for determining the missegregation rates of individual human chromosomes in a high-throughput manner. Using this system I have shown that certain chromosomes are more prone to missegregation, across multiple cell lines and stresses. Furthermore, I have started to elucidate the important contribution of centromere integrity to chromosome missegregation rates.

Finally I have, for the first time, shown that chromosome arrangement in the unperturbed metaphase plate is non-random, with certain chromosomes having a preference for alignment in average territories at the spindle equator. This has revealed the existence of aneuploidy-prone regions which are subject to high rates of chromosome missegregation. Taken together, these data have important implications for understanding the recurrent patterns of aneuploidy observed in human disease.

Following the development of a drug-inducible chromosome missegregation strategy and aneuploidy reporter cell line I was able to isolate a population of cells enriched for monosomic cells. However, there are some important issues which are likely obscuring the aneuploidy responses. Firstly, the monosomy 6 rate in the EGFP-negative population after FACS was only 74.9 %, implying that I have a ~ 25 % contamination of non-monosomic cells which may be cloaking some of the earliest responses. Moreover, the preparation of samples by FISH following FACS is a harsh procedure which may be introducing artefacts, as a 75 % monosomy should be have detectable by SNP array.

Furthermore, it is a possibility that some cells transiently dysregulate the *dsEGFP* gene following mitotic arrest, thus appearing EGFP-negative, despite remaining diploid. This is supported by the observation in the literature that gene transcription is down-regulated globally as cells enter mitosis[427–429]. Therefore, a fraction of the EGFP-negative population, which are in-fact diploid, may simply not have started to express *dsEGFP* in the subsequent G_1.

Additionally, the presence of EGFP-negative cells arrested in G_1, but still alive (and not in apoptosis) at 24 hours post-nocodazole, suggests that some cells in this population may have arrested for aneuploidy-independent reasons. One such possibility may be as a result of unavoidable FACS-induced cellular stress. This is supported by the observation that the percentage of EGFP-negative diploid cells is similar to that percentage of cells not in apoptosis at the 24 hour time-point (~ 32 % alive *vs.* ~ 20 % diploid).

An alternative strategy to elevate chromosome missegregation, which is currently under development in the McClelland laboratory, is to induce the specific missegregation of single chromosomes without the need for a mitotic arrest. One advantage of such system would abrogate any effects of nocodazole wash-out which are not manifesting solely as DNA damage. This would more faithfully

recapitulate the missegregation of chromosomes following merotely and therefore a fairer comparison of the early transcriptional responses to aneuploidy.

Interestingly, at 12 hours following EGFP loss, I did not detect a change in the expression of p53. This suggests that p53-mediated cell cycle arrest in the earliest stages of the aneuploidy response is entirely due to translocation of p53 into the nucleus rather than an increase in p53 transcription, resembling a global DNA damage response phenotype[430–432]. In support of this, I observed the transcriptional upregulation of MDM2, a known repressor of p53 activity. This is important as it is known that stabilisation of p53 in the nucleus activates transcription of MDM2, thereby providing a regulatory negative-feedback loop on p53 activity; the greater the p53 stabilisation in the nucleus, the higher MDM2 transcription and, in-turn, p53 inhibition[433,434].

There was also significant upregulation of the DNA-damage response protein ATM. This is important as it is known that ATM activates p53 by phosphorylation on serine 15, causing translocation to the nucleus[435,436]. ATM also phosphorylates Chk2, which together form the ATM-Chk2 DNA damage response pathway[172,197]. Interestingly, I did not observe an increase in transcription of CHK2, suggesting that ATM acts independently of the ATM/ATR DNA damage response pathway in response to aneuploidy. These data demonstrate that nascent aneuploid cells stabilise p53 in the nucleus through ATM-dependent phosphorylation; in agreement the p53-mediated cell cycle arrest observed in the literature[176,177,431].

It has already been shown that apoptosis induction is increased when the expression of two regulators of apoptosis are perturbed, namely BCL6 and BCL2[437]. Confirming the literature, I also observed a significant increase in expression of the pro-apoptotic protein Bcl6 and downregulation of Bcl2. Additionally, Bcl2 has been shown to inhibit the pro-apoptotic Bax/Bak1 complex, and therefore downregulation of Bcl2 would expect to increase the fidelity of Bax/Bak1-mediated apoptosis[438].

Finally, I observed an upregulation of BCL2L11, encoding the protein BIM, which diminishes the activity of Bcl-xL, an anti-apoptotic protein which inhibits p53[438,439]. These data suggest that chromosome missegregation leads to apoptosis through transcriptional upregulation of pro-apoptotic proteins, and simultaneously upregulating proteins that inhibit pro-survival Bcl2-family members (**fig. 8.1c**).

Following nocodazole wash-out, I observed unequal rates of individual chromosome missegregation between transformed and untransformed cell lines (**Table 8.1**). It is already known that chromosome 1 has a large region of pericentromeric heterochromatin and is frequently missegregated following hypomethylating treatments[440,441]. This suggests that changes in centromeric and/or pericentromeric integrity may influence chromosome missegregation rates. This is supported by my observation that chromosome 1 was frequently observed with premature sister chromatid separation (PSCS) at metaphase which suggests that chromosome 1 is vulnerable to the disruption of centromeric cohesin following a prolonged mitotic arrest. This phenomenon has been previously reported in the literature, however it has not been associated with specific chromosomes[442].

This raises an important question: do individual chromosomes displaying PSCS evade the spindle assembly checkpoint (SAC)? If so, they may be frequently missegregated and contribute to the high aneuploidy rate observed for particular chromosomes. In support of this hypothesis, it has recently been shown that premature sister chromatid separation does not elicit a robust SAC response, followed by abnormal mitotic exit after a short delay[443]. Moreover, there is mounting evidence that aneuploidy in human disease is linked to cohesin complex malfunction, in some instances[443,444]. The mechanistic basis for chromosome-specific cohesion loss is still unclear, given that there is little evidence of a correlation

between chromosome length and centromere size, which would dictate levels of centromeric cohesin.

The idea that cohesion defects may predispose to aneuploidy of individual chromosomes is supported by the observation that weakened sister chromatid cohesion is prevalent in ageing oocytes, indicating that age-related pathological aneuploidies may be caused by intrinsic properties of individual chromosomes[445]. Further supporting this hypothesis, it has been observed that nearly two-thirds of failed-fertilised oocytes display chromatid abnormalities, with the most frequent aneuploidies involving chromosome 1, 4, 16 and 22[446,447]. Strikingly, chromosome 1 aneuploidy in oocytes is common (15.8 %) but not related to maternal age, indicating that chromosome 1 is particularly vulnerable to missegregation in meiosis I, independent of age-related replication stress[448].

A further explanation for the non-random lagging chromosome and PSCS rates is related to centromeric Aurora B levels. It is known that Aurora B is recruited to centromeres where it participates in the removal of the cohesin complex and destabilises merotelic kinetochore-microtubule attachments[449–454]. Therefore, reduced centromeric cohesin on vulnerable chromosomes would reduce the capacity for Aurora B-dependent erroneous attachment correction. This may promote elevated rates of merotely for subsets of chromosomes with weakened cohesion, thereby generating high rates of lagging chromosomes at anaphase. In some cases, where biorientation is achieved, microtubule tension in the absence of merotely may overwhelm centromeric cohesin forces for particular chromosomes, especially chromosomes 1 and 2, promoting the PSCS phenotype (**fig. 8.1a**). This is important because it highlights how chromosome-level differences in intrinsic routes to aneuploidy may obscure the conventional assessment of segregation error rates, depending upon whether the observer is scoring lagging, bridges or non-disjunction rates, and for which chromosome(s).

Remarkably, when RPE-1 cells are released from nocodazole following p53 knockdown, there is significant chromothripsis for chromosomes 1, 2, 3, 4, 9, 16, 18 and 20 which are trapped in micronuclei[455]. The only chromosome subject to loss in micronuclei following p53 knock-down alone was chromosome 1. These data are in striking agreement with the unequal missegregation, and segregation error, rates observed in both RPE-1 and BJ cells in my hands. Taken together, this implies that the increased merotely present in cancer cells may perpetuate the instability of a select few chromosomes through illicit chromothripsis in micronuclei.

Additionally, I observed chromosome-level differences between merotely and replication stress. For example, chromosome 16 was missegregated at high rates following replication stress, but not in nocodazole wash-out. This is in support of the literature in which the replication stress fragile sites, FRA3B and FRA16D have been shown to predispose chromosomes 3 and 16 to high rates of non-disjunction following replication stress[456,457]. Furthermore, previous data have described age-related chromosome-specific aneuploidies arising in the ageing mouse brain[457]. Of particular interest, chromosome 18 was missegregated at high frequency, suggesting that chromosome 18 may be particularly vulnerable to age-related replication stress and contributes to CIN in ageing cells.

One possibility linking the similar patterns between stresses is that structural rearrangements which perturb faithful attachment to the mitotic spindle, such as those which disrupt centromeric integrity, may account for some of the observed aneuploidy rates. Moreover, it has been shown that replication stress-induced DNA bridges are subject to down-stream DNA damage through breakage-fusion-bridge (BFB) cycles[410,458,459]. Patterns of aneuploidy following replication stress may therefore represent a subset of chromosomes which are most vulnerable to illegitimate centromere rearrangements caused by BFB cycles in the preceding cell cycle.

The data in this thesis therefore contradicts the conventional wisdom in which conditions thought to elevate chromosome missegregation uniformly across the genome are actually inducing the missegregation of a small subset of chromosomes. This has consequences for the design of experimental mouse models trying to recapitulate tumour karyotypic complexity, where aneuploidy induced using certain strategies may predispose particular chromosomes to missegregation. It is therefore unclear whether the current literature describing recurrent patterns of aneuploidy *in vivo* are faithfully recapitulating those observed in human disease.

Cell line	Aneuploidies
RPE1 nocodazole w/o	1, 3, 4, 7, 10, 18 (Fig. 6.2)
RPE1 replication stress	2, 3, 4, 6, 16, 18, 20 (Fig.6.7)
RPE1 CENP-A depletion	4, 9, 15, 16, X (Fig.6.12)
RPE1 12/3 nocodazole w/o	1, 3, 4, 10 (Fig. 6.6)
RPE1 12/3 replication stress	2, 3, 4, 7, 13, 14, 16, 18, X (Fig.6.10)
BJ nocodazole w/o	1, 3, 4, 10, 18, 20 (Fig. 6.4)
BJ replication stress	2, 3, 4, 18, 20 (Fig. 6.8)
HCT116 nocodazole w/o	3, 4, 9, 15, 18, 20, X (Fig. 6.5)
HCT116 replication stress	4, 6, 7, 15, 18, 21, X (Fig. 6.9)
DLD1 CENPA depletion	1, 6, 7, 18 (Fig.6.13)

Table 8.1. Significantly elevated aneuploidies display recurrent biases. Patterns of aneuploidy are observed between cell lines and stresses of different tissue origin and tumorigenic status. Chromosomes shown are missegregated significantly more frequently than the mean of all other chromosomes ($p<0.05$). Red = gain rate greater than loss rate. Blue = loss rate greater than gain rate. Black = Gain and loss rates approximately equal.

The highly-repetitive α-satellite DNA of human centromeres contains an element which is important for centromere integrity, the CENP-B box. CENP-B boxes, together with the N-terminal domains of CENP-A, recruit CENP-B to centromeres. In humans, it has already been shown that CENP-B fulfils at least two roles at the centromere including establishing neocentromeres and inhibiting multiple centromere formation[460]. In agreement with these data, abolition of CENP-A reduces centromeric CENP-B levels by >50 %[461]. CENP-A is also known to be important for the stability of the centromere and faithful segregation of chromosomes. In this way, CENP-A can be used as a surrogate measure of centromere strength.

Following CENP-A depletion I revealed distinct patterns of aneuploidy in RPE-1 and DLD1 cells, suggesting that certain chromosomes are more contingent on centromere viability for faithful segregation behaviour. In support of this hypothesis, recent data have described the role of CENP-A in protecting against illegitimate centromere rearrangements[462]. This suggests that patterns of chromosome missegregation in the absence of CENP-A are, in-part, reflected by the intrinsic susceptibility of individual centromeres to structural aberrations. Furthermore, super-resolution microscopy of α-satellite DNA has revealed the existence of a CENP-A-dependent mechanism for preventing promiscuous α-satellite rearrangements[34,462]. It is therefore likely that patterns of aneuploidy in CENP-A depleted cells are also defined by the integrity of the base pair sequence in addition to down-stream assembly of kinetochore components. One important consideration is that CENP-A might not be totally depleted, leaving just enough to assemble a functional kinetochore. This would explain why global aneuploidy is not as high as would be expected following complete CENP-A removal.

Chromosome missegregation in the absence of CENP-A was variable between RPE-1 and DLD1 cells, which is surprising as α-satellite array length polymorphisms

have not been shown to be significantly different between cell types. It is known, however, that CENP-A levels are proportional to chromosome size[408].

Surprisingly, I did not observe size-dependent patterns of chromosome loss following CENP-A depletion in either cell line, suggesting that the maintenance of chromatin architecture, described above, are likely the primary driver of chromosome missegregation in the absence of CENP-A. In agreement with this hypothesis, under-condensation of centromeric chromatin and high rates of aneuploidy have been observed following hypomethylation treatment with 5-azacytidine, specifically for chromosomes 1, 9, 15 and 16[463,464]. Importantly, I also observed elevated rates of missegregation for chromosomes 9, 15 and 16 when CENP-A is depleted in RPE-1 cells, suggesting that CENP-A may dictate centromeric chromatin environments which are required for faithful segregation of a subset of chromosomes. I had already observed high rates of chromosome 1 missegregation under other cellular stresses (nocodazole and replication stress) but did not report a similar phenotype in the absence of CENP-A. Therefore, chromosome 1 may be less susceptible to centromere integrity defects than aberrant kinetochore-microtubule attachments and structural rearrangements.

Given that centromeric α-satellite sequence length is likely to vary at each centromere, it is plausible that less aneuploidy-prone chromosomes have reduced dependence on CENP-A-mediated centromere specification. The pattern of chromosome missegregation in DLD1 cells depleted of CENP-A is surprising, given the absence of shared aneuploidy-prone chromosomes compared to RPE-1 cells. To understand these data more fully would require further karyotype analysis and characterisation of CENP-A levels in DLD1 cells to ask if there are differences in centromeric CENP-A establishment, maintenance or function between RPE-1 and DLD1 cells, specifically.

It is pertinent that I observed a size-dependent chromosome positioning phenomenon at metaphase. Strikingly, large chromosomes congressed to the periphery of the spindle equator whereas smaller chromosome were generally located towards to centre of the spindle equator. This phenotype had already been reported in human interphase and prophase cells and therefore highlights the maintenance of chromosome arrangement during congression to the spindle equator[465,466].

Importantly, I observed similar positioning patterns for both RPE-1 and BJ cells, indicating that metaphase chromosome positioning is conserved and may influence pathological aneuploidy patterns observed in human disease. Indeed, the average position of chromosomes at metaphase correlated with their likelihood to missegregate under cellular stress.

This suggests that chromosomes may missegregate depending on where they are located in the metaphase plate, possibly due to a transient deviation from bipolar spindle geometry, and complexity of kinetochore-microtubule dynamics, which has been observed to generate CIN in cancer cells[242,467]. This is supported by the recent discovery that peripherally-located sister kinetochores are rotationally flexible[420]. Although kinetochore flexibility was shown to broadly aid attachment to microtubule K-fibres, it is plausible the metaphase periphery represents a region of elevated instability following microtubule disruption with nocodazole. These data are further supported by the notion that centrally-located chromosomes are captured by microtubules in early prophase, therefore achieving rapid biorientation in most cases, while chromosomes at either pole display increased propensity to become mono-oriented and merotelically attached to microtubules[468–470]. My data are in agreement with this observation given that size-dependent chromosome positioning at metaphase increases the mass of DNA at the spindle equator poles, therefore

potentially shielding kinetochores from erroneous microtubule reorganisation and correction.

Early work characterising the territories of metaphase chromosomes in cultured Indian deer cells has also established a size-dependent positioning phenomenon[471]. Here, the authors additionally describe homologous chromosomes as being significantly closer to each other than would be expected if there were no mechanisms regulating the spacing between chromosomes pairs at metaphase. This is in good agreement with my data in which homologous chromosomes were most frequently within 25 %, and rarely greater than 50 %, of the metaphase axis length apart in RPE-1 and BJ cells.

Taken together, these data suggest that the arrangement of homologous chromosomes at metaphase is both tightly coordinated and conserved across species. It is currently unclear whether there is homologue-specific missegregation of vulnerable chromosomes, and the McClelland laboratory is currently trying to optimise fluorescent live-cell-based approaches to determine this. It is already known that homologous chromosomes display recurrent patterns of differential chromatin condensation[472,473]. It is therefore plausible that there are homologue-specific chromatin differences which may influence missegregation rates.

Sister chromatid geometry also displayed recurrent patterns which may further perpetuate differential missegregation rates. For example, I observed an increase in inter-centromere distance for chromosomes 1, 2, 7 and 9 which correlated with their geography at the metaphase periphery in BJ cells. This further supports the hypothesis that, although there are mechanisms to promote microtubule stability at the spindle periphery, chromosomes may be vulnerable to microtubule pulling forces depending on their relative position at metaphase.

8.5. Conclusions and models

Interpreting the data presented in this thesis, I propose three models for aneuploidy mechanisms and responses in human cells.

Firstly, the unequal missegregation rates for a small number of chromosomes are influenced by their intrinsic properties and premature loss of sister chromatid cohesion, in some cases. This is most apparent for chromosomes 1 and 2, which display high rates of lagging at anaphase and precocious separation of sister chromatids in late prometaphase. One explanation is that reduced centromeric cohesin for some chromosomes causes a reduced Aurora-B localisation to the inner kinetochore, preventing the efficient destabilisation of merotelic kinetochore-microtubule attachments (**figure 8.1a**, upper pathway). Occasionally, under microtubule tension, sister chromatids with weakened cohesion (or complete loss) are frequently separated despite biorientation (**figure 8.1a**, lower pathway).

Secondly, chromosome alignment at metaphase is non-random, which is in agreement with the early observation that chromosomes occupy size-dependent positions in interphase. I propose that, in addition to the intrinsic chromosome vulnerabilities described above, regions of the spindle equator are more prone to missegregation (**figure 8.1b**). This is supported by >85 % of significantly aneuploidy-vulnerable chromosomes occupying average positions in these 'aneuploidy prone' regions following nocodazole wash-out.

Finally, I have started to elucidate the transcriptome responses to chromosome missegregation in nascent aneuploid cells. These data have highlighted the potential for expeditious, ATM-activated nuclear stabilisation of p53 in aneuploid cells (**figure 8.1c**). The subsequent onset of cell-cycle arrest and apoptosis may be mediated by both the DNA damage response and BLC2 family proteins, respectively.

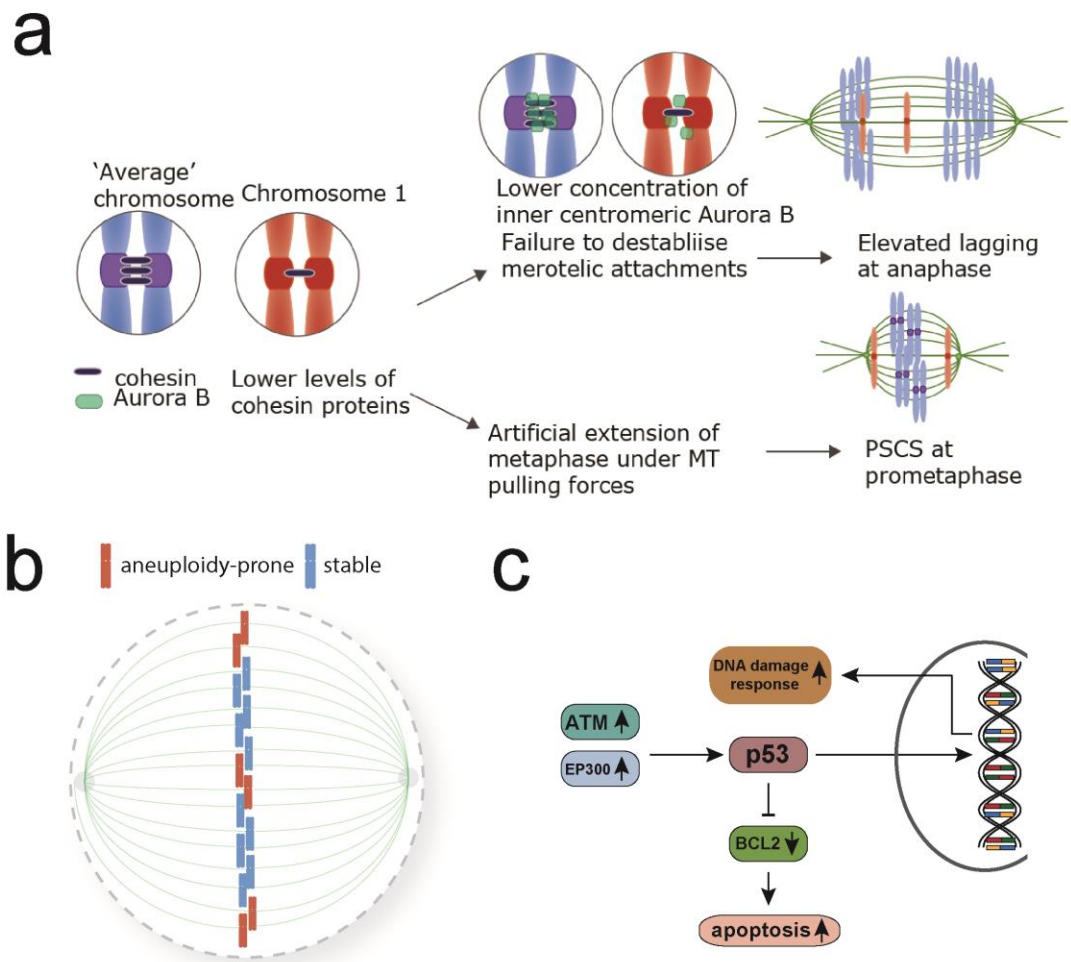

Figure 8.1. Models for aneuploidy mechanisms and responses in human cells. (a) Model for how lower cohesin levels at centromeres of chromosomes 1 and 2 may promote both the failure to destabliise merotelic attachments by deregulation of the ICS (upper pathway) and complete separation of sisters during artificially extended metaphase (lower pathway). (b) Model for how chromosome position at metaphase elevates missegregation of aneuploidy-prone chromosomes in particular regions of the spindle equator. (c) Cell cycle arrest and apoptosis in nascent aneuploid cells are likely induced by ATM and p53-dependent mechanisms.

9. References

1. Bayani JM, Squire JA. Applications of SKY in cancer cytogenetics. *Cancer Invest*. 2002;20(3):373-386. doi:10.1081/CNV-120001183.

2. Rensen FB, Kristensen IB, Grymer F, Jakobsen A. DNA-index and stereological estimation of nuclear volume in primary and metastatic malignant melanomas: A comparative study with analysis of heterogeneity. *APMIS*. 1990;98(1-6):61-70. doi:10.1111/j.1699-0463.1990.tb01003.x.

3. Vogelmann J, Valeri A, Guillou E, Cuvier O, Nollmann M. Roles of chromatin insulator proteins in higher-order chromatin organization and transcription regulation. *Nucleus*. 2011;2(5):358-369. doi:10.4161/nucl.2.5.17860.

4. Wu C. Chromatin Remodeling and the Control of Gene Expression. *J Biol Chem*. 1997;272(45):28171-28174. doi:10.1074/jbc.272.45.28171.

5. Richmond TJ, Finch JT, Rushton B, Rhodes D, Klug A. Structure of the nucleosome core particle at 7 a resolution. *Nature*. 1984;311(5986):532-537. doi:10.1038/311532a0.

6. Xiao B, Freedman BS, Miller KE, Heald R, Marko JF. Histone H1 compacts DNA under force and during chromatin assembly. *Mol Biol Cell*. 2012;23(24):4864-4871. doi:10.1091/mbc.e12-07-0518.

7. Mario-Ramirez L, Kann MG, Shoemaker BA, Landsman D. Histone structure and nucleosome stability. *Expert Rev Proteomics*. 2005;2(5):719-729. doi:10.1586/14789450.2.5.719.

8. Li B, Carey M, Workman JL. The Role of Chromatin during Transcription. *Cell*. 2007;128(4):707-719. doi:10.1016/j.cell.2007.01.015.

9. Yu X, Lin J, Zack DJ, Qian J. Identification of tissue-specific cis-regulatory modules based on interactions between transcription factors. *BMC Bioinformatics*. 2007;8(1):437. doi:10.1186/1471-2105-8-437.

10. Tirosh I, Barkai N. Two strategies for gene regulation by promoter nucleosomes. *Genome Res*. 2008;18(7):1084-1091. doi:10.1101/gr.076059.108.

11. Field Y, Kaplan N, Fondufe-Mittendorf Y, et al. Distinct Modes of Regulation by Chromatin Encoded through Nucleosome Positioning Signals. *PLoS Comput Biol*. 2008;4(11):e1000216. doi:10.1371/journal.pcbi.1000216.

12. Radman-Livaja M, Rando OJ. Nucleosome positioning: How is it established, and why does it matter? *Dev Biol*. 2010;339(2):258-266. doi:10.1016/j.ydbio.2009.06.012.

13. Struhl K, Segal E. Determinants of nucleosome positioning. *Nat Struct Mol Biol*. 2013;20(3):267-273. doi:10.1038/nsmb.2506.

14. Bai L, Ondracka A, Cross F. Multiple Sequence-Specific Factors Generate the Nucleosome-Depleted Region on CLN2 Promoter. *Mol Cell*. 2011;42(4):465-476. doi:10.1016/j.molcel.2011.03.028.

15. Segal E, Widom J. Poly(dA:dT) tracts: major determinants of nucleosome organization. *Curr Opin Struct Biol*. 2009;19(1):65-71. doi:10.1016/j.sbi.2009.01.004.

16. Segal E, Fondufe-Mittendorf Y, Chen L, et al. A genomic code for nucleosome positioning. *Nature*. 2006;442(7104):772-778. doi:10.1038/nature04979.

17. Lowary PT, Widom J. New DNA sequence rules for high affinity binding to histone octamer and sequence-directed nucleosome positioning. *J Mol Biol*. 1998;276(1):19-42. doi:10.1006/jmbi.1997.1494.

18. Cao X-Q, Zeng J, Yan H. Structural property of regulatory elements in human promoters. *Phys Rev E*. 2008;77(4). doi:10.1103/physreve.77.041908.

19. Becker PB, Herz W. ATP-Dependent Nucleosome Remodeling. *Annu Rev Biochem*. 2002;71(1):247-273. doi:10.1146/annurev.biochem.71.110601.135400.

20. Struhl K. Naturally occurring poly(dA-dT) sequences are upstream promoter elements for constitutive transcription in yeast. *Proc Natl Acad Sci*. 1985;82(24):8419-8423. doi:10.1073/pnas.82.24.8419.

21. Yella VR, Bansal M. DNA structural features of eukaryotic TATA-containing and TATA-less promoters. *FEBS Open Bio*. 2017;7(3):324-334. doi:10.1002/2211-5463.12166.

22. Martinez-Campa C, Politis P, Moreau J-L, et al. Precise Nucleosome Positioning and the TATA Box Dictate Requirements for the Histone H4 Tail and the Bromodomain Factor Bdf1. *Mol Cell*. 2004;15(1):69-81. doi:10.1016/j.molcel.2004.05.022.

23. Longst G, Bonte EJ, Corona DF V, Becker PB. Nucleosome Movement by CHRAC and ISWI without Disruption or trans-Displacement of the Histone Octamer. *Cell*. 1999;97(7):843-852. doi:10.1016/s0092-8674(00)80797-7.

24. Whitehouse I, Flaus A, Owen-Hughes T. Catalytic nucleosome mobilisation mediated by the SWI/SNF complex. *Biochem Soc Trans*. 1999;27(3):A96.1-A96. doi:10.1042/bst027a096.

25. Mizuguchi G. ATP-Driven Exchange of Histone H2AZ Variant Catalyzed by SWR1 Chromatin Remodeling Complex. *Science (80-)*. 2004;303(5656):343-348. doi:10.1126/science.1090701.

26. Westhorpe FG, Straight AF. Functions of the centromere and kinetochore in chromosome segregation. *Curr Opin Cell Biol*. 2013;25(3):334-340. doi:10.1016/j.ceb.2013.02.001.

27. Antonin W, Neumann H. Chromosome condensation and decondensation during mitosis. *Curr Opin Cell Biol*. 2016;40:15-22. doi:10.1016/j.ceb.2016.01.013.

28. Ris H, Witt PL. Structure of the mammalian kinetochore. *Chromosoma*. 1981;82(2):153-170. doi:10.1007/bf00286101.

29. Gascoigne KE, Takeuchi K, Suzuki A, Hori T, Fukagawa T, Cheeseman IM. Induced ectopic kinetochore assembly bypasses the requirement for CENP-A nucleosomes. *Cell*. 2011;145(3):410-422. doi:10.1016/j.cell.2011.03.031.

30. Shelby RD, Vafa O, Sullivan KF. Assembly of CENP-A into Centromeric Chromatin Requires a Cooperative Array of Nucleosomal DNA Contact Sites. *J Cell Biol*. 1997;136(3):501-513. doi:10.1083/jcb.136.3.501.

31. Nechemia-Arbely Y, Fachinetti D, Cleveland DW. Replicating centromeric chromatin: Spatial and temporal control of CENP-A assembly. *Exp Cell Res*. 2012;318(12):1353-1360. doi:10.1016/j.yexcr.2012.04.007.

32. Sullivan KF. A solid foundation: functional specialization of centromeric chromatin. *Curr Opin Genet Dev*. 2001;11(2):182-188. doi:10.1016/s0959-437x(00)00177-5.

33. Shelby RD, Monier K, Sullivan KF. Chromatin Assembly at Kinetochores Is Uncoupled from DNA Replication. *J Cell Biol*. 2000;151(5):1113-1118. doi:10.1083/jcb.151.5.1113.

34. Black BE, Foltz DR, Chakravarthy S, Luger K, Woods VL, Cleveland DW. Structural determinants for generating centromeric chromatin. *Nature*. 2004;430(6999):578-582. doi:10.1038/nature02766.

35. Ikeno M, Masumoto H, Okazaki T. Distribution of CENP-B boxes reflected in CREST centromere antigenic sites on long-range a-satellite DNA arrays of human chromosome 21. *Hum Mol Genet*. 1994;3(8):1245-1257. doi:10.1093/hmg/3.8.1245.

36. Kitagawa K, Masumoto H, Ikeda M, Okazaki T. Analysis of protein-DNA and protein-protein interactions of centromere protein B (CENP-B) and properties of the DNA-CENP-B complex in the cell cycle. *Mol Cell Biol*. 1995;15(3):1602-1612. doi:10.1128/mcb.15.3.1602.

37. Tanaka Y, Tachiwana H, Yoda K, et al. Human Centromere Protein B Induces Translational Positioning of Nucleosomes on a-Satellite Sequences. *J Biol Chem*. 2005;280(50):41609-41618. doi:10.1074/jbc.m509666200.

38. Sugimoto K, Yata H, Muro Y, Himeno M. Human Centromere Protein C (CENP-C) Is a DNA-Binding Protein Which Possesses a Novel DNA-Binding Motif1. *J Biochem*. 1994;116(4):877-881. doi:10.1093/oxfordjournals.jbchem.a124610.

39. Allshire RC, Karpen GH. Epigenetic regulation of centromeric chromatin: old dogs, new tricks? *Nat Rev Genet*. 2008;9(12):923-937. doi:10.1038/nrg2466.

40. Brown WRA, Thomas G, Lee NCO, et al. Kinetochore assembly and heterochromatin formation occur autonomously inSchizosaccharomyces pombe. *Proc Natl Acad Sci*. 2014;111(5):1903-1908. doi:10.1073/pnas.1216934111.

41. Boyarchuk E, Filipescu D, Vassias I, Cantaloube S, Almouzni G. The histone variant composition of centromeres is controlled by the pericentric heterochromatin state during the cell cycle. *J Cell Sci*. 2014;127(15):3347-3359. doi:10.1242/jcs.148189.

42. Zhang W, Lee H-R, Koo D-H, Jiang J. Epigenetic Modification of Centromeric Chromatin: Hypomethylation of DNA Sequences in the CENH3-Associated Chromatin in Arabidopsis thaliana and Maize. *PLANT CELL ONLINE*. 2008;20(1):25-34. doi:10.1105/tpc.107.057083.

43. Zheng Y-L, Hu N, Sun Q, Wang C, Taylor PR. Telomere Attrition in Cancer Cells and Telomere Length in Tumor Stroma Cells Predict Chromosome Instability in Esophageal Squamous Cell Carcinoma: A Genome-Wide Analysis. *Cancer Res*. 2009;69(4):1604-1614. doi:10.1158/0008-5472.can-08-3028.

44. Palm W, de Lange T. How Shelterin Protects Mammalian Telomeres. *Annu Rev Genet*. 2008;42(1):301-334. doi:10.1146/annurev.genet.41.110306.130350.

45. Diede SJ, Gottschling DE. Telomerase-Mediated Telomere Addition In Vivo Requires DNA Primase and DNA Polymerases a and d. *Cell*. 1999;99(7):723-733. doi:10.1016/s0092-8674(00)81670-0.

46. Garvik B, Carson M, Hartwell L. Single-stranded DNA arising at telomeres in cdc13 mutants may constitute a specific signal for the RAD9 checkpoint. *Mol Cell Biol*. 1995;15(11):6128-6138. doi:10.1128/mcb.15.11.6128.

47. Lipps HJ, Rhodes D. G-quadruplex structures: in vivo evidence and function. *Trends Cell Biol*. 2009;19(8):414-422. doi:10.1016/j.tcb.2009.05.002.

48. Zhao Y, Hoshiyama H, Shay JW, Wright WE. Quantitative telomeric overhang determination using a double-strand specific nuclease. *Nucleic Acids Res*. 2007;36(3):e14-e14. doi:10.1093/nar/gkm1063.

49. Bianchi A, Shore D. How Telomerase Reaches Its End: Mechanism of Telomerase Regulation by the Telomeric Complex. *Mol Cell*. 2008;31(2):153-165. doi:10.1016/j.molcel.2008.06.013.

50. Zhao Y, Sfeir AJ, Zou Y, et al. Telomere Extension Occurs at Most Chromosome Ends and Is Uncoupled from Fill-In in Human Cancer Cells. *J End-to-End-testing*. 2009;138(3):463-475. doi:10.1016/s9999-9994(09)20385-0.

51. Riethman H, Ambrosini A, Paul S. Human subtelomere structure and variation. *Chromosom Res*. 2005;13(5):505-515. doi:10.1007/s10577-005-0998-1.

52. Riethman H. Mapping and Initial Analysis of Human Subtelomeric Sequence Assemblies. *Genome Res*. 2003;14(1):18-28. doi:10.1101/gr.1245004.

53. Luo K. Rap1-Sir4 binding independent of other Sir, yKu, or histone interactions initiates the assembly of telomeric heterochromatin in yeast. *Genes Dev*. 2002;16(12):1528-1539. doi:10.1101/gad.988802.

54. Tutton S, Azzam GA, Stong N, et al. Subtelomeric p53 binding prevents accumulation of DNA damage at human telomeres. *EMBO J*. 2015;35(2):193-207. doi:10.15252/embj.201490880.

55. Marvin ME, Griffin CD, Eyre DE, Barton DBH, Louis EJ. In Saccharomyces cerevisiae, yKu and Subtelomeric Core X Sequences Repress Homologous Recombination Near Telomeres as Part of the Same Pathway. *Genetics*. 2009;183(2):441-451. doi:10.1534/genetics.109.106674.

56. Croft JA, Bridger JM, Boyle S, Perry P, Teague P, Bickmore WA. Differences in the Localization and Morphology of Chromosomes in the Human Nucleus. *J Cell Biol*. 1999;145(6):1119-1131. doi:10.1083/jcb.145.6.1119.

57. Neusser M, Schubel V, Koch A, Cremer T, Muller S. Evolutionarily conserved, cell type and species-specific higher order chromatin arrangements in interphase nuclei of primates. *Chromosoma*. 2007;116(3):307-320. doi:10.1007/s00412-007-0099-3.

58. Ganai N, Sengupta S, Menon GI. Chromosome positioning from activity-based segregation. *Nucleic Acids Res*. 2014;42(7):4145-4159. doi:10.1093/nar/gkt1417.

59. Stanislav Kozubek. Spatial arrangement of the human genome, its possible functional role. *Atlas Genet Cytogenet Oncol Haematol*. 2006;10(1):40-55. http://atlasgeneticsoncology.org/Deep/SpatialArrangGenomID20051.html.

60. Cornforth MN, Greulich-Bode KM, Loucas BD, et al. Chromosomes are predominantly located randomly with respect to each other in interphase human cells. *J Cell Biol*. 2002;159(2):237-244. doi:10.1083/jcb.200206009.

61. Chuang C-H, Belmont AS. Moving chromatin within the interphase nucleus-controlled transitions? *Semin Cell Dev Biol*. 2007;18(5):698-706. doi:10.1016/j.semcdb.2007.08.012.

62. Abney JR, Cutler B, Fillbach ML, Axelrod D, Scalettar BA. Chromatin dynamics in interphase nuclei and its implications for nuclear structure. *J Cell Biol*. 1997;137(7):1459-1468. doi:10.1083/jcb.137.7.1459.

63. Levi V, Ruan Q, Plutz M, Belmont AS, Gratton E. Chromatin dynamics in interphase cells revealed by tracking in a two-photon excitation microscope. *Biophys J*. 2005;89(6):4275-4285. doi:10.1529/biophysj.105.066670.

64. Branco MR, Pombo A. Intermingling of Chromosome Territories in Interphase Suggests Role in Translocations and Transcription-Dependent Associations. *PLoS Biol*. 2006;4(5):e138. doi:10.1371/journal.pbio.0040138.

65. Zhang Y, McCord R, Ho Y-J, et al. Spatial Organization of the Mouse Genome and Its Role in Recurrent Chromosomal Translocations. *Cell*. 2012;148(5):908-921. doi:10.1016/j.cell.2012.02.002.

66. Tanabe H, Muller S, Neusser M, et al. Evolutionary conservation of chromosome territory arrangements in cell nuclei from higher primates. *Proc Natl Acad Sci*. 2002;99(7):4424-4429. doi:10.1073/pnas.072618599.

67. Manvelyan M, Hunstig F, Mrasek K, et al. Position of chromosomes 18, 19, 21 and 22 in 3D-preserved interphase nuclei of human and gorilla and white hand gibbon. *Mol Cytogenet*. 2008;1(1):9. doi:10.1186/1755-8166-1-9.

68. Kalhor R, Tjong H, Jayathilaka N, Alber F, Chen L. Genome architectures revealed by tethered chromosome conformation capture and population-based modeling. *Nat Biotechnol*. 2011;30(1):90-98. doi:10.1038/nbt.2057.

69. Tolhuis B, Blom M, Kerkhoven RM, et al. Interactions among polycomb domains are guided by chromosome architecture. *PLoS Genet*. 2011;7(3). doi:10.1371/journal.pgen.1001343.

70. Hakim O, Sung MH, Voss TC, et al. Diverse gene reprogramming events occur in the same spatial clusters of distal regulatory elements. *Genome Res*. 2011;21(5):697-706. doi:10.1101/gr.111153.110.

71. Morey C, Kress C, Bickmore WA. Lack of bystander activation shows that localization exterior to chromosome territories is not sufficient to up-regulate gene expression. *Genome Res*. 2009;19(7):1184-1194. doi:10.1101/gr.089045.108.

72. Franke M, Ibrahim DM, Andrey G, et al. Formation of new chromatin domains determines pathogenicity of genomic duplications. *Nature*. 2016;538(7624):265-269. doi:10.1038/nature19800.

73. Yaffe E, Tanay A. Probabilistic modeling of Hi-C contact maps eliminates systematic biases to characterize global chromosomal architecture. *Nat Genet*. 2011;43(11):1059-1065. doi:10.1038/ng.947.

74. Desprat R, Thierry-Mieg D, Lailler N, et al. Predictable dynamic program of timing of DNA replication in human cells. *Genome Res*. 2009;19(12):2288-2299. doi:10.1101/gr.094060.109.

75. O'Keefe RT, Henderson SC, Spector DL. Dynamic organization of DNA replication in mammalian cell nuclei: Spatially and temporally defined replication of chromosome-specific ??-satellite DNA sequences. *J Cell Biol*. 1992;116(5):1095-1110. doi:10.1083/jcb.116.5.1095.

76. Mekhail K, Moazed D. The nuclear envelope in genome organization, expression and stability. *Nat Rev Mol Cell Biol*. 2010;11(5):317-328. doi:10.1038/nrm2894.

77. Gonzalez-Suarez I, Gonzalo S. Nurturing the genome: A-type lamins preserve genomic stability. *Nucleus*. 2010;1(2):129-135. doi:10.4161/nucl.1.2.10797.

78. Steensel B van, Henikoff S. Identification of in vivo DNA targets of chromatin proteins using tethered Dam methyltransferase. *Nat Biotechnol*. 2000;18(4):424-428. doi:10.1038/74487.

79. Pickersgill H, Kalverda B, de Wit E, Talhout W, Fornerod M, van Steensel B. Characterization of the Drosophila melanogaster genome at the nuclear lamina. *Nat Genet*. 2006;38(9):1005-1014. doi:10.1038/ng1852.

80. Csink AK, Henikoff S. Genetic modification of heterochromatic association and nuclear organization in Drosophila. *Nature*. 1996;381(6582):529-531. doi:10.1038/381529a0.

81. Casolari JM, Brown CR, Komili S, West J, Hieronymus H, Silver PA. Genome-Wide Localization of the Nuclear Transport Machinery Couples Transcriptional Status and Nuclear Organization. *Cell*. 2004;117(4):427-439. doi:10.1016/s0092-8674(04)00448-9.

82. Brown CR, Kennedy CJ, Delmar VA, Forbes DJ, Silver PA. Global histone acetylation induces functional genomic reorganization at mammalian nuclear pore complexes. *Genes Dev*. 2008;22(5):627-639. doi:10.1101/gad.1632708.

83. Sung P, Klein H. Mechanism of homologous recombination: mediators and helicases take on regulatory functions. *Nat Rev Mol Cell Biol*. 2006;7(10):739-750. doi:10.1038/nrm2008.

84. Mekhail K, Seebacher J, Gygi SP, Moazed D. Role for perinuclear chromosome tethering in maintenance of genome stability. *Nature*. 2008;456(7222):667-670. doi:10.1038/nature07460.

85. Torres-Rosell J, Sunjevaric I, De Piccoli G, et al. The Smc5-Smc6 complex and SUMO modification of Rad52 regulates recombinational repair at the ribosomal gene locus. *Nat Cell Biol*. 2007;9(8):923-931. doi:10.1038/ncb1619.

86. Taddei A, Gasser SM. Repairing subtelomeric DSBs at the nuclear periphery. *Trends Cell Biol*. 2006;16(5):225-228. doi:10.1016/j.tcb.2006.03.005.

87. Bupp JM, Martin AE, Stensrud ES, Jaspersen SL. Telomere anchoring at the nuclear periphery requires the budding yeast Sad1-UNC-84 domain protein Mps3. *J Cell Biol*. 2007;179(5):845-854. doi:10.1083/jcb.200706040.

88. Taddei A, Van Houwe G, Nagai S, Erb L, Van Nimwegen E, Gasser SM. The functional importance of telomere clustering: Global changes in gene expression result from SIR factor dispersion. *Genome Res*. 2009;19(4):611-625. doi:10.1101/gr.083881.108.

89. Nagai S, Dubrana K, Tsai-Pflugfelder M, et al. Functional Targeting of DNA Damage to a Nuclear Pore-Associated SUMO-Dependent Ubiquitin Ligase. *Science (80-)*. 2008;322(5901):597-602. doi:10.1126/science.1162790.

90. Capell BC, Collins FS. Human laminopathies: nuclei gone genetically awry. *Nat Rev Genet*. 2006;7(12):940-952. doi:10.1038/nrg1906.

91. Andres V, Gonzalez JM. Role of A-type lamins in signaling, transcription, and chromatin organization. *J Cell Biol*. 2009;187(7):945-957. doi:10.1083/jcb.200904124.

92. Lamm N, Ben-David U, Golan-Lev T, Storchova Z, Benvenisty N, Kerem B. Genomic Instability in Human Pluripotent Stem Cells Arises from Replicative Stress and Chromosome Condensation Defects. *Cell Stem Cell*. 2016;18(2):253-261. doi:10.1016/j.stem.2015.11.003.

93. Coschi CH, Martens AL, Ritchie K, et al. Mitotic chromosome condensation mediated by the retinoblastoma protein is tumor-suppressive. *Genes Dev*. 2010;24(13):1351-1363. doi:10.1101/gad.1917610.

94. Jeppsson K, Kanno T, Shirahige K, Sjogren C. The maintenance of chromosome structure: positioning and functioning of SMC complexes. *Nat Rev Mol Cell Biol*. 2014;15(9):601-614. doi:10.1038/nrm3857.

95. Gruber S, Haering CH, Nasmyth K. Chromosomal Cohesin Forms a Ring. *Cell*. 2003;112(6):765-777. doi:10.1016/s0092-8674(03)00162-4.

96. Nasmyth K, Uhlmann F, Lottspeich F. Sister-chromatid separation at anaphase onset is promoted by cleavage of the cohesin subunit Scc1. *Nature*. 1999;400(6739):37-42. doi:10.1038/21831.

97. Cuylen S, Metz J, Haering CH. Condensin structures chromosomal DNA through topological links. *Nat Struct Mol Biol*. 2011;18(8):894-901. doi:10.1038/nsmb.2087.

98. Kimura K, Hirano T. ATP-Dependent Positive Supercoiling of DNA by 13S Condensin: A Biochemical Implication for Chromosome Condensation. *Cell*. 1997;90(4):625-634. doi:10.1016/s0092-8674(00)80524-3.

99. Strick TR, Kawaguchi T, Hirano T. Real-Time Detection of Single-Molecule DNA Compaction by Condensin I. *Curr Biol*. 2004;14(10):874-880. doi:10.1016/j.cub.2004.04.038.

100. Maeshima K, Laemmli UK. A Two-Step Scaffolding Model for Mitotic Chromosome Assembly. *Dev Cell*. 2003;4(4):467-480. doi:10.1016/s1534-5807(03)00092-3.

101. Bembenek J, Verbrugghe KC, Khanikar J, Csankovszki G, Chan R. Condensin and the Spindle Midzone Prevent Cytokinesis Failure Induced by Chromatin Bridges in C. elegans Embryos. *Curr Biol*. 2013;23(11):937-946. doi:10.1016/j.cub.2013.04.028.

102. Amaral N, Vendrell A, Funaya C, et al. The Aurora-B-dependent NoCut checkpoint prevents damage of anaphase bridges after DNA replication stress. *Nat Cell Biol*. 2016;18(5):516-526. doi:10.1038/ncb3343.

103. Martin CA, Murray JE, Carroll P, et al. Mutations in genes encoding condensin complex proteins cause microcephaly through decatenation failure at mitosis. *Genes Dev*. 2016;30(19):2158-2172. doi:10.1101/gad.286351.116.

104. Wignall SM, Deehan R, Maresca TJ, Heald R. The condensin complex is required for proper spindle assembly and chromosome segregation inXenopusegg extracts. *J Cell Biol*. 2003;161(6):1041-1051. doi:10.1083/jcb.200303185.

105. Stear JH. Characterization of HCP-6, a C. elegans protein required to prevent chromosome twisting and merotelic attachment. *Genes Dev*. 2002;16(12):1498-1508. doi:10.1101/gad.989102.

106. Hagstrom KA. C. elegans condensin promotes mitotic chromosome architecture, centromere organization, and sister chromatid segregation during mitosis and meiosis. *Genes Dev*. 2002;16(6):729-742. doi:10.1101/gad.968302.

107. Guacci V. Sister chromatid cohesion: the cohesin cleavage model does not ring true. *Genes to Cells*. 2007;12(6):693-708. doi:10.1111/j.1365-2443.2007.01093.x.

108. Zheng G, Yu H. Regulation of sister chromatid cohesion during the mitotic cell cycle. *Sci China Life Sci*. 2015;58(11):1089-1098. doi:10.1007/s11427-015-4956-7.

109. Sun Y, Kucej M, Fan H-Y, Yu H, Sun Q-Y, Zou H. Separase Is Recruited to Mitotic Chromosomes to Dissolve Sister Chromatid Cohesion in a DNA-Dependent Manner. *Cell*. 2009;137(1):123-132. doi:10.1016/j.cell.2009.01.040.

110. Hauf S. Cohesin Cleavage by Separase Required for Anaphase and Cytokinesis in Human Cells. *Science (80-)*. 2001;293(5533):1320-1323. doi:10.1126/science.1061376.

111. Peters J-M, Tedeschi A, Schmitz J. The cohesin complex and its roles in chromosome biology. *Genes Dev*. 2008;22(22):3089-3114. doi:10.1101/gad.1724308.

112. Gerlich D, Koch B, Dupeux F, Peters J-M, Ellenberg J. Live-Cell Imaging Reveals a Stable Cohesin-Chromatin Interaction after but Not before DNA Replication. *Curr Biol*. 2006;16(15):1571-1578. doi:10.1016/j.cub.2006.06.068.

113. Yeh E, Haase J, Paliulis L V, et al. Pericentric Chromatin Is Organized into an Intramolecular Loop in Mitosis. *Curr Biol*. 2008;18(2):81-90. doi:10.1016/j.cub.2007.12.019.

114. Arumugam P, Gruber S, Tanaka K, Haering CH, Mechtler K, Nasmyth K. ATP Hydrolysis Is Required for Cohesin's Association with Chromosomes. *Curr Biol*. 2003;13(22):1941-1953. doi:10.1016/j.cub.2003.10.036.

115. Arumugam P, Nishino T, Haering CH, Gruber S, Nasmyth K. Cohesin's ATPase Activity Is Stimulated by the C-Terminal Winged-Helix Domain of Its Kleisin Subunit. *Curr Biol*. 2006;16(20):1998-2008. doi:10.1016/j.cub.2006.09.002.

116. Seitan VC, Banks P, Laval S, et al. Metazoan Scc4 homologs link sister chromatid cohesion to cell and axon migration guidance. *PLoS Biol*. 2006;4(8):1411-1425. doi:10.1371/journal.pbio.0040242.

117. Watrin E, Schleiffer A, Tanaka K, Eisenhaber F, Nasmyth K, Peters JM. Human Scc4 Is Required for Cohesin Binding to Chromatin, Sister-Chromatid Cohesion, and Mitotic Progression. *Curr Biol*. 2006;16(9):863-874. doi:10.1016/j.cub.2006.03.049.

118. Gillespie PJ, Hirano T. Scc2 Couples Replication Licensing to Sister Chromatid Cohesion in Xenopus Egg Extracts. *Curr Biol*. 2004;14(17):1598-1603. doi:10.1016/j.cub.2004.07.053.

119. Bernard P, Drogat J, Maure J-F, et al. A Screen for Cohesion Mutants Uncovers Ssl3, the Fission Yeast Counterpart of the Cohesin Loading Factor Scc4. *Curr Biol*. 2006;16(9):875-881. doi:10.1016/j.cub.2006.03.037.

120. Michaelis C, Ciosk R, Nasmyth K. Cohesins: Chromosomal Proteins that Prevent Premature Separation of Sister Chromatids. *Cell*. 1997;91(1):35-45. doi:10.1016/s0092-8674(01)80007-6.

121. Jeppsson K, Carlborg KK, Nakato R, et al. The Chromosomal Association of the Smc5/6 Complex Depends on Cohesion and Predicts the Level of Sister Chromatid Entanglement. *PLoS Genet*. 2014;10(10). doi:10.1371/journal.pgen.1004680.

122. Cortes-Ledesma F, Aguilera A. Double-strand breaks arising by replication through a nick are repaired by cohesin-dependent sister-chromatid exchange. *EMBO Rep*. 2006;7(9):919-926. doi:10.1038/sj.embor.7400774.

123. Takahashi TS, Yiu P, Chou MF, Gygi S, Walter JC. Recruitment of Xenopus Scc2 and cohesin to chromatin requires the pre-replication complex. *Nat Cell Biol*. 2004;6(10):991-996. doi:10.1038/ncb1177.

124. Takahashi TS, Basu A, Bermudez V, Hurwitz J, Walter JC. Cdc7-Drf1 kinase links chromosome cohesion to the initiation of DNA replication in Xenopus egg extracts. *Genes Dev*. 2008;22(14):1894-1905. doi:10.1101/gad.1683308.

125. Hauf S, Roitinger E, Koch B, Dittrich CM, Mechtler K, Peters J-M. Dissociation of Cohesin from Chromosome Arms and Loss of Arm Cohesion during Early Mitosis Depends on Phosphorylation of SA2. *PLoS Biol*. 2005;3(3):e69. doi:10.1371/journal.pbio.0030069.

126. Gandhi R, Gillespie PJ, Hirano T. Human Wapl Is a Cohesin-Binding Protein that Promotes Sister-Chromatid Resolution in Mitotic Prophase. *Curr Biol*. 2006;16(24):2406-2417. doi:10.1016/j.cub.2006.10.061.

127. Kueng S, Hegemann B, Peters BH, et al. Wapl Controls the Dynamic Association of Cohesin with Chromatin. *Cell*. 2006;127(5):955-967. doi:10.1016/j.cell.2006.09.040.

128. Salic A, Waters JC, Mitchison TJ. Vertebrate Shugoshin Links Sister Centromere Cohesion and Kinetochore Microtubule Stability in Mitosis. *Cell*. 2004;118(5):567-578. doi:10.1016/j.cell.2004.08.016.

129. McGuinness BE, Hirota T, Kudo NR, Peters J-M, Nasmyth K. Shugoshin Prevents Dissociation of Cohesin from Centromeres During Mitosis in Vertebrate Cells. *PLoS Biol*. 2005;3(3):e86. doi:10.1371/journal.pbio.0030086.

130. Uhlmann F, Wernic D, Poupart M-A, Koonin E V, Nasmyth K. Cleavage of Cohesin by the CD Clan Protease Separin Triggers Anaphase in Yeast. *Cell*. 2000;103(3):375-386. doi:10.1016/s0092-8674(00)00130-6.

131. Stemmann O, Zou H, Gerber SA, Gygi SP, Kirschner MW. Dual Inhibition of Sister Chromatid Separation at Metaphase. *Cell*. 2001;107(6):715-726. doi:10.1016/s0092-8674(01)00603-1.

132. Huang X, Andreu-Vieyra C V, York JP, et al. Inhibitory Phosphorylation of Separase Is Essential for Genome Stability and Viability of Murine Embryonic Germ Cells. *PLoS Biol*. 2008;6(1):e15. doi:10.1371/journal.pbio.0060015.

133. Huang X, Andreu-Vieyra C V, Wang M, Cooney AJ, Matzuk MM, Zhang P. Preimplantation Mouse Embryos Depend on Inhibitory Phosphorylation of Separase To Prevent Chromosome Missegregation. *Mol Cell Biol*. 2009;29(6):1498-1505. doi:10.1128/mcb.01778-08.

134. Musacchio A, Salmon ED. The spindle-assembly checkpoint in space and time. *Nat Rev Mol Cell Biol*. 2007;8(5):379-393. doi:10.1038/nrm2163.

135. Ellermeier C, Smith GR. Cohesins are required for meiotic DNA breakage and recombination in Schizosaccharomyces pombe. *Proc Natl Acad Sci U S A*. 2005;102(31):10952-10957. doi:10.1073/pnas.0504805102.

136. Strom L, Lindroos HB, Shirahige K, Sjogren C. Postreplicative Recruitment of Cohesin to Double-Strand Breaks Is Required for DNA Repair. *Mol Cell*. 2004;16(6):1003-1015. doi:10.1016/j.molcel.2004.11.026.

137. Onal E, Arbel-Eden A, Sattler U, et al. DNA Damage Response Pathway Uses Histone Modification to Assemble a Double-Strand Break-Specific Cohesin Domain. *Mol Cell*. 2004;16(6):991-1002. doi:10.1016/j.molcel.2004.11.027.

138. Petronczki M, Siomos MF, Nasmyth K. Un Menage et Quatre. *Cell*. 2003;112(4):423-440. doi:10.1016/s0092-8674(03)00083-7.

139. Bannister LA, Reinholdt LG, Munroe RJ, Schimenti JC. Positional cloning and characterization of mousemei8, a disrupted allele of the meiotic cohesinRec8. *genesis*. 2004;40(3):184-194. doi:10.1002/gene.20085.

140. Houtgraaf JH, Versmissen J, van der Giessen WJ. A concise review of DNA damage checkpoints and repair in mammalian cells. *Cardiovasc Revascularization Med*. 2006;7(3):165-172. doi:10.1016/j.carrev.2006.02.002.

141. Ciccia A, Elledge SJ. The DNA Damage Response: Making It Safe to Play with Knives. *Mol Cell*. 2010;40(2):179-204. doi:10.1016/j.molcel.2010.09.019.

142. Jiang G, Sancar A. Recruitment of DNA Damage Checkpoint Proteins to Damage in Transcribed and Nontranscribed Sequences. *Mol Cell Biol*. 2005;26(1):39-49. doi:10.1128/mcb.26.1.39-49.2006.

143. Zhou B-BS, Chaturvedi P, Spring K, et al. Caffeine Abolishes the Mammalian G2/M DNA Damage Checkpoint by Inhibiting Ataxia-Telangiectasia-mutated Kinase Activity. *J Biol Chem*. 2000;275(14):10342-10348. doi:10.1074/jbc.275.14.10342.

144. Ganem NJ, Pellman D. Linking abnormal mitosis to the acquisition of DNA damage. *J Cell Biol*. 2012;199(6):871-881. doi:10.1083/jcb.201210040.

145. Ohashi A, Ohori M, Iwai K, et al. Aneuploidy generates proteotoxic stress and DNA damage concurrently with p53-mediated post-mitotic apoptosis in SAC-impaired cells. *Nat Commun*. 2015;6:7668. doi:10.1038/ncomms8668.

146. Blank HM, Sheltzer JM, Meehl CM, Amon A. Mitotic entry in the presence of DNA damage is a widespread property of aneuploidy in yeast. *Mol Biol Cell*. 2015;26(8):1440-1451. doi:10.1091/mbc.e14-10-1442.

147. McNamee LM, Brodsky MH. p53-Independent Apoptosis Limits DNA Damage-Induced Aneuploidy. *Genetics*. 2009;182(2):423-435. doi:10.1534/genetics.109.102327.

148. McCullough AK, Dodson ML, Lloyd RS. Initiation of Base Excision Repair: Glycosylase Mechanisms and Structures. *Annu Rev Biochem*. 1999;68(1):255-285. doi:10.1146/annurev.biochem.68.1.255.

149. Matsumoto Y, Kim K. Excision of deoxyribose phosphate residues by DNA polymerase beta during DNA repair. *Science (80-)*. 1995;269(5224):699-702. doi:10.1126/science.7624801.

150. Roberts RJ, Cheng X. Base Flipping. *Annu Rev Biochem*. 1998;67(1):181-198. doi:10.1146/annurev.biochem.67.1.181.

151. Mol CD, Parikh SS, Putnam CD, Lo TP, Tainer JA. DNA repair mechanisms for the recognition and removal of damaged DNA bases. *Annu Rev Biophys Biomol Struct*. 1999;28(1):101-128. doi:10.1146/annurev.biophys.28.1.101.

152. Canitrot Y, Cazaux C, Frechet M, et al. Overexpression of DNA polymerase B in cell results in a mutator phenotype and a decreased sensitivity to anticancer drugs. *Proc Natl Acad Sci*. 1998;95(21):12586-12590. doi:10.1073/pnas.95.21.12586.

153. Sancar A. DNA Excision Repair. *Annu Rev Biochem*. 1996;65(1):43-81. doi:10.1146/annurev.bi.65.070196.000355.

154. Mu D, Park C-H, Matsunaga T, Hsu DS, Reardon JT, Sancar A. Reconstitution of Human DNA Repair Excision Nuclease in a Highly Defined System. *J Biol Chem*. 1995;270(6):2415-2418. doi:10.1074/jbc.270.6.2415.

155. Staresincic L, Fagbemi AF, Enzlin JH, et al. Coordination of dual incision and repair synthesis in human nucleotide excision repair. *EMBO J*. 2009;28(8):1111-1120. doi:10.1038/emboj.2009.49.

156. Branum ME, Reardon JT, Sancar A. DNA Repair Excision Nuclease Attacks Undamaged DNA. *J Biol Chem*. 2001;276(27):25421-25426. doi:10.1074/jbc.m101032200.

157. Howlett N. Nucleotide excision repair deficiency causes elevated levels of chromosome gain in Saccharomyces cerevisiae. *DNA Repair (Amst)*. 2004;3(2):127-134. doi:10.1016/j.dnarep.2003.10.003.

158. Jackson SP, Jeggo P a. DNA double-strand break repair and V(D)J recombination: involvement of DNA-PK. *Trends Biochem Sci*. 1995;20(10):412-415. http://www.ncbi.nlm.nih.gov/pubmed/8533154.

159. Lieber MR. Pathological and Physiological Double-Strand Breaks. *Am J Pathol*. 1998;153(5):1323-1332. doi:10.1016/s0002-9440(10)65716-1.

160. Murakami H, Keeney S. Regulating the formation of DNA double-strand breaks in meiosis. *Genes Dev*. 2008;22(3):286-292. doi:10.1101/gad.1642308.

161. Sung P. Catalysis of ATP-dependent homologous DNA pairing and strand exchange by yeast RAD51 protein. *Science (80-)*. 1994;265(5176):1241-1243. doi:10.1126/science.8066464.

162. Nick McElhinny SA, Snowden CM, McCarville J, Ramsden DA. Ku recruits the XRCC4-ligase IV complex to DNA ends. *Mol Cell Biol*. 2000;20(9):2996-3003. doi:10.1128/MCB.20.9.2996-3003.2000.

163. Lakhani SR, Jacquemier J, Sloane JP, et al. Multifactorial analysis of differences between sporadic breast cancers and cancers involving BRCA1 and BRCA2 mutations. *J Natl Cancer Inst*. 1998;90(15):1138-1145. doi:10.1093/jnci/90.15.1138.

164. Yarden RI, Pardo-Reoyo S, Sgagias M, Cowan KH, Brody LC. BRCA1 regulates the G2/M checkpoint by activating Chk1 kinase upon DNA damage. *Nat Genet*. 2002;30(3):285-289. doi:10.1038/ng837.

165. Bessho T, Mu D, Sancar A. Initiation of DNA interstrand cross-link repair in humans: the nucleotide excision repair system makes dual incisions 5' to the cross-linked base and removes a 22- to 28-nucleotide-long damage-free strand. *Mol Cell Biol*. 1997;17(12):6822-6830. doi:10.1128/mcb.17.12.6822.

166. De Silva IU, McHugh PJ, Clingen PH, Hartley JA. Defining the Roles of Nucleotide Excision Repair and Recombination in the Repair of DNA Interstrand Cross-Links in Mammalian Cells. *Mol Cell Biol*. 2000;20(21):7980-7990. doi:10.1128/MCB.20.21.7980-7990.2000.

167. Vermeulen,K.,Van Bockstaele,D.R.,Berneman ZN, Vermeulen K, Van Bockstaele DR, Berneman ZN. The cell cycle:a review of regulation,deregulation and therapeutic targets in cancer. *Cell Prolif*. 2003;36(3):131-149. doi:10.1306/74D715D2-2B21-11D7-8648000102C1865D.

168. Hochegger H, Takeda S, Hunt T. Cyclin-dependent kinases and cell-cycle transitions: does one fit all? *Nat Rev Mol Cell Biol*. 2008;9(11):910-916. doi:10.1038/nrm2510.

169. Deng C-X. BRCA1: cell cycle checkpoint, genetic instability, DNA damage response and cancer evolution. *Nucleic Acids Res*. 2006;34(5):1416-1426. doi:10.1093/nar/gkl010.

170. Laiho M, Latonen L. Cell cycle control, DNA damage checkpoints and cancer. *Ann Med*. 2003;35(6):391-397. doi:10.1080/07853890310014605.

171. Hyka-Nouspikel N, Desmarais J, Gokhale PJ, et al. Deficient DNA Damage Response and Cell Cycle Checkpoints Lead to Accumulation of Point Mutations in Human Embryonic Stem Cells. *Stem Cells*. 2012;30(9):1901-1910. doi:10.1002/stem.1177.

172. Bartek J, Lukas J. Chk1 and Chk2 kinases in checkpoint control and cancer. *Cancer Cell*. 2003;3(5):421-429. doi:10.1016/s1535-6108(03)00110-7.

173. Holland AJ, Cleveland DW. Boveri revisited: chromosomal instability, aneuploidy and tumorigenesis. *Nat Rev Mol Cell Biol*. 2009;10(7):478-487. doi:10.1038/nrm2718.

174. Donzelli M, Draetta GF. Regulating mammalian checkpoints through Cdc25 inactivation. *EMBO Rep*. 2003;4(7):671-677. doi:10.1038/sj.embor.embor887.

175. Bartek J, Lukas J. Mammalian G1- and S-phase checkpoints in response to DNA damage. *Curr Opin Cell Biol*. 2001;13(6):738-747. doi:10.1016/s0955-0674(00)00280-5.

176. Banin S. Enhanced Phosphorylation of p53 by ATM in Response to DNA Damage. *Science (80-)*. 1998;281(5383):1674-1677. doi:10.1126/science.281.5383.1674.

177. Canman CE. Activation of the ATM Kinase by Ionizing Radiation and Phosphorylation of p53. *Science (80-)*. 1998;281(5383):1677-1679. doi:10.1126/science.281.5383.1677.

178. Skladanowski A, Bozko P, Sabisz M. DNA Structure and Integrity Checkpoints during the Cell Cycle and Their Role in Drug Targeting and Sensitivity of Tumor Cells to Anticancer Treatment. *Chem Rev*. 2009;109(7):2951-2973. doi:10.1021/cr900026u.

179. Ehrlich LA, Yang-Iott K, Bassing CH. Tcrδ translocations that delete the Bcl11b haploinsufficient tumor suppressor gene promote atm-deficient T cell acute lymphoblastic leukemia. *Cell Cycle*. 2014;13(19):3076-3082. doi:10.4161/15384101.2014.949144.

180. Li M, Fang X, Baker DJ, et al. The ATM – p53 pathway suppresses aneuploidy- induced tumorigenesis. *Pnas*. 2010;107(32):14188-14193. doi:10.1073/pnas.1005960107/-/DCSupplemental.www.pnas.org/cgi/doi/10.1073/pnas.1005960107.

181. Campomenosi P, Assereto P, Bogliolo M, et al. p53 mutations and DNA ploidy in colorectal adenocarcinomas. *Anal Cell Pathol*. 1998;17(1):1-12.

182. Williams BR, Prabhu VR, Hunter KE, et al. Aneuploidy Affects Proliferation and Spontaneous Immortalization in Mammalian Cells. *Science (80-)*. 2008;322(5902):703-709. doi:10.1126/science.1160058.

183. Toledo F, Wahl GM. Regulating the p53 pathway: in vitro hypotheses, in vivo veritas. *Nat Rev Cancer*. 2006;6(12):909-923. doi:10.1038/nrc2012.

184. Brush GS. Phosphorylation of the replication protein A large subunit in the Saccharomyces cerevisiae checkpoint response. *Nucleic Acids Res*. 2000;28(19):3725-3732. doi:10.1093/nar/28.19.3725.

185. Gitig DM, Koff A. Cdk Pathway: Cyclin-Dependent Kinases and Cyclin-Dependent Kinase Inhibitors. *Mol Biotechnol*. 2001;19(2):179-188. doi:10.1385/mb:19:2:179.

186. Heffernan TP, Simpson DA, Frank AR, et al. An ATR- and Chk1-Dependent S Checkpoint Inhibits Replicon Initiation following UVC-Induced DNA Damage. *Mol Cell Biol*. 2002;22(24):8552-8561. doi:10.1128/mcb.22.24.8552-8561.2002.

187. Kim S-T. Involvement of the cohesin protein, Smc1, in Atm-dependent and independent responses to DNA damage. *Genes Dev*. 2002;16(5):560-570. doi:10.1101/gad.970602.

188. Ouchi M, Ouchi T. Regulation of ATM/DNA-PKcs Phosphorylation by BRCA1-Associated BAAT1. *Genes Cancer*. 2010;1(12):1211-1214. doi:10.1177/1947601911404222.

189. Unsal-Kacmaz K, Makhov AM, Griffith JD, Sancar A. Preferential binding of ATR protein to UV-damaged DNA. *Proc Natl Acad Sci*. 2002;99(10):6673-6678. doi:10.1073/pnas.102167799.

190. Hekmat-Nejad M, You Z, Yee M, Newport JW, Cimprich KA. Xenopus ATR is a replication-dependent chromatin-binding protein required for the DNA replication checkpoint. *Curr Biol*. 2000;10(24):1565-1573. doi:10.1016/s0960-9822(00)00855-1.

191. Costanzo V, Shechter D, Lupardus PJ, Cimprich KA, Gottesman M, Gautier J. An ATR- and Cdc7-Dependent DNA Damage Checkpoint that Inhibits Initiation of DNA Replication. *Mol Cell*. 2003;11(1):203-213. doi:10.1016/s1097-2765(02)00799-2.

192. Osborn AJ, Elledge SJ, Zou L. Checking on the fork: the DNA-replication stress-response pathway. *Trends Cell Biol*. 2002;12(11):509-516. doi:10.1016/s0962-8924(02)02380-2.

193. Ii M, Brill SJ. Roles of SGS1, MUS81, and RAD51 in the repair of lagging-strand replication defects in Saccharomyces cerevisiae. *Curr Genet*. 2005;48(4):213-225. doi:10.1007/s00294-005-0014-5.

194. Sogo JM. Fork Reversal and ssDNA Accumulation at Stalled Replication Forks Owing to Checkpoint Defects. *Science (80-)*. 2002;297(5581):599-602. doi:10.1126/science.1074023.

195. Liberi G. Rad51-dependent DNA structures accumulate at damaged replication forks in sgs1 mutants defective in the yeast ortholog of BLM RecQ helicase. *Genes Dev*. 2005;19(3):339-350. doi:10.1101/gad.322605.

196. Casper AM, Nghiem P, Arlt MF, Glover TW. ATR Regulates Fragile Site Stability. *Cell*. 2002;111(6):779-789. doi:10.1016/s0092-8674(02)01113-3.

197. Abraham RT. Cell cycle checkpoint signaling through the ATM and ATR kinases. *Genes Dev*. 2001;15(17):2177-2196. doi:10.1101/gad.914401.

198. Sorensen CS, Syljuosen RG, Falck J, et al. Chk1 regulates the S phase checkpoint by coupling the physiological turnover and ionizing radiation-induced accelerated proteolysis of Cdc25A. *Cancer Cell*. 2003;3(3):247-258. doi:10.1016/s1535-6108(03)00048-5.

199. Gong X, Liu A, Ming X, Deng P, Jiang Y. UV-induced interaction between p38 MAPK and p53 serves as a molecular switch in determining cell fate. *FEBS Lett*. 2010;584(23):4711-4716. doi:10.1016/j.febslet.2010.10.057.

200. Warmerdam DO, Brinkman EK, Marteijn J a, Medema RH, Kanaar R, Smits V a J. UV-induced G2 checkpoint depends on p38 MAPK and minimal activation of ATR-Chk1 pathway. *J Cell Sci*. 2013;126(Pt 9):1923-1930. doi:10.1242/jcs.118265.

201. Champeris Tsaniras S, Kanellakis N, Symeonidou IE, Nikolopoulou P, Lygerou Z, Taraviras S. Lice;nsing of DNA replication, cancer, pluripotency and differentiation: An interlinked world? *Semin Cell Dev Biol*. 2014;30:174-180. doi:10.1016/j.semcdb.2014.03.013.

202. Blow JJ, Hodgson B. Replication licensing Origin licensing: defining the proliferative state? *Trends Cell Biol*. 2002;12(2):72-78. doi:10.1016/s0962-8924(01)02203-6.

203. Fragkos M, Ganier O, Coulombe P, Michali M. DNA replication origin activation in space and time. *Nat Rev Mol Cell Biol*. 2015;16(6):360-374. doi:10.1038/nrm4002.

204. Nishitani H, Lygerou Z. Control of DNA replication licensing in a cell cycle. *Genes to Cells*. 2002;7(6):523-534. doi:10.1046/j.1365-2443.2002.00544.x.

205. Beresova L, Vesela E, Chamrad I, et al. Role of DNA Repair Factor Xeroderma Pigmentosum Protein Group C in Response to Replication Stress As Revealed by DNA Fragile Site Affinity Chromatography and Quantitative Proteomics. *J Proteome Res*. 2016;15(12):4505-4517. doi:10.1021/acs.jproteome.6b00622.

206. Kanu N, Cerone MA, Goh G, et al. DNA replication stress mediates APOBEC3 family mutagenesis in breast cancer. *Genome Biol*. 2016;17(1):185. doi:10.1186/s13059-016-1042-9.

207. Mazouzi A, Velimezi G, Loizou JI. DNA replication stress: Causes, resolution and disease. *Exp Cell Res*. 2014;329(1):85-93. doi:10.1016/j.yexcr.2014.09.030.

208. Ward IM, Minn K, Chen J. UV-induced Ataxia-telangiectasia-mutated and Rad3-related (ATR) Activation Requires Replication Stress. *J Biol Chem*. 2004;279(11):9677-9680. doi:10.1074/jbc.c300554200.

209. Marechal A, Zou L. DNA Damage Sensing by the ATM and ATR Kinases. *Cold Spring Harb Perspect Biol*. 2013;5(9):a012716-a012716. doi:10.1101/cshperspect.a012716.

210. Flynn RL, Zou L. ATR: a master conductor of cellular responses to DNA replication stress. *Trends Biochem Sci*. 2011;36(3):133-140. doi:10.1016/j.tibs.2010.09.005.

211. Barlow JH, Faryabi RB, Callén E, et al. Identification of early replicating fragile sites that contribute to genome instability. *Cell*. 2013;152(3):620-632. doi:10.1016/j.cell.2013.01.006.

212. Bermejo R, Capra T, Jossen R, et al. The replication checkpoint protects fork stability by releasing transcribed genes from nuclear pores. *Cell*. 2011;146(2):233-246. doi:10.1016/j.cell.2011.06.033.

213. Aguilera A, Garcia-Muse T. R Loops: From Transcription Byproducts to Threats to Genome Stability. *Mol Cell*. 2012;46(2):115-124. doi:10.1016/j.molcel.2012.04.009.

214. Bermejo R, Capra T, Gonzalez-Huici V, et al. Genome-Organizing Factors Top2 and Hmo1 Prevent Chromosome Fragility at Sites of S phase Transcription. *Cell*. 2009;138(5):870-884. doi:10.1016/j.cell.2009.06.022.

215. Tuduri S, Crabbé L, Conti C, et al. Topoisomerase I suppresses genomic instability by preventing interference between replication and transcription. *Nat Cell Biol*. 2009;11(11):1315-1324. doi:10.1038/ncb1984.

216. Ragland RL, Patel S, Rivard RS, et al. RNF4 and PLK1 are required for replication fork collapse in ATR-deficient cells. *Genes Dev*. 2013;27(20):2259-2273. doi:10.1101/gad.223180.113.

217. Tercero JA, Diffley JFX. Regulation of DNA replication fork progression through damaged DNA by the Mec1/Rad53 checkpoint. *Nature*. 2001;412(6846):553-557. doi:10.1038/35087607.

218. Hanada K, Budzowska M, Davies SL, et al. The structure-specific endonuclease Mus81 contributes to replication restart by generating double-strand DNA breaks. *Nat Struct Mol Biol*. 2007;14(11):1096-1104. doi:10.1038/nsmb1313.

219. Chanoux RA, Yin B, Urtishak KA, Asare A, Bassing CH, Brown EJ. ATR and H2AX Cooperate in Maintaining Genome Stability under Replication Stress. *J Biol Chem*. 2008;284(9):5994-6003. doi:10.1074/jbc.m806739200.

220. Betous R, Mason AC, Rambo RP, et al. SMARCAL1 catalyzes fork regression and Holliday junction migration to maintain genome stability during DNA replication. *Genes Dev*. 2012;26(2):151-162. doi:10.1101/gad.178459.111.

221. Kim Y, Kipreos ET. Cdt1 degradation to prevent DNA re-replication: conserved and non-conserved pathways. *Cell Div*. 2007;2(1):18. doi:10.1186/1747-1028-2-18.

222. Wohlschlegel JA. Inhibition of Eukaryotic DNA Replication by Geminin Binding to Cdt1. *Science (80-)*. 2000;290(5500):2309-2312. doi:10.1126/science.290.5500.2309.

223. Liontos M, Koutsami M, Sideridou M, et al. Deregulated overexpression of hCdt1 and hCdc6 promotes malignant behavior. *Cancer Res*. 2007;67(22):10899-10909. doi:10.1158/0008-5472.CAN-07-2837.

224. Li A, Blow JJ. Cdt1 downregulation by proteolysis and geminin inhibition prevents DNA re-replication in Xenopus. *EMBO J*. 2004;24(2):395-404. doi:10.1038/sj.emboj.7600520.

225. Davidson IF, Li A, Blow JJ. Deregulated Replication Licensing Causes DNA Fragmentation Consistent with Head-to-Tail Fork Collision. *Mol Cell*. 2006;24(3):433-443. doi:10.1016/j.molcel.2006.09.010.

226. Burrell R a, McClelland SE, Endesfelder D, et al. Replication stress links structural and numerical cancer chromosomal instability. *Nature*. 2013;494(7438):492-496. doi:10.1038/nature11935.

227. Smith L, Liu SJ, Goodrich L, et al. Duplication of ATR inhibits MyoD, induces aneuploidy and eliminates radiation-induced G1 arrest. *Nat Genet*. 1998;19(1):39-46. doi:10.1038/ng0598-39.

228. Abdel-Fatah TMA, Middleton FK, Arora A, et al. Untangling the ATR-CHEK1 network for prognostication, prediction and therapeutic target validation in breast cancer. *Mol Oncol*. 2015;9(3):569. doi:10.1016/j.molonc.2014.10.013.

229. Murga M, Campaner S, Lopez-Contreras AJ, et al. Exploiting oncogene-induced replicative stress for the selective killing of Myc-driven tumors. *Nat Struct Mol Biol*. 2011;18(12):1331-1335. doi:10.1038/nsmb.2189.

230. Gilad O, Nabet BY, Ragland RL, et al. Combining ATR Suppression with Oncogenic Ras Synergistically Increases Genomic Instability, Causing Synthetic Lethality or Tumorigenesis in a Dosage-Dependent Manner. *Cancer Res*. 2010;70(23):9693-9702. doi:10.1158/0008-5472.can-10-2286.

231. Koniaras K, Cuddihy a R, Christopoulos H, Hogg a, O'Connell MJ. Inhibition of Chk1-dependent G2 DNA damage checkpoint radiosensitizes p53 mutant human cells. *Oncogene*. 2001;20(51):7453-7463. doi:10.1038/sj.onc.1204942.

232. Lopez-Contreras AJ, Gutierrez-Martinez P, Specks J, Rodrigo-Perez S, Fernandez-Capetillo O. An extra allele of Chk1 limits oncogene-induced replicative stress and promotes transformation. *J Exp Med*. 2012;209(3):455-461. doi:10.1084/jem.20112147.

233. Lara-Gonzalez P, Westhorpe F, Taylor S. The Spindle Assembly Checkpoint. *Curr Biol*. 2012;22(22):R966-R980. doi:10.1016/j.cub.2012.10.006.

234. Gregan J, Polakova S, Zhang L, Tolic-Norrelykke IM, Cimini D. Merotelic kinetochore attachment: causes and effects. *Trends Cell Biol*. 2011;21(6):374-381. doi:10.1016/j.tcb.2011.01.003.

235. Cimini D, Howell B, Maddox P, Khodjakov A, Degrassi F, Salmon ED. Merotelic Kinetochore Orientation Is a Major Mechanism of Aneuploidy in Mitotic Mammalian Tissue Cells. *J Cell Biol*. 2001;153(3):517-528. doi:10.1083/jcb.153.3.517.

236. Thompson SL, Compton D a. Examining the link between chromosomal instability and aneuploidy in human cells. *J Cell Biol*. 2008;180(4):665-672. doi:10.1083/jcb.200712029.

237. Hanks S, Coleman K, Reid S, et al. Constitutional aneuploidy and cancer predisposition caused by biallelic mutations in BUB1B. *Nat Genet*. 2004;36(11):1159-1161. doi:10.1038/ng1449.

238. Cahill DP, da Costa LT, Carson-Walter EB, Kinzler KW, Vogelstein B, Lengauer C. Characterization of MAD2B and other mitotic spindle checkpoint genes. *Genomics*. 1999;58(2):181-187. doi:10.1006/geno.1999.5831.

239. Haruta M, Matsumoto Y, Izumi H, et al. Combined BubR1 protein down-regulation and RASSF1A hypermethylation in Wilms tumors with diverse cytogenetic changes. *Mol Carcinog*. 2008;47(9):660-666. doi:10.1002/mc.20412.

240. Fu J, Bian M, Jiang Q, Zhang C. Roles of Aurora Kinases in Mitosis and Tumorigenesis. *Mol Cancer Res*. 2007;5(1):1-10. doi:10.1158/1541-7786.mcr-06-0208.

241. Ganem NJ, Godinho SA, Pellman D. A mechanism linking extra centrosomes to chromosomal instability. *Nature*. 2009;460(7252):278-282. doi:10.1038/nature08136.

242. Silkworth WT, Nardi IK, Scholl LM, Cimini D. Multipolar Spindle Pole Coalescence Is a Major Source of Kinetochore Mis-Attachment and Chromosome Mis-Segregation in Cancer Cells. *PLoS One*. 2009;4(8):e6564. doi:10.1371/journal.pone.0006564.

243. Bakhoum SF, Thompson SL, Manning AL, Compton DA. Genome stability is ensured by temporal control of kinetochore-microtubule dynamics. *Nat Cell Biol*. 2008;11(1):27-35. doi:10.1038/ncb1809.

244. Kumar A, Rajendran V, Sethumadhavan R, Purohit R. Evidence of Colorectal Cancer-Associated Mutation in MCAK: A Computational Report. *Cell Biochem Biophys*. 2013;67(3):837-851. doi:10.1007/s12013-013-9572-1.

245. Nasmyth K. Cohesin: a catenase with separate entry and exit gates? *Nat Cell Biol*. 2011;13(10):1170-1177. doi:10.1038/ncb2349.

246. Welch JS, Ley TJ, Link DC, et al. The origin and evolution of mutations in acute myeloid leukemia. *Cell*. 2012;150(2):264-278. doi:10.1016/j.cell.2012.06.023.

247. Dorsett D. Cohesin: genomic insights into controlling gene transcription and development. *Curr Opin Genet Dev*. 2011;21(2):199-206. doi:10.1016/j.gde.2011.01.018.

248. Torres EM, Williams BR, Amon A. Aneuploidy: Cells losing their balance. *Genetics*. 2008. doi:10.1534/genetics.108.090878.

249. Sunshine AB, Payen C, Ong GT, Liachko I, Tan KM, Dunham MJ. The Fitness Consequences of Aneuploidy Are Driven by Condition-Dependent Gene Effects. *PLOS Biol*. 2015;13(5):e1002155. doi:10.1371/journal.pbio.1002155.

250. Dephoure N, Hwang S, O'Sullivan C, et al. Quantitative proteomic analysis reveals posttranslational responses to aneuploidy in yeast. *Elife*. 2014;3:e03023. doi:10.7554/eLife.03023.

251. Stingele S, Stoehr G, Peplowska K, Cox J, Mann M, Storchova Z. Global analysis of genome, transcriptome and proteome reveals the response to aneuploidy in human cells. *Mol Syst Biol*. 2012. doi:10.1038/msb.2012.40.

252. Sheltzer JM, Blank HM, Pfau SJ, et al. Aneuploidy Drives Genomic Instability in Yeast. *Science (80-)*. 2011;333(6045):1026-1030. doi:10.1126/science.1206412.

253. Potapova TA, Zhu J, Li R. Aneuploidy and chromosomal instability: a vicious cycle driving cellular evolution and cancer genome chaos. *Cancer Metastasis Rev*. 2013;32(3-4):377-389. doi:10.1007/s10555-013-9436-6.

254. Sheltzer JM, Torres EM, Dunham MJ, Amon A. Transcriptional consequences of aneuploidy. *Proc Natl Acad Sci*. 2012;109(31):12644-12649. doi:10.1073/pnas.1209227109.

255. Swanton C, Nicke B, Schuett M, et al. Chromosomal instability determines taxane response. *Proc Natl Acad Sci*. 2009;106(21):8671-8676. doi:10.1073/pnas.0811835106.

256. McClelland SE, Burrell R a., Swanton C. Chromosomal instability: A composite phenotype that influences sensitivity to chemotherapy. *Cell Cycle*. 2009;8(20):3262-3266.

257. Tan Z, Hays M, Cromie GA, et al. Aneuploidy underlies a multicellular phenotypic switch. *Proc Natl Acad Sci*. 2013;110(30):12367-12372. doi:10.1073/pnas.1301047110.

258. Weaver BAA, Cleveland DW. Decoding the links between mitosis, cancer, and chemotherapy: The mitotic checkpoint, adaptation, and cell death. *Cancer Cell*. 2005;8(1):7-12. doi:10.1016/j.ccr.2005.06.011.

259. Darrbaum M, Storchova Z. Effects of aneuploidy on gene expression: implications for cancer. *FEBS J*. 2015;283(5):791-802. doi:10.1111/febs.13591.

260. Torres EM, Sokolsky T, Tucker CM, et al. Effects of Aneuploidy on Cellular Physiology and Cell Division in Haploid Yeast. *Science (80-)*. 2007;317(5840):916-924. doi:10.1126/science.1142210.

261. Gordon DJ, Resio B, Pellman D. Causes and consequences of aneuploidy in cancer. *Nat Rev Genet*. 2012;13(3):189-203. doi:10.1038/nrg3123.

262. Lingle WL, Barrett SL, Negron VC, et al. Centrosome amplification drives chromosomal instability in breast tumor development. *Proc Natl Acad Sci U S A*. 2002;99(4):1978-1983. doi:10.1073/pnas.032479999.

263. Lengauer C, Kinzler KW, Vogelstein B. Genetic instability in colorectal cancers. *Nature*. 1997;386(6625):623-627. doi:10.1038/386623a0.

264. Cahill DP, Lengauer C, Yu J, et al. Mutations of mitotic checkpoint genes in human cancers. *Nature*. 1998;392(6673):300-303. doi:10.1038/32688.

265. Kops GJPL, Weaver BAA, Cleveland DW. On the road to cancer: aneuploidy and the mitotic checkpoint. *Nat Rev Cancer*. 2005;5(10):773-785. doi:10.1038/nrc1714.

266. Gascoigne KE, Taylor SS. Cancer Cells Display Profound Intra- and Interline Variation following Prolonged Exposure to Antimitotic Drugs. *Cancer Cell*. 2008;14(2):111-122. doi:10.1016/j.ccr.2008.07.002.

267. Thompson SL, Compton D a. Proliferation of aneuploid human cells is limited by a p53-dependent mechanism. *J Cell Biol*. 2010;188(3):369-381. doi:10.1083/jcb.200905057.

268. Reish O, Regev M, Kanesky A, Girafi S, Mashevich M. Sporadic Aneuploidy in PHA-Stimulated Lymphocytes of Trisomies 21, 18, and 13. *Cytogenet Genome Res*. 2011;133(2-4):184-189. doi:10.1159/000323504.

269. Reish O, Brosh N, Gobazov R, Rosenblat M, Libman V, Mashevich M. Sporadic aneuploidy in PHA-stimulated lymphocytes of Turner's syndrome patients. *Chromosom Res*. 2006;14(5):527-534. doi:10.1007/s10577-006-1050-9.

270. Gasch a P, Spellman PT, Kao CM, et al. Genomic expression programs in the response of yeast cells to environmental changes. *Mol Biol Cell*. 2000;11(12):4241-4257. doi:10.1091/mbc.11.12.4241.

271. Jiang J, Jing Y, Cost GJ, et al. Translating dosage compensation to trisomy 21. *Nature*. 2013;500(7462):296-300. doi:10.1038/nature12394.

272. Tang Y-C, Williams BR, Siegel JJ, Amon A. Identification of Aneuploidy-Selective Antiproliferation Compounds. *Cell*. 2011;144(4):499-512. doi:10.1016/j.cell.2011.01.017.

273. Gupta S. Hepatic polyploidy and liver growth control. *Semin Cancer Biol*. 2000;10:161-171. doi:10.1006/scbi.2000.0317.

274. Yurov YB, Iourov IY, Vorsanova SG, et al. Aneuploidy and confined chromosomal mosaicism in the developing human brain. *PLoS One*. 2007;2(6). doi:10.1371/journal.pone.0000558.

275. Carter SL, Cibulskis K, Helman E, et al. Absolute quantification of somatic DNA alterations in human cancer. *Nat Biotechnol*. 2012;30(5):413-421. doi:10.1038/nbt.2203.

276. Mitelman F, Johansson B, Mertens B. Database of Chromosome Aberrations and Gene Fusions in Cancer. 2017. http://www.cgap.nci.nih.gov/Chromosomes/Mitelman.

277. Hanna J, Hathaway NA, Tone Y, et al. Deubiquitinating Enzyme Ubp6 Functions Noncatalytically to Delay Proteasomal Degradation. *Cell*. 2006;127(1):99-111. doi:10.1016/j.cell.2006.07.038.

278. Peth A, Besche HC, Goldberg AL. Ubiquitinated Proteins Activate the Proteasome by Binding to Usp14/Ubp6, which Causes 20S Gate Opening. *Mol Cell*. 2009;36(5):794-804. doi:10.1016/j.molcel.2009.11.015.

279. Tomasini R, Mak TW, Melino G. The impact of p53 and p73 on aneuploidy and cancer. *Trends Cell Biol*. 2008;18(5):244-252. doi:10.1016/j.tcb.2008.03.003.

280. Donner EM, Preston RJ. The relationship between p53 status, DNA repair and chromatid aberration induction in G2 mouse embryo fibroblast cells treated with bleomycin. *Carcinogenesis*. 1996;17(5):1161-1165. doi:10.1093/carcin/17.5.1161.

281. GOEPFERT TM. Progesterone facilitates chromosome instability (aneuploidy) in p53 null normal mammary epithelial cells. *FASEB J*. 2000;14(14):2221-2229. doi:10.1096/fj.00-0165com.

282. McGranahan N, Burrell RA, Endesfelder D, Novelli MR, Swanton C. Cancer chromosomal instability: therapeutic and diagnostic challenges. *EMBO Rep*. 2012;13(6):528-538. doi:10.1038/embor.2012.61.

283. Giam M, Rancati G. Aneuploidy and chromosomal instability in cancer: a jackpot to chaos. *Cell Div*. 2015;10(1). doi:10.1186/s13008-015-0009-7.

284. Komarova NL, Wodarz D. The optimal rate of chromosome loss for the inactivation of tumor suppressor genes in cancer. *Proc Natl Acad Sci*. 2004;101(18):7017-7021. doi:10.1073/pnas.0401943101.

285. P??rez de Castro I, de C??rcer G, Malumbres M. A census of mitotic cancer genes: New insights into tumor cell biology and cancer therapy. *Carcinogenesis*. 2007;28(5):899-912. doi:10.1093/carcin/bgm019.

286. Sotillo R, Hernando E, Diaz-Rodriguez E, et al. Mad2 Overexpression Promotes Aneuploidy and Tumorigenesis in Mice. *Cancer Cell*. 2007;11(1):9-23. doi:10.1016/j.ccr.2006.10.019.

287. Sotillo R, Schvartzman J-M, Socci ND, Benezra R. Mad2-induced chromosome instability leads to lung tumour relapse after oncogene withdrawal. *Nature*. 2010;464(7287):436-440. doi:10.1038/nature08803.

288. Hernando E, Nahlé Z, Juan G, et al. Rb inactivation promotes genomic instability by uncoupling cell cycle progression from mitotic control. *Nature*. 2004;430(7001):797-802. doi:10.1038/nature02820.

289. Duijf PHG, Schultz N, Benezra R. Cancer cells preferentially lose small chromosomes. *Int J Cancer*. 2012;132(10):2316-2326. doi:10.1002/ijc.27924.

290. Kaur A, Singh A, Kaur S, Singh J. Karyotypic findings in chronic myeloid leukemia cases undergoing treatment. *Indian J Hum Genet*. 2012;18(1):66. doi:10.4103/0971-6866.96654.

291. Chmital L, Gabriel S, Mitsainas G, et al. Centromere Strength Provides the Cell Biological Basis for Meiotic Drive and Karyotype Evolution in Mice. *Curr Biol*. 2014;24(19):2295-2300. doi:10.1016/j.cub.2014.08.017.

292. Martin RH, Ko E, Rademaker A. Distribution of aneuploidy in human gametes: Comparison between human sperm and oocytes. *Am J Med Genet*. 1991;39(3):321-331. doi:10.1002/ajmg.1320390315.

293. Pellestor F. Differential distribution of aneuploidy in human gametes according to their sex. *Hum Reprod*. 1991;6(9):1252-1258. doi:10.1093/oxfordjournals.humrep.a137522.

294. Goldacre MJ, Wotton CJ, Seagroatt V, Yeates D. Cancers and immune related diseases associated with Down's syndrome: a record linkage study. *Arch Dis Child*. 2004;89(11):1014-1017. doi:10.1136/adc.2003.046219.

295. Xavier AC, Ge Y, Taub JW. Down Syndrome and Malignancies: A Unique Clinical Relationship. *J Mol Diagnostics*. 2009;11(5):371-380. doi:10.2353/jmoldx.2009.080132.

296. Jefford CE, Irminger-Finger I. Mechanisms of chromosome instability in cancers. *Crit Rev Oncol Hematol*. 2006;59(1):1-14. doi:10.1016/j.critrevonc.2006.02.005.

297. Pino MS, Chung DC. The Chromosomal Instability Pathway in Colon Cancer. *Gastroenterology*. 2010;138(6):2059-2072. doi:10.1053/j.gastro.2009.12.065.

298. Kops GJPL, Foltz DR, Cleveland DW. Lethality to human cancer cells through massive chromosome loss by inhibition of the mitotic checkpoint. *Proc Natl Acad Sci*. 2004;101(23):8699-8704. doi:10.1073/pnas.0401142101.

299. Satg?? D, Sommelet D, Geneix A, Nishi M, Malet P, Vekemans M. A tumor profile in Down syndrome. *Am J Med Genet*. 1998;78(3):207-216. doi:10.1002/(SICI)1096-8628(19980707)78:3<207::AID-AJMG1>3.0.CO;2-M.

300. Baek K, Zaslavsky A, Lynch RC, et al. Down syndrome suppression of tumor growth and the role of the calcineurin inhibitor DSCR1. *Nature*. 2009;459(7250):1126-1130. doi:10.1038/nature08062.Down.

301. Weaver BAA, Silk AD, Montagna C, Verdier-Pinard P, Cleveland DW. Aneuploidy Acts Both Oncogenically and as a Tumor Suppressor. *Cancer Cell*. 2007;11(1):25-36. doi:10.1016/j.ccr.2006.12.003.

302. Gartner EM, Silverman P, Simon M, et al. A phase II study of 17-allylamino-17-demethoxygeldanamycin in metastatic or locally advanced, unresectable breast cancer. *Breast Cancer Res Treat*. 2011;131(3):933-937. doi:10.1007/s10549-011-1866-7.

303. Heath EI, Hillman DW, Vaishampayan U, et al. A Phase II trial of 17-allylamino-17-demethoxygeldanamycin in patients with hormone-refractory metastatic prostate cancer. *Clin Cancer Res*. 2008;14(23):7940-7946. doi:10.1158/1078-0432.CCR-08-0221.

304. Kwon M, Godinho SA, Chandhok NS, et al. Mechanisms to suppress multipolar divisions in cancer cells with extra centrosomes. *Genes Dev*. 2008;22(16):2189-2203. doi:10.1101/gad.1700908.

305. Kantarjian HM, Padmanabhan S, Stock W, et al. Phase I/II multicenter study to assess the safety, tolerability, pharmacokinetics and pharmacodynamics of AZD4877 in patients with refractory acute myeloid leukemia. *Invest New Drugs*. 2012;30(3):1107-1115. doi:10.1007/s10637-011-9660-2.

306. Infante JR, Kurzrock R, Spratlin J, et al. A Phase i study to assess the safety, tolerability, and pharmacokinetics of AZD4877, an intravenous Eg5 inhibitor in patients with advanced solid tumors. *Cancer Chemother Pharmacol*. 2012;69(1):165-172. doi:10.1007/s00280-011-1667-z.

307. Kallioniemi A. CGH microarrays and cancer. *Curr Opin Biotechnol*. 2008;19(1):36-40. doi:10.1016/j.copbio.2007.11.004.

308. Pinkel D, Albertson DG. Array comparative genomic hybridization and its applications in cancer. *Nat Genet*. 2005;37(6s):S11-S17. doi:10.1038/ng1569.

309. Shinawi M, Cheung SW. The array CGH and its clinical applications. *Drug Discov Today*. 2008;13(17-18):760-770. doi:10.1016/j.drudis.2008.06.007.

310. Ligon AH, Beaudet AL, Shaffer LG. Simultaneous, Multilocus FISH Analysis for Detection of Microdeletions in the Diagnostic Evaluation of Developmental Delay and Mental Retardation. *Am J Hum Genet*. 1997;61(1):51-59. doi:10.1086/513904.

311. Speicher MR, Carter NP. The new cytogenetics: blurring the boundaries with molecular biology. *Nat Rev Genet*. 2005;6(10):782-792. doi:10.1038/nrg1692.

312. Knouse KA, Wu J, Whittaker CA, Amon A. Single cell sequencing reveals low levels of aneuploidy across mammalian tissues. *Proc Natl Acad Sci*. 2014;111(37):13409-13414. doi:10.1073/pnas.1415287111.

313. Falconer E, Hills M, Naumann U, et al. DNA template strand sequencing of single-cells maps genomic rearrangements at high resolution. *Nat Methods*. 2012;9(11):1107-1112. doi:10.1038/nmeth.2206.

314. Bakker B, Taudt A, Belderbos ME, et al. Single-cell sequencing reveals karyotype heterogeneity in murine and human malignancies. *Genome Biol*. 2016;17(1):115. doi:10.1186/s13059-016-0971-7.

315. Dong X, Zhang L, Milholland B, et al. Accurate identification of single-nucleotide variants in whole-genome-amplified single cells. *Nat Methods*. 2017;14(5):491-493. doi:10.1038/nmeth.4227.

316. Van Loo P, Voet T. Single cell analysis of cancer genomes. *Curr Opin Genet Dev*. 2014;24:82-91. doi:10.1016/j.gde.2013.12.004.

317. Korbel J, Campbell P. Criteria for Inference of Chromothripsis in Cancer Genomes. *Cell*. 2013;152(6):1226-1236. doi:10.1016/j.cell.2013.02.023.

318. Macaulay IC, Voet T. Single Cell Genomics: Advances and Future Perspectives. *PLoS Genet*. 2014;10(1):e1004126. doi:10.1371/journal.pgen.1004126.

319. Blanco R, Rengifo CE, Cedeño M, Frómeta M, Rengifo E. Flow Cytometric Measurement of Aneuploid DNA Content Correlates with High S-Phase Fraction and Poor Prognosis in Patients with Non-Small-Cell Lung Cancer. *ISRN Biomarkers*. 2013;2013:1-8. doi:10.1155/2013/354123.

320. Abad M, Ciudad J, Rincon MR, et al. DNA Aneuploidy by Flow Cytometry Is an Independent Prognostic Factor in Gastric Cancer. *Anal Cell Pathol*. 1998;16(4):223-231. doi:10.1155/1998/158243.

321. Frankfurt OS, Slocum HK, Rustum YM, et al. Flow cytometric analysis of DNA aneuploidy in primary and metastatic human solid tumors,. *Cytometry*. 1984;5(1):71-80. doi:10.1002/cyto.990050111.

322. van den Ingh HF, Griffioen G, Cornelisse CJ. Flow cytometric detection of aneuploidy in colorectal adenomas. *Cancer Res*. 1985;45(JULY):3392-3397.

323. Jensen RH. Chromomycin A3 as a fluorescent probe for flow cytometry of human gynecologic samples. *J Histochem Cytochem*. 1977;25(7):573-579. doi:10.1177/25.7.70448.

324. Pozarowski P, Darzynkiewicz Z. Analysis of cell cycle by flow cytometry. *Methods Mol Biol*. 2004;281:301-311. doi:10.1385/1-59259-811-0:301.

325. Minderman H, Humphrey K, Arcadi JK, et al. Image cytometry-based detection of aneuploidy by fluorescence in situ hybridization in suspension. *Cytom Part A*. 2012;81A(9):776-784. doi:10.1002/cyto.a.22101.

326. Carter NP. Bivariate chromosome analysis using a commercial flow cytometer. *Methods Mol Biol*. 1994;29:187-204.

327. Dey P. Aneuploidy and malignancy: an unsolved equation. *J Clin Pathol*. 2004;57(12):1245-1249. doi:10.1136/jcp.2004.018952.

328. Howe B, Umrigar A, Tsien F. Chromosome Preparation From Cultured Cells. *J Vis Exp*. 2014;(83). doi:10.3791/50203.

329. WILKINSHAUG L, SANDSTROM M, WEREMOWICZ S. Fluorescence in situ hybridization for the detection of aneuploidy from archived fetal cells. *Obstet Gynecol*. 1996;88(4):684-687. doi:10.1016/0029-7844(96)00277-3.

330. Das K, Tan P. Molecular cytogenetics: recent developments and applications in cancer. *Clin Genet*. 2013;84(4):315-325. doi:10.1111/cge.12229.

331. Monzon FA. Guidance for Fluorescence in Situ Hybridization Testing in Hematologic Disorders. *Yearb Pathol Lab Med*. 2008;2008:295-296. doi:10.1016/s1077-9108(08)70716-3.

332. Iourov IY, Soloviev I V, Vorsanova SG, Monakhov V V, Yurov YB. An Approach for Quantitative Assessment of Fluorescence In Situ Hybridization (FISH) Signals for Applied Human Molecular Cytogenetics. *J Histochem Cytochem*. 2005;53(3):401-408. doi:10.1369/jhc.4a6419.2005.

333. Carter NP. Cytogenetic analysis by chromosome painting. *Cytometry*. 1994;18(1):2-10. doi:10.1002/cyto.990180103.

334. Ried T. Chromosome painting: a useful art. *Hum Mol Genet*. 1998;7(10):1619-1626. doi:10.1093/hmg/7.10.1619.

335. KRAKER WJ, BORELL TJ, SCHAD CR, et al. Fluorescent In Situ Hybridization: Use of Whole Chromosome Paint Probes to Identify Unbalanced Chromosome Translocations. *Mayo Clin Proc*. 1992;67(7):658-662. doi:10.1016/s0025-6196(12)60721-6.

336. Passerini V, Ozeri-Galai E, de Pagter MS, et al. The presence of extra chromosomes leads to genomic instability. *Nat Commun*. 2016;7:10754. doi:10.1038/ncomms10754.

337. Thompson SL, Compton DA. Proliferation of aneuploid human cells is limited by a p53-dependent mechanism. *J Cell Biol*. 2010;188(3):369-381. doi:10.1083/jcb.200905057.

338. Knutsen T, Padilla-Nash HM, Wangsa D, et al. Definitive molecular cytogenetic characterization of 15 colorectal cancer cell lines. *Genes, Chromosom Cancer*. 2009:NA-NA. doi:10.1002/gcc.20730.

339. McClelland SE, Tamura N. Personal communication. 2017.

340. Kelder T, Pico AR, Hanspers K, Van Iersel MP, Evelo C, Conklin BR. Mining biological pathways using WikiPathways web services. *PLoS One*. 2009;4(7). doi:10.1371/journal.pone.0006447.

341. Pfau SJ, Silberman RE, Knouse KA, Amon A. Aneuploidy impairs hematopoietic stem cell fitness and is selected against in regenerating tissues in vivo. *Genes Dev*. 2016;30(12):1395-1408. doi:10.1101/gad.278820.116.

342. Deutschbauer AM. Mechanisms of Haploinsufficiency Revealed by Genome-Wide Profiling in Yeast. *Genetics*. 2005;169(4):1915-1925. doi:10.1534/genetics.104.036871.

343. Thompson SL, Compton DA. Examining the link between chromosomal instability and aneuploidy in human cells. *J Cell Biol*. 2008;180(4):665-672. doi:10.1083/jcb.200712029.

344. Shapiro E, Biezuner T, Linnarsson S. Single-cell sequencing-based technologies will revolutionize whole-organism science. *Nat Rev Genet*. 2013;14(9):618-630. doi:10.1038/nrg3542.

345. Vasquez RJ, Howell B, Yvon AM, Wadsworth P, Cassimeris L. Nanomolar concentrations of nocodazole alter microtubule dynamic instability in vivo and in vitro. *Mol Biol Cell*. 1997;8(6):973-985. doi:10.1091/mbc.8.6.973.

346. Zimmermann FK, Mayer VW, Scheel I. Induction of aneuploidy by oncodazole (nocodazole), an anti-tubulin agent, and acetone. *Mutat Res Lett*. 1984;141(1):15-18. doi:10.1016/0165-7992(84)90030-7.

347. Mayer VW, Goin CJ. Aneuploidy induced by nocodazole or ethyl acetate is suppressed by dimethyl sulfoxide. *Mutat Res Toxicol*. 1987;187(1):31-35. doi:10.1016/0165-1218(87)90073-5.

348. Fenech M. The Cytokinesis-Block Micronucleus Technique and Its Application to Genotoxicity Studies in Human Populations. *Environ Health Perspect*. 1993;101:101. doi:10.2307/3431708.

349. Fenech M, Kirsch-Volders M, Natarajan AT, et al. Molecular mechanisms of micronucleus, nucleoplasmic bridge and nuclear bud formation in mammalian and human cells. *Mutagenesis*. 2010;26(1):125-132. doi:10.1093/mutage/geq052.

350. Dalton WB, Nandan MO, Moore RT, Yang VW. Human Cancer Cells Commonly Acquire DNA Damage during Mitotic Arrest. *Cancer Res*. 2007;67(24):11487-11492. doi:10.1158/0008-5472.can-07-5162.

351. Uetake Y, Sluder G. Prolonged Prometaphase Blocks Daughter Cell Proliferation Despite Normal Completion of Mitosis. *Curr Biol*. 2010;20(18):1666-1671. doi:10.1016/j.cub.2010.08.018.

352. Orth JD, Loewer A, Lahav G, Mitchison TJ. Prolonged mitotic arrest triggers partial activation of apoptosis, resulting in DNA damage and p53 induction. *Mol Biol Cell*. 2011;23(4):567-576. doi:10.1091/mbc.e11-09-0781.

353. Vassilev LT. Cell cycle synchronization at the G2/M phase border by reversible inhibition of CDK1. *Cell Cycle*. 2006;5(November):2555-2556. doi:10.4161/cc.5.22.3463.

354. Vassilev LT, Tovar C, Chen S, et al. Selective small-molecule inhibitor reveals critical mitotic functions of human CDK1. *Proc Natl Acad Sci*. 2006;103(28):10660-10665. doi:10.1073/pnas.0600447103.

355. Mah L-J, El-Osta a, Karagiannis TC. gammaH2AX: a sensitive molecular marker of DNA damage and repair. *Leuk Off J Leuk Soc Am Leuk Res Fund, UK*. 2010;24(4):679-686. doi:10.1038/leu.2010.6.

356. Podhorecka M, Skladanowski A, Bozko P. H2AX Phosphorylation: Its Role in DNA Damage Response and Cancer Therapy. *J Nucleic Acids*. 2010;2010:1-9. doi:10.4061/2010/920161.

357. Mariotti LG, Pirovano G, Savage KI, et al. Use of the ?-H2AX Assay to Investigate DNA Repair Dynamics Following Multiple Radiation Exposures. *PLoS One*. 2013;8(11):e79541. doi:10.1371/journal.pone.0079541.

358. Giunta S, Belotserkovskaya R, Jackson SP. DNA damage signaling in response to double-strand breaks during mitosis. *J Cell Biol*. 2010;190(2):197-207. doi:10.1083/jcb.200911156.

359. Branzei D, Foiani M. Regulation of DNA repair throughout the cell cycle. *Nat Rev Mol Cell Biol*. 2008;9(4):297-308. doi:10.1038/nrm2351.

360. Kaye JA, Melo JA, Cheung SK, Vaze MB, Haber JE, Toczyski DP. DNA Breaks Promote Genomic Instability by Impeding Proper Chromosome Segregation. *Curr Biol*. 2004;14(23):2096-2106. doi:10.1016/j.cub.2004.10.051.

361. Thompson SL, Compton DA. Chromosome missegregation in human cells arises through specific types of kinetochore-microtubule attachment errors. *Proc Natl Acad Sci*. 2011;108(44):17974-17978. doi:10.1073/pnas.1109720108.

362. Wang Z-B, Schatten H, Sun Q-Y. Why is Chromosome Segregation Error in Oocytes Increased With Maternal Aging? *Physiology*. 2011;26(5):314-325. doi:10.1152/physiol.00020.2011.

363. Kleyman M, Kabeche L, Compton DA. STAG2 promotes error correction in mitosis by regulating kinetochore-microtubule attachments. *J Cell Sci*. 2014;127(19):4225-4233. doi:10.1242/jcs.151613.

364. Kumari G, Ulrich T, Krause M, Finkernagel F, Gaubatz S. Induction of p21CIP1 Protein and Cell Cycle Arrest after Inhibition of Aurora B Kinase Is Attributed to Aneuploidy and Reactive Oxygen Species. *J Biol Chem*. 2014;289(23):16072-16084. doi:10.1074/jbc.m114.555060.

365. Shen KC, Heng H, Wang Y, et al. ATM and p21 Cooperate to Suppress Aneuploidy and Subsequent Tumor Development. *Cancer Res*. 2005;65(19):8747-8753. doi:10.1158/0008-5472.can-05-1471.

366. Fenech M, Kirsch-Volders M, Natarajan a. T, et al. Molecular mechanisms of micronucleus, nucleoplasmic bridge and nuclear bud formation in mammalian and human cells. *Mutagenesis*. 2011;26(1):125-132. doi:10.1093/mutage/geq052.

367. Li X, Zhao X, Fang Y, et al. Generation of Destabilized Green Fluorescent Protein as a Transcription Reporter. *J Biol Chem*. 1998;273(52):34970-34975. doi:10.1074/jbc.273.52.34970.

368. Ward WW, Bokman SH. Reversible denaturation of Aequorea green-fluorescent protein: physical separation and characterization of the renatured protein. *Biochemistry*. 1982;21(19):4535-4540. doi:10.1021/bi00262a003.

369. Cubitt AB, Heim R, Adams SR, Boyd AE, Gross LA, Tsien RY. Understanding, improving and using green fluorescent proteins. *Trends Biochem Sci*. 1995;20(11):448-455. doi:10.1016/s0968-0004(00)89099-4.

370. Franke CA, Rice CM, Strauss JH, Hruby DE. Neomycin resistance as a dominant selectable marker for selection and isolation of vaccinia virus recombinants. *Mol Cell Biol*. 1985;5(8):1918-1924. doi:10.1128/mcb.5.8.1918.

371. Kisselev AF, Goldberg AL. Proteasome inhibitors: from research tools to drug candidates. *Chem Biol*. 2001;8(8):739-758. doi:10.1016/s1074-5521(01)00056-4.

372. Schneider-Poetsch T, Ju J, Eyler DE, et al. Inhibition of eukaryotic translation elongation by cycloheximide and lactimidomycin. *Nat Chem Biol*. 2010;6(3):209-217. doi:10.1038/nchembio.304.

373. Cummings BS, Schnellmann RG. Measurement of Cell Death in Mammalian Cells. *Curr Protoc Pharmacol*. 2004. doi:10.1002/0471141755.ph1208s25.

374. LaFramboise T. Single nucleotide polymorphism arrays: a decade of biological, computational and technological advances. *Nucleic Acids Res*. 2009;37(13):4181-4193. doi:10.1093/nar/gkp552.

375. Gryfe R, Gallinger S. Microsatellite instability, mismatch repair deficiency, and colorectal cancer. *Surgery*. 2001;130(1):17-20. doi:10.1067/msy.2001.112738.

376. Potapova TA, Unruh JR, Box AC, et al. Karyotyping human and mouse cells using probes from single-sorted chromosomes and open source software. *Biotechniques*. 2015;59(6). doi:10.2144/000114362.

377. Prestel M, Feller C, Becker PB. Dosage compensation and the global re-balancing of aneuploid genomes. *Genome Biol*. 2010;11(8):216. doi:10.1186/gb-2010-11-8-216.

378. Hose J, Yong CM, Sardi M, Wang Z, Newton MA, Gasch AP. Correction: Dosage compensation can buffer copy-number variation in wild yeast. *Elife*. 2016;5. doi:10.7554/elife.15743.

379. Margolis RL, Lohez OD, Andreassen PR. G1 tetraploidy checkpoint and the suppression of tumorigenesis. *J Cell Biochem*. 2003;88(4):673-683. doi:10.1002/jcb.10411.

380. Lohez OD, Reynaud C, Borel F, Andreassen PR, Margolis RL. Arrest of mammalian fibroblasts in G1 in response to actin inhibition is dependent on retinoblastoma pocket proteins but not on p53. *J Cell Biol*. 2003;161(1):67-77. doi:10.1083/jcb.200208140.

381. Niwa O, Tange Y, Kurabayashi A. Growth arrest and chromosome instability in aneuploid yeast. *Yeast*. 2006;23(13):937-950. doi:10.1002/yea.1411.

382. Santaguida S, Richardson A, Iyer DR, et al. Chromosome Mis-segregation Generates Cell-Cycle-Arrested Cells with Complex Karyotypes that Are Eliminated by the Immune System. *Dev Cell*. 2017;41(6):638-651.e5. doi:10.1016/j.devcel.2017.05.022.

383. Elmore S. Apoptosis: A Review of Programmed Cell Death. *Toxicol Pathol*. 2007;35(4):495-516. doi:10.1080/01926230701320337.

384. Davoli T, Xu A, Mengwasser K, et al. Cumulative Haploinsufficiency and Triplosensitivity Drive Aneuploidy Patterns and Shape the Cancer Genome. *Cell*. 2013;155(4):948-962. doi:10.1016/j.cell.2013.10.011.

385. Flintoft L. Cancer genomics: Explaining aneuploidy patterns. *Nat Rev Genet*. 2013;14(12):825. doi:10.1038/nrg3634.

386. Bakker B, van den Bos H, Lansdorp PM, Foijer F. How to count chromosomes in a cell: An overview of current and novel technologies. *BioEssays*. 2015;37(5):570-577. doi:10.1002/bies.201400218.

387. Shaffer LG, Bui T-H. Molecular cytogenetic and rapid aneuploidy detection methods in prenatal diagnosis. *Am J Med Genet Part C Semin Med Genet*. 2007;145C(1):87-98. doi:10.1002/ajmg.c.30114.

388. Weissenberg R. Concurrent use of flow cytometry and fluorescence in-situ hybridization techniques for detecting faulty meiosis in a human sperm sample. *Mol Hum Reprod*. 1998;4(1):61-66. doi:10.1093/molehr/4.1.61.

389. Kay DB, Cambier JL, Wheeless LL. Imaging in flow. *J Histochem Cytochem*. 1979;27(1):329-334. doi:10.1177/27.1.374597.

390. Cambier JL, Kay DB, Wheeless LL. A multidimensional slit-scan flow system. *J Histochem Cytochem*. 1979;27(1):321-324. doi:10.1177/27.1.374595.

391. Basiji DA, Ortyn WE, Liang L, Venkatachalam V, Morrissey P. Cellular Image Analysis and Imaging by Flow Cytometry. *Clin Lab Med*. 2007;27(3):653-670. doi:10.1016/j.cll.2007.05.008.

392. Compton DA. Mechanisms of aneuploidy. *Curr Opin Cell Biol*. 2011;23(1):109-113. doi:10.1016/j.ceb.2010.08.007.

393. Tanaka K, Hirota T. Chromosome segregation machinery and cancer. *Cancer Sci*. 2009;100(7):1158-1165. doi:10.1111/j.1349-7006.2009.01178.x.

394. Taylor SS, McKeon F. Kinetochore Localization of Murine Bub1 Is Required for Normal Mitotic Timing and Checkpoint Response to Spindle Damage. *Cell*. 1997;89(5):727-735. doi:10.1016/s0092-8674(00)80255-x.

395. Gorbsky GJ, Chen R-H, Murray AW. Microinjection of Antibody to Mad2 Protein into Mammalian Cells in Mitosis Induces Premature Anaphase. *J Cell Biol*. 1998;141(5):1193-1205. doi:10.1083/jcb.141.5.1193.

396. Abrieu A, Magnaghi-Jaulin L, Kahana JA, et al. Mps1 Is a Kinetochore-Associated Kinase Essential for the Vertebrate Mitotic Checkpoint. *Cell*. 2001;106(1):83-93. doi:10.1016/s0092-8674(01)00410-x.

397. Burhans WC, Weinberger M. DNA replication stress, genome instability and aging. *Nucleic Acids Res*. 2007;35(22):7545-7556. doi:10.1093/nar/gkm1059.

398. Gaillard H, Garcia-Muse T, Aguilera A. Replication stress and cancer. *Nat Rev Cancer*. 2015;15(5):276-289. doi:10.1038/nrc3916.

399. Brambati A, Colosio A, Zardoni L, Galanti L, Liberi G. Replication and transcription on a collision course: eukaryotic regulation mechanisms and implications for DNA stability. *Front Genet*. 2015;6. doi:10.3389/fgene.2015.00166.

400. Helmrich A, Ballarino M, Tora L. Collisions between Replication and Transcription Complexes Cause Common Fragile Site Instability at the Longest Human Genes. *Mol Cell*. 2011;44(6):966-977. doi:10.1016/j.molcel.2011.10.013.

401. Liu B, Alberts B. Head-on collision between a DNA replication apparatus and RNA polymerase transcription complex. *Science (80-)*. 1995;267(5201):1131-1137. doi:10.1126/science.7855590.

402. Hou C, Li L, Qin Z, Corces V. Gene Density, Transcription, and Insulators Contribute to the Partition of the Drosophila Genome into Physical Domains. *Mol Cell*. 2012;48(3):471-484. doi:10.1016/j.molcel.2012.08.031.

403. Spadari S, Sala F, Pedrali-Noy G. Aphidicolin: a specific inhibitor of nuclear DNA replication in eukaryotes. *Trends Biochem Sci*. 1982;7(1):29-32. doi:10.1016/0968-0004(82)90061-5.

404. Regnier V, Vagnarelli P, Fukagawa T, et al. CENP-A Is Required for Accurate Chromosome Segregation and Sustained Kinetochore Association of BubR1. *Mol Cell Biol*. 2005;25(10):3967-3981. doi:10.1128/mcb.25.10.3967-3981.2005.

405. Hori T, Shang W-H, Takeuchi K, Fukagawa T. The CCAN recruits CENP-A to the centromere and forms the structural core for kinetochore assembly. *J Cell Biol*. 2012;200(1):45-60. doi:10.1083/jcb.201210106.

406. Orthaus S, Biskup C, Hoffmann B, et al. Assembly of the Inner Kinetochore Proteins CENP-A and CENP-B in Living Human Cells. *ChemBioChem*. 2008;9(1):77-92. doi:10.1002/cbic.200700358.

407. Guse A, Carroll CW, Moree B, Fuller CJ, Straight AF. In vitro centromere and kinetochore assembly on defined chromatin templates. *Nature*. 2011;477(7364):354-358. doi:10.1038/nature10379.

408. Irvine D V, Amor DJ, Perry J, et al. Chromosome size and origin as determinants of the level of CENP-A incorporation into human centromeres. *Chromosom Res*. 2004;12(8):805-815. doi:10.1007/s10577-005-5377-4.

409. Holland AJ, Fachinetti D, Han JS, Cleveland DW. Inducible, reversible system for the rapid and complete degradation of proteins in mammalian cells. *Proc Natl Acad Sci*. 2012;109(49):E3350-E3357. doi:10.1073/pnas.1216880109.

410. Janssen A, van der Burg M, Szuhai K, Kops GJ, Medema RH. Chromosome segregation errors as a cause of DNA damage and structural chromosome aberrations. *Science (80-)*. 2011;333(6051):1895-1898. doi:10.1126/science.1210214.

411. Potapova T, Gorbsky G. The Consequences of Chromosome Segregation Errors in Mitosis and Meiosis. *Biology (Basel)*. 2017;6(1):12. doi:10.3390/biology6010012.

412. Nakagawa S, FitzHarris G. Intrinsically Defective Microtubule Dynamics Contribute to Age-Related Chromosome Segregation Errors in Mouse Oocyte Meiosis-I. *Curr Biol*. 2017;27(7):1040-1047. doi:10.1016/j.cub.2017.02.025.

413. El-Labban A, Arteta C, Zisserman A, Bird AW, Hyman A. Mitotic phase based detection of chromosome segregation errors in embryonic stem cells. *2013 IEEE 10th Int Symp Biomed Imaging*. 2013. doi:10.1109/isbi.2013.6556619.

414. Hoque MT, Ishikawa F. Cohesin Defects Lead to Premature Sister Chromatid Separation, Kinetochore Dysfunction, and Spindle-assembly Checkpoint Activation. *J Biol Chem*. 2002;277(44):42306-42314. doi:10.1074/jbc.m206836200.

415. Cohen-Fix O. Sister chromatid separation: Falling apart at the seams. *Curr Biol*. 2000;10(22):R816-R819. doi:10.1016/s0960-9822(00)00799-5.

416. Wang S, Su J-H, Beliveau BJ, et al. Spatial organization of chromatin domains and compartments in single chromosomes. *Science (80-)*. 2016;353(6299):598-602. doi:10.1126/science.aaf8084.

417. Hoo JJ, Cramer H. On the position of chromosomes in prepared mitosis figures of human fibroblasts. *Humangenetik*. 1971;13(2):166-170. doi:10.1007/bf00295800.

418. Juricek D. Non-random chromosome distribution in radial metaphases from the Chinese hamster. *Chromosoma*. 1975;50(3). doi:10.1007/bf00283474.

419. Cremer T, Cremer M. Chromosome Territories. *Cold Spring Harb Perspect Biol*. 2010;2(3):a003889-a003889. doi:10.1101/cshperspect.a003889.

420. Smith CA, McAinsh AD, Burroughs NJ. Human kinetochores are swivel joints that mediate microtubule attachments. *Elife*. 2016;5. doi:10.7554/elife.16159.

421. Liang Z, Zickler D, Prentiss M, et al. Chromosomes Progress to Metaphase in Multiple Discrete Steps via Global Compaction/Expansion Cycles. *Cell*. 2015;161(5):1124-1137. doi:10.1016/j.cell.2015.04.030.

422. Gillego I, Castro-Hartmann P, Caravaca JM, Caio S, Daban J-R. Dense chromatin plates in metaphase chromosomes. *Eur Biophys J*. 2009;38(4):503-522. doi:10.1007/s00249-008-0401-1.

423. Fernandez P, Maier M, Lindauer M, Kuffer C, Storchova Z, Bausch AR. Mitotic Spindle Orients Perpendicular to the Forces Imposed by Dynamic Shear. *PLoS One*. 2011;6(12):e28965. doi:10.1371/journal.pone.0028965.

424. Gardner MK, Bouck DC, Paliulis L V., et al. Chromosome Congression by Kinesin-5 Motor-Mediated Disassembly of Longer Kinetochore Microtubules. *Cell*. 2008;135(5):894-906. doi:10.1016/j.cell.2008.09.046.

425. Stumpff J, Wordeman L. Chromosome Congression: The Kinesin-8-Step Path to Alignment. *Curr Biol*. 2007;17(9):R326-R328. doi:10.1016/j.cub.2007.03.013.

426. Wandke C, Barisic M, Sigl R, et al. Human chromokinesins promote chromosome congression and spindle microtubule dynamics during mitosis. *J Cell Biol*. 2012;198(5):847-863. doi:10.1083/jcb.201110060.

427. Tanenbaum ME, Stern-Ginossar N, Weissman JS, Vale RD. Regulation of mRNA translation during mitosis. *Elife*. 2015;4. doi:10.7554/elife.07957.

428. Halley-Stott RP, Jullien J, Pasque V, Gurdon J. Mitosis Gives a Brief Window of Opportunity for a Change in Gene Transcription. *PLoS Biol*. 2014;12(7):e1001914. doi:10.1371/journal.pbio.1001914.

429. Parsons GG, Spencer CA. Mitotic repression of RNA polymerase II transcription is accompanied by release of transcription elongation complexes. *Mol Cell Biol*. 1997;17(10):5791-5802. doi:10.1128/mcb.17.10.5791.

430. Lakin ND, Jackson SP. Regulation of p53 in response to DNA damage. *Oncogene*. 1999;18(53):7644-7655. doi:10.1038/sj.onc.1203015.

431. Cheng Q, Chen J. Mechanism of p53 stabilization by ATM after DNA damage. *Cell Cycle*. 2010;9(3):472-478. doi:10.4161/cc.9.3.10556.

432. Boehme KA, Kulikov R, Blattner C. p53 stabilization in response to DNA damage requires Akt/PKB and DNA-PK. *Proc Natl Acad Sci*. 2008;105(22):7785-7790. doi:10.1073/pnas.0703423105.

433. Ard PG, Chatterjee C, Kunjibettu S, Adside LR, Gralinski LE, McMahon SB. Transcriptional Regulation of the mdm2 Oncogene by p53 Requires TRRAP Acetyltransferase Complexes. *Mol Cell Biol*. 2002;22(16):5650-5661. doi:10.1128/mcb.22.16.5650-5661.2002.

434. Manfredi JJ. The Mdm2-p53 relationship evolves: Mdm2 swings both ways as an oncogene and a tumor suppressor. *Genes Dev*. 2010;24(15):1580-1589. doi:10.1101/gad.1941710.

435. Lambert PF, Kashanchi F, Radonovich MF, Shiekhattar R, Brady JN. Phosphorylation of p53 Serine 15 Increases Interaction with CBP. *J Biol Chem*. 1998;273(49):33048-33053. doi:10.1074/jbc.273.49.33048.

436. Loughery J, Cox M, Smith LM, Meek DW. Critical role for p53-serine 15 phosphorylation in stimulating transactivation at p53-responsive promoters. *Nucleic Acids Res*. 2014;42(12):7666-7680. doi:10.1093/nar/gku501.

437. Bai M, Agnantis NJ, Skyrlas A, et al. Increased Expression of the bcl6 and CD10 Proteins Is Associated with Increased Apoptosis and Proliferation in Diffuse Large B-Cell Lymphomas. *Mod Pathol*. 2003;16(5):471-480. doi:10.1097/01.mp.0000067684.78221.6e.

438. Yang E, Zha J, Jockel J, Boise LH, Thompson CB, Korsmeyer SJ. Bad, a heterodimeric partner for Bcl-xL and Bcl-2, displaces bax and promotes cell death. *Cell*. 1995;80(2):285-291. doi:10.1016/0092-8674(95)90411-5.

439. O'Connor L, Strasser A, O'Reilly LA, et al. Bim: A novel member of the Bcl-2 family that promotes apoptosis. *EMBO J*. 1998;17(2):384-395. doi:10.1093/emboj/17.2.384.

440. Hernandez R, Frady A, Zhang X-Y, Varela M, Ehrlich M. Preferential induction of chromosome 1 multibranched figures and whole-arm deletions in a human pro-B cell line treated with 5-azacytidine or 5-azadeoxycytidine. *Cytogenet Genome Res*. 1997;76(3-4):196-201. doi:10.1159/000134548.

441. Lavia P, Ferraro M, Micheli A, Olivieri G. Effect of 5-azacytidine (5-azaC) on the induction of chromatid aberrations (CA) and sister-chromatid exchanges (SCE). *Mutat Res Mol Mech Mutagen*. 1985;149(3):463-467. doi:10.1016/0027-5107(85)90164-2.

442. Stevens D, Gassmann R, Oegema K, Desai A. Uncoordinated Loss of Chromatid Cohesion Is a Common Outcome of Extended Metaphase Arrest. *PLoS One*. 2011;6(8):e22969. doi:10.1371/journal.pone.0022969.

443. Mirkovic M, Hutter L, Novak B, Oliveira R. Premature Sister Chromatid Separation Is Poorly Detected by the Spindle Assembly Checkpoint as a Result of System-Level Feedback. *Cell Rep*. 2015;13(3):469-478. doi:10.1016/j.celrep.2015.09.020.

444. Losada A. Cohesin in cancer: chromosome segregation and beyond. *Nat Rev Cancer*. 2014;14(6):389-393. doi:10.1038/nrc3743.

445. Chiang T, Duncan FE, Schindler K, Schultz RM, Lampson MA. Weakened Centromere Cohesion Is the Primary Cause of Age-Related Aneuploidy in Oocytes. *Biol Reprod*. 2010;83(Suppl_1):9. doi:10.1093/biolreprod/83.s1.9.

446. Gutierrez-Mateo C. Aneuploidy study of human oocytes first polar body comparative genomic hybridization and metaphase II fluorescence in situ hybridization analysis. *Hum Reprod*. 2004;19(12):2859-2868. doi:10.1093/humrep/deh515.

447. Munne S. Preimplantation genetic diagnosis of numerical and structural chromosome abnormalities. *Reprod Biomed Online*. 2002;4(2):183-196. doi:10.1016/s1472-6483(10)61938-4.

448. Weier JF, Weier H-UG, Nureddin A, Pedersen RA, Racowsky C. Aneuploidy involving chromosome 1 in failed-fertilized human oocytes is unrelated to maternal age. *J Assist Reprod Genet*. 2005;22(7-8):285-293. doi:10.1007/s10815-005-5999-7.

449. Nishiyama T, Sykora MM, Huis In 't Veld PJ, Mechtler K, Peters J-M. Aurora B and Cdk1 mediate Wapl activation and release of acetylated cohesin from chromosomes by phosphorylating Sororin. *Proc Natl Acad Sci U S A*. 2013;110(33):13404-13409. doi:10.1073/pnas.1305020110.

450. Tanno Y, Kitajima TS, Honda T, Ando Y, Ishiguro K -i., Watanabe Y. Phosphorylation of mammalian Sgo2 by Aurora B recruits PP2A and MCAK to centromeres. *Genes Dev*. 2010;24(19):2169-2179. doi:10.1101/gad.1945310.

451. Kim H-S, Kim S-H, Park H-Y, et al. Functional interplay between Aurora B kinase and Ssu72 phosphatase regulates sister chromatid cohesion. *Nat Commun*. 2013;4. doi:10.1038/ncomms3631.

452. Dai J, Sullivan BA, Higgins JMG. Regulation of Mitotic Chromosome Cohesion by Haspin and Aurora B. *Dev Cell*. 2006;11(5):741-750. doi:10.1016/j.devcel.2006.09.018.

453. Knowlton AL, Lan W, Stukenberg PT. Aurora B Is Enriched at Merotelic Attachment Sites, Where It Regulates MCAK. *Curr Biol*. 2006;16(17):1705-1710. doi:10.1016/j.cub.2006.07.057.

454. Cimini D. Detection and Correction of Merotelic Kinetochore Orientation by Aurora B and its Partners. *Cell Cycle*. 2007;6(13):1558-1564. doi:10.4161/cc.6.13.4452.

455. Zhang C-Z, Spektor A, Cornils H, et al. Chromothripsis from DNA damage in micronuclei. *Nature*. 2015;522(7555):179-184. doi:10.1038/nature14493.

456. Minocherhomji S, Ying S, Bjerregaard VA, et al. Replication stress activates DNA repair synthesis in mitosis. *Nature*. 2015;528(7581):286-290. doi:10.1038/nature16139.

457. Faggioli F, Wang T, Vijg J, Montagna C. Chromosome-specific accumulation of aneuploidy in the aging mouse brain. *Hum Mol Genet*. 2012;21(24):5246-5253. doi:10.1093/hmg/dds375.

458. Gisselsson D, Pettersson L, Höglund M, et al. Chromosomal breakage-fusion-bridge events cause genetic intratumor heterogeneity. *Proc Natl Acad Sci U S A*. 2000;97(10):5357-5362. doi:10.1073/pnas.090013497.

459. Hu L, Filippakis H, Huang H, Yen TJ, Gjoerup O V. Replication Stress and Mitotic Dysfunction in Cells Expressing Simian Virus 40 Large T Antigen. *J Virol*. 2013;87(24):13179-13192. doi:10.1128/jvi.02224-13.

460. Okada T, Ohzeki J, Nakano M, et al. CENP-B Controls Centromere Formation Depending on the Chromatin Context. *Cell*. 2007;131(7):1287-1300. doi:10.1016/j.cell.2007.10.045.

461. Fachinetti D, Han JS, McMahon MA, et al. DNA Sequence-Specific Binding of CENP-B Enhances the Fidelity of Human Centromere Function. *Dev Cell*. 2015;33(3):314-327. doi:10.1016/j.devcel.2015.03.020.

462. Giunta S, Funabiki H. Integrity of the human centromere DNA repeats is protected by CENP-A, CENP-C, and CENP-T. *Proc Natl Acad Sci*. 2017;114(8):1928-1933. doi:10.1073/pnas.1615133114.

463. Mart?nez P, Bouza C, Vi?as A, S?nchez L. Differential digestion of the centromeric heterochromatic regions of the 5-azacytidine-decondensed human chromosomes 1, 9, 15, and 16 by NdeII and Sau3AI restriction endonucleases. *Genetica*. 1995;96(3):235-238. doi:10.1007/bf01439577.

464. Prada D, Gonzalez R, Sanchez L, Castro C, Fabian E, Herrera LA. Satellite 2 demethylation induced by 5-azacytidine is associated with missegregation of chromosomes 1 and 16 in human somatic cells. *Mutat Res Mol Mech Mutagen*. 2012;729(1-2):100-105. doi:10.1016/j.mrfmmm.2011.10.007.

465. Chen B, Yusuf M, Hashimoto T, Estandarte AK, Thompson G, Robinson I. Three-dimensional positioning and structure of chromosomes in a human prophase nucleus. *Sci Adv*. 2017;3(7):e1602231. doi:10.1126/sciadv.1602231.

466. Cremer M, Kopper K, Wagler B, et al. Inheritance of gene density-related higher order chromatin arrangements in normal and tumor cell nuclei. *J Cell Biol*. 2003;162(5):809-820. doi:10.1083/jcb.200304096.

467. Bakhoum SF, Genovese G, Compton DA. Deviant Kinetochore Microtubule Dynamics Underlie Chromosomal Instability. *Curr Biol*. 2009;19(22):1937-1942. doi:10.1016/j.cub.2009.09.055.

468. Magidson V, O'Connell CB, Lončarek J, Paul R, Mogilner A, Khodjakov A. The spatial arrangement of chromosomes during prometaphase facilitates spindle assembly. *Cell*. 2011;146(4):555-567. doi:10.1016/j.cell.2011.07.012.

469. Paul R, Wollman R, Silkworth WT, Nardi IK, Cimini D, Mogilner A. Computer simulations predict that chromosome movements and rotations accelerate mitotic spindle assembly without compromising accuracy. *Proc Natl Acad Sci*. 2009;106(37):15708-15713. doi:10.1073/pnas.0908261106.

470. Levesque AA, Compton DA. The chromokinesin Kid is necessary for chromosome arm orientation and oscillation, but not congression, on mitotic spindles. *J Cell Biol*. 2001;154(6):1135-1146. doi:10.1083/jcb.200106093.

471. Heneen WK, Nichols WW. Nonrandom arrangement of metaphase chromosomes in cultured cells of the Indian deer, *Muntiacus muntjak*. *Cytogenet Genome Res*. 1972;11(3):153-164. doi:10.1159/000130185.

472. Khan WA, Rogan PK, Knoll JHM. Localized, non-random differences in chromatin accessibility between homologous metaphase chromosomes. *Mol Cytogenet*. 2014;7(1). doi:10.1186/s13039-014-0070-y.

473. SCHNEIDERMAN LJ, SMITH CAB. Non-Random Distribution of Certain Homologous Pairs of Normal Human Chromosomes in Metaphase. *Nature*. 1962;195(4847):1229-1230. doi:10.1038/1951229a0.

10. Appendix

10.1. Macros and programming scripts

10.1.1. Fluorescence intensity within the nucleus – ImageJ macro

```
{
dir = getDirectory("image");
processedDir=dir + "\Text Data\\";
File.makeDirectory(processedDir);
title = getTitle();
dotIndex = indexOf(title, ".");
title1 = substring(title, 0, dotIndex);
setBatchMode('false');
run("Set Measurements...", "mean redirect=None decimal=3");
selectWindow(title);
run("Z Project...", "start=1 stop=50 projection=[Max Intensity]");
selectWindow(title);
run("Z Project...", "start=51 stop=100 projection=[Max Intensity]");
selectWindow(title);
run("Z Project...", "start=101 stop=150 projection=[Max Intensity]");
selectWindow("MAX_"+title);
setAutoThreshold("Default dark");
//run("Threshold...");
run("Analyze Particles...", "size=100-Infinity add");
name = title + " - Cell Identification";
saveAs("Tiff", processedDir +name);
selectWindow("MAX_"+title1+"-1.dv");
run("Show Overlay");
roiManager("Multi Measure");
run("Input/Output...", "jpeg=85 gif=-1 file=.txt use_file save_column");
name = title + " p21" + ".txt";
saveAs("Results", processedDir +name);
selectWindow("MAX_"+title1+"-2.dv");
run("Show Overlay");
roiManager("Multi Measure");
```

```
run("Input/Output...", "jpeg=85 gif=-1 file=.txt use_file save_column");
name = title + " p53" + ".txt";
saveAs("Results", processedDir +name);
selectWindow("Results");
run("Close");
selectWindow("ROI Manager");
run("Close");
run("Close All");
}
```

10.1.2. Metaphase plate positioning – ImageJ macro

```
{
title = getTitle();
dotIndex = indexOf(title, ".");
title1 = substring(title, 0, dotIndex);
run("Set Measurements...", "centroid fit invert redirect=None decimal=3");
selectWindow(title);
run("Z Project...", "projection=[Standard Deviation]");
run("Split Channels");
selectWindow("C1-STD_"+title);
setAutoThreshold("Default dark");
setOption("BlackBackground", false);
run("Convert to Mask");
run("Analyze Particles...", "size=50-Infinity pixel circularity=0.00-1.00 show=Overlay
exclude clear add");
selectWindow("C2-STD_"+title);
setAutoThreshold("Intermodes dark");
setOption("BlackBackground", false);
run("Convert to Mask");
roiManager("Select", 0);
run("Find Maxima...", "noise=10 output=[Point Selection] light");
roiManager("Add");
array1 = newArray("0");;
for (i=1;i<roiManager("count");i++){
        array1 = Array.concat(array1,i);
}
roiManager("select", array1);
roiManager("Measure");
selectWindow("C3-STD_"+title);
setAutoThreshold("Intermodes dark");
setOption("BlackBackground", false);
run("Convert to Mask");
roiManager("Select", 0);
```

```
run("Find Maxima...", "noise=10 output=[Point Selection] light");
roiManager("Add");
array2 = newArray("0");;
for (i=1;i<roiManager("count");i++){
        array2 = Array.concat(array2,i);
}
roiManager("select", array2);
roiManager("Measure");
}
```

10.1.3. Metaphase plate positioning – R script

```
install.packages("ggplot2")
library(ggplot2)
setwd("   ")                    # set working directory for analysis file
df <- read.table("    ",        # point to analysis file (.txt)
  header = TRUE, fill = TRUE)
ggplot(df, aes(x = chromosome, y = angle)) + geom_bin2d() +
 scale_fill_gradient(low = "white", high = "red")
```

10.1.4. Sister chromatid angle rose plot – R script

```
install.packages("ggplot2")
library(ggplot2)
setwd("   ")                    # set working directory for analysis file
df <- read.table("    ",        # point to analysis file (.txt)
  header = TRUE, fill = TRUE)
ggplot(df, aes(x = angle, y = frequency)) +
  coord_polar(theta = "x", direction = 1) +
  geom_bar(stat = "identity", width=1, fill="slategray3", colour="black") +
  scale_x_continuous(limits = c(0,45), breaks = seq(0, 360, 60)) +
  scale_y_sqrt(breaks = seq(0,6)) +
  theme(panel.grid.major = element_blank())
```

10.1.5. Inter-homologue distance – R script

```
install.packages("ggplot2")
library(ggplot2)
setwd("   ")                    # set working directory for analysis file
df <- read.table("    ",        # point to analysis file (.txt)
  header = TRUE, fill = TRUE)
ggplot(df, aes(x = chromosome, y = distance)) + geom_bin2d(bins=23) +ylim(0,1) +
  scale_fill_gradient(low = "light grey", high = "green")
```

10.1.6. Chromatid geometry – Microsoft Excel function macro

10.1.6.1. Cell definitions

C2	ellipse centre raw x position
D2	ellipse centre raw y position
E2	major axis length
F2	minor axis length
G2	metaphase rotation angle
C3	sister chromatid raw x position
D3	sister chromatid raw y position
H3	Δx
I3	Δy
J3	Hypotenuse of Δx Δy
K3	Angle between Δx Δy and x-axis (radians)
L3	Angle between Δx Δy and x-axis (degrees)
M3	Chromatid quadrant check
N3	Angle between Δx Δy and the metaphase major axis (degrees)
O3	Chromatid position
P3	Chromatid position normalised to metaphase plate length
P3:P6	All chromatid positions normalised to metaphase plate length
Q3	Number of individual chromatid signals
R3	Number of resolved sister chromatid pairs
S3	Inter-centromere distance between sister chromatid pairs
T3	Inter-centromere angle (radians)
U3	Inter-centromere angle (degrees)
V3	Inter-centromere angle sister chromatid qualifier
W3	Normalised inter-homologue distance

10.1.6.2. Cell functions

H3 =(C3-C2)

I3 =(D3-D2)

J3 =(SQRT((I3^2)+(H3^2)))

K3 =(ABS(ATAN(I3/H3)))

L3 =(K3*(180/3.14159265358979))

M3 =IF(G2<0, (G2+180), G2)

N3 =IF(M3>90, (IF((180-M3-L3)<0, ABS(180-M3-L3), (IF(AND((H3>=0), (I3>=0)), (M3-L3), (180-M3-L3))))), (IF(L3<M3, SUM(M3-L3), SUM((L3-M3)))))

O3 =ABS((J3*(COS(N3*(3.14159265359/180)))))

P3 =(O3/(E2/2))

Q3 =COUNT(P3:P6)

R3 =IF(Q3=4,2,(IF(Q3=3,2,(IF(Q3=2,0,IF(Q3=1,0,0))))))

S3 =IF(Q3=1,0,IF(Q3=2,0,IF(Q3=4,IF(SUM(LARGE(P3:P6,1)-LARGE(P3:P6,2))<0.1,(SQRT((((INDEX(H3:H6,MATCH(LARGE(P3:P6,1),(P3:P6),0)))-(INDEX(H3:H6,MATCH(LARGE(P3:P6,2),(P3:P6),0))))^2)+(((INDEX(I3:I6,MATCH(LARGE(P3:P6,1),(P3:P6),0)))-(INDEX(I3:I6,MATCH(LARGE(P3:P6,2),(P3:P6),0))))^2))),0),(IF(Q3=3,IF(SUM(LARGE(P3:P6,1)-LARGE(P3:P6,2))<0.1,(SQRT((((INDEX(H3:H6,MATCH(LARGE(P3:P6,1),(P3:P6),0)))-(INDEX(H3:H6,MATCH(LARGE(P3:P6,2),(P3:P6),0))))^2)+(((INDEX(I3:I6,MATCH(LARGE(P3:P6,1),(P3:P6),0)))-(INDEX(I3:I6,MATCH(LARGE(P3:P6,2),(P3:P6),0))))^2))),SQRT((((INDEX(H3:H6,MATCH(LARGE(P3:P6,2),(P3:P6),0)))-(INDEX(H3:H6,MATCH(LARGE(P3:P6,3),(P3:P6),0))))^2)+(((INDEX(I3:I6,MATCH(LARGE(P3:P6,2),(P3:P6),0)))-(INDEX(I3:I6,MATCH(LARGE(P3:P6,3),(P3:P6),0))))^2))),0)))))

T3 =IF(Q3=1,0,IF(Q3=2,0,IF(Q3=4,IF(SUM(LARGE(P3:P6,1)-LARGE(P3:P6,2))<0.1,(ABS(ACOS(((LARGE(P3:P6,1)-(LARGE(P3:P6,2)))))))),0), IF(Q3=3,IF(SUM(LARGE(P3:P6,1)-LARGE(P3:P6,2))<0.1,(ABS(ACOS(((LARGE(P3:P6,1)-(LARGE(P3:P6,2)))))))), (ABS(ACOS(((LARGE(P3:P6,2)-(LARGE(P3:P6,3)))))))),0))))

U3 =(T3*(180/3.14159265358979))

V3 =IF(AND(Q3>=3, U3>0),(90-U3),0)

W3 =IF(Q3=2, (ABS(P3-P4)), 0)